Dissertation

submitted to the
Combined Faculty of Natural Sciences and Mathematics
of Heidelberg University, Germany
for the degree of
Doctor of Natural Sciences

Put forward by
Marleen Lausecker, M. Sc.
born in Nürtingen
Oral examination: 19.10.2021

Insights into Atlantic thermocline seawater temperatures from cold-water corals since the last glacial

Referees:

Prof. Dr. Norbert Frank

Prof. Dr. Werner Aeschbach

Einblicke in die thermoklinen Temperaturen des Atlantik durch Kaltwasserkorallen seit dem letzten Glazial

Der mittlere, globale Temperaturanstieg des Ozeans seit dem letzten glazialen Maximum (LGM) wurde kürzlich auf etwa 2,6 °C abgeschätzt (Bereiter *et al.*, 2018). Dieser Temperaturunterschied verteilt sich allerdings nicht gleichmäßig. Während der Oberflächen- und tiefe Ozean vergleichsweise gut untersucht ist, wurde der dynamische thermokline Ozean lange vernachlässigt. Kaltwasserkorallen (KWK) bewohnen diese dynamischen Wassertiefen, was sie zu wertvollen Archiven für paläoozeanographische Studien macht.
In dieser Arbeit wird das Li/Mg-Verhältnis in KWK genutzt um Wassertemperaturen zu rekonstruieren. In einer ersten Studie wurden KWK vor der Küste Angolas untersucht. Es zeigt sich ein Temperaturunterschied von -6 °C während des Glazials im Vergleich zu heute, was auf eine flachere Thermokline während des Glazials hinweist. Zudem wurden KWK von sechs verschiedenen Lokationen im Atlantik untersucht. Dabei wurden überall ähnliche Temperaturmuster entdeckt. ^{14}C Messungen wurden genutzt um Reservoiralter und Änderungen der Wasserbewegungen zu rekonstruieren.
Während des LGM werden in Regionen hoher vulkanische Aktivität extrem hohe Li/Mg-Verhältnisse gemessen. Dies könnte auf eine erhöhte Li-Konzentration im Meerwasser hinweisen. Im zweiten Teil dieser Arbeit wird die Hypothese lokalen Li Eintrags durch hydrothermal Fluide als Ursache erhöhter Li-Konzentration in KWK untersucht. Die Li-Isotopie von sechs Korallen wurde analysiert. Alle KWK zeigen die gleiche Li-Isotopie. Ein Einfluss hydrothermaler Fluide auf das Li/Mg-Verhältnis der KWK ist daher unwahrscheinlich und der Ursprung hoher Li/Mg-Verhältnisse bleibt weiter unbekannt.

Insights into Atlantic thermocline seawater temperatures from cold-water corals since the last glacial

The mean global ocean temperature increase since the last glacial maximum was recently estimated to be about 2.6 °C (Bereiter *et al.*, 2018). This temperature increase is not homogeneously distributed throughout the ocean. While the surface and deep ocean are well studied, the dynamic thermocline ocean was long neglected. As cold-water corals (CWCs) inhabit these highly dynamic water depths, they are valuable archives for paleoceanographic studies.
In this thesis, CWCs are used to reconstruct thermocline water temperatures using their Li/Mg ratio. A first study focuses on the Angolan margin. Here, glacial cooling of about 6 °C indicating a shoaling of the thermocline was found. Furthermore, CWCs from six locations throughout the Atlantic were studied. Similar temperature patterns over the last 40 ka were found at all locations. Radiocarbon data was used to estimate reservoir ages and changes in water mass pathways. An aging of thermocline waters south of 35 °N in the Atlantic is observed.
During the LGM, extremely high Li/Mg ratios were found in regions with volcanic activity. These might be influenced through increased Li concentrations in the seawater. Thus, in the second part of the thesis, the hypothesis of locally increased Li input through hydrothermal fluids was tested. Therefore, the lithium isotopic composition of six CWCs was analysed. The isotopic composition of the CWCs does not vary, excluding an influence of hydrothermal fluids on the Li/Mg ratio of the CWCs. Hence, the origin of unusal high Li/Mg ratios of glacial corals remains unknown.

Contents

1 Motivation

The mean ocean temperature increase during the last glacial transition was recently estimated to be about 2.6 °C through noble gases trapped in ice cores (Bereiter *et al.*, 2018). This temperature increase, however, is not uniformly distributed throughout the ocean. While temperature changes in the deep ocean are rather small at 2 °C to 3 °C (Bereiter *et al.*, 2018; Adkins *et al.*, 2002), the upper ocean is more dynamic. Furthermore, strong latitudinal and longitudinal gradients are observed, as the surface water masses in the tropics receive thermal energy through solar radiation while polar waters feed the deep sea in the North Atlantic. A lot of effort went into the reconstruction of surface water temperatures based on temperature reconstructions of planktonic microfossils (e.g. MARGO Project Members, 2009). These studies have revealed a southward displacement of the polar front with temperature decreasing up to 12 °C in the Northern North Atlantic.

Various proxies were developed over the last decades to reconstruct seawater properties like temperature, water mass origin or nutrient contents (e.g. Penaud *et al.*, 2011; Keigwin and Boyle, 1989; Adkins and Boyle, 1997; Frank, 2002). These analyses have long focused on the surface and the deep ocean while the thermocline ocean was often neglected. Thermocline water masses are highly dynamic, but remain far less constrained. Various model simulations of past ocean circulation patterns have revealed the importance of thermocline water temperature changes of up to 6 °C during times of major climate changes (Stocker and Johnsen, 2003; Schiller *et al.*, 1997; Stocker *et al.*, 1992).

These dynamic thermocline water masses are inhabited by cold-water corals representing a highly valuable environmental archive for mid-depth water studies. Trace elements, incorporated into the coralline carbonate skeletons, are used as proxies to reconstruct past climate conditions. Vital effexts during calcification, however, can strongly influence elemental distributions and classical isotope tools (Robinson *et al.*, 2014). In 2010, Case *et al.* proposed the Li/Mg ratio in cold-water corals as a new promising proxy to reconstruct thermocline temperatures. Montagna *et al.* (2014) then published an empirically observed calibration between Li/Mg ratios in coralline skeletons and ambient seawater temperature. This calibration was recently affirmed

by Cuny-Guirriec *et al.* (2019) and Stewart *et al.* (2020).
In this thesis, the Li/Mg coralline thermometer is used to reconstruct thermocline temperatures in six different locations throughout the Atlantic. Since models infer highly variable temperatures in the thermocline associated with major ocean reorganisations during climate change cold water coral temperature reconstructions can provide a archive to measure the ocean interior heat content since the last glacial. The implications of a strong thermocline cooling during the last glacial on the Atlantic water pathways are discussed.
The Li/Mg thermometer is not yet fully understood. At times, reconstructed thermocline temperatures using this method reveal physically unreasonable low temperatures. These temperatures primarily occur at locations with volcanic activity like the Azores and the Gulf of Cadiz. This lead to the hypothesis of locally influenced lithium content of the ambient seawater, possibly through the input of hydrothermal fluids. This hypothesis is here tested through the analysis of the lithium isotopic composition of corals. The global seawater lithium composition is fairly constant and does not change on glacial/interglacial timescales (Hall *et al.*, 2005; Cuny-Guirriec, 2020) while its lithium isotopic composition strongly deviates from the highly concentrated hydrothermal fluids. A local input of lithium through hydrothermal fluids, therefore, would also change the lithium isotopic composition of seawater and, thus, of the coralline skeletons. If locally altered seawater lithium concentrations are the reason for physically unreasonably low reconstructed temperatures, measurements of the lithium isotopic composition might be used to correct these temperatures.
The main part of this thesis is, thus, divided into two parts: Part I, containing two chapters, does focus on reconstructed thermocline temperatures using the Li/Mg thermometer. In chapter 5, corals off the coast of Angola were analysed for their Li/Mg ratio and ^{14}C reservoir ages. At this location, cold-water corals are found during glacial and interglacial times, making it a unique location to observe the last deglaciation. The corals reveal a gradual water mass aging during the Last Glacial Maximum. Furthermore, a strong and abrupt temperature increase of about 6 °C was observed at the beginning of Heinrich Event 1 about 17 ka ago. In chapter 6, a compilation of nearly 200 thermocline temperature values spanning the last 40 ka is presented. Cold-water corals at six different locations throughout the Atlantic were analysed, revealing similar temperature patterns. At the end of the chapter, the reconstructed thermocline temperatures are complemented by compiled coralline radiocarbon data to gain more information on the internal flow patterns of the glacial Atlantic ocean.
In the second main part of this thesis (see part II), the hypothesis on local Li influences on the thermometer described above is tested. In chapter 8, a method to extract lithium

from carbonate and seawater samples as well as their measurement is established. This is followed by the analysis of six different cold-water coral samples from the Azores archipelago indicating a volcanic influence on the corals through the water mass provenance proxy ϵ_{Nd}. A change in the lithium isotopic composition, however, is not found. Hence, a significant local input of lithium into the seawater is unlikely to be the cause for physically unreasonable low seawater temperatures. This leaves this observation unexplained.

2 Fundamentals

2.1 Oceanography

The upper Atlantic ocean is dominated by wind-driven gyres and wind-driven tropical transport (see figure 2.1). There are two subtropical gyres, one in the North and one in the South Atlantic. In the North Atlantic, an additional subpolar gyre is formed north of 50 °N, centered in the Labrador and Irmminger Sea. In the tropics, circulation predominantly occurs zonal. The conversion towards cooler and denser waters in the northern North Atlantic leads to the formation of intermediate and deep waters associated with the thermohaline overturning circulation. This also affects the upper ocean as it increases the northward transport in the Gulf Stream and North Atlantic Current by about 10 % (Talley *et al.*, 2011), resulting in a net northward heat transport for the Atlantic. In the South Atlantic, the poleward direction of the heat transport is reversed (Talley *et al.*, 2011).

The South Atlantic surface circulation is characterised by the anticyclonic subtropical gyre with the Brazil current as its westward boundary current flowing southwards along the South American coastline. The eastward flow in the south is the South Atlantic Current (SAC), which is divided from the Antarctic Circumpolar Current (ACC) by the subantarctic Front. On the eastern boundary, the Benguela Current (BeC) carries about 20 Sv from the southern tip of Africa and polar Southern Ocean north-westward (Stramma and Peterson, 1989; Garzoli *et al.*, 1996; Boyer and Hampton, 2001; Veitch *et al.*, 2010) containing contributions of a warm and saline water mass from the Indian ocean through the Agulhas leakage (Biastoch *et al.*, 2008, 2015; Weijer and van Sebille, 2014). Equatorward winds along the eastern margin produce a westward Ekman transport in the upper ocean resulting in a strong upwelling and tongue of cold surface waters at the Benguela Upwelling System (BUS).

The Benguela Current meets the Angola Current (AC) at the Angola-Benguela-Front (ABF). The ABF separates the warmer North and South Equatorial Counter Currents (NECC and SECC) from the colder BeC at a seasonally varying latitude of about 15 ± 3 °S (Meeuwis and Lutjeharms, 1990). The SECC is a quasi-permanent Current at about 7 - 8 °S which is associated with the is redirected at the coast of Africa, turns

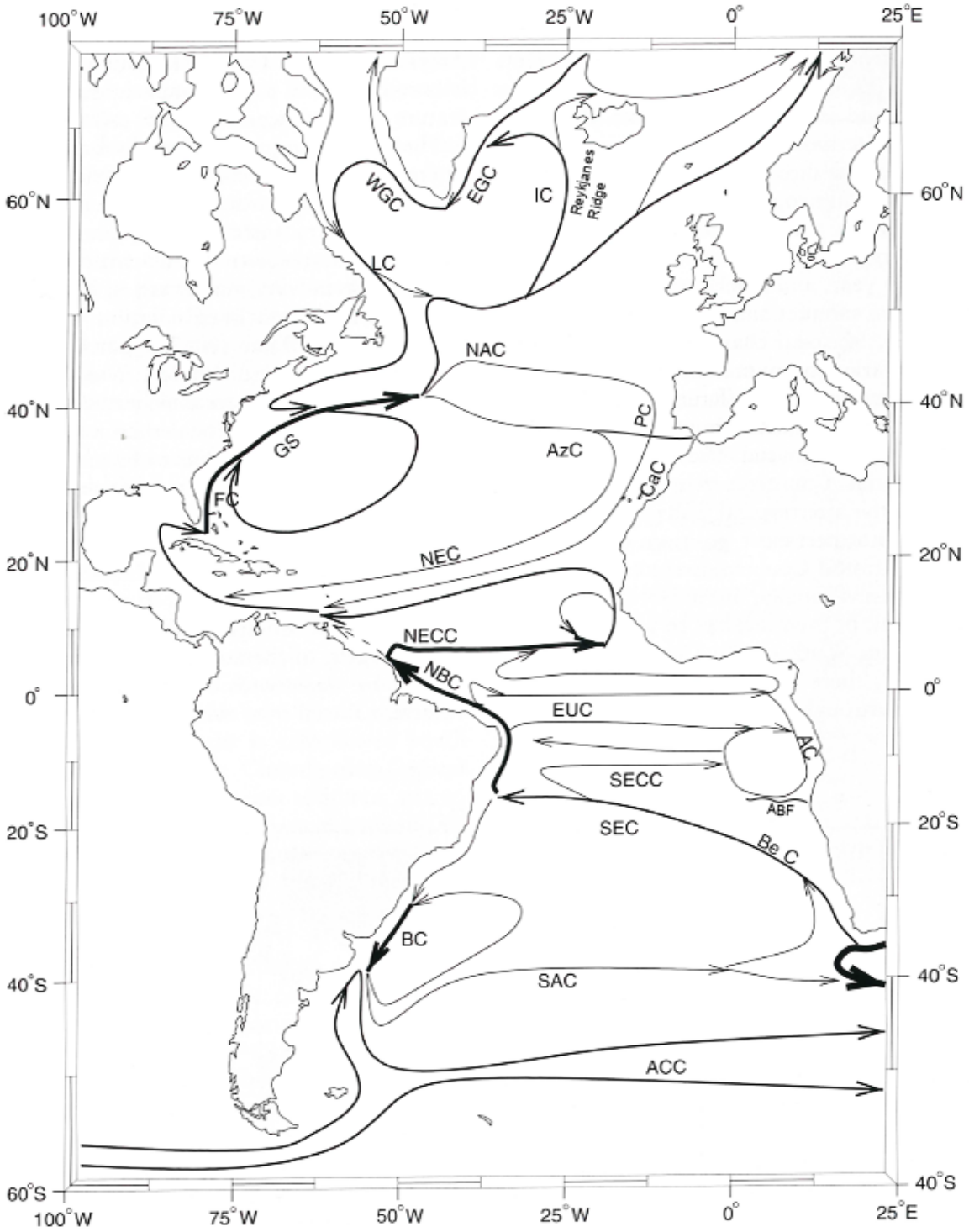

Figure 2.1: Map of the major subsurface currents in the Atlantic. Abbreviations are used as follows: WGC: West Greenland Current, EGC East Greenland Current, IC: Irminger Current, LC: Labrador Current, NAC: North Atlantic Current, PC: Portugal Current, CaC: Canary Current, AzC: Azores Current, GS: Gulf Stream, NEC: North Equatorial Current, NECC: North Equatorial Countercurrent, EUC: Equatorial Under Current, SECC: South Equatorial Countercurrent, SEC; South Equatorial Current, NBC: North Brazil Current, BC: Brazil Current, AC: Angola Current, ABF: Angola Benguela Front, BeC: Benguela Current, SAC: South Atlantic Current, ACC: Antarctic Circumpolar Current. Figure modified from Stramma (2001).

south and forms the Angola Current (AC) (Talley *et al.*, 2011). This leads to a cyclonic upwelling system, the so-called Angola Dome (Wacongne and Piton, 1992).
The northern component of the South Atlantic subtropical gyre is formed by the South Equatorial Current (SEC). On the western boundary the SEC divides into the BC, moving towards the South, and the North Brazil Current (NBC), moving towards the north and feeding into the Gulf Stream (GS). Hence, the westward directed equatorial currents contribute directly to the interhemispheric exchange of water at the surface, forming a cross-equatorial flow.
In the north, the surface water pathways are dominated by the anticyclonic subtropical gyre and the cyclonic subpolar gyre, which stretches into the Nordic Seas (Talley *et al.*, 2011). The subtropical gyre is an asymmetric gyre with strong and narrow western boundary currents and a broad southward flow through the central and eastern subtropics. It is dominantly formed through the GS system on the western boundary. The GS moves along the North American coast towards the north before it continues eastwards splitting into the Azores Current (AzC) and the North Atlantic Current (NAC). On the eastern boundary, the Canary (CaC) and Portugal Current (PC) form the southward component before they turn westwards and feed the North Equatorial Current (NEC), which completes the northern subtropical gyre (Talley *et al.*, 2011). The Canary and the Portugal system are, again, eastern boundary upwelling systems that are separated by the AzC, which is associated with the Mediterranean inflow (New *et al.*, 2001).
The subpolar gyre (SPG) is a cyclonic circulation north of 50 °N. Separating the STG and the SPG, the eastward components of the Gulf Stream form the southern branch of the SPG. At this line of separation, where the SPG and the STG compete against each other, also knwon as line of zero-Ekman pumping, the Azores Front is formed. It is characterised by the 15 °C isotherm between 200 m and 300 m water depth and a strong meridional temperature gradient (Schiebel *et al.*, 2002).
On the western margin, the NAC then splits up into the southern branch forming the PC and two northwards branches (Fratantoni, 2001; Flatau *et al.*, 2003; Brambilla and Talley, 2008) separated through the Reykjanes Ridge. The western branch forms a cyclonic gyre in the Irminger and Labrador Seas, while the eastern part gets separated into several branches. Their pathways are mainly controlled through topography (Talley *et al.*, 2011), moving into the Nordic Seas. Through the EGC, the branches meet again, turning towards a northward flow into the Labrador Sea and moving towards the south in the Labrador Current (LC) following the coastline.
Apart from these major surface currents, there are three major Atlantic intermediate water masses at depths between 500 m and 2000 m. The low salinity Labrador Seawater

(LSW) in the northern North Atlantic, the high salinity Mediterranean Water (MW) in the subtropical South Atlantic and the low salinity Antarctic Intermediate Water (AAIW) in the South and tropical Atlantic. Here, only the MW and the AAIW will be further described. The Mediterranean Water (also called Mediterranean Outflow Water) enters the Atlantic as a dense, high salinity water mass through the Strait of Gibraltar. Following the topography, it turns northward into the Gulf of Cadiz. As it moves along the Iberian margin, anticyclonic eddies, so-called 'Meddies', of almost pure MW are spun off at different topographic features (e.g. Candela, 2001; Richardson *et al.*, 2000). The resulting Meddies are about 9 km in diameter and retain their high salinity and coherence over long distances and for about 2 to 3 years. Over time, their radius becomes larger at about 20 - 100 km with a thickness of about 650 m centred around about 1000 m water depth (Richardson *et al.*, 2000). This way, up to 50 % of the MW is carried into the North Atlantic.
Another characteristic in the North Atlantic is the 'Mediterranean salt tongue' which is formed by advection of high salinity MW through eddies into the subtropical North Atlantic (Bashmachnikov *et al.*, 2015).
The Antarctic Intermediate Water is a major intermediate water mass in the South and tropical Atlantic. It is characterised through a low salinity layer at about 1000 m water depth with a salinity minimum originating near the Drake passage (Talley, 1996). The net northward transport of AAIW into the Atlantic is estimated to be 5 - 7 Sv (Talley, 2008). In the South Atlantic, AAIW is advected to the east, followed by a northward and westward flow around the subtropical gyre. As it returns to the South American coast, it enters the NBC system where it moves north into the Gulf Stream system. In the tropics, the AAIW is eroded from above (Talley, 1996) and the remnants of the AAIW are marked by increased nutrients rather than low salinity (Tsuchiya, 1989). The northern boundary of the AAIW is at about 20 °N coinciding with the southern boundary of the MW (Talley *et al.*, 2011).

This complex sub-surface recircuation pattern, which is observed today in the Atlantic Ocean is predominantly a result of wind forcing and a flow along the topographic boundaries of this narrow, elongated ocean. The slow thermocline flow covers a large depth interval up to about 1200 m water depth, thus, lengthening the mixing pathways storing properties over timescales of up to centuries Lozier (1999). Through climate change, surface and thermocline circulation are expected to change significantly due to a realignment of the atmospheric circulation, the ice cover and the resulting changes in the seawater salt content. The relevant climate changes of the last 40 ka will be

described in the next section.

2.2 Climate variability of the last 40 ka

Through $\delta^{18}O$ analysis of deep-sea sediment cores, long-term climate patterns that follow the Milankovich cycles can be identified in marine sediments. A close correlation between marine and ice-core records was found (Imbrie *et al.*, 1984). In oceanic records, these long-term patterns are called Marine Isotope Stages (MIS), where odd numbers denote interglacials and even numbers denote glacials. In this thesis, the focus will be on the last 40 ka (see figure 2.2). These are mainly characterised by the Last Glacial Maximum (LGM) which had its maximum global ice volume between 26.5 ka and 19 ka (Clark *et al.*, 2009). This also corresponds to MIS 2 and is followed by the deglaciation (Termination 1). The deglaciation was enhanced from 14.7 ka to 14.1 ka, at the beginning of an abrupt warm and moist interstadial period, the so-called Bølling-Allerød stadial (Rasmussen *et al.*, 2006), concurrent with a sea level rise of about 20 m (Weaver, 2003). This led to a subsequent cooling which is terminated by the Younger Dryas (YD, 12.5-11.7 ka), an event of strong, punctuated cooling leading to a near reversal to glacial conditions (Dansgaard *et al.*, 1993; Rasmussen *et al.*, 2006). The subsequent warming period completes the deglaciation and leads to the Holocene (MIS 1) which lasts until today.

These long-term patterns are interrupted by short-term events, namely Heinrich stadials (HS) and Dansgaard-Oeschger cycles (D/O-events). Heinrich stadials are extremely cold periods in the Northern hemisphere provoked by Heinrich events (here H1-H3). Heinrich events are characterised by massive iceberg and freshwater discharges into the North Atlantic from the Laurentide ice sheet (Hemming, 2004; Heinrich, 1988). These immense changes in the freshwater discharge are thought to have led to a weakened or even halted deep water formation in the North Atlantic leading to a weakened northward flow and therefore reduced northward heat transport in the Atlantic (Clark *et al.*, 2002; Clement and Peterson, 2008). These Heinrich stadials only lasted for about 500 years (Hemming, 2004).

Dansgaard-Oeschger cycles are periods of abrupt warming followed by gradual cooling, particularly during MIS 3 (57 ka to 29 ka ago) (Rahmstorf, 2003; Dansgaard *et al.*, 1993; Johnsen *et al.*, 1992; Clement and Peterson, 2008). As D/O often follow Heinrich Stadials, possible links between the two are discussed (e.g. Bond and Lotti, 1995; Zhang *et al.*, 2014), but the origin of these events and their full global extent remain unclear. These events and their characteristics are mainly present in the Greenland ice core data

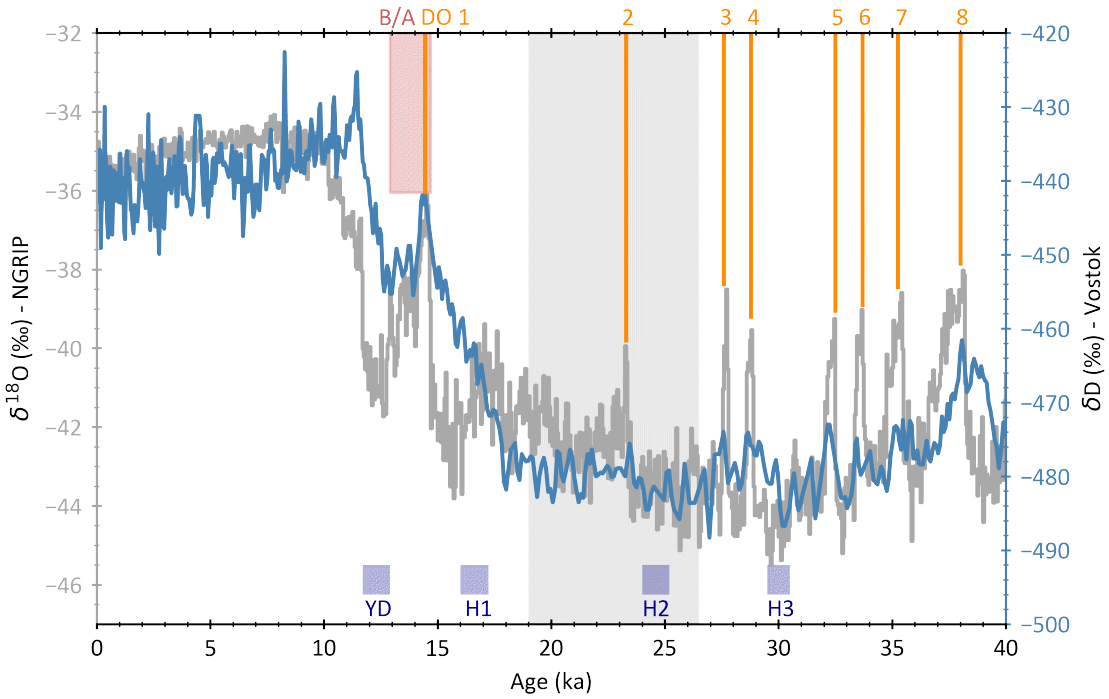

Figure 2.2: Climate variability of the last 40 ka as recorded in Greenlandic NGRIP and Antarctic Vostok ice cores. Periods of distinct climate variability are indicated by blue rectangles for Heinrich stadials (H1 - 3) and the Younger Dryas (YD). Orange lines show the Dansgaard-Oeschger cycles (DO1 - 8) and the grey shaded area represents the Last Glacial Maxium (LGM) (Clark *et al.*, 2009; Hemming, 2004; Dansgaard *et al.*, 1993; Bazin *et al.*, 2013b,a).

of NGRIP (Bazin *et al.*, 2013b). The Antarctic ice core data of Vostok (Bazin *et al.*, 2013a) reveals far fewer fluctuations and more gradual warming rather than abrupt warming events in the southern hemisphere. Furthermore, during the deglaciation, a phase shift in the warming behaviour between the Greenland and Antarctic ice core data is present. While the southern hemisphere warms up, the northern hemisphere cools or remains at its mean conditions and vice versa during e.g. during the Younger Dryas. This phenomenon is known as the 'bipolar seesaw' (e.g. Freeman *et al.*, 2015; Stocker and Johnsen, 2003; Knutti *et al.*, 2004).
These modelling studies have demonstrated that changes in the AMOC through increased fresh water discharges may cause massive changes in thermocline temperatures in the subtropics. Therefore, the thermocline ocean may hold the key to prove the 'thermal bipolar seesaw', including a heat reservoir as proposed by Stocker and Johnsen (2003). Hence, marine archives, such as cold-water corals, are needed to trace large temperature changes in thermocline waters.

2.3 Cold-water Corals

When most people hear about corals, they think about colourful reefs in the tropics that can be visited while snorkelling or diving. However, there is another, even more diverse, yet less colourful, group of corals living in the depth of the ocean without any need for sunlight. In 2007, 5160 different corals species were known, 3356 (or 65 %) of which occur in water depths lower than 50 m, showing that corals are mostly deep and cold-water inhabitants (Roberts *et al.*, 2009). These corals are so-called *deep-sea corals* or *cold-water corals (CWCs)*[1]. In contrast to most of their tropical relatives, CWCs do not live in symbioses with photosynthesizing algae as they mostly live beneath the euphotic zone. Therefore, they are called *azooxanthellate*.
CWCs can be found in all major ocean basins, in all latitudes and water depths of about 40 m to more than 6000 m (Roberts *et al.*, 2009) (see Fig. 2.3) and grow either solitary or form reefs in small patches up to huge mounds as high as 300 m and with a horizontal expansion of several kilometres (Freiwald and Roberts, 2005). These reefs can be thousands to millions of years old (e.g. Kano *et al.*, 2007). When forming their carbonate skeleton, CWCs incorporate trace elements from the seawater. This way, CWCs indirectly record past seawater parameters like temperature and ventilation (Robinson *et al.*, 2014; Sherwood and Risk, 2007), which can be reconstructed using

[1] In this thesis, I will refer to these corals as *cold-water corals (CWCs)*, as their uniting characteristic is less the deep than the cold water they live in.

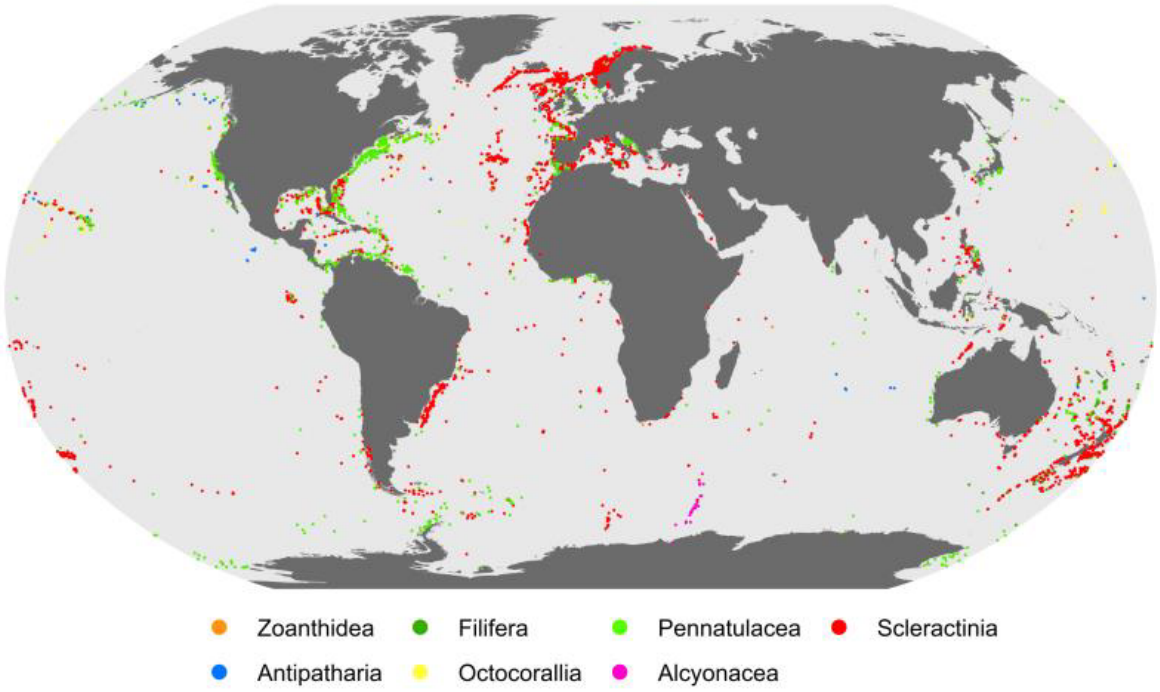

Figure 2.3: Worldwide occurrence of cold water corals. It should be noted, that the particularly dense reef occurance in the North Atlantic is most certainly a sampling bias and reflects the intensity of research in the region. Taken from Freiwald *et al.* (2017)

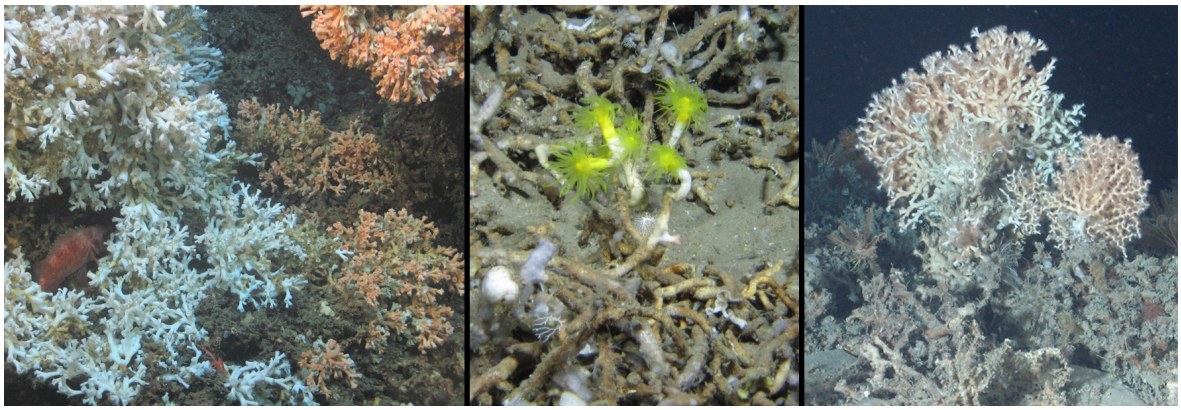

Figure 2.4: Pictures of cold-water coral reefs in the Atlantic taken during ROV-dives. Left: White and pink Lophelia pertusa off Iceland. Picture taken during NO Thalassa research cruise ICE-CTD with ROV Victor 6000 (IFREMER). Middle: Eguchipsammia cornucopia on José Gaspar seamount south of the Azores. Picture taken during RV Meteor research cruise M151 Athena with ROV Squid (Marum). Right: Lophelia pertusa (left) and Madrepora oculata (right) in the Bay of Biscay. Picture taken during NO Pourquois Pas research cruise BOBECO with ROV Victor 6000 (IFREMER).

different proxies. Corals forming giant reefs can provide a high-resolution long-term record of the ocean parameters (e.g. Robinson, 2004; Chen *et al.*, 2016; Frank *et al.*, 2011; Raddatz and Rüggeberg, 2019; Raddatz *et al.*, 2013; Montero-Serrano *et al.*, 2011; Colin *et al.*, 2010), making CWCs a valuable paleoclimate archive for the intermediate ocean.

2.3.1 Scleractinia

The corals used in this thesis are all of the order *Scleractinia*. Some exemplary pictures of Scleractinian CWCs are shown in figure 2.4. There are about 711 species of azooxanthellate *Scleractinia* known, 622 (or 87 %) of which inhabit water depths deeper than 50 m (Roberts *et al.*, 2009). However, only 26 % of these cold-water scleractinian corals build colonies and only 17 of them are framework forming, while the vast majority of them live solitary (Cairns, 2007). *Scleractinia* are a widespread order in both geographical latitude and water depth as they are found from off continental Antarctica up to the Barents Sea within the Arctic circle. They are not found yet only in the Bering Sea and high in the Arctic regions. They also occur in water temperatures as low as –1.1 °C and water depths as deep as 6328 m in the Aleutian Trench in the North Pacific (Roberts *et al.*, 2009). However, most *Scleractinian corals* inhabit intermediate water depths of 200 m to 1000 m (Freiwald, 2002).

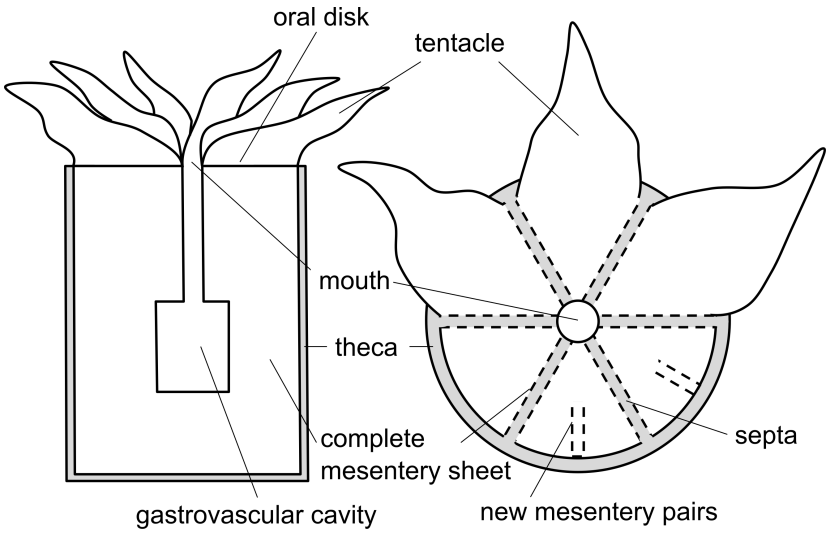

Figure 2.5: Cross section through a coral polyp from top down and lateral. Calcium carbonate skeleton is shown in grey. Figure from Spooner *et al.* (2016).

There are two main characteristics to distinguish *Scleractinia* from the other five cold-water coral groups. These are their calcareous exoskeleton, which can also be used to help distinguish different *Scleractinia* species and their complete mesenteries. Mesenteries are membranes that extend from the body wall of the polyp into the gastrovascular cavity of the coral. 'Complete' means that the mesenteries meet the 'pharynx' of the corals in comparison to 'incomplete mesenteries' which only extend partly into the gastrovascular cavity (see figure 2.5).
The most common family of *Scleractinian corals* are *Caryophillidae* including most of the corals used in this thesis. In the following the most relevant reef-building CWC species are described.

Lophelia pertusa *Lophelia pertusa* are by far the most common reef-building, framework-forming corals. The genus *Lophelia* is a monospecific one, meaning that *Lophelia pertusa* is the only species of the genus (Freiwald, 2002). In recent years there has been a discussion to rename *Lophelia pertusa* to *Desmophyllum pertusum* due to new genetic findings suggesting a close relationship between these two genera (Addamo *et al.*, 2016). As the discussion on this matter is still ongoing, I will stick to the name *Lophelia pertusa*, to prevent confusion with former publications.
Lophelia pertusa is a cosmopolitan occurring all over the Atlantic, in parts of the Mediterranean Sea, the Gulf of Mexico, the Caribbean Sea, the Indian and the Pacific Ocean (Freiwald, 2002; Cairns, 1984). Their specimen are found as south as 51°S on the sub-antarctic Macquarie Ridge off New Zealand and as north as the southwestern Barents Sea in 71°N (Fosså and Mortensen, 2000) and from 39 m water depth in the

Trondheimfjord to 3383 m water depth on the New England Seamount chain and 2775 m off Morocco (Roberts *et al.*, 2009).
Lophelia pertusa form bush-like colonies that can span several meters across consisting of several thousand polyps (Freiwald and Roberts, 2005). Their skeleton is relatively thick and solid and as the colony grows, they develop anastomoses, which denotes crosslinks between single branches of the colony, to strengthen the framework (e.g. Hennige *et al.*, 2014). Early observations of *Lophelia pertusa* estimated growth rates of 4 mm/yr to 8 mm/yr. However, under optimal conditions, their growth rate can reach up to about 25 mm per year (Adkins *et al.*, 2004). Their tissue does occur in several nuances of yellow, orange or red, but is most often white resulting in *Lophelia pertusa* also being called the 'white coral' (Freiwald *et al.*, 2004).

Madrepora oculata *Madrepora oculata* is the most common species of the genus. Their skeletons are more fragile, 'zig-zag shaped' branches limiting their capacity to build large colonies. However, *Madrepora oculata* often co-occur with the more robust *Lophelia pertusa* (Freiwald *et al.*, 2004).
They are found all over the world and are even the dominant coral species in some areas of the northeastern Atlantic and the Mediterranean Sea. The northernmost known occurrence of *Madrepora oculata* is in the Andfjord in Northern Norway at 69°N (Freiwald *et al.*, 2004) and they can be found as south as the sub-Antarctic Drake Passage at 59° S (Cairns, 1982).

Solenosmilia variabilis Also a framework-forming species with a solid skeleton is *Solenosmilia variabilis*. They are in principle cosmopolitan, except for the sub-Antarctic region and the North and East Pacific, where they are not yet found. They occur in water depths from about 220 m to 2165 m (Roberts *et al.*, 2009).

2.3.2 Environmental Conditions on Cold-water Coral Growth

Apart from what their denotation as *deep-sea corals* implies, water depth is not the primary control on coral occurrence in certain places. However, water depth is often associated with coral occurrence patterns as the data is widely available (Vaughan, 1940; Roberts *et al.*, 2009). Yet there are other environmental conditions controlling coral growth, the main controls being temperature, food supply and the need for a hard substrate to settle on (Mortensen *et al.*, 2001; Cairns, 2007; Davies *et al.*, 2009; Roberts *et al.*, 2009; Davies and Guinotte, 2011; Flögel *et al.*, 2014; Henry *et al.*, 2014). Every coral species has probably its own optimal temperature to thrive in; A factor that strongly regulates which coral species can be found in which area of the world's oceans.

Scleractinia corals were found in water temperatures as low as -1.8 °C (Davies *et al.*, 2008) whereas the most common reef-building CWC is not found in water temperatures lower than 4 °C (Roberts *et al.*, 2003).
Corals need an appropriate substratum to settle and build their skeletons on. This should give enough support even for large colonies in strong bottom currents. Therefore, corals most often can be found on a hard substrate which is either of calcareous or volcanic nature (Freiwald *et al.*, 2004), but also man-made objects like cables and submerged parts of oil rigs offer substrate for corals to settle on (Bell and Smith, 1999; Wilson, 1979).
Another important factor for coral habitats is a constant or periodic flow of water which provides two essential needs of corals. On the one hand, bottom currents can provide food and oxygen to the sessile corals and, on the other hand, remove sediments and wastes from the corals, preventing them to be buried (Dorschel *et al.*, 2005; White, 2006). This need for water flow leads to increased coral occurrence on ridges or rocky outcrops, where currents are accelerated (Messing *et al.*, 1990; Freiwald *et al.*, 2004; Wienberg and Titschack, 2017).
Apart from these most important factors coral occurrences are also dependent on salinity, dissolved oxygen concentrations and carbonate chemistry. As these are fairly constant in deep water, they are thought to not be a significant factor at local scales, but over large geographic and depth scales (Roberts *et al.*, 2009). Recent findings by Hebbeln *et al.* (2020) showed, however, that corals might be able to adapt to hypoxic water conditions in combination with extensive food supply indicating that corals or at least the most prominent reef-building species *Lophelia pertusa* might be even more stress resistant and less sensitive to oxygen supply under certain conditions.
Taking these points into account, particularly good conditions for coral habitats can be mostly found at summits and flanks of seamounts, at the flanks of steep-sloped islands and at continental slopes, where we can also find coral mounds (like e.g. off Angola) (Wienberg and Titschack, 2017).

2.3.3 Cold-water coral geochemistry

Inorganic calcium carbonate is precipitated from seawater into its crystallised state in thermodynamic equilibrium whereas corals, as most marine calcifiers, calcify in disequilibrium (e.g. Allemand *et al.*, 2010), altering the isotopic and trace metal composition of the precipitated calcium carbonate (e.g. Emiliani *et al.*, 1978; Spiro *et al.*, 2000; Sinclair *et al.*, 2006; Thiagarajan *et al.*, 2011; Robinson *et al.*, 2014). The geochemical composition deviating from equilibrium aragonite precipitation is summarised under the term *vital effects*(Sinclair *et al.*, 2006; Robinson *et al.*, 2014).

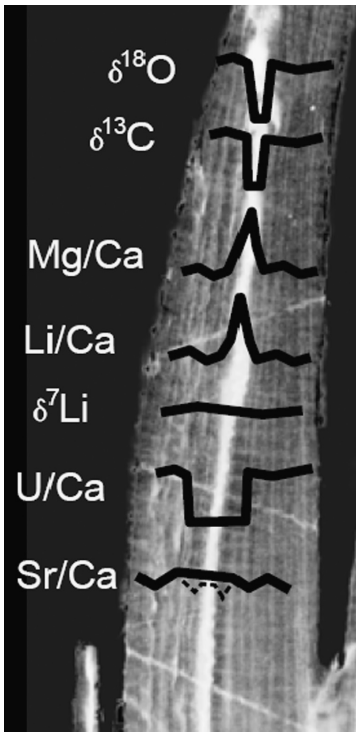

Figure 2.6: Variations of proxies within a coral skeleton due to vital effects. Taken from Robinson *et al.* (2014)

.

It wasfound to depend in corals on growth rate and pH (Weber and Woodhead, 1970; McConnaughey, 1989; Cohen *et al.*, 2002; Rollion-Bard *et al.*, 2003; Reynaud *et al.*, 2007).

As CWCs mostly grow in relatively homogenous environments with strongly damped seasonal variations in temperature and water composition, these vital effects are much more apparent in CWCs than in surface/warm-water corals and often play a dominant role in proxy variability obscuring direct relationships between proxies and environmental parameters (Thiagarajan *et al.*, 2011; Robinson *et al.*, 2014). This, however, also brings a valuable opportunity: Studying the offset from equilibrium calcium carbonate precipitation in corals for different Metall/Ca ratios and isotopic systems like δ^{18}O or δ^{13}C, can help to understand the biological processes of calcification (Thiagarajan *et al.*, 2011; Robinson *et al.*, 2014). The research that went into paleothermometers revealed systematic patterns in vital effects showing significant differences in the microstructure of a coralline skeleton especially between aragonitic fibres and the centres of calcification (COC) (see Fig. 2.6, e.g. Sinclair *et al.*, 2006; Meibom *et al.*, 2008; Case *et al.*, 2010; Robinson *et al.*, 2014; Montagna *et al.*, 2014). Centres of calcification are areas of disorganized aragonite crystals that are supposedly the result of nucleation events (Gladfeiter, 1982; Stolarski, 2003). The improved understanding of vital effects is also

fundamental to the development and improvement of robust proxies and, therefore, an essential part in the process to find accurate past climate records (Robinson *et al.*, 2014). Not all proxies are, however, affected by vital effects leading to the hunt for a temperature proxy to overcome the influences of vital effects.

2.4 A Temperature Proxy for Cold-water Corals

The main focus in this thesis is seawater temperature reconstruction. However, classical proxies to evaluate past seawater temperatures from marine archives like foraminifera and tropical corals such as $\delta^{18}O$ and Metal/Calcium elemental ratios (Mitsuguchi *et al.*, 1996) are found to be altered in CWCs. Hence, they not only depend on seawater temperature but also on other chemical and physical properties like salinity and vital effects (Weber, 1973; Shen and Dunbar, 1995; Smith *et al.*, 2002; Adkins *et al.*, 2003; Cohen *et al.*, 2006; Gagnon *et al.*, 2007; Mitsuguchi *et al.*, 2008; Rollion-Bard *et al.*, 2010; Montagna *et al.*, 2014). Especially in tropical corals Sr/Ca ratios are used as a temperature proxy (e.g. Beck *et al.*, 1992; Guilderson *et al.*, 1994; Hughen *et al.*, 1999), but concerns have been raised about the Sr heterogeneity in coralline skeletons, which was found to be higher than expected (Allison *et al.*, 2001). Furthermore, temporal variations in the Sr/Ca content of the ocean (Stoll *et al.*, 1999) and vital effects, strongly altering the Sr/Ca ratio in corals were found (de Villiers *et al.*, 1995). In CWCs Sr/Ca shows large scatter making the negative correlation of Sr/Ca and temperature impractical (Shirai *et al.*, 2005; Cohen *et al.*, 2006). Mg/Ca ratios, widely applied in foraminifera (e.g. Anand *et al.*, 2003), however, do not show a strong relationship with temperature in CWCs (Shirai *et al.*, 2005; Case *et al.*, 2010).
Another promising temperature proxy are clumped isotopes (Δ_{47}), based on the abundance of the double substituted CO_2 isotopologue $^{13}C^{18}O^{16}O$ (Ghosh *et al.*, 2006; Thiagarajan *et al.*, 2011, 2014; Spooner *et al.*, 2016). This thermometer has the advantage that it is based on solely thermodynamical assumptions and thus independent of the stable isotope composition of the seawater (Ghosh *et al.*, 2006) and was thought to show little to no vital effects (Thiagarajan *et al.*, 2011). However, more recent work showed, that some CWC genera underestimate the seawater temperature by 9°C (or overestimate Δ_{47} by 0.05 ‰) indicating the influence of an unknown vital effect and the need for species or genera specific calibration (Spooner *et al.*, 2016).
In 2004, Marriott *et al.* studied the temperature dependence of Li/Ca in a *Porites*, a tropical Scleractinia, and in inorganic calcite and found an inverse temperature dependence, which is particularly sensitive at low temperatures. Bryan and Marchitto

(2008) used the Li/Ca ratio in benthic foraminifera to further refine the Mg/Ca thermometer and suggested that the influence of the carbonate ion concentration on Mg/Ca can be adjusted by combining Li/Ca and Mg/Ca ratios. With a stronger temperature correlation in Mg/Li compared to Mg/Ca they suggested the corraline Mg/Li ratio as a potential new temperature proxy.
Case *et al.* (2010) studied the microscale distributions of Mg/Ca and Li/Ca in CWCs and found similar variations for both. Furthermore, they found no evidence for a dependence on salinity or carbon ion concentrations but a significant temperature correlation with $r^2 = 0.62$. However, the maximal precision of their calibration was $\pm 1.6\,°C$, calling for further calibration efforts. In 2013, further studies showed dependencies on pH, coralline growth and calcification rates for Mg/Ca and Li/Ca ratios which were ruled out in Mg/Li ratios (Raddatz *et al.*, 2013). Hathorne *et al.* (2013) published an inter-archive comparison of the correlation between Li/Mg and temperature in benthic foraminifera, tropical corals and cold-water corals. For the first time different coral genera and even different archives were brought together in an exponential relationship ($\mathrm{Li/Mg}\,[mmol/mol] = 5.16 \exp(-0.0492 \times \mathrm{T}\,[°C])$, $r^2 = 0.97$) hinting at *"an overarching mechanism controlling the temperature response of Li and Mg incorporation into aragonite"* (Hathorne *et al.*, 2013) which would potentially make an Li/Mg calibration inter-species applicable. By combining an exponential approach and living or young corals from seven different genera in the temperature range from 0 °C to 28 °C, Montagna *et al.* (2014) determined a robust calibration curve for Li/Mg ratios valid in a wide range of Scleractinian corals:

$$\mathrm{Li/Mg}\,[mmol/mol] = 5.41[mmol/mol] \exp\left(-0.049\,[\pm 0.002][1/°C] \times \mathrm{T}\,[°C]\right) \quad (2.1)$$

Recently more Similar to Hathorne *et al.* (2013) the authors found a strong correlation between Li/Mg and temperature ($r^2 = 0.975$) following an exponential regression decreasing at 5 % per °C. Furthermore, the authors examined the microstructural composition of the skeleton finding strong variation over several orders of magnitude in Li/Ca and Mg/Ca ratios that are ruled out when using the Li/Mg elemental ratio. Enriched Li and Mg concentrations are mainly found in the centers of calcification where primary coralline growth is initiated. In the slower growing aragonitic fibers, a more unbiased environmental signal is suggested as lower Li/Ca and Mg/Ca ratios indicate growth close to thermodynamic equilibrium.
work was done on the the chemical preparation of coral samples for Li/Mg measurements as well as adding further species to the calibration. Cuny-Guirriec *et al.* (2019) added an oxidative cleaning procedure to the method of mechanical cleaning and weak acid leaching in order to remove organic material, especially chlorophyll

from green algae living in symbioses on tropical corals. Additionally they recalculated the calibration curve published by Montagna *et al.* (2014) with additional corals and more coral genera from the Antarctic region, the Caribbean Sea and the Pacific. Their updated exponential regression was determined to $\mathrm{Li/Mg}\,[mmol/mol] = 5.19 \pm 0.04 \exp(-0.046 \pm 0.001 \times \mathrm{T}\,[^{\circ}C])$, $\mathrm{r}^2 = 0.99$. Stewart *et al.* (2020) also added steps of oxidative cleaning to their method, but mainly expanded the Li/Mg method to other corals of an even different class (*Stylasteridae*). By combining all aragonitic biocarbonates, i.e. Scleractininae, Stylasteridae and foraminifera, they propose a calibration universal to all biogenic aragonites and calculate a refined exponential relationship within uncertainty of the calibration by Montagna *et al.* (2014) ($\mathrm{r}^2 = 0.97$):

$$\mathrm{Li/Mg}\,[\frac{\mathrm{mmol}}{\mathrm{mol}}] = 5.42[\frac{\mathrm{mmol}}{\mathrm{mol}}]\,[\pm 0.04] \exp\left(-0.50\,[\pm 0.0004][\frac{1}{^{\circ}\mathrm{C}}] \times \mathrm{T}\,[^{\circ}\mathrm{C}]\right). \tag{2.2}$$

This strong, inter-archive relationship between Li/Mg and temperature suggests an abiogenic trace metal incorporation similar for Li and Mg far beyond vital effects (Stewart *et al.*, 2020).

2.5 Li as a tracer for weathering

Lithium is an alkali metal with two naturally occurring isotopes, ^{6}Li and ^{7}Li. The ^{7}Li isotope is by far the more abundant with 92.5 % natural occurrence, while ^{6}Li has an abundance of about 7.5 %. Its large relative mass difference of about 16 % has significant potential for mass-dependent fractionation during natural exchange processes such as water-rock interaction. This was already demonstrated by early experiments by Taylor and Urey (1938).

As one of few elements, lithium was produced during the Big Bang nucleosynthesis within the first three minutes of the Universe (e.g. Spite and Spite, 1982; Burles *et al.*, 2001) and is still produced during stellar nucleosynthesis. Stellar processes tend to destroy lithium leaving an abundance in the solar system lower than expected from comparison with elements of higher or lower atomic numbers (Korn *et al.*, 2006). Lithium is also widely distributed on Earth but does not occur in elemental form due to its high reactivity (Burton and Vigier, 2011). While abundances in mantle rocks are 0.1 ppm to 7.7 ppm, abundances in crustal rocks range between 1 ppm and 80 ppm with an average of about 22 ppm. Therefore, lithium is the 25^{th} most abundant element in the Earth's crust (Burton and Vigier, 2011). With 91 % most of the Earth's

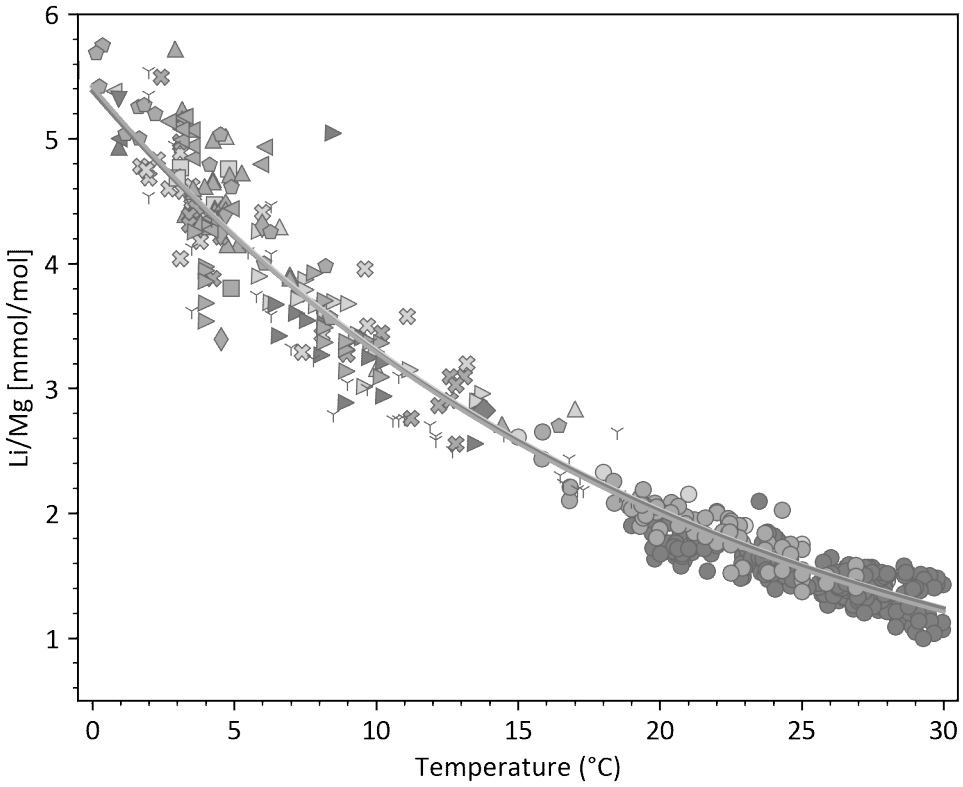

Figure 2.7: All data used for the various Li/Mg calibration curves. Light grey symbols denote all samples used for calibration curve by Montagna *et al.* (2014), middle grey samples are additional samples used in Cuny-Guirriec *et al.* (2019), dark grey samples are additionally used in Stewart *et al.* (2020). Please note, that all three calibration curves are shown but are indistinguishable from each other.

Li is located in the mantle and, as Li is incompatible during magmatic processes, the oceanic crust (1 %) contains less Li compared to the continental crust (7 %) (Teng *et al.*, 2004). Inorganic and biogenic carbonates play only a minor role in the overall lithium budget of the Earth, as carbonates have low lithium contents of about 1 ppm in pure carbonate (Hoefs and Sywall, 1997). For seawater, an average Li concentration of about 180 ppb is given in the literature (e.g. Riley and Tongudai, 1964; You and Chan, 1996; Vigier *et al.*, 2015).
The lithium isotopic composition of different materials is commonly given in δ - notation referenced to the NIST reference standard LSVEC:

$$\delta^7\mathrm{Li} = \frac{(^7\mathrm{Li}/^6\mathrm{Li})_{sample}}{(^7\mathrm{Li}/^6\mathrm{Li})_{LSVEC}} - 1 \tag{2.3}$$

The δ-value is typically given in ‰. The LSVEC standard material is a lithium carbonate produced from Li-ore (Flesch *et al.*, 1973). It has a natural $^6\mathrm{Li}/^7\mathrm{Li}$ ratio of 0.08215 ± 0.00023 (Qi *et al.*, 1997) and was assigned a $\delta^7\mathrm{Li}$ value of 0 ‰.
Mid-oceanic ridge basalts (MORB) reveal a $\delta^7\mathrm{Li}$ value of 3.7 ± 1.9 ‰ (Tomascak *et al.*, 2008), which is close to the estimated value for the undepleted upper mantle of about 3.5 ‰ (Jeffcoate *et al.*, 2007). A compilation by Carignan *et al.* (2004) of $\delta^7\mathrm{Li}$ values in filtered seawater showed values between 28.9 ‰ and 33.4 ‰. For the North Atlantic a $\delta^7\mathrm{Li}$ value of 31.2 ± 0.4 ‰ was determined (Millot *et al.*, 2010; Jeffcoate *et al.*, 2004). This high variation for seawater was unexpected, as lithium is supposed to be homogeneously distributed throughout the ocean due to its long residence time of about 1 Ma, which is some orders of magnitude higher than the overturning time of the ocean at about 1 ka. Furthermore, the $\delta^7\mathrm{Li}$ values found in seawater are significantly higher than their principal sources, which are hydrothermal fluids and continental weathering. High temperature oceanic hydrothermal fluids contain about 20-50 times the Li concentration of seawater (Chan *et al.*, 1993, 1994) and a $\delta^7\mathrm{Li}$ value of about 3 ‰ to 11 ‰ (Chan *et al.*, 1993, 1994; Foustoukos *et al.*, 2004). Continental weathering provides Li through rivers, groundwater and aeolian dust and displays a high variation of $\delta^7\mathrm{Li}$ values at an average of 23.4 ‰ (Huh *et al.*, 1998; Chan *et al.*, 1992; Falkner *et al.*, 1997). This leads to the best evidence of high fractionation of lithium during low-temperature weathering, as natural waters are systematically enriched in $^7\mathrm{Li}$ when compared to their bedrock. Additional processes can also significantly alter its isotopic signature. These processes are mainly lithium sinks for seawater through sea-floor alteration when Li is incorporated into secondary minerals, through high-temperature hydrothermal recrystallisation and through adsorption (Burton and Vigier, 2011). Given their low Li content, the precipitation of marine carbonates and biogenic silica

only play a minor role in the removal of Li from the seawater (Chan *et al.*, 2006; Hoefs and Sywall, 1997; Milliman, 1993; Hathorne and James, 2006). The contribution of diffusive flux from the sediment is likely to be also minor at about 1 % to 2 % (Stoffynegli and Mackenzie, 1984; Chan *et al.*, 1992, 2002, 2006; Wheat and Mottl, 2000).
Due to low Li concentrations present in marine carbonates (typically < 1 ppm) and high levels of Li (» 10 ppm) in potential contaminants like marine clays, δ^7Li values are difficult to determine in marine carbonates like foraminifera resulting in few published data. Vigier *et al.* (2007) showed the importance of rigorous cleaning of foraminiferal tests to remove any influence of materials included during the shell growth. Corals, however, are a potential recorder of the Li isotopic composition of seawater as Vigier *et al.* (2007) did not find the same contamination in coral skeletons. Performing in situ microscale measurements of coral skeletons using a SIMS, Rollion-Bard *et al.* (2009) found that tropical and CWC are isotopically homogeneous within the 1.1 ‰ uncertainty range of the method. Therefore, the biomineralization process is thought to not influence the Li isotopic composition as centres of calcification and the fibrous parts are not distinguishable through δ^7Li values. Solely the fractionation occurring during calcite and aragonite formation differs strongly. While inorganic precipitated calcite is only fractionated by -2 ‰ to -5 ‰, inorganic aragonite is more fractionated at -7 ‰ to -12 ‰ (Dellinger *et al.*, 2018). In addition, CWCs which grew under highly different pCO_2 and pH conditions do not differ in their Li isotopic composition (Burton and Vigier, 2011). Species related fractionation might occur (Marriott *et al.*, 2004a; Rollion-Bard *et al.*, 2009). Marriott *et al.* (2004a) noted an approximately 2 ‰ difference in two different species of shallow-water corals.
Recently, Cuny-Guirriec (2020) studied CWCs to analyse a change in the seawater Li content, and therefore changes in the sources and/or sinks, over the last glacial/interglacial cycle. The author found constant δ^7Li values and thus, no variation in the Li content of the seawater. This confirms a previous δ^7Li study of Hall *et al.* (2005) using foraminifera in the North Atlantic. As expected, due to its long residence time in the ocean, no glacial/interglacial changes in the lithium isotopic composition of seawater can be measured (Cuny-Guirriec, 2020).

2.6 U/Th dating

U/Th dating is a powerful geochronological tool to reconstruct the earth's history on timescales of up to 800 ka before present (BP). It is based on the radioactive decay chain of the mother nucleus ^{238}U into ^{230}Th via two α and two β decays (see figure 2.8). As

the half-lives of ^{234}Th and ^{234}Pa are several orders of magnitude shorter than those of the U isotopes, these decays can be neglected. The radioactive decay of the remaining isotopes ^{238}U, ^{234}U and ^{230}Th can be described in a set of differential equations from which the *marine age equation* can be derived (Ivanovich and Harmon, 1982), which has to be solved iteratively to determine the sample time t:

$$\left(\frac{^{230}\mathrm{Th}}{^{238}\mathrm{U}}\right)_t = 1+\left[\left(\frac{^{230}\mathrm{Th}}{^{238}\mathrm{U}}\right)_0 - 1\right]\cdot e^{-\lambda_{230}\cdot t}+\left[\left(\frac{^{234}\mathrm{U}}{^{238}\mathrm{U}}\right)_t - 1\right]\frac{\lambda_{230}}{\lambda_{230}-\lambda_{234}}\left[1-e^{(\lambda_{234}-\lambda_{230})\cdot t}\right] \tag{2.4}$$

Parentheses denote activity ratios at the time of measurement (index t) or at t = 0

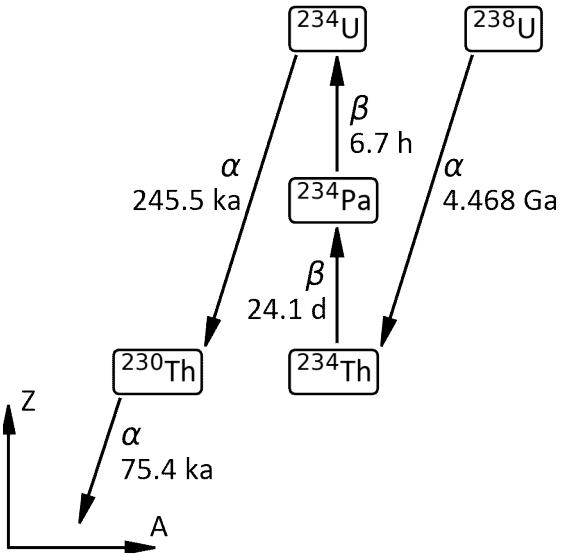

Figure 2.8: Part of the ^{238}U decay chain relevant for U/Th dating. Half life of the respective nuclei and type of radioactive decay are given. Due to their short half life, ^{234}Th and ^{234}Pa can be neglected here.

(index 0). The activity ratio (^{234}U / ^{238}U) is commonly expressed in δ - notation relative to the secular equilibrium of $(^{234}\mathrm{U} / ^{238}\mathrm{U})_{eq} = 1$:

$$\delta^{234}\mathrm{U} = \frac{(^{234}\mathrm{U}/^{238}\mathrm{U})_t - (^{234}\mathrm{U}/^{238}\mathrm{U})_{eq}}{(^{234}\mathrm{U}/^{238}\mathrm{U})_{eq}} = \left(\frac{^{234}\mathrm{U}}{^{238}\mathrm{U}}\right)_t - 1 \tag{2.5}$$

Based on the decay equations of ^{238}U and ^{234}U, the activity ratio of both isotopes at time t can be described by

$$\left[\left(\frac{^{234}\mathrm{U}}{^{238}\mathrm{U}}\right)_t - 1\right] = \left[\left(\frac{^{234}\mathrm{U}}{^{238}\mathrm{U}}\right)_0 - 1\right] \cdot e^{-\lambda_{234} \cdot t} \tag{2.6}$$

Assuming $(^{230}\mathrm{Th} / {}^{238}\mathrm{U})_0 = 0$, i.e. no initial ^{230}Th is found in the sample, from equations 2.4 and 2.6, the following theoretical *seawater evolution curve* can be derived:

$$\left(\frac{^{230}\mathrm{Th}}{^{238}\mathrm{U}}\right) = 1 - e^{\frac{\lambda_{230}}{\lambda_{234}} \cdot ln\left(\frac{\delta^{234}\mathrm{U}}{\delta^{234}\mathrm{U}_0}\right)} + \delta^{234}\mathrm{U} \cdot \frac{\lambda_{230}}{\lambda_{230} - \lambda_{234}} \cdot \left(1 - e^{\frac{\lambda_{230} - \lambda_{234}}{\lambda_{234}} \cdot ln\left(\frac{\delta^{234}\mathrm{U}}{\delta^{234}\mathrm{U}_0}\right)}\right) \tag{2.7}$$

The residence time of ^{238}U in the ocean is, with about 400 ka (Ivanovich and Harmon, 1982), considerably longer than the global ocean mixing time of about 1000 years. Therefore, it is homogeneously distributed throughout the ocean. In contrast, ^{230}Th is highly particle reactive and is effectively removed from the water column via reverse scavenging processes and adsorption leading to a residence time of only about 40 years (Ivanovich and Harmon, 1982). This radioactive disequilibrium in seawater sets the basis for U/Th dating in marine calcifiers such as CWCs.

As CWCs precipitate calcium carbonate from their surrounding seawater to build their skeleton, some places of Ca in the $CaCO_3$ crystal lattice can be replaced by uranium atoms. This results in a U concentration in CWC skeletons of about 2 - 5 ppm (e.g. Frank and Hemsing, 2020). Once the CWC polyp dies, no more U is incorporated into the skeleton and Th is produced by the decay of ^{238}U.

Regardless of the short residence time of Th in seawater, the initial ^{230}Th concentration in CWCs cannot be assumed to be zero as Th concentrations increase with water depth (Vogler *et al.*, 1998). Therefore, non-radiogenic ^{230}Th may have been incorporated into the skeleton during growth which must be corrected. To correct for any initial $^{230}\mathrm{Th}_i$, the most abundant thorium isotope ^{232}Th is measured (e.g. Frank *et al.*, 2004; Cheng *et al.*, 2000a). For this purpose, the initial activity ratio of $(^{230}\mathrm{Th}/^{238}\mathrm{U})_i$ (see equation 2.4) is rewritten to:

$$\left(\frac{^{230}\mathrm{Th}}{^{238}\mathrm{U}}\right)_0 = \left(\frac{^{232}\mathrm{Th}}{^{238}\mathrm{U}}\right) \cdot \left(\frac{^{230}\mathrm{Th}}{^{232}\mathrm{Th}}\right)_0 \tag{2.8}$$

The measured $(^{232}\mathrm{Th}/^{238}\mathrm{U})$ activity ratio can be assumed to be constant since the formation of the CWC skeleton due to the long half-lives of both isotopes. The initial $(^{230}\mathrm{Th}/^{232}\mathrm{Th})_0$ activity ratio can be estimated from measurements of both isotopes in the water column as no fractionation is known to occur for these isotopes during incorporation into the CWC skeleton. Seawater $(^{230}\mathrm{Th}/^{232}\mathrm{Th})$ measurements range

from 0 to 30 for the upper 1600 m water depth (e.g. Guo *et al.*, 1995; Roy-Barman *et al.*, 1996; Cheng *et al.*, 2000a).
Another crucial point of U series dating is for the CWCs to remain in a closed system, i.e. the isotopic composition of the corals only changes due to radioactive decay (Edwards *et al.*, 2003). Potential disturbances can occur through diagenesis of the skeletons, like dissolution or recrystallisation (e.g. Pons-Branchu *et al.*, 2005; Allison *et al.*, 2007). Open system behaviour of the samples can be identified by comparing the samples ($^{230}Th/^{238}U$) and $\delta^{234}U$ to the seawater evolution curve (see equation 2.7). A closed system sample must follow this curve. A present-day initial $\delta^{234}U_0$ of 146.8 ‰ is assumed (Andersen *et al.*, 2010). Recently, climate driven changes of initial $\delta^{234}U_0$ have been quantified (Krengel, 2020). Largest expected changes in initial $\delta^{234}U_0$ occur in the North Atlantic above 35 °N. Nevertheless, variability remains small at < 8 ‰ for the last 400 ka. The North Atlantic, however, freshwater runoff may cause a variation of initial $\delta^{234}U_0$ of < 15 ‰ (Krengel, 2020; Chen *et al.*, 2016). Furthermore, only recently Border (2020) found small but significant variations in modern seawater $\delta^{234}U$ revealing a surprisingly dynamic system of oceanic $\delta^{234}U$. This, however, needs to be further studied in the future.

2.7 Radiocarbon dating and reservoir ages

The radiocarbon dating method is a commonly used method to date fossil materials. It was developed in 1946 by W.F. Libby (Libby, 1946), who was awarded the Nobel prize in chemistry in 1960 for this discovery.
The dating method is based on ^{14}C, the sole naturally occurring radioactive isotope of carbon, which is produced through cosmic radiation and atmospheric nitrogen. In the atmosphere radiocarbon mainly occurs as $^{14}CO_2$ molecules at a ratio of $^{14}C/^{12}C \approx 10^{-12}$ (Currie, 2004). At a half-life of $t_{1/2} = 5730 \pm 40$ years (Godwin, 1962), ^{14}C decays to nitrogen.
When alive, all organisms take up ^{14}C at the atmospheric $^{14}C/^{12}C$ ratio into their system. After their death, no more ^{14}C is brought into the system and the radioactive decay of ^{14}C can be used to determine the time elapsed since the last exchange of carbon with the atmosphere:

$$\left(\frac{^{14}C}{^{12}C}\right)_t = \left(\frac{^{14}C}{^{12}C}\right)_0 \cdot e^{-\lambda_L \cdot t} \tag{2.9}$$

Here, index t denotes the ratio at time t, index 0 denotes the initial ratio and λ_L is the Libby decay constant of $\lambda_L = (8033 \text{ years})^{-1}$. Libby determined a half-life of $t_{1/2_{Libby}} = 5568$ years, which was later found to be incorrect as Libby assumed a constant atmospheric ^{14}C concentration through time. As early publications used the 'Libby half-life', this is still used to calculate the so-called 'conventional ^{14}C ages' for reasons of comparability (Stuiver and Polach, 1977). The half-life of ^{14}C limits the datable ages to about 200 to 50000 years depending on the condition of the archive.
The ^{14}C ages, however, do not reflect the real ages of the samples and they have to be calibrated to determine calendar ages. The ^{14}C content of the atmosphere has not been constant over the last 50000 years due to changes in the Earth's magnetic field and the carbon cycle (Stuiver and Suess, 1966). Therefore, a calibration for the initial $^{14}C/^{12}C$ ratio must be applied to correctly date samples. These calibration curves, derived from tree rings and different other archives, are regularly updated with the most recent versions being the IntCal20 (Reimer *et al.*, 2020) for the northern hemisphere and the SHCal20 (Hogg *et al.*, 2020) for the southern hemisphere. These past $^{14}C/^{12}C$ signatures are reported in reference to the $^{14}C/^{12}C$ ratio in 1950 and are commonly given in $\Delta^{14}C$ values:

$$\Delta^{14}\text{C} = \left(\frac{e^{-^{14}\text{C age}/8033\,a}}{e^{-\text{Cal age}/8266\,a}} - 1 \right) \tag{2.10}$$

Furthermore, a correction due to isotope fractionation has to be considered which occurs during physical and chemical processes at carbonate precipitation as well as during the measurement. To correct for any deviations in the isotopic ratio due to fractionation, the sample $^{13}C/^{12}C$ ratio is compared to the $^{13}C/^{12}C$ of the Vienna Pee Dee Belemnite-standard (VPDB-standard):

$$\delta^{13}C = \left(\frac{(^{13}\text{C}/^{12}\text{C})_{sample}}{(^{13}\text{C}/^{12}\text{C})_{VPDB}} - 1 \right) \tag{2.11}$$

The VPDB-standard is an artificial reference standard based on the PDB-standard which originated from a cretaceous marine fossil (Friedman *et al.*, 1982). The measured $^{13}C/^{12}C$ is normalised to a $\delta^{13}C$ value of -25 ‰ which is the mean value of wood. This normalization is now applied to the ^{14}C signature assuming that the fractionation of the $^{14}C/^{12}C$ ratio is the square of the $^{13}C/^{12}C$ fractionation.

For especially benthic marine archives another effect must be taken into account. Only the surface ocean has direct contact with the atmosphere and thus, exchanges carbon. However, not even the surface ocean is in equilibrium with the atmosphere as surface

waters mix with water masses underneath. Therefore, surface water masses have a lower $^{14}C/^{12}C$ signature than the atmosphere. However, this so-called 'reservoir effect' is not constant through time (e.g. Waelbroeck *et al.*, 2001; Bondevik, 2006). Furthermore, the CWCs 'see' water masses that have not been in contact with the atmosphere for up to more than 1000 years. Some of the radiocarbon already decays before arriving at the CWCs and being incorporated into the skeleton. Therefore, the ^{14}C age derived from CWCs is the sum of the age of the CWC and the age of the ambient water mass (Mangini *et al.*, 1998). In surface and mid-depth water masses, this effect is typically rather small with water ages of decades to centuries. For the deep water masses, e.g. in the Pacific Ocean, this can add up to about 1500 years. Using the ^{14}C age of the sample in combination with its U/Th age, the $\Delta^{14}C$ concentration of the water (index dw, *deep water*) can be calculated (Adkins and Boyle, 1997):

$$\Delta^{14}C_{dw} = \left(\frac{e^{-^{14}\text{C age}/8033\,a}}{e^{-\text{U/Th age}/8266\,a}} - 1 \right) \tag{2.12}$$

Certain rare circumstances can lead to a vanishing reservoir effect. This is e.g. the case in todays North Atlantic were surface waters have taken up bomb radiocarbon from nuclear weapon testing, while the atmospheric concentration has decreased rapidely due to the carbon exchange with all reservoirs, e.g. ocean and biosphere (Miltner, 2020). The offset of the deep water to the atmospheric $\Delta^{14}C$ can be described by two parameters. Firstly, the offset $\Delta\Delta^{14}C = \Delta^{14}C_{dw} - \Delta^{14}C_{atm}$ can be used, which is always negative apart from the exception described above. A constant offset indicates a constant reservoir effect and current pattern at the CWC location whereas changes in the $\Delta\Delta^{14}C$ hint towards changes in the pathways of the water masses. This means either changes in the horizontal transport or vertical mixing of differently ^{14}C aged waters. Low $^{14}C_{dw}$ concentrations imply a longer time since the water mass was in contact with the atmosphere. These water masses are also called 'old' water masses. In contrast to this, high $^{14}C_{dw}$ concentrations imply well ventilated, 'young' water masses.

This nomenclature already hints towards the second possibility to describe the offset between measured coralline and atmospheric $\Delta^{14}C$: Calculating the reservoir age R. Assuming a closed system ^{14}C decay in the CWC, the $\Delta^{14}C$ signal of the CWC can be traced back to the intersect with the atmospheric calibration curves IntCal20 (Reimer *et al.*, 2020) and SHCal20 (Hogg *et al.*, 2020). The difference between the extrapolated age of the intersect and the measured U/Th age of the coral is called the reservoir age R of the water mass (Adkins and Boyle, 1997). If both the reservoir effect r and the reservoir age R of a sample are known, the time since the last contact of the water

mass to the atmosphere, the so-called ventilation age, can be calculated via $\Delta R = R\text{-}r$ (Mangini *et al.*, 1998; Adkins, 1998; Skinner *et al.*, 2017). However, the reservoir effect of different regions is not precisely known and is, therefore, a large source of uncertainty for the ventilation ages.

In the following chapters, the Li/Mg thermometer and ^{14}C reservoir ages will be explored in more detail to observe thermocline circulation changes over the last 40 ka. The U/Th dating will not be discussed in detail but plays a major role for the chronological frame of the temporal evolution of the thermocline circulation patterns.

Part I

Reconstruction of seawater temperatures using cold-water corals

3 Introduction

In the following chapters the thermal history of the Atlantic mid-depth ocean will be reconstructed using CWCs from various locations in the Atlantic. According to the models by e.g. Stocker and Johnsen (2003) and Knutti *et al.* (2004), major warming of the subtropical thermocline waters is expected shortly after the decrease in the strength of the AMOC associated with increased freshwater discharge into the North Atlantic between 18.5 ka and 15 ka ago. The thermal history of the upper thermocline, however, is poorly constrained. As there are several explanations for temperature changes in thermocline, like up- and downwelling as well as horizontal advection of water masses, ^{14}C measurements of the CWCs are explored to gain further insights in the water mass pathways.

In the next chapter, the required methods for U/Th dating, ^{14}C and Li/Mg measurements will be described in detail, before, in chapter 5, the results are described and discussed for a location off Angola in the southern hemisphere. In chapter 6, Li/Mg measurements at six different locations throughout the Atlantic are compiled, all showing similar patterns on glacial/interglacial timescales. For further discussions of the water pathways, a compilation of coralline ^{14}C measurements was used. A well-ventilated water mass in the North Atlantic and 'older' water masses in the South Atlantic was observed. However, the dividing line is rather the Azores Front than at the equator. Afterwards, resulting from new findings in these chapters, in part II, disturbances of the Li/Mg thermometer from possible seawater Li variability will be explored.

4 Methods

4.1 U-series dating

For U-series dating, coral samples were mechanically cleaned and U and Th were extracted using the method after Frank *et al.* (2004) and Wefing *et al.* (2017). Between 40 mg and 60 mg of the sample material was leached carefully, dried over night and dissolved in 7 M HNO_3. Afterwards, samples were spiked using the artifical isotopes ^{229}Th, ^{233}U and ^{236}U before purification from matrix elements by ion exchange column chemistry using UTEVA resin. The columns were cleaned with high purity water with a resistance of 18.2 MΩ.cm (MilliQ water) and filled with 0.25 ml of UTEVA resin. The resin was washed again with 0.25 ml of MilliQ before it was loaded with 0.25 ml of 7 M HNO_3 and the samples was added. Afterwards, the matrix fraction was washed from the column with 3×0.5 ml of 7 M HNO_3. When the acid has completely passed the column U and Th were eluted by adding 3×0.5 ml of 1 M HCl and 3 M HCl respectively before MilliQ water was added once more. In the end the eluted samples were evaporated to full dryness on a hot plate and the columns were filled with MilliQ water, capped and stored for a second column.
For the second column, the samples were redissolved in 0.3 ml of 7 M HNO_3, the columns were opened and loaded again with 7 M HNO_3 after the water drained out. The procedure for the second column is similar to the first one. However, as the matrix fraction in the sample is already greatly diminished, the column was only washed with 0.75 ml 7 M HNO_3 before eluting the samples similar to the first column. At the end an additional step of adding 3×0.5 ml 1 M HF was conducted. The samples solution is evaporated again and redissolved in a mixture of 1 % $HNO_3 + 0.05$ % HF for isotope measurements.
High precision isotope measurements were conducted on a multicollector inductively coupled plasma mass spectrometer (MC-ICP-MS, Thermo Fisher Neptune Plus) equipped with an desolvator (ESI Aridus) and an autosampler (ESI SC-d DX) at the Institute of Environmental Physics (IUP), Heidelberg University, Germany. Detailed description of the measurement procedure and data treatment including blank, mass bias and interfering corrections, can be found in Arps (2017). Samples were analysed

for their ^{229}Th, ^{230}Th, ^{232}Th, ^{233}U, ^{234}U, ^{235}U, ^{236}U and ^{238}U content using a standard bracketing method with the reference material Hu-1. A reproducibility of (^{234}U/^{238}U) = 0.9997 ± 0.0003 and (^{230}Th/^{238}U) = 1.0002 ± 0.0005 (weighted mean and standard deviation) was achieved (Arps, 2017). A precision of < 1 ‰ for U isotope ratios and < 3 ‰ for Th isotope ratios is reached, analytical blanks are frequently assessed but insignificant with respect to the measurement precision (< 0.05 fg for ^{230}Th and < 0.3 fg for ^{234}U) (Arps, 2017). For age calculations ^{234}U and ^{230}Th half-lives published in Cheng *et al.* (2000b) were used.

4.2 Radiocarbon ventilation ages

For radiocarbon measurements, CO_2 must be extracted from the CWC samples and transformed into graphite for measurements. This extraction and graphitization process took place at the IUP, Heidelberg University, Germany and will be described in the following section.

Before dissolving the corals and extracting CO_2, 15 mg to 20 mg of the mechanically cleaned coral samples were carefully leached using 4 % HCl and dried afterwards. For the extraction of CO_2, the coral samples were hydrolized using 0.5 ml of 3 M HCl in an evacuated glass extraction line, causing the following chemical reaction:

$$CaCO_3 + 2HCl \longrightarrow CO_2 + H_2O + CaCl_2 \tag{4.1}$$

This gas mixture of carbon dioxide and water vapour was directed into a freezing trap cooled by a combination of dry ice and acetone to a temperature of approximately -78 °C. Here, the water vapour was removed from the gas mixture as it freezes at the greatly increased inner surface of the freezing trap. The carbon dioxide, remaining gaseous, is then collected in a glass container cooled by liquid nitrogen to -196 °C. For detailed description of the extraction process and extraction line see Therre *et al.* (2021).

Afterwards, the carbon dioxide sample was, together with pure hydrogen gas, injected into an evacuated chemical reactor heated to about 575 °C and filled with an iron catalyst. The carbon dioxide was then reduced to graphite over the course of three to four hours and precipitated on the iron catalyst. At the end the iron-graphite compound is stored in a small glass vial and measurend on an accelerator mass spectrometer (AMS, MICADAS) at the Curt-Engelhorn-Center Archaeometry (CEZA) in Mannheim, Germany (Kromer *et al.*, 2013).

Procedual blanks obtained from a marble and IAEA C1 - standard show apparent

^{14}C - ages are >50000 years (Therre *et al.*, 2021). The reproducibility of radiocarbon measurements was determined using the IAEA C2 standard material. The mean value was measured at (41.058 ± 0.225) pmC (n = 33) and is in accordance to the literature value of (41.14 ± 0.03) pmC (Rozanski *et al.*, 1992) and translates to a reproducability of 0.547 % (Therre *et al.*, 2021).

4.3 Li/Mg

From the U-series dated sample archives, mechanically cleaned aliquots of 10 mg to 15 mg were taken for Li/Mg analysis. During mechanical preparation the outer surface, bioerosion and septae were removed thoroughly as these might influence the Li/Mg ratio of the coral and do not reflect the Li- and Mg- content of the coral theca. Afterwards, coral samples were washed with MilliQ water to remove any residual powder from the mechanical cleaning procedure, dissolved in 10 ml 0.5 M HNO_3 and diluted to samples containing 10 ppm Ca for measurement. Dilution factors are calculated from the sample weight under the assumption that coral samples are purely made out of $CaCO_3$.
Measurements were carried out on a quadrupole mass spectrometer (Thermo Fischer ICapQ) connected to a desolvating nebulizer system (ESI Apex HF) to improve sensibility at the Institute of Environmental Physics (IUP), Heidelberg University, Germany, according to the method described in Förstel (2014) and Lausecker (2015). The measurements were performed using nickel cones with a high-matrix insert as the samples were not purified in terms of separating Li and Mg from the matrix. The mass spectrometer was tuned to achieve maximum Li sensitivity, deviations from reference Li/Mg ratios of the reference material was corrected later on in the evaluation. The ICap Q is equipped with a collision cell, that can be flooded with an additional gas (e.g. He) to remove e.g. molecules from the sample aerosol. This was not used for Li/Mg measurements, as it strongly suppresses Li (Förstel, 2014), however, the lenses affiliated to the collision cell were used to focus the ion beam. Typical tune parameters used during Li/Mg measurements are found in tab. 4.1. Samples were analysed using a standard bracketing method. Therefore, the in-house reference coral ICE (<100a young CWC ICE-CTD 20PL501-6-C4 from Iceland, collected from water at a temperature of about 6 °C cool water) was analysed at the beginning and as every sixth sample. To determine the external reproducibility for various days of the measurements two in-house external reference corals were analysed: One warm-water coral from the Seychelles (PF-2, 6.2 [$\pm$ 0.2] ka) and a cold-water coral from the Azores (Acor-1, 15.2 [$\pm$ 0.8] ka).

Table 4.1: Typical mass spectrometer settings used during Li/Mg analyses.

Parameter	Value
Resolution	high
Main runs	10
Sweeps	50
Channels	3
Spacing [u]	0,05
Dwell time [s]:	
^{7}Li	0,05
^{25}Mg/^{26}Mg	0,02
collision gas [$\frac{\text{ml}}{\text{min}}$]	0,0
U_{CCT} [V]	-21,25
U_{Pole} [V]	0,795

The isotopes analysed to obtain Li/Mg ratios are ^{7}Li for lithium, as the abundance of the only other lithium isotope, ^{6}Li, is too low to be measured precisely at this concentration (order of about 10 ppt). For the concentration measurements of magnesium ^{25}Mg and ^{26}Mg are used. The last and most abundant magnesium isotope was discarded, as there might be interference with $^{48}Ca^{2+}$ (Förstel, 2014). Mainly for control reasons calcium was also analysed using the low abundance isotopes of ^{43}Ca and ^{48}Ca.
During evaluation, measurements were drift and mass-bias corrected using the in-house reference coral ICE. For temperature reconstruction the calibration curve published by Montagna *et al.* (2014) was used (after eq. 2.1):

$$T\,[^{\circ}C] = -\frac{1}{0,049\,[\pm 0.002]}\,[^{\circ}C] \times \ln\left(\frac{\frac{[\text{Li}]}{[\text{Mg}]}\,[mmol/mol]}{5,41\,[mmol/mol]}\right)\,^{\circ}\text{C}. \tag{4.2}$$

The methods and calibration of Cuny-Guirriec *et al.* (2019) and Stewart *et al.* (2020) give the same results within uncertainty (Rampmeier, 2021). The reliability of in-house measurements was tested by reconstructing the calibration curve of Montagna *et al.* (2014) using < 100 a old corals (see figure 4.1a, Lausecker, 2015), as well as an interlaboratory comparison experiment between the IUP and the LSCE (Laboratoire des Sciences du Climat et de l'Environnement, Gif-sur-Yvette, France), in which 19 sample aliquots were measured in both laboratories (Krengel, 2016). The results of this experiment agree well with each other (see figure 4.1b). The Li/Mg ratio of the in-house standard ICE is 4.08 ± 0.08 mmol/mol, the external reproducibility for the Li/Mg measurements was determined to 1.24 ± 0.14 mmol/mol (n = 33, 33 months) for the in-house reference coral PF-2 and to 4.50 ± 0.12 mmol/mol (n = 37, 4 months) using reference coral Acor-1.

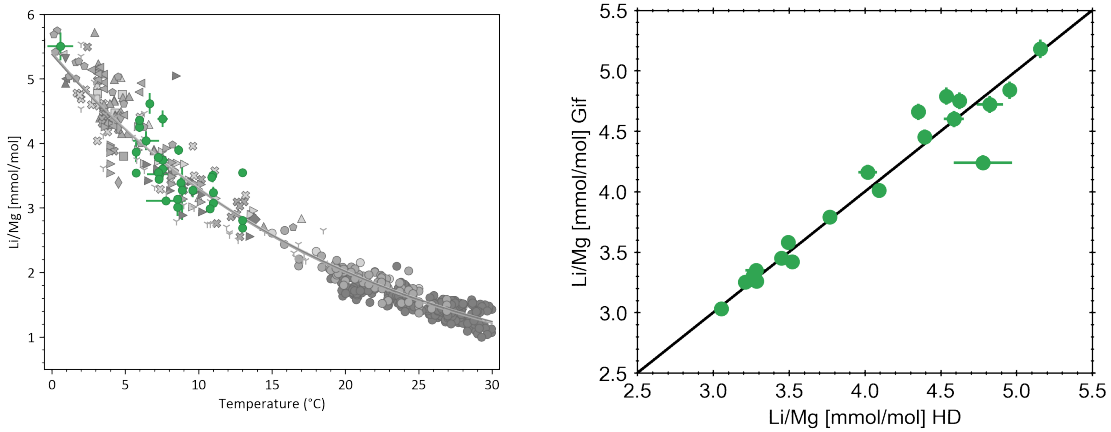

a) In-house Li/Mg calibration.

b) Interlaboratory comparison.

Figure 4.1: Results of the interlaboratory comparison of Li/Mg samples. a) Analysis of modern CWC samples added to the published calibration curves. Data measured here agrees well with the published data within scatter. b) Aliquots of the same samples were measured in two different laboratories at the LSCE in Gif-sur-Yvette and at the Institute of Environmental Physics in Heidelberg (Krengel, 2016). The black line indicates the 1:1 line. Samples show the same results. Uncertainties are smaller than symbols when not apparent.

5 Thermal and ventilation changes across Termination I in the eastern South Atlantic

5.1 Introduction

The thermocline waters of the south-eastern Atlantic basin are today dominated by the cold and nutrient-rich waters of the Benguela current flowing in northwestern direction. The pathways of water advection in the eastern South Atlantic are strongly dependent on the intensity of the Agulhas leakage at the southern tip of Africa (Veitch *et al.*, 2010). Another important feature are the local upwelling cells, greatly influencing the regional heat budget of the surface and thermocline waters. While the Angola Dome is a flow induced upwelling system, the coastal upwelling of Angola and Namibia are wind induced.

Major past changes in the Benguela Current (BC) and Benguela Upwelling System were (BUS) formely recorded in marine sediments (Mollenhauer *et al.*, 2002; Romero *et al.*, 2003; Rutberg *et al.*, 2005) and sea surface temperatures (SST) reconstructions find a strong LGM cooling of 5 °C (e.g. Schneider *et al.*, 1996; Sachs *et al.*, 2001). It was further shown that the origin of particles in the Agulhas leakage changed during the last glacial (Rutberg *et al.*, 2005), suggesting a strong decrease in the strength of the Agulhas leakage resulting from a northward displacement of the southern hemispheric ocean polar front (Little *et al.*, 1997a; Veitch *et al.*, 2010). This would lead to an increase in the advection of cold polar waters from the Antarctic Circumpolar Current (ACC) into the South Atlantic (Little *et al.*, 1997a).

Consequently, one would expect an aging of the thermocline water driven by the influx of cold polar water masses from the Southern Ocean possibly including radiocarbon depleted Pacific carbon-rich waters. Additionally, one would expect the thermocline to rise bringing cold nutrient-rich waters closer to the surface. A northward shift of the polar front probably triggered a displacement of the Hadley cell or modulation of the strength of surface winds that may resulted in a northward migration and strengthening

of coastal upwelling systems and a relocation of the surface ABF.
To verify the hypothesis of polar water advection, water mass aging and the rise of the thermocline, a thermocline water perspective of major thermal and ventilation changes as observed in CWCs is added in this chapter. To obtain information on the thermal and ventilation changes of the thermocline water masses, CWCs from a CWC province off Angola north of today's ABF were studied, recording an even stronger cooling as well as major water mass aging during the LGM compared to the Holocene.

5.2 Materials

One hundred and fifty-two CWC samples from three gravity cores and 16 surface samples collected by a ROV, grab sampler or giant box corer were analysed for this study. All sample material was recovered during the research cruise M122 *ANNA* onboard RV Meteor off the coast of Angola in January 2016.
Gravity core GeoB 20933–1 (9°49.331' S, 12°46.565' E, 338 m), containing well-preserved CWCs throughout its 9.83 m length, was recovered on 80 m-high *Scary mounds* (Hebbeln *et al.*, 2017). A first Uranium-series chronology of this core was presented by Wefing *et al.* (2017) (n = 34 samples), revealing quasi-continuous CWC ages between 0.5 ka and 33.6 ka. However, the analysed samples showed three major hiatuses of 4 - 5 ka duration between 13.9 ka and 19.3 ka, between 19.3 ka and 23.3 ka and between 26.8 ka and 31.4 ka. To further encircle the hiatuses and thus minimizing the time span of little to no CWC growth at this core location, additional samples (n = 14) of this gravity core were analysed by Roesch (2017).
In a multi-core approach that reveals a broader and more accurate view of CWC growth periods in a CWC mound province two more cores were analysed. Sixty-three CWC samples from CWC bearing gravity core GeoB20928–1 (9°43.388' S, 12°42.899' E, 457 m) were analysed for their U-series age. This gravity core was recovered from the nearby *Valentine mounds* and also contained well-preserved CWCs throughout its 7.57 m length.
In close proximity to GeoB20928–1, GeoB20908–2 (9°43.605' S; 12°42.893' E, 439 m) was also recovered from *Valentine mounds*. From this shorter CWC-bearing gravity core of only 4.52 m length, additional 41 CWC samples were analysed.
To complement the time series of the gravity cores, 17 fossil surface CWC samples obtained during ROV dives (GeoB20930–4, –30–6, –17–1, –27–1, –51–1), with a giant box core (GeoB20953–2) and a grab sampler (GeoB 20909–1, –34–1, –13–1, –35–1, –58–1, –07–1, –B08–1, –10–1, –55–1) were analysed. These samples were collected from water depths between 259 m and 517 m in the same CWC province as the studied

gravity cores, eight of which originate from the same CWC mounds as the gravity cores (Hebbeln *et al.*, 2017).

All 168 CWC samples were U-series dated and 56 of the CWCs were additionally analysed for their ^{14}C age (Beisel, 2021) to record water mass ventilation of the last 31.7 ka BP using the approach by Mangini *et al.* (1998) and Adkins *et al.* (1998). Finally, the Li/Ca and Mg/Ca ratios of 69 CWC samples (Roesch, 2017, this thesis) were measured to retrieve thermocline water temperatures (ThWT) during the last 33.6 ka using the Li/Mg thermometer (Montagna *et al.*, 2014).

5.3 Results

All U-series ages can be found in figure 5.1. The newly measured ages of samples from gravity core GeoB20933-1 confirm the hiatuses previously determined. However, the measurements allowed to slightly reduce the time spans lacking CWCs to: 30.98 ± 0.16 ka to 26.83 ± 0.06 ka, 22.68 ± 0.27 ka to 19.31 ± 0.04 ka and 19.00 ± 0.22 ka to 13.81 ± 0.05 ka. Apart from these hiatuses, gravity core GeoB20933-1 shows continous, flourishing CWC growth for the last 33.58 ± 0.08 ka as can be seen by high aggradation rates of up to 200 cm ka^{-1} (see figure 5.1).
Gravity core GeoB20928-1 shows CWC growth between 3.79 ± 0.02 ka and 25.31 ± 0.09 ka ago. Three hiatuses occur between 23.92 ± 0.07 ka to 17.67 ± 0.05 ka, 16.65 ± 0.04 ka to 13.59 ± 0.07 ka and 8.07 ± 0.03 ka to 5.34 ± 0.03 ka. Hence, hiatus 2 and 3 overlap with the hiatus 1 and 2 in the core GeoB 20933-1. At all other times high mound aggradation rates between 20 cm ka^{-1} and 110 cm ka^{-1} are found.
GeoB20908-2 covers the shortest time span of only the last 6.1 ka. Large CWC mound aggradation rates were also found for this core with values of 30 cm ka^{-1} to 115 cm ka^{-1}.
CWC ages of the surface samples coincide with the ages found in the gravity cores and span a time range of 21.90 ± 0.08 ka to 0.09 ± 0.01 ka.
Combining all CWC ages and thus, eliminating the sample bias of just one core, flourishing CWC growth is observed during glacial and interglacial times for the last 34 ka. However, little to no CWC growth was found between 30.9 ka and 25.3 ka, between 22.6 ka and 19.3 ka and 16.6 ka and 13.9 ka possibly hinting towards strongly reduced or even absent CWC reef activity at these times.

For the following description and further discussion of the CWC data, all samples will be viewed as one data set and no differentiation will be made between the gravity cores. This is a valid approach as all samples were recovered in close proximity to

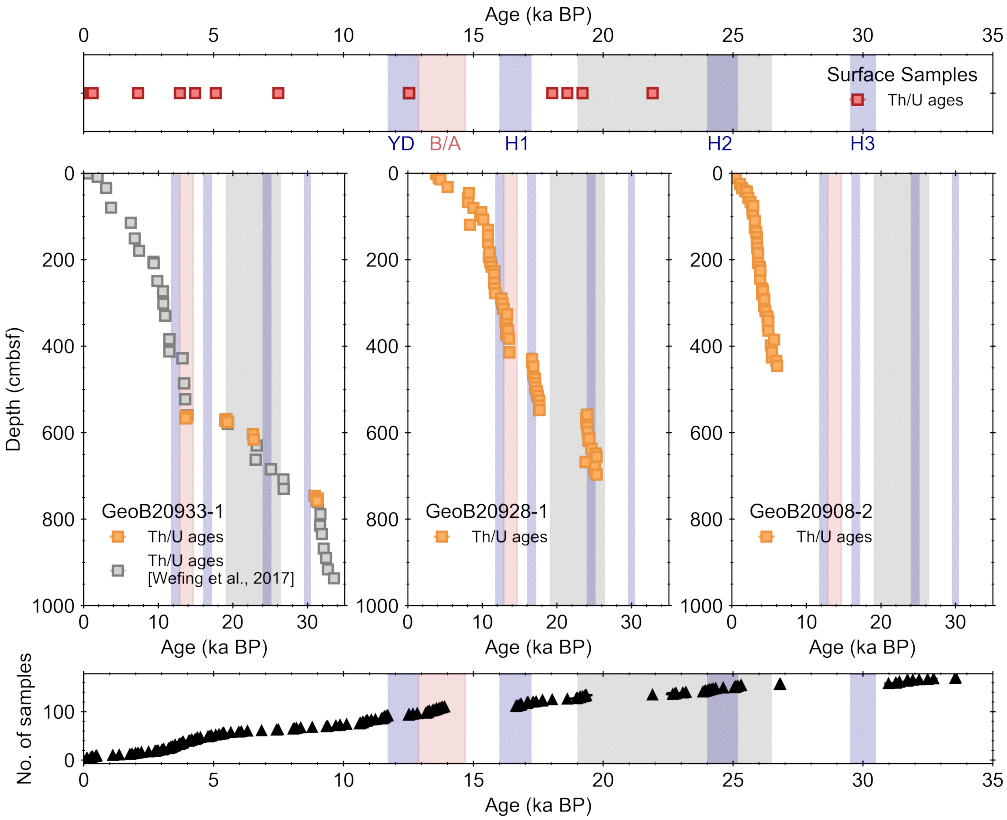

Figure 5.1: Dating results of U-series measurements (squares) of all CWC samples. Upper panel shows results of all surface samples. Middle panels show results of the three gravity cores. From left to right: GeoB20933-1, GeoB20928-1, GeoB20908-2. Grey squares in the first middle panel are U-series ages published in Wefing et al. (2017). Orange squares are newly established U-series ages resulting from this study. The lower panel contains all U-series data merged into one data set to illustrate times of reduced to no CWC growth. Grey vertical bars illustrate the Younger Dryas (YD), Heinrich events 1-3 (H1, H2, H3) and the Last Glacial Maximum (LGM) as outlined in the upper panel.

each other, i.e. in similar water temperatures and water depths, with the bulk of data originating from a water depth between 338 m and 457 m. Assuming a local sea level drop of 120 m to 130 m during th LGM (Lambeck *et al.*, 2014; Gowan *et al.*, 2021), this modern depth interval corresponds to a paleo sea level corrected depth interval of about 210 m to 340 m depth.

As described in chapter 2.7, past seawater $\Delta^{14}C$ values can be determined from combining U-series ages and ^{14}C measurements to measure the state of ventilation

of the ocean interior (Adkins *et al.*, 1998; Mangini *et al.*, 1998), here the upper thermocline waters. For detailed information on the calculation of the uncertainty ellipses of the radiocarbon fraction using a Monte-Carlo approach, the reader is referred to Ruckelshausen (2013). A detailed description of the quality control can be found in Beisel (2021).

The Δ^{14}C values vary between -90 ‰ and 450 ‰ over the last 32 ka (see fig. 5.2). The oldest three samples analysed at at 31.67 ± 0.14 ka BP to 31.20 ± 0.12 ka BP only show a minor offset $\Delta\Delta^{14}$C from the atmosphere (SHCal20, Hogg *et al.*, 2020) pointing to low reservoir ages of the thermocline waters. Hence, reservoir ages between 196 ± 284 years and 429 ± 238 years are very young for these three CWCs. Moving towards the LGM, reservoir ages and the offset $\Delta\Delta^{14}$C of the CWCs samples from the atmosphere (SHCal20, Hogg *et al.*, 2020) seem to steadily increase from 30.92 ± 0.16 ka BP to the LGM indicating the advection of a less ventilated water mass at the CWC site during the LGM. For the time span from 24.98 ± 0.09 ka BP to 16.66 ± 0.03 ka BP, $\Delta\Delta^{14}$C values between -126 ± 18 ‰ and -231 ± 26 ‰ are calculated with one sample at -299 ± 30 ‰. This corresponds to large mean reservoir ages of 1224 ± 229 years (n = 14). During most of the last 13.8 ka, $\Delta\Delta^{14}$C was fairly constant at about -79 ± 19 ‰ (n = 19). This converts into a mean reservoir age of 746 ± 140 years. However, between 12.61 ± 0.03 ka BP and 12.45 ± 0.03 ka BP, Δ^{14}C shows a sharp increase to values between -97 ± 15 ‰ and -196 ± 17 ‰.

Li/Ca, Mg/Ca and Li/Mg ratios were determined for CWC samples with an age between 33.58 ± 0.08 ka to 0.47 ± 0.03 ka. Li/Ca ratios vary between 1.64 ± 0.02 µg g^{-1} and 2.74 ± 0.07 µg g^{-1} while Mg/Ca ratios are more stable between 1.51 ± 0.04 mg g^{-1} and 2.18 ± 0.02 mg g^{-1}. This translates into Li/Mg ratios between 3.26 ± 0.06 mmol mol^{-1} and 4.96 ± 0.18 mmol mol^{-1}, which can be converted into thermocline water temperatures (ThWT) between 1.8 ± 1 °C and 10.4 ± 1 °C using the calibration curve of Montagna *et al.* (2014) (see figure 5.3). More recent calibration curves by Cuny-Guirriec *et al.* (2019) and Stewart *et al.* (2020) do not influence the temperature range or time series behaviour. Starting with the oldest samples, Li/Mg ratios and reconstructed temperatures are fairly constant between 33.58 ± 0.08 ka and 17.07 ± 0.04 ka at a mean of 4.68 ± 0.30 mmol mol^{-1} corresponding to 3.0 ± 1.2 °C (n = 36). During the following 400 years to 16.69 ± 0.03 ka, reconstructed temperatures increase to about 6.7 ± 1.5 °C (n = 3). For the last 13.9 ka, Li/Mg ratios and reconstructed temperatures are fairly constant again with a mean value of 3.49 ± 0.28 mmol mol^{-1} and 9.0 ± 1.4 °C (n = 22). The variability is in the same range as the systematic uncertainty of about 1.0 °C of the calibration curve in this temperature interval. Moreover, reconstructed measurements are in good accordance with today's thermocline temperature measured

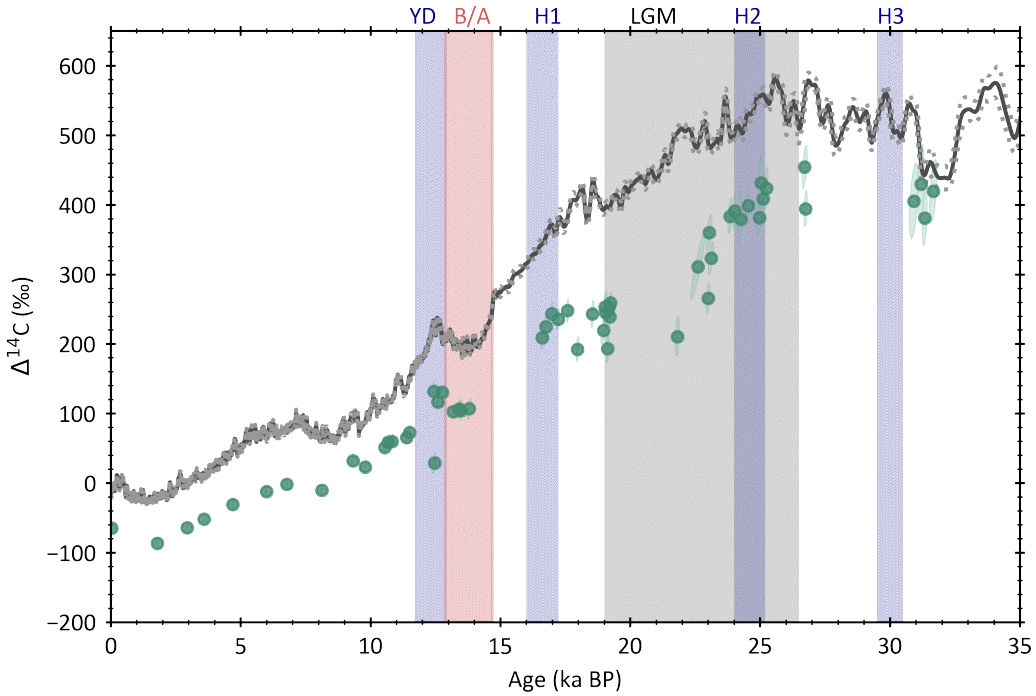

Figure 5.2: Thermocline water $\Delta^{14}C$ from combined U-series and 14C dating of CWCs off Angola (green dots), SHCal20 atmospheric 14C-values (grey line, Hogg *et al.*, 2020). Light grey dots show CWC data collected in the mid-depth equatorial North Atlantic (only 500 – 1100 m depth) (Chen *et al.*, 2015).

at the water depth of the CWC location at 8 - 12 °C (ROV-CTD-data, Hebbeln *et al.*, 2020). Consequently, the last glacial and Holocene differ by a Li/Mg-reconstructed ThWT of 6 ± 1.8 °C, with potentially a very rapid centennial half-way increase of 3 °C centered at 16.7 ka.

5.4 Discussion

Cold-water corals in the south-east Atlantic lived in the eastern South Atlantic during the last glacial and recent interglacial periods until today. However, short time ranges of missing or very little CWC growth in the combined record of three gravity cores and multiple surface samples partly coincide with events of ocean circulation disruption, namely the Heinrich events H1 (14.7 ka to 17.1 ka) and H3 (29 ka to 31 ka). Furthermore, few CWCs are found so far during the LGM (19 ka to 24 ka) when ice sheet extension was maximal (e.g. Batchelor *et al.*, 2019). However, during H2 (24.1 ka to 24.9 ka), the present of CWCs was only documented in one of the gravity cores, which indicate that CWCs were growing at least in sime of the Angolan coral mounds

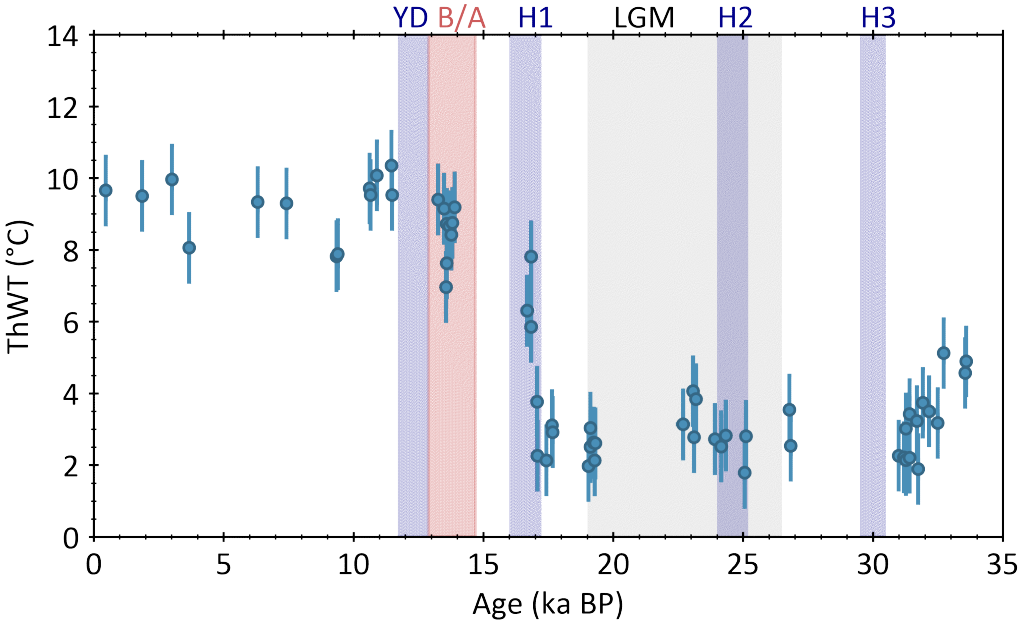

Figure 5.3: Thermocline water temperatures (ThWT) reconstructed from Li/Mg ratios using the calibration ofMontagna *et al.* (2014). Grey vertical bars illustrate the Younger Dryas (YD), Heinrich events 1-3 (H1, H2, H3) and the last glacial maximum (LGM). The red dashed line indicates the timing of the Bølling-Allerød (B/A).

during these times. CWC mound evolution often follows complex, non-linear patterns as formerly described e.g. for the Mediterranean Sea (Krengel, 2020) and the Golf of Cadiz (Hemsing, 2017). Therefore, even massive CWC growth activity is possible at times no CWCs were found in the studied gravity cores, as these cores cover and represent only a very tiny area of the CWC mound province. This, however, can only be speculated on and more studies are needed to reveal the nature of CWC appearance off the coast of Angola.

Since Heinrich events occur during times of northern hemispheric climate instabilities, the concurrence of Heinrich events and the absence of CWC growth in the south-east Atlantic might hint towards a teleconnection between CWC growth conditions in the south east Atlantic and the northern hemisphere climate changes as inferred by Henry *et al.* (2014).

Increasing reservoir ages towards the LGM indicate poorer ventilated, 'aged' water masses at the CWC location. When compared to published CWC radiocarbon data by Chen *et al.* (2015), a similar increase in reservoir ages can be seen in intermediate water masses (< 1100 m water depth) in the equatorial North Atlantic (5° N to 10° N,

see fig. 5.4).

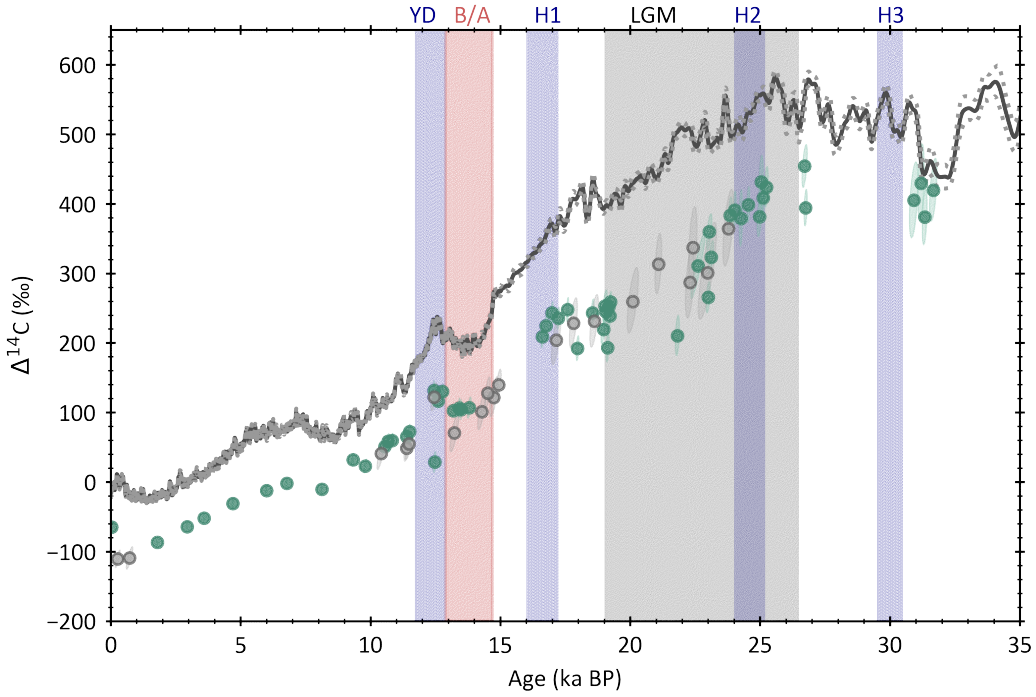

Figure 5.4: Thermocline water $\Delta^{14}C$ from combined U-series and 14C dating of CWCs off Angola (green dots), SHCal20 atmospheric 14C-values (grey line, Hogg *et al.*, 2020).

Just before the YD cold reversal, $\Delta^{14}C$ reached Holocene values of well-ventilated waters before getting more variant during the YD and stabilizing for the rest of the Holocene.

Li/Mg ratios and reconstructed ThWT do not show the same temporal pattern as the ^{14}C measurements. Temperatures are at a constant low value of $3.0 \pm 1.2\,°C$ up to the beginning of H1, when temperatures start rising coinciding with the onset of southern hemisphere warming as shown by Vostok ice core data (see fig. 5.5). Shortly after the beginning of H1, CWC growth ceases and no statement can be made on the further temperature evolution until 13.9 ka BP, when CWCs reappear on the Angolan coral mounds and waters have reached a temperature of $9.0 \pm 1.4\,°C$ as is still found today (Hebbeln *et al.*, 2020).

One explanation for these large differences between glacial and interglacial reconstructed temperatures might be a major change in the Li/Mg ratio of seawater. As residence times of Li and Mg in the ocean are larger than 1 Ma and 10 Ma (Huh *et al.*, 1998; Berner and Berner, 2012), respectively, changes in ocean Li/Mg ratios are likely

to occur only very local and to be insignificant on the studied time range of 34 ka. Furthermore, the influence of biomineralisation or diagenesis on the Li/Mg ratios of these CWCs can be ruled out, as one would expect these to result in a larger scatter rather than a systematic shift towards colder temperatures during the glacial. Cuny-Guirriec *et al.* (2019) suggested a strong effect of up to 50 % variance in Li/Mg from organic matter in CWCs and tested different cleaning protocols on organic rich tropical corals. Rampmeier (2021) tested this method on CWC and found no benefit from the cleaning protocol Cuny-Guirriec *et al.* (2019) proposed for surface CWCs when applied to CWC. Moreover, residual organic matter would also be expected to result in a larger scatter, which cannot be seen in the presented data. The same applies to variances in the CWCline microstructure. It is known that Li/Mg ratios in COCs slightly differ from that of fibrous aragonite within the CWC skeleton (Case *et al.*, 2010). This can be excluded as the reason for glacial-interglacial variance, due to the lack of scatter seen in the presented CWC data.

As alteration processes cannot explain the variation found in the data set, a strong and sharp temperature increase of 6.0 ± 1.9 °C starting at the beginning of H1, coinciding with southern hemisphere deglacial warming, must be invoked. This agrees with model predicitons of a strong warming of up to 5 °C in the upper 1000 m of the South Atlantic within 200 to 300 years after the AMOC intermits due to freshwater influx in the North Atlantic (Stocker and Johnsen, 2003; Pedro *et al.*, 2018). Rühlemann *et al.* (2004) investigated sediment core ODP1078C (11° 55'S, 13° 24'E, 426 water depth) south of the Angolan CWC mound province as well as an earth system model of intermediate complexity and found an intense and rapid warming during AMOC slowdown as well. The data set of benthic foraminifera collected in sediment core ODP1078C suggests a temperature increase of 0.8 °C per century at the onset of H1, which agrees well with the temperature increase documented by the CWCs.

CWCs show modern-day thermocline temperature long before the end of the deglaciation. At 13.9 ka BP, when CWCs reappear on the Angolan coral mounds and warm state temperatures are observed, global sea levels were still 80 m below modern values (Lambeck *et al.*, 2014). However, SST reconstructed from alkenones in sediment core GeoB1016-3, which was recovered nearby on the Angolan margin, reveal a SST of about 22.6 ± 0.3 °C at 13.9 ka BP (see figure 5.5) and hence, surfaces waters have not yet reached their warm state temperatures of about 25 ± 1 °C at that time (Schneider *et al.*, 1996). Therefore, estimated temperature gradients are constant at 3.5 to 5.0 °C per 100 m water depth since 13.9 ka BP. To explain this constant temperature gradient, the thermocline must have deepened simultaneously to the sea level rise and global atmosphere warming as indicated bei NGRIP and Vostok ice cores.

The same consideration must be made for the glacial period. Schneider *et al.* (1996) found a SST of about 21 ± 1 °C, only about 4°C colder compared to the Holocene, while CWCs show a glacial thermocline temperature of about 3.0 ± 1.2 °C, about 6 °C colder as in the Holocene. Furthermore, during the LGM, sea levels were about 110 m to 125 m below modern sea levels (Lambeck *et al.*, 2014). Combining this information, a stronger glacial temperature gradient of 5.5 to 8 °C per 100 m water depth and a therefore shallower thermocline during the glacial can be estimated.

Combining the results of radiocarbon reservoir ages and Li/Mg temperature reconstructions during the glacial, water masses at the Angolan CWC site get progressively older from 32 ka BP towards the LGM at constant temperatures while during most of the Holocene modern conditions are observed. This suggests a strong change in solubility of old respired carbon within the thermocline ocean. There are three possible origins for these glacial-interglacial differences:
(1) The displacement of the Angola-Benguela-Front (ABF) to the north, allowing cold and aged polar waters forming the Benguela current (BeC) to reach the Angolan CWC site,
(2) vertical upwelling of cold and radiocarbon-depleted water masses from water depths or
(3) advection of cold and aged waters from the Southern Ocean ACC forming the BeC recirculating towards the CWCs under the Angola Dome.
The ABF is known to have varied in its position during the last 200 ka in response to the position and intensity of the subtropical convergence (STC) (e.g. Jansen *et al.*, 1996). Its southernmost position was reached, e.g. during the beginning of MIS 1 (14 ka), between today's location at 15 °S and 20 °S, while the northernmost position between 9 °S and 6.5 °S was reached e.g. between 50 ka BP and 40 ka BP (Jansen *et al.*, 1996; Little *et al.*, 1997a). However, this displacement does not follow glacial-interglacial patterns. During the last 34 ka in focus here, the ABF was never found north of 9 °S. In fact, the most northern position of the ABF between 6. °S and 9 °S was found between 50 ka BP and 40 ka BP, followed by a rapid southwards move during the LGM (Jansen *et al.*, 1996). If a displacement of the ABF was the (only) reason for changes in temperature and reservoir ages of water masses at the Angolan CWC site, one would not expect the aging of the water masses and might even expect a slight increase in water temperature as warmer water masses of the Angola Current advance to the south. Therefore, displacement of the ABF cannot be the reason for the observed changes in water mass properties.
Changes in intensity and zonality of the trade wind system do not only affect the position of the ABF, but also the upwelling intensity off the coast of Angola. Enhanced

upwelling could bring cold and aged intermediate water masses from below to the thermocline. Off Angola potential candidates are the Antarctic Intermediate Waters (AAIW) in 700 m to 1200 m water depth with water temperatures of 3-7 °C and reservoir ages of 600 years to 800 years and the even deeper North Atlantic Deep Water (2-4 °C, 1500-3500 m water depth) (Talley *et al.*, 2011). Little *et al.* (1997b) found indications for increased upwelling in the glacial Benguela upwelling system, whereas Schneider *et al.* (1996) found similar SST changes off Namibia as observed off Angola. This supports the hypothesis of strong upwelling as a possible explanation for the cooling and aging of the glacial thermocline waters. However, increased upwelling was studied off Namibia (Little *et al.*, 1997a) and occurs in rather sharp events simultaneously to H1 and H3. This cannot explain the gradually aging water masses as they were found in this study. Furthermore, as Little *et al.* (1997a) stated, the correlation of upwelling events in the South Atlatnic to the Heinrich events in the North Atlantic further hints towards a teleconnection via heat transfer and the trade wind systems of the North and South Atlantic. Although it is unlikely that upwelling was the main source of cold and radiocarbon depleted waters at the CWCs location, it cannot completely be rule out and likely contributed to the observed changes.

The last hypothesis is a large-scale advection of cold and aged water masses from the ACC. A schematic of this explanation is given in figure 5.6. A northward movement of the STC during glacial periods limits the advection of the Agulhas current into the Atlantic by forming a thermal barrier off the southern tip of Africa (Little *et al.*, 1997a; Veitch *et al.*, 2010). This allows an increase in cold water advection from the ACC (Little *et al.*, 1997a) and an intensification of the eastern boundary current (Lu *et al.*, 2007). Veitch and Penven (2017) also showed in a regional model that the warm waters of the Agulhas leakage caused intense mixing in the southern Benguela and that a removal of the Angulhas leakage results in a rather strong cooling of southeastern Atlantic water masses as well as a loss in eddy kinetic energy. This cools the thermocline effectively and increases the temperature gradient between the thermocline and surface waters, as it is documented in our data showing a glacial gradient of up to 8 °C per 100 m, which is doubled compared to today (3.5 to 5 °C per 100 m). This hypothesis of advected ACC water masses to the north is supported by paleoclimatic and model data. A large radiocarbon depletion of up to 500 ‰ or 2500 years (Burke and Robinson, 2012; Freeman *et al.*, 2015) and a cooling of about 3 °C (Lynch-Stieglitz *et al.*, 2016; Elmore *et al.*, 2015) of the ACC during the glacial was observed in different archives supported by models of Annan and Hargreaves (2013) and Annan and Hargreaves (2015). Butzin *et al.* (2005) found in model simulations that a reduced AMOC during the glacial leads to a significant water mass aging in the thermocline South Atlantic waters to

about 1000 years from present day values of about 600 years and simultaneous shoaling of thermocline waters between about 300 m and 700 m water depth. This increase in reservoir ages of about 400 to 500 years is in accordance to the CWC data obtained in this study.
Some models predict a glacial intensification of the southern hemispheric together with a smaller vertical and latitudinal extension of the southern hemispheric Hadley cell (Murakami *et al.*, 2008). As the BeC is wind-driven, this would favour an enhanced BeC supplying cold polar waters to the tropical and subtropical thermocline and influencing the global heat transport system (Jansen *et al.*, 1996) as the BeC is an important component of the surface interhemisphric heat transport from the south across the equator (Gordon *et al.*, 1987). This might, therefore, also be a possible explanation for the glacial aging of water masses found in the equatorial North Atlantic (Chen *et al.*, 2015).
These models and observations can support the immense cooling and aging of thermocline water masses as found in this study and the theory of a larger contribution of cold and aged polar waters of the ACC into the eastern South Atlantic. Furthermore, that might also, together with an enhanced BeC, explain radiocarbon depleted glacial water masses found in the equatorial North Atlantic (Chen *et al.*, 2015).

5.5 Conclusions

The thermal and ventilation patterns for the upper thermocline eastern South Atlantic over the past 34 ka were presented. CWCs were precisely dated using U/Th dating, while radiocarbon and Li/Mg measurements were used to obtain changes in glacial thermocline water properties near todays ABF.
While temperatures are constantly low during the glacial, reservoir ages increase towards the LGM coinciding with the aging of thermocline equatorial North Atlantic and Antarctic circumpolar current waters (Chen *et al.*, 2015). Li/Mg temperatures show a strong thermocline cooling during the last glacial and are indicative for a shoaling of the thermocline. At the start of H1, Li/Mg temperatures begin to rise in a sharp and intense increase and modern-day temperatures are observed for the last 14 ka.
An enhanced Hadley circulation and, thus, an enhanced BeC are a likely scenario for the observed water mass properties. When the BeC lacks the influx of warm water from the Indian ocean via the Angulhas leakage, cut off by a thermal barrier at the tip of Africa during the glacial periods, it transports even colder waters towards the north

as under conditions marked by an active Agulhas leakage. Alternatively, an enhanced coastal upwelling could lead to the observed cooling and aging of thermocline waters. However, as changes in upwelling intensity occur in sharp events (Little *et al.*, 1997a), this cannot explain the gradually aging of thermocline waters. Furthermore, increased upwelling is not supported by changes in CWC mound aggradation accounting for an increased food flux. Nevertheless, increased upwelling cannot be completely ruled out. Both hypothesis imply enhanced northward winds most likely caused by an intensification of the Hadley circulation. If the hypothesis of an advection of cold an aged polar water masses is valid, a major temperature drop during the glacial throughout the entire thermocline Atlantic would be expected. A shoaling of the thermocline would, furthermore, reduce vertical mixing near the surface in the mid-depth Atlantic Ocean. In the following chapter a compilation of Li/Mg temperatures from various locations throughout the Atlantic will be presented opening the discussion of the proposed mechanisms to a wider view and the impact of such an enhanced Hadley circulation on the entire Atlantic.

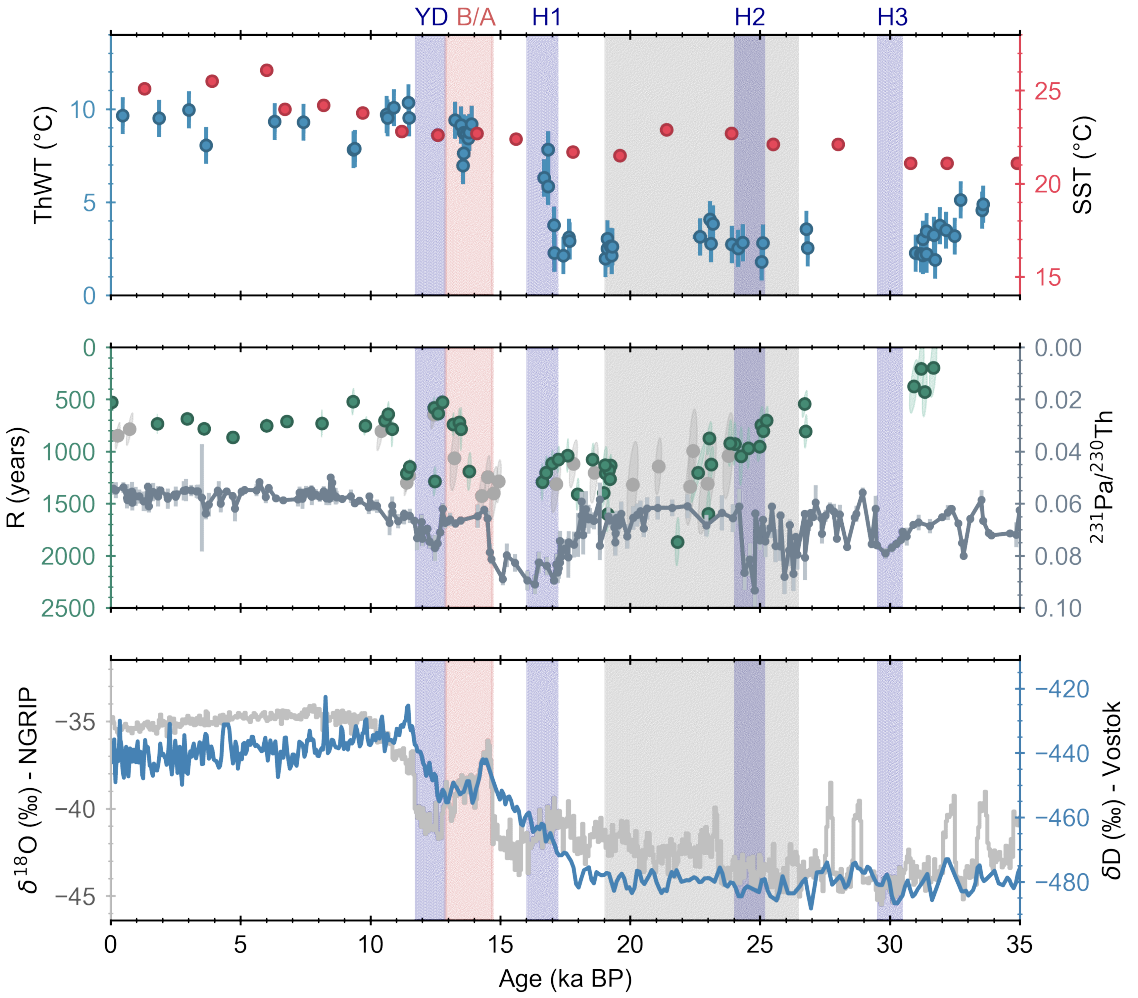

Figure 5.5: Upper panel: Thermocline water temperatures (ThWT) reconstructed from CWCs using Li/Mg ratios (blue dots, this study) and sea surface temperatures (SST) reconstructed from sediment core GeoB1016-3 using alkenones (Schneider *et al.*, 1996). Middle panel: Thermocline reservoir ages R reconstructed using CWCs off Angola (green dots, this study) agree well with CWC data from the equatorial North Atlantic (light grey, Chen *et al.*, 2015). ^{231}Pa/^{230}Th records of sediments from the Bermuda rise (grey line, McManus *et al.*, 2004; Böhm *et al.*, 2015; Lippold *et al.*, 2019) reflect AMOC changes. High values (>0.08) are indicative of times of a weak AMOC. Lower panel: δD record of Vostok ice core, Antarctica (blue line, Bazin *et al.*, 2013b) and δ^{18}O record of NGRIP ice core, Greenland (light grey line, Bazin *et al.*, 2013a). Blue vertical bars illustrate the Younger Dryas (YD) and Heinrich events 1-3 (H1, H2, H3). The last glacial maximum (LGM) is given as the grey shaded area. The red bar indicates the Bølling-Allerød stadial (B/A).

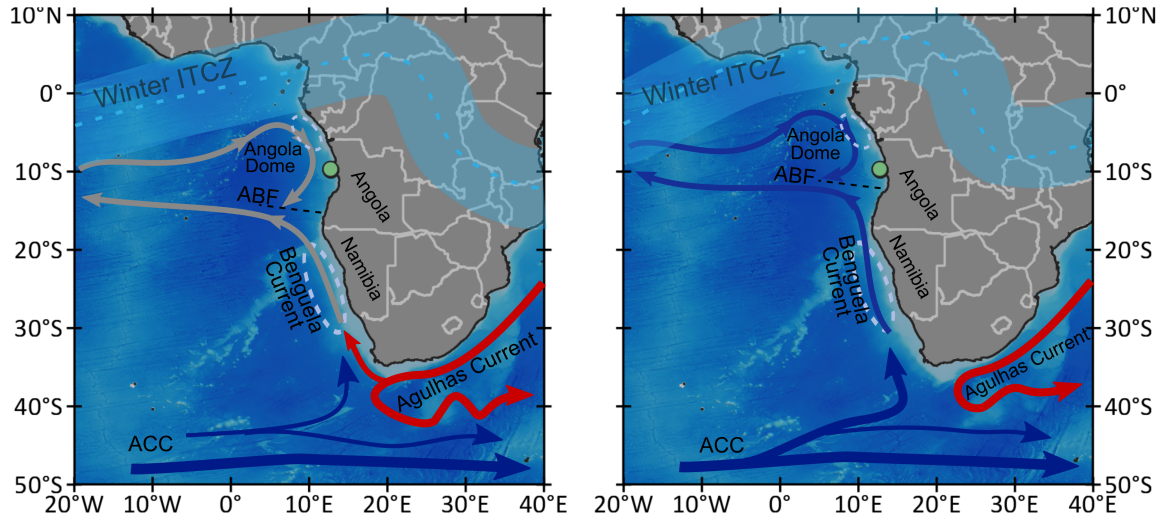

a) Holocene. **b)** Last Glacial Maximum.

Figure 5.6: Schematics of mid-depth circulation changes. The green dot denotes the sample location. a) Holocene situation with a BeC carrying 20 Sv of water northward and upwelling centers off Namibia and Angola (light blue dashed ellipses). b) During the glacial, warm water leakage through the Agulhas Current is cut off through water of the Polar Front. The Polar Front and ACC water induce massive thermocline water cooling and vertical stratification in the tropics via a glacial BeC.

6 A glacial polar Atlantic?

The data shown and discussed in this chapter is a compilation of results collected during various Bachelor's projects (Lausecker, 2015; Nakajima, 2016; Dardoufas, 2019; Rampmeier, 2021; Roesch, 2017; Rosenthal, 2018) and Master's projects (Glasder, 2018; Schneider, 2018) as well as this PhD project. It represents work that was initiated during the Bachelor's thesis of Förstel (2014) and Lausecker (2015) which was followed up over the past 6 years through these numerous subsequent projects. While individual Bachelor's and Master's projects where restricted to the individual locations, this compilation will present a first glance of the thermocline ocean temperature distribution during the past 40 ka using the Li/Mg thermometer.

6.1 Introduction

The ocean has a crucial role in buffering the global heat budget of the earth climate system. During the last glacial the mean sea level was up to 140 m lower (Lambeck *et al.*, 2014), the Atlantic Meridional Overturning Circulation (AMOC) was more shallow (e.g. Rahmstorf, 2002; Böhm *et al.*, 2015) and northern hemisphere ice sheet extend was large (Batchelor *et al.*, 2019) resulting in a global increase in salinity. As a consequence, the deep ocean became haline straified (Adkins *et al.*, 2002). Recently, Bereiter *et al.* (2018) studied noble gases in ice cores and determined the mean global ocean temperature increase during the last glacial transition to 2.57 ± 0.24 °C. The ocean, however, is highly heterogenic with respect to its internal temperature both in latitudes and water depths. While temperature changes in the deep ocean are small at about 2 - 3 °C (Bereiter *et al.*, 2018; Adkins *et al.*, 2002), the upper ocean is more dynamic.

The internal structure of the ocean is strongly impacted by the temperatures and salinities of the water masses. Therefore, quantitative temperature reconstructions of the ocean are important to understand the glacial ocean dynamics. Adkins *et al.* (2002) reconstructed glacial deep ocean temperatures from oxygen isotopic compostitions of pore fluids of deep ocean sediment cores and found similar glacial temperatures near the freezing point of seawater for all deep waters (Atlantic, Pacific and Southern Ocean).

Furthermore, a lot of effort went into the reconstruction of sea surface temperatures (SST) since the last glacial maximum (e.g. MARGO Project Members, 2009), based on measurements of planktonic microfossils. Temperatures of the glacial thermocline ocean are, however, less well constraint.
Here, thermocline water temperatures reconstructed from Li/Mg ratios in CWCs will be discussed for their implications on the internal structure of the ocean flow domain. Therefore, CWC data from six different sites across the Atlantic was compiled, all revealing similar and synchronous temporal patterns. Furthermore, in the last part of the discussion, reconstructed thermocline temperatures will be complemented by compiled coralline radiocarbon data to gain more information on the internal flow patterns of the glacial Atlantic Ocean.

6.2 Materials

Fossil CWCs from six sites across the Atlantic in 330 m to 1250 m water depth and multiple research cruises were analysed for their U/Th age and their Li/Mg temperature. Sampling methods include various devices adjusted to the conditions found at the sample site. A map of the sample sites can be found in figure 6.1. All sample locations can also be found in A.1.
Thirty-four samples from six different dredges were analysed at Galicia Bank off the coast of the Iberian peninsula. Five of these dredges (DR17 (42° 40.866', –11° 36.642', 813 m); DR20 (42° 34.536', –11° 44.262', 806 m); DR23 (42° 48.618', –11° 43.350', 861.5 m); DR19(42° 43.632', –11° 50.232', 796 m); DR22 (42° 39.780', –11° 56.964', 919 m)) were centered around 800 m to 900 m water depth. Twenty-nine of the analysed corals were taken during these dredges, seven samples originated from water depths between 1200 m and 1300 m (DR24 (42° 48.618', –12° 5.148', 1241.5 m)). For further information about the samples the interested reader is refered to Glasder (2018).
Near the Azores, 48 coral samples were collected during various cruises using different sampling gears. Eight samples were recovered during ROV dives and by TV-grabs during RV Meteor research cruise M128 in 2016, 18 samples were recovered during RV Meteor cruise M151 *ATHENA* by a ROV and by grab samplers. The remaining 23 samples were recovered in 2010 during different cruises. Due to the large number of sample origins, precise locations can be found in table A.1. These samples were, in part, already described in Lausecker (2015), Nakajima (2016), Rosenthal (2018) and Rampmeier (2021).
Thirty-one coral samples were analysed from the Great Meteor seamount, about 1000 km south of the Azores near the mid-Atlantic ridge. These samples were recovered

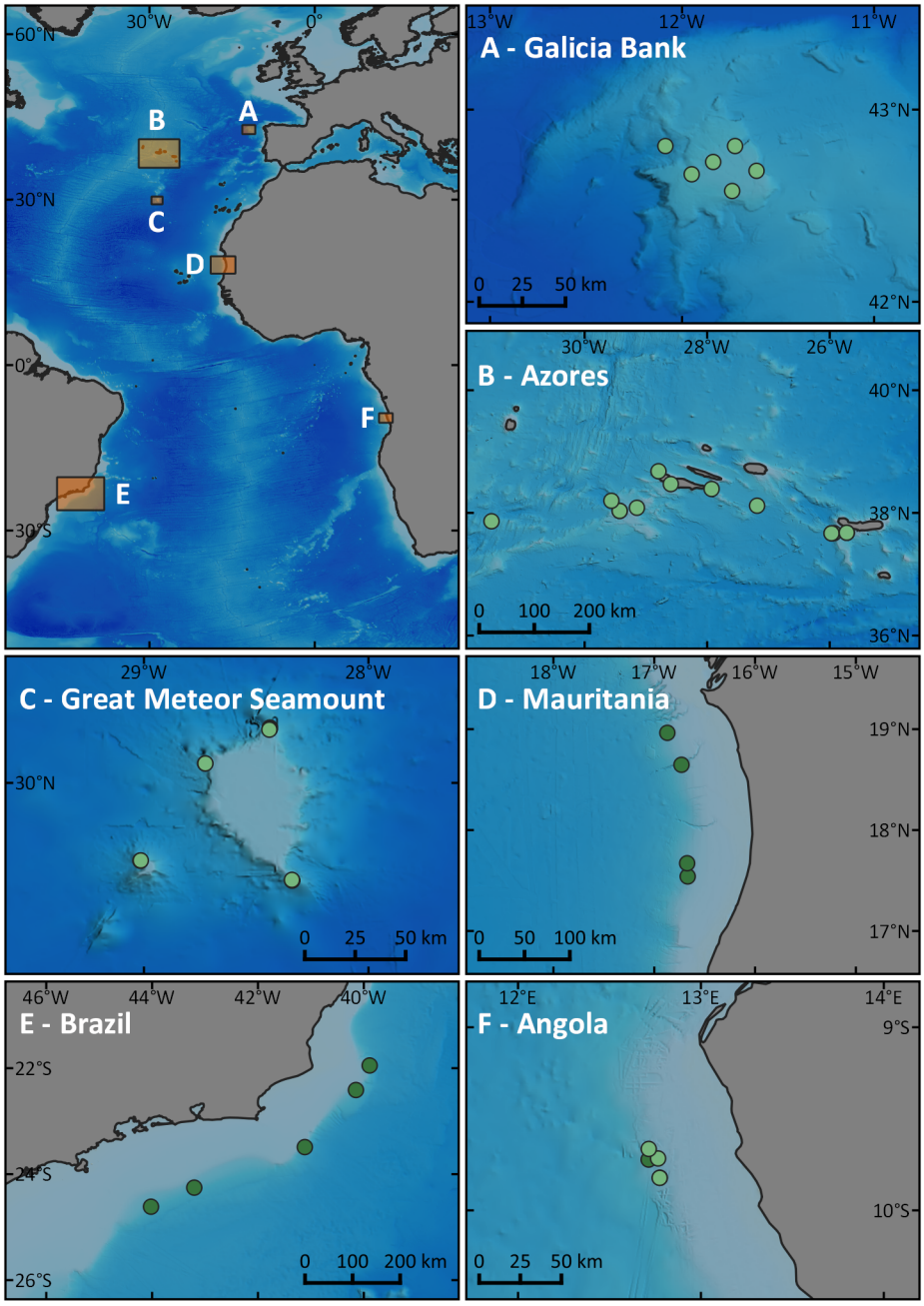

Figure 6.1: Map of all six analysed sample locations. Upper left: Overview over locations in the Atlantic Ocean. Panels A - F: detailed maps of the sample locations. Dark green dots indicate coral bearing sediment core samples, light green dots denote surface samples. The orange boxes in the overview map show area covered in detailed maps (A-F correspondingly).

during research cruise M151 *ATHENA* in 2018 during ROV dives from the northern (GeoB23415-1), north-western (GeoB23429-1) and southern (GeoB23425-1) slope of the Great Meteor Bank as well as samples recovered on the northern slopes of the Little Meteor seamount in close proximity. Here, samples were recovered during a

ROV-dive (GeoB23434-1) and by a grab sampler (GeoB23436-1 and GeoB23437-1). Precise locations can be found in table A.1. Detailed description of the samples can be found in Dardoufas (2019) and Rampmeier (2021).
Off the coast of Mauritania four gravity cores were analysed (n = 31 CWC samples). GeoB14905-2 (17° 32.456', –16° 39.999') and GeoB14884-1 (18° 57.803', –16° 52.123') and GeoB14899-2 (17° 40.191', –16° 40.329') were taken in 495 m, 492 m and 485 m, respectively. The other core GeoB14890-2 (18° 38.792', –16° 43.698') originates from 580 m water depth. These samples were already analysed and described in Schneider (2018).
On the shelf off Brazil, 20 CWC samples from five coral-bearing sediment cores from two different research cruises were sampled. Cores C1 (–22° 24.767', –40° 8.683', 621 m), K–GLC–PPT-06 (–23° 29.450', –41° 06.667', 626 m), C2 (–24° 15.400', –43° 12.100', 781 m) and MXL–030 (-24° 37.567', –44° 01.150', 808 m) are piston cores. These cores are already further discribed in Mangini *et al.* (2010) and Ruckelshausen (2013). The coral bearing gravity core M125-34-2 (–21° 56.957', –39° 53.117', 866 m) was obtained during research cruise M125 *SAMBA*.

6.3 Results

Two hundred and thirty-four coral samples from six locations spread over the Atlantic were analysed for their Li/Mg ratio in order to reconstruct thermocline water temperatures (see appendix B and fig. 6.2). For the description of the results, the six locations will be viewed individually starting in the North Atlantic moving to the south (see figure 6.1).

Thirty-four CWCs sampled at Galicia Bank off the coast of the Iberian peninsula revealed one sample from the LGM 21.60 ± 0.05 ka, nine CWCs grew during Termination I between 14.98 ± 0.03 ka and 11.74 ± 0.04 ka and mostly Holocene ages (1.09 ± 0.01 ka to 0.081 ± 0.002 ka; n = 31) (Glasder, 2018). There are two ranges of water depth that need to be considered seperately: For corals ranging between 800 m and 900 m water depth Li/Mg ratios between 2.74 ± 0.03 mmol mol^{-1} and 4.63 ± 0.08 mmol mol^{-1} were measured. Reconstructed thermocline temperatures are 3.16 ± 1.0 °C for the LGM coral, vary between 7.4 ± 1.0 °C and 11.7 ± 1.5 °C during Termination I (n = 8) and are between 9.4 ± 1.2 °C and 13.9 ± 1.3 °C (n = 17) with one exception at 0.71 ± 0.02 ka (3.7 ± 1.0 °C) during the Holocene. Corals in the lower depth range of 1200 m to 2000 m are all from the Holocene (n = 10) with one exception at an age of 14.01 ± 0.03 ka. The Li/Mg ratio of the older sample was determined to 4.22 ± 0.05 mmol mol^{-1}, while Li/Mg

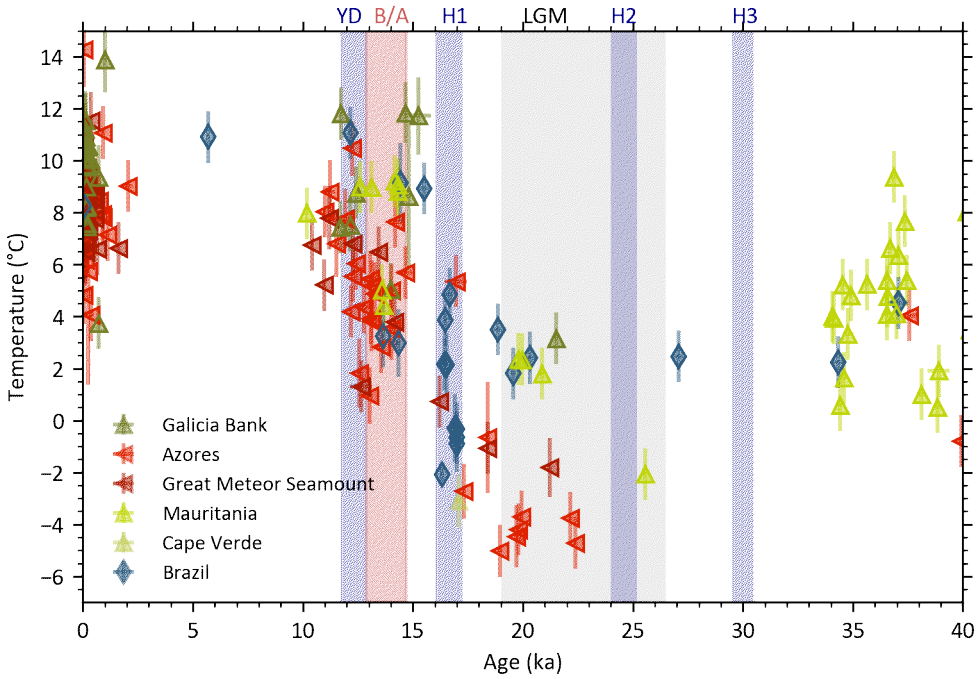

Figure 6.2: All compiled results from the six locations studied here. Heinrich events and the Younger Dryas are indicated by the blue shaded areas. Furthermore, the Bølling-Allerød stadial is marked in red and the LGM in grey.

ratios between 2.74 ± 0.04 mmol mol^{-1} and 3.92 ± 0.04 mmol mol^{-1} were measured for the Holocene CWCs. This corresponds to reconstructed ThWT of 5.1 ± 1.0 °C for the 14 ka year old CWC and a reconstructed temperature 6.6 ± 1.0 °C to 13.9 ± 1.3 °C for the Holocene CWCs.

Fourty-eight different CWC samples were analysed from the region south of the Azores archipelago. The two oldest samples were determined to an age of 39.9 ± 0.1 ka and 37.6 ± 0.3 ka and a subsequent large gap of sample ages with the third oldest coral at 22.4 ± 0.1 ka. Most of the analysed CWCs (n = 30) are between 22.4 ± 0.1 ka and 11.0 ± 0.1 ka old, followed by a cluster of CWCs (n = 16) that grew during the past 2.1 ± 0.2 ka. Li/Mg ratios were measured between 2.69 ± 0.05 mmol mol^{-1} and 6.95 ± 0.16 mmol mol^{-1}. This translates into reconstructed temperatures between -5.1 ± 1.0 °C to 10.5 ± 1.0 °C for CWCs older than 11.2 ka and are between 4.1 ± 1.0 °C and 14.3 ± 1.4 °C for CWCs younger than 2.1 ka. These reconstructed temperatures are, in part, physically unreasonable. This will be discussed in section 6.4.1.

Coral samples from the Great Meteor Seamount reveal ages between 21.2 ± 0.04 ka and 0.08 ± 0.01 ka in two main time ranges. The older samples are between 21.22 ± 0.04 ka and 10.41 ± 0.07 ka old (n = 10), while younger samples are found for the last

1.61 ± 0.02 ka (n = 21). Measured Li/Mg ratios range between 3.07 ± 0.05 mmol mol^{-1} and 5.91 ± 0.16 mmol mol^{-1}. This converts into temperatures between -1.8 ± 1.1 °C and 7.8 ± 1.2 °C for CWCs older than 10.41 ka and into temperatures between 6.1 ± 1.0 °C and 11.5 ± 1.1 °C for CWCs younger than 1.6 ka.
A data set of 31 CWCs in the analysed time range of the last 40 ka was compiled from the Mauritanian margin. Ages range between 39.05 ± 0.10) ka and 10.23 ± 0.03 ka, with the majority of coral ages between 39.05 ± 0.10 ka and 34.18 ± 0.09 ka (n = 20) (Schneider, 2018). The CWC samples recovered from shallower water depths between 492 m and 495 m showed Li/Mg ratios between 3.42 ± 0.03) and 4.95 ± 0.05 mmol mol^{-1}, while Li/Mg ratios of CWC samples collected from 580 m to 590 m water depth were measured at 3.66 ± 0.06 mmol mol^{-1} to 5.99 ± 0.11 mmol mol^{-1}. This translates into reconstructed temperatures of 1.8 ± 1.0 °C during the LGM to 9.4 ± 1.0 °C during the Bølling-Allerød stadial 14.7 ka to 12.9 ka) for the shallower CWC samples and into temperatures between -2.1 ± 1.0 °C and 9.0 ± 1.0 °C for the deeper samples.
On the western boundary of the Atlantik, 20 different CWC samples from the shelf of Brazil were sampled. The shallowest samples were recovered from 621 m to 626 m water depth and span coral ages between 27.1 ± 0.2 ka and 14.4 ± 0.3 ka (n = 5). For these CWCs, Li/Mg ratios between 3.33 mmol mol^{-1} and 4.95 mmol mol^{-1} were measured. This corresponds to reconstructed temperatures of 1.8 ± 1.0 °C to 9.9 ± 1.0 °C. Six samples were collected in a water depth between 781 m and 808 m and cover ages between 37.06 ± 0.45 ka and 5.69 ± 0.07 ka. Li/Mg ratios of 3.17 ± 0.05 mmol mol^{-1} to 5.99 ± 0.05 mmol mol^{-1} and, thus, reconstructed temperatures of - 2.08 ± 1.0 °C to 10.9 ± 1.0 °C were determined [1]. These samples were analysed at the LSCE in Gif-sur-Yvette, France. The deepest samples origin from a water depth of 866 m and revealed ages between 17.00 ± 0.12 ka and 13.65 ± 0.06 ka (n = 10). Li/Mg ratios for these CWCs were measured to 4.26 ± 0.06 mmol mol^{-1} to 5.65 ± 0.16 mmol mol^{-1}. This converts into reconstructed temperatures of - 0.9 ± 1.1 °C to 4.9 ± 1.0 °C.

Twenty-five of these corals from various locations, were sampled at least twice for Li/Mg analysis (see appendix B). Twenty-three of these agree well with each other within $2\,\sigma$ uncertainty. Only two CWCs from the Azores have larger deviations. The mean reproducibility of these samples is ± 0.9 °C ($2\,\sigma$) and, thus, within the uncertainty that can be achieved using the calibration curves (Montagna *et al.*, 2014; Cuny-Guirriec *et al.*, 2019; Stewart *et al.*, 2020).

[1] reported uncertainties here are external uncertainties rather than analytical uncertainties

6.4 Discussion

6.4.1 Qualiy control

Reconstructed thermocline water temperatures (ThWT) during the LGM are extremely cold, reaching down to -5.1 ± 1.0 °C. These temperatures have to be considered in greater detail, as, from a physical point of view, such temperatures cannot be reached in seawater. Due to its mean salinity of about 34.5 psu, the freezing point of seawater is reached at about -1.9 °C. However, even temperatures like -1.0 ± 1.0 °C to -1.8± 1.0 °C, as they were obtained at the Great Meteor Seamount, are highly unlikely to reflect real temperatures during the LGM at this location as temperatures lower than 0 °C are presently only found in polar regions or bottom waters at abyssal depths (e.g. Antarctic Bottom Water).

There are different reasons that need to be considered for these physically non-reasonable temperatures. As already described in chapter 5.4, one reason for changes in coralline Li/Mg ratios could be changes in seawater Li or Mg concentrations. This is, as described before, highly unlikely on global scales. However, this might have an influence on local scales, as, e.g. hydrothermal fluids and mud volcano fluids are highly enriched in Li but slightly depleted in Mg with respect to seawater (Hensen *et al.*, 2007; Tomascak *et al.*, 2016). This might especially influence the corals collected near hydrothermal vents like the Menez Gwen hydrothermal vent field near the Azores and will also be discussed in chapter 9. Mud volcanoes are present e.g. in the Golf of Cadiz (e.g. Hensen *et al.*, 2007). Reconstructed temperatures from these sites might have to be considered with caution. Middleton *et al.* (2016) studied the hydrothermal flux variability over the last 50 ka at about 26 °N on the Mid-Atlantic Ridge. Massively increased Fe and Cu deposits in the sediment records between 28 ka and 15 ka indicate an increased hydrothermal flux between the onset of the LGM and the Bølling-Allerød stadial. Similar results were found on the Mid-Atlantic Ridge south of the Azores and in the Pacific on the southern East Pacific Rise and on the Galapagos Microplate hinting towards a globally increased hydrothermal flux during the LGM (Frank *et al.*, 1994; Auffret *et al.*, 1996; Lund *et al.*, 2016; Middleton *et al.*, 2016). This, however, cannot explain extremely low temperatures found near Mauritania, Cape Verde and Brazil, as no sources for hydrothermal fluids are present in these regions.

Another argument might be, that the empirically determined calibration curve for Li/Mg needs revision. In this study, the calibration curve of Montagna *et al.* (2014) is used which is based on a data set of corals that grew in water temperatures between 0.75 °C and 28 °C. However, there is only one data point of very low temperatures below 1.7 °C used in this calibration curve. Recently the calibration curve published

by Stewart *et al.* (2020) focussed, amongst others, on the low temperature regime of the calibration curve and confirmed the result of Montagna *et al.* (2014) within uncertainty. A closer inspection of the low temperature range of the calibration curve shows that for data points below 1 °C mostly Li/Mg ratios above the calibration curve were measured. This might lead to an underestimation of reconstructed temperatures for very cold waters. Hence, a further investigation of the very low temperature regime of the calibration curve is advisable, yet the used calibration curve by Montagna *et al.* (2014) was validated by more recent studies (Cuny-Guirriec *et al.*, 2019; Stewart *et al.*, 2020).

Another important aspect that needs to be considered are coralline vital effects (see chapter 2.3.3). In this study, mostly the reef-building CWCs *Lophelia pertusa* and *Madrepora oculata* were investigated. While these CWCs are, at present, sparsely found in waters as cold as -1.8 °C (Davies *et al.*, 2008), most active reef-building CWC growth is presently found in temperatures between 5 °C and 10 °C (Davies and Guinotte, 2011; Wienberg and Titschack, 2017). During the LGM, temperatures must still have been tolerable for CWC growth, as corals from this time were found on various sites throughout the Atlantic. However, reconstructed temperatures -5 °C to 4 °C) are well below their comfortable temperature range. This might lead to an additional vital effect due to temperature stress affecting the biomineralization process of the coralline skeleton and, therefore, the incorporation of trace metals like Li and Mg. This vital effect would not be reproduced by the calibration curve, as the data sets used for calibration only contain corals that are grown in their preferred temperature range.

As mentioned before (see chapter 5.4), coral diagenesis could also play a role in Li/Mg ratio alteration. Especially diagentic calcite is known to influence the Li/Mg ratio (Cuny-Guirriec *et al.*, 2019). CWCs showing signs of diagenesis are already removed during the quality control of U-series age determination. As U/Ca ratios are much smaller than Li/Ca ratios and Mg/Ca ratios (e.g Raddatz *et al.*, 2014; Montagna *et al.*, 2014), they are more easily altered and are, therefore, thought to be an effective measure for coralline skeleton alteration through diagenetic processes. There are no processes known, yet, to alter the Li/Mg ratio, but not the U composition in CWC skeletons. Furthermore, diagenetic calcite is especially enriched in Mg with respect to coralline aragonite (Cuny-Guirriec *et al.*, 2019). This would lead to an extreme overestimation of reconstructed Li/Mg temperatures and can, therefore, not explain extreme low reconstructed temperatures found in the CWCs.

One last aspect to consider is the influence of organic matter on the Li/Mg ratios of CWC. Organic matter left on the sample after the cleaning process can lead to an alteration of the measured coralline Li/Mg ratio. Cuny-Guirriec *et al.* (2019)

analysed the organic matter in tropical corals and found highly enriched Mg (and to a lesser degree Li) contents in the organic bands. This would also lead to an underestimation of Li/Mg and, therefore, to an overestimation of reconstructed temperatures. Furthermore, Lausecker (2015) and Rampmeier (2021) did show that, if CWC samples are properly mechanically cleaned, acidic and oxidative cleaning does not improve the Li/Mg measurements. Organic matter can, therefore, be excluded as a reason for extremely low reconstructed temperatures found in CWC samples.

Even though there are still open questions concerning the calibration curve and the

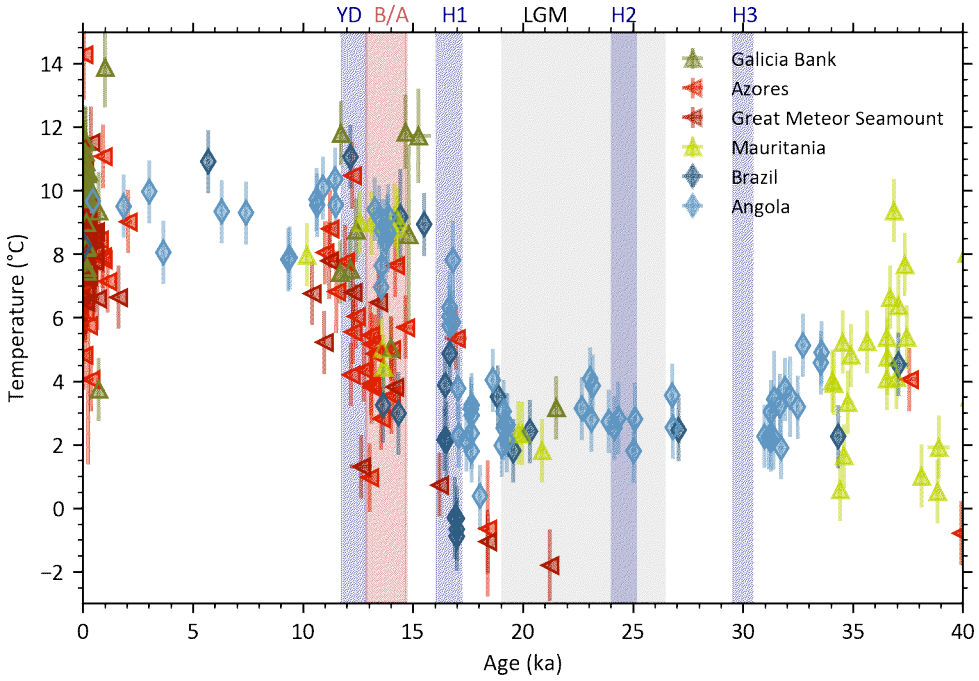

Figure 6.3: All compiled results after the quality control. Heinrich events and the Younger Dryas are indicated by the blue shaded areas. The Bølling-Allerød stadial is marked in red and the LGM in grey.

Li/Mg temperature proxy, a remarkable correlation is found between reconstructed ThWT variations and atmospheric climate patterns, as seen in ice core data (Bazin *et al.*, 2013b,a). This cannot be explained from randomly distributed influences of the different factors mentioned above and, therefore, supports the reconstruction of ThWT using coralline Li/Mg ratios.

Since reconstructed temperatures below -1.8 °C are physically not reasonable as stated above, obtained temperatures $<$ -1.8 °C are excluded from further discussion (n = 10). The same applies to samples known to be collected in close proximity to hydrothermal vents (n = 1) (see figure 6.3).

6.4.2 Polar glacial Atlantic?

The remaining data is assumed to reflect changes in thermocline water temperatures at the different coral sites. Here, the data will be discussed in its entirety, for closer discussion of the single site data, the interested reader is referred to the various Master's and Bachelor's thesis. The Angolan data set will be added to the following discussion (see figure 6.3).

Li/Mg data shows a consistent pattern throughout the entire Atlantic during the LGM and the Holocene. Starting at 40 ka ago, coral data off Mauritania shows a short and strong temperature oscillation of about ± 6 °C coinciding with Dansgaard/Oeschger event 8 (D/O 8). Due to a lack of data, this feature cannot be seen in the other data sets. Subsequently, temperatures are relatively stable at 2 ± 1 °C until the end of the LGM. The last gacial is mostly represented in temperature data from the southern hemisphere (Angolan and Brazilian margin). Contrary to the radiocarbon data (see chapter 5.4), in Li/Mg temperature reconstructions the data of these locations agree well with each other. This indicates that two water masses of different origins but at similar temperatures were present in the eastern and western South Atlantic. Comparing the southern hemisphere data to data from the Gulf of Cadiz in the North Atlantic (Hemsing, 2017) and the Azores, reveals a very similar temperature pattern in the northern hemisphere during the time between the D/O 8 and the LGM (see figure 6.5). No statement can be made on the temperature changes in the Gulf of Cadiz during the deglaciation as CWC growth halts after the LGM.

At the end of the LGM, reconstructed temperatures start to rise in the South Atlantic (see chapter 5.4), simultaneously on the eastern and western margin. Temperatures at the Galicia Bank and off the Mauritanian margin are also at modern day values (10 ± 1 °C and 10 ± 1 °C, respectively (Schlitzer, 2020)) about 15 ka ago. This might hint towards an early rise in temperatures at these locations as well, but missing CWCs prevent statements on the exact timing of the local temperature increase. Temperatures off Angola stay at modern day values between the Bølling-Allerød stadial and the Younger Dryas. In contrast, temperatures off Mauritania, off Brazil and at the Galicia Bank drop by 4 °C to 5 °C for about 1000 ± 500 years before recovering and reaching modern day values after the Younger Dryas cold reversal.

Temperatures at the Great Meteor Seamount and off the Azores, on the other hand, seem to stay at lower values, oscillating between about 3 °C and 6 °C until the end of the Younger Dryas when they first reach modern day values 8.5 °C to 10 °C in 800 m to 900 m water depth (World Ocean Atlas 2018, Schlitzer, 2020)). Near the Azores Front, where the subpolar and subtropical waters meet, a large scatter of reconstructed temperatures is also observed the last 250 years, when CWCs collected in water depths

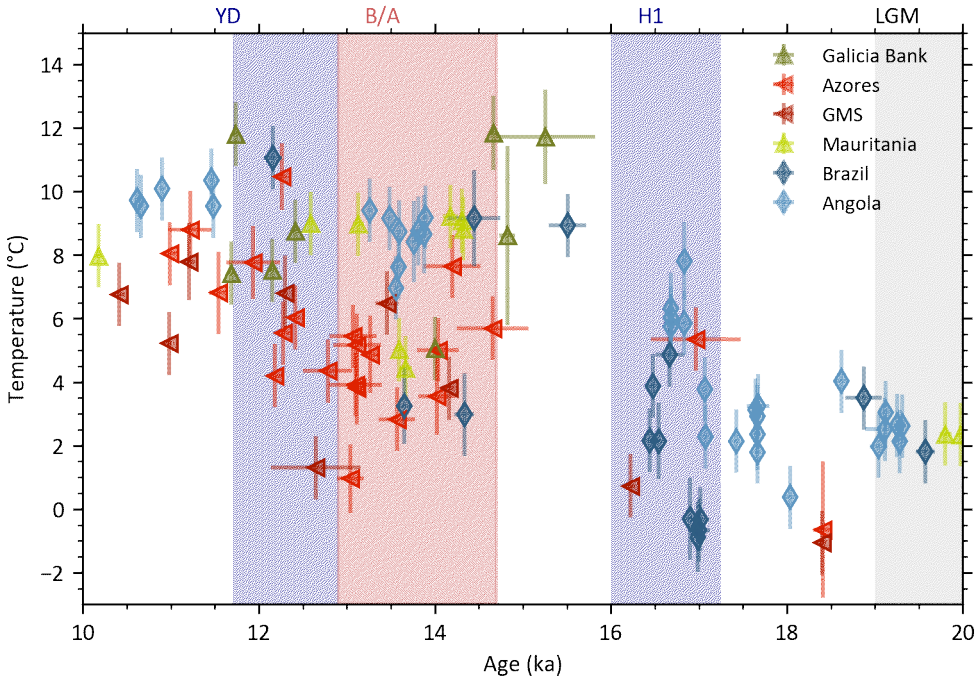

Figure 6.4: Compiled results in the time period between 10 ka and 20 ka. Heinrich events and the Younger Dryas are indicated by the blue shaded areas. The Bølling-Allerød stadial is marked in red and the LGM in grey.

between 300 m and 400 m reveal a mean reconstructed temperature of 8.9 ± 6.6 °C. Similar to the reconstructed temperatures off Angola, published Holocene data from the Rockall Bank (Bonneau *et al.*, 2018) reveal only minor temperature variability (7.7 ± 1.0 °C) for the last 8 ka in the eastern North Atlantic (see figure 6.5). This shows that, apart from locations near oceanic fronts, seawater temperatures are unlikely to change detectable by the Li/Mg method during the Holocene.

However, apart from these local dynamics a strong glacial-interglacial trend is visible in all analysed data. While temperatures are highly variable and similar in the North Atlantic 1.4 ± 2.5 °C) and the South Atlantic 2.5 ± 2.2 °C) during the last glacial 27 ka to 17 ka), they differ to about 1.7 ± 1 °C during the Holocene. This is in good agreement with modern seawater temperatures at the respective study sites (Schlitzer, 2020). While CWCs from the Angolan and Brazilian margin show a synchronous rise in temperature, northern hemisphere corals do not show a coherent pattern of temperature increase. This might hint towards a separation through oceanic frontal lines of the temperature increase rather than a northern-southern hemisphere division. Furthermore, coral samples off Mauritania and off Morocco show only minor to no coral growth during the termination and the Holocene. This was associated to a decrease in

local upwelling strength, resulting in a decrease in food availability (Wienberg *et al.*, 2010; Eisele *et al.*, 2011). Therefore, no statement can be made on the specific timing of the changes along the eastern basin boundary.
After the Younger Dryas corals start to flourish further north at Rockall Bank. Little to no coral growth was observed during the termination here to provide information on the thermal evolution of the water masses.
The only northern hemisphere sites able to provide information on the thermal evolution during the termination are the Azores region and sparsely scattered samples from the Galicia Bank. These samples might hint towards an early increase in temperature on the eastern basin boundary during H1, reaching modern day values at the end of H1. Meanwhile, coral samples off the Azores are indicative of warm and cold water masses oscillating along the Azores Front throughout the termination. Temperatures hereby follow northern hemisphere perturbations e.g. major Atlantic freshwater influxes causing the Younger Dryas (e.g. Broecker *et al.*, 1988; Keigwin *et al.*, 1991) until modern day temperatures are reached at about 11.5 ka.
The consistency of temperature reconstructions from the southern and northern Atlantic during the last glacial might hint towards an Atlantic wide glacial cooling rather than a local phenomenon as described for corals off Angola (see chapter 5). As presented before, these similar patterns across the northern and southern Atlantic cannot be explained by changes in seawater Li/Mg ratios or coralline vital effects. Therefore it is proposed, that changes in ocean dynamics are causing the observed temperature patterns.
A potential first mechanism to explain the observed temperature variations might be an increase in upwelling strength. Increased upwelling can provide nutrients and, thus, food to the corals in thermocline water depths (e.g. Wienberg *et al.*, 2010). This is well documented for the coral regions e.g. off Mauritania and off Morocco, were nutrient (and oxygen) depleted waters recently prevent coral growth (Mienis *et al.*, 2012; Glogowski *et al.*, 2015; Ramos *et al.*, 2017; Wienberg *et al.*, 2018). However, no upwelling is observed near the lines of zero Ekman pumping in the Azores region and the Galicia Bank.
As described before for the Angolan margin (see chapter 5.4), upwelling does not only provide nutrients to shallower water depths but also cooler water masses. This would explain the observed increased cooling in thermocline water masses. However, increased cooling would also be observed in surface waters showing a temperature drop similar to that found for thermocline waters. Such a strong glacial cooling was not found in SST reconstructions in subtropical regions. SST anomalies in these regions are in the order of 2 °C to 4 °C (MARGO Project Members, 2009; Schneider *et al.*, 1996; Penaud

et al., 2011; Annan and Hargreaves, 2013), which is about half the temperature drop observed in thermocline waters. Thus, increased upwelling cannot be the sole reason for glacial cooling at the coral locations.

Another possible explanation might by the strengthened flux of polar waters along the mid-depth eastern and western basin boundary in the Atlantic. As described in chapter 5, for the South Atlantic this might be explained by an equatorward displacement of polar waters due to an equatorward shift of the Hadley cell. As the corals off Brazil occur in deeper water depths, cooling at this coral location might even be explained by an enhanced equatorward flow of Antarctic Intermediate Water (AAIW) (Pahnke *et al.*, 2008).

It was shown for the northern hemisphere, that the polar front shifted south during the LGM and H1 letting subpolar and arctic waters advance towards the Galicia Bank respectively (Eynaud *et al.*, 2009; Penaud *et al.*, 2010, 2011). Additionally, the Azores Front dividing subtropical and subpolar waters in the North Atlantic, was displaced to the south (Keffer *et al.*, 1988; Rogerson *et al.*, 2004; Schwab *et al.*, 2012). This promotes the advance of subpolar waters as far south as the Azores.

This equatorward advection of polar waters during times of reduced AMOC strength seems most reasonable to explain the synchronous North and South Atlantic thermocline glacial cooling. Though, the cooling most likely has different origins in the north and south. This however, cannot be traced using Li/Mg temperature reconstructions. Furthermore, the absolute values of cooling might need revision, due to different influences on the Li/Mg thermometer as discussed above.

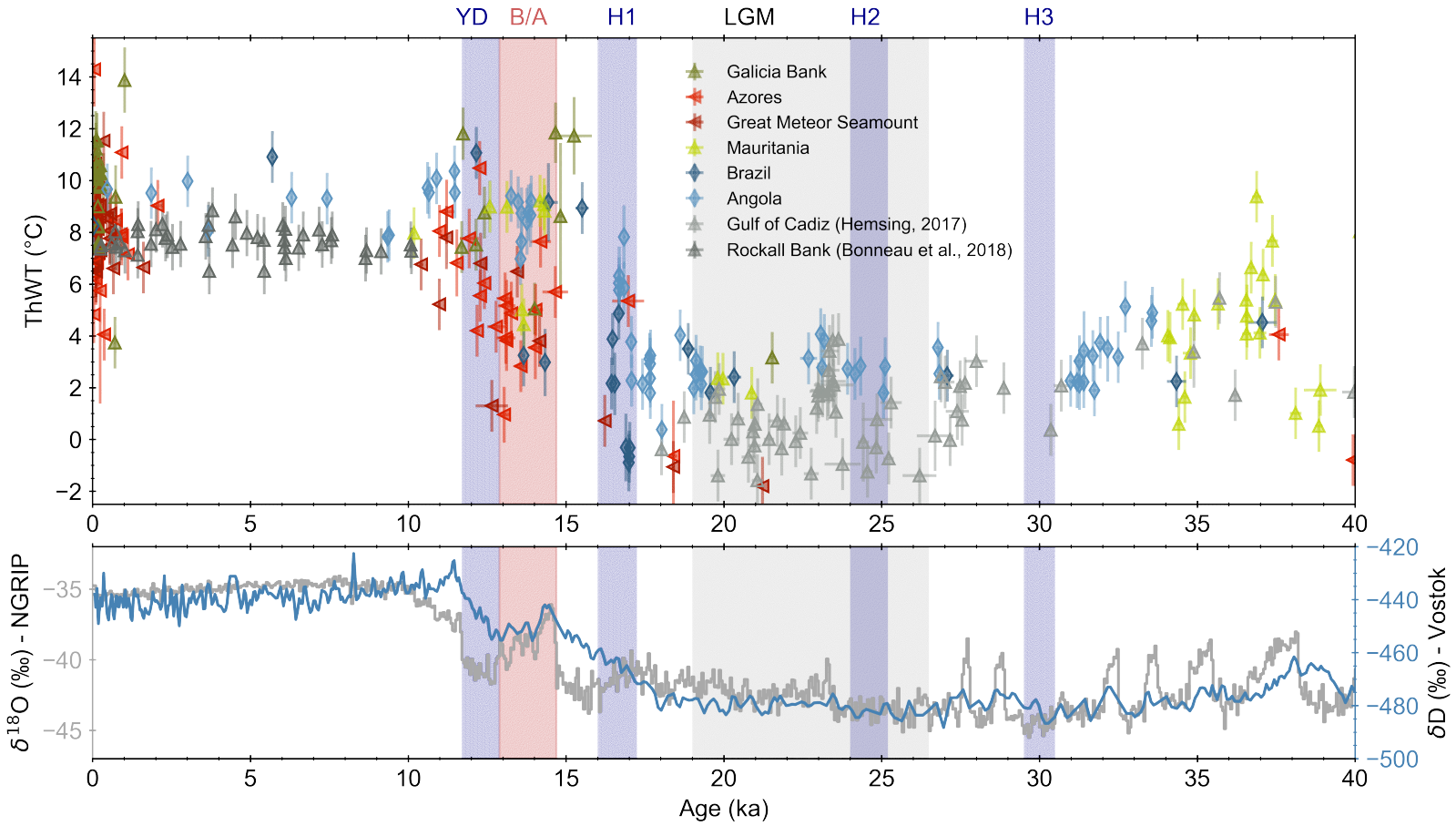

Figure 6.5: Li/Mg results in comparison to published data and ice core data. Upper panel: Compiled Li/Mg temperature data. Published data is given additionally given as grey triangles (data from Hemsing (2017) is given in lightgrey, Bonneau *et al.* (2018) is given in dark grey). Lower panel: Atmospheric climate development over the last 40 ka from the Greenlandic (NGRIP, Bazin *et al.*, 2013a) and Antarctic (Vostok, Bazin *et al.*, 2013b) ice cores. The Last Glacial Maxium is shown as the grey shaded area, the YD and Heinrich stadials are shown as blue bars, the Bølling-Allerød stadial is shown in red.

6.4.3 Do reservoir ages provide further information on the glacial Atlantic water pathways?

As temperature reconstructions are not able to provide any information about the provenance of the waters masses at the different coral locations, radiocarbon data and therefrom derived reservoir ages are discussed in the following section. For the glacial ocean, published CWC data as well as data obtained during the Master's thesis of Beisel (2021) from the thermocline Atlantic waters above 1100 m water depth were compiled (see figure 6.6). This depth threshold was applied to solely focus on the upper thermocline water depths from which the CWCs of the temperature study originate.
To obtain further information about glacial thermocline water pathways and to further constrain the origin of cold water masses found in large parts of the Atlantic, coralline radiocarbon ages from 14 studies were compiled (Burke and Robinson, 2012; Robinson and van de Flierdt, 2009; Chen *et al.*, 2015; Schröder-Ritzrau *et al.*, 2003; Frank *et al.*, 2011; Mienis *et al.*, 2009; Adkins, 1998; López Correa *et al.*, 2012; Douarin *et al.*, 2016; Hemsing, 2017; Beisel, 2021; Mangini *et al.*, 1998; Ruckelshausen, 2013; Mangini *et al.*, 2010). To compare the coralline data to modern seawater data, the GLODAP-database (Olsen *et al.*, 2019) and a North Atlantic seawater study by Miltner (2020) were referred to.

As described before (see chapter 5.4), the south-eastern Atlantic thermocline waters become continuously less ventilated during the LGM. This pattern extents to the northern equatorial Atlantic, where CWC data shows the same $\Delta^{14}C$ values. CWCs off Brazil revealed heavily aged thermocline waters for the western South Atlantic during the LGM (Mangini *et al.*, 2010; Ruckelshausen, 2013). However, these $\Delta^{14}C$ values are explained through a strongly depleted saline deep water mass, isolated from the atmosphere for thousands of years. Such a depleted water mass has never been identified in the Southern or Pacific Ocean (Hain *et al.*, 2011). As the about 3800 year old deep Southern Ocean reveals a $\Delta\Delta^{14}C$ of about -120 ‰(Skinner *et al.*, 2010), and therefore less negative than the mid-depth anomalies, the existence of such a highly depleted water mass is unlikely (Hain *et al.*, 2011; Adkins, 2013). Thornalley *et al.* (2015), however, analysed foraminifera in the deep Arctic Ocean and the Nordic Seas and found ventilation ages of up to 10000 years. Therefore, extremely poor ventilated water masses on the western basin boundary might be a result from Arctic waters propagating towards the south. As no further data is available from the western margin, this hypothesis, however cannot be proved yet.
For the North Atlantic, thermocline CWC data is mainly available from the eastern Atlantic margin. Furthermore, data is mostly missing from 17 ka to 15 ka BP. However, it is clearly visible, that thermocline waters are better ventilated in the North Atlantic

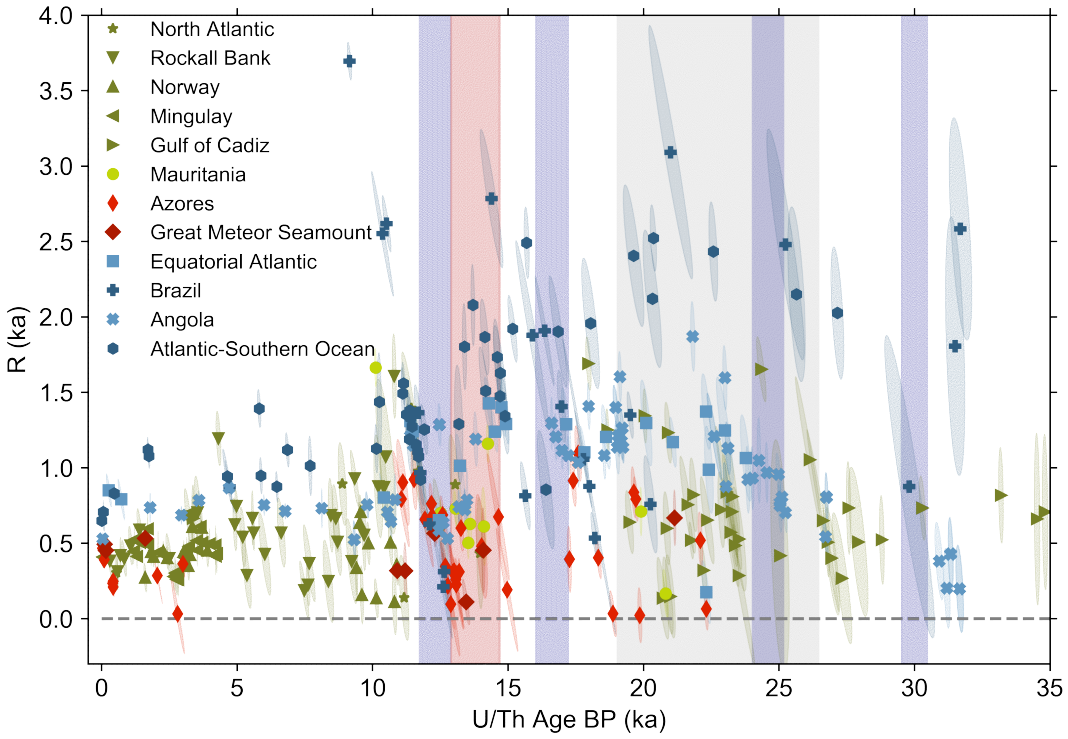

Figure 6.6: Compiled CWC $\Delta^{14}C$ data of the upper Atlantic <1100 m water depth. Original datasets can be found in the following publications: general North Atlantic (Schröder-Ritzrau *et al.*, 2003; Cao *et al.*, 2007), Rockall Bank (Frank *et al.*, 2011; Mienis *et al.*, 2009), Norway (López Correa *et al.*, 2012), Mingulay (Douarin *et al.*, 2016), Gulf of Cadiz (Hemsing, 2017), Mauritania, Azores and Great Meteor Seamount (Beisel, 2021), equatorial Atlantic (Chen *et al.*, 2015; Mangini *et al.*, 1998), Brazil (Ruckelshausen, 2013; Mangini *et al.*, 2010), Angola (Roesch, 2017; Beisel, 2021), Southern Ocean (Burke and Robinson, 2012). The Last Glacial Maxium is shown as the grey shaded area, the YD and Heinrich stadials are shown as blue bars, the Bølling-Allerød stadial is shown in red.

compared to the South Atlantic at the end of the last glacial. Nevertheless, short appearences of aged waters can be found e.g. in the Golf of Cadiz during the LGM, which was interpreted as short periods of inreased Eastern Antarctic Intermediate Water (EAAIW) influences in the Golf of Cadiz (Hemsing, 2017) and was also traced in Nd isotopes (Dubois-Dauphin *et al.*, 2016).

After the YD, data from the Rockall Bank seems to indicate a steady increase in ventilation until reaching its modern day state at about 10 ka ago (Mienis *et al.*, 2009; Frank *et al.*, 2011), while CWC data off Norway, further north, record well ventilated waters since the Younger Dryas (López Correa *et al.*, 2012). Unfortunately, no glacial data is available from this location.

Data from the Azores region and the Great Meteor seamount show mainly well venti-

lated waters with larger variation between the end of the Holocene and Termination 1. Despite missing data between the start of H1 and the B/A, CWCs in this region record well ventilated waters during the LGM as well as during the B/A stadial. Only during the Younger Dryas a 'dip' towards lesser ventilated waters is found before the water masses show a well ventilated signal again. As seen before in the temperature data, large variability is also found in $\Delta^{14}C$ values from the Azores region. This further hints towards a strong influence of the Azores Front on this region. Sparsely scattered data from off Mauritania does also show a mainly well ventilated water body from the LGM to the YD. Solely one coral after the YD shows poorly ventilated waters at the CWC location. Since there is only one coral showing poor ventilated waters off Mauritania, this will be discarded from further discussion to prevent over interpretation.
The combination of data of all locations all over the Atlantic leads to a bigger picture of the glacial ventilation. While reservoir ages in the southern Atlantic are significantly increased and show major variation during the LGM and Termination 1, corals in the subtropical North Atlantic show an overall well-ventilated thermocline water mass.

When comparing the modern seawater data from the South Atlantic (Olsen *et al.*, 2019) to the modern CWC radiocarbon measurements as described before (see chapter 5; Beisel, 2021), the data agrees well revealing a well ventilated south-east Atlantic. The same applies to the south-west Atlantic as seen in the GLODAP-compilation (Olsen *et al.*, 2019).

Miltner (2020) studied radiocarbon in North Atlantic seawater on a North-South transect between Iceland and the Great Meteor seamount at 25 °W. Well ventilated, bomb-testing influenced waters where found throughout the upper 500 m water depths. Between 500 m and 1500 m water depth of the studied corals in the North Atlantic were found, a clear distinction can be made in the radiocarbon content of the analysed seawater. While North of the Azores the bomb-testing influence on the radiocarbon content is clearly visible in the mid-depth ocean, the thermocline waters at the Great Meteor seamount are depleted in radiocarbon (see figure 6.7). The line of distinction therefore seems to be at the Azores Front (Miltner, 2020). This shows a clear influence of the Azores Front on the seawater pathways and ventilation in the North Atlantic at present time.
Overall, the modern Atlantic is well ventilated at all locations, however a clear distinction between the waters north and south of the Azores Front as manifested by the influence of bomb-testing on the radiocarbon content can be made.
The combination of modern and glacial radiocarbon data might hint towards a large-scale influence of the Azores Front on the Atlantic thermocline water pathways in

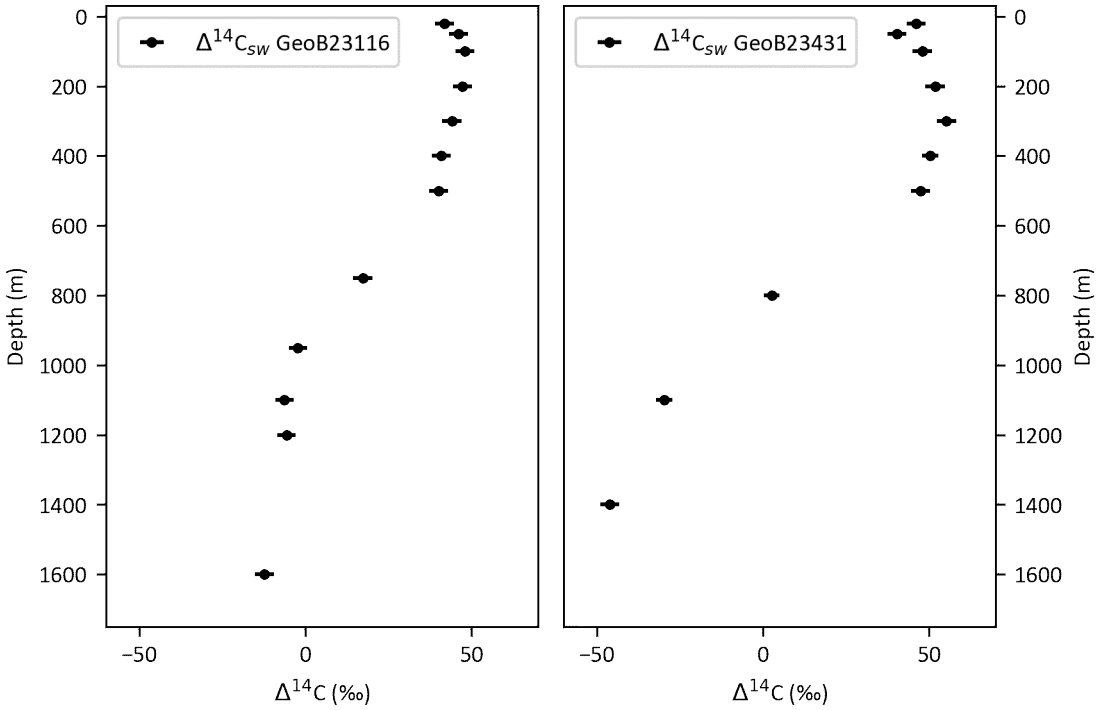

Figure 6.7: Comparison of seawater $\Delta^{14}C$ data north (GeoB23116) and south (GeoB23431) of Azores Front. North of the Azores Front. While north of the Azores Front, the profile shows bomb influence throughout, south of the Azores Front, the mid-depth water masses are not yet influenced by bomb produced ^{14}C (data from Miltner (2020)).

present times as well as during the LGM. The better ventilated separation line between poorer ventilated water masses does not seem to occur between the hemispheres but at the Azores Front. Furthermore, the glacial reconstructed temperatures discussed here are unlikely to have the same origin, but rather originate from the northern and southern polar regions. To acquire even more information about the detailed provenance of the glacial water masses an additional water mass tracer like ϵ_{Nd} would be helpful. First indications of northward propagating southern hemisphere waters have been identified through this proxy by Dubois-Dauphin *et al.* (2016). A recent study by Lütkes (2021), however, shows a complex picture of the thermocline ocean Nd isotopic composition possibly also related and influenced by regional isotope exchange along active spreading ridges. Hence, a confirmation of the water mass pathways and heat transport proposed here may be only achieved through climate models.

6.5 Conclusions

Reconstructed Li/Mg temperatures of 234 CWC from various locations throughout the Atlantic revealed similar and synchronous temporal patterns coinciding with atmospheric ice core data. Temporal changes in temperatures are systematic and cannot be explained by vital effects, diagenesis, incorporated organic matter or changes in seawater Li/Mg ratios as these would produce more randomly distributed data. Therefore, the presented CWC temperature data is assumed to reflect changes in thermocline water temperatures (ThWT). During the LGM ThWT are at similar low values of about $2 \pm 1\,°C$ in the North and South Atlantic. While temperatures in the South Atlantic start to rise at the beginning of H1, coinciding with the Vostok ice core, CWC in the North Atlantic disappear and reappear at modern day temperatures just before the Bølling-Allerød stadial at about 15 ka. CWC data near the Azores Front shows a different pattern as temperatures stay relatively low and highly variant during the termination 1 until modern day temperatures are observed just after the Younger Dryas at about 11.5 ka. A reasonable explanation for the glacial cooling is the equatorward advection of polar waters.

To obtain further information on the origin of the water masses and their pathways reservoir ages were obtained through coralline radiocarbon ages. These seem to confirm the hypothesis of polar water advection as water masses in the South Atlantic become poorer ventilated during the LGM. Coralline radiocarbon data near the Azores Front reveal better ventilated northern sourced water masses. Furthermore reservoir ages during the glacial and the deglacation are highly variable, while Holocene reservoir ages are more stable. Hence, the variability of the ocean interior decreased since the LGM simultaneously with a depending of the thermocline due to the global warming and deglaciation. A comparison between coralline paleo- and modern seawater $\Delta^{14}C_{sw}$ data further hints towards a strong influence of the Azores Front on the Atlantic thermocline water pathways.

Part II

Li-isotopes in cold-water corals

7 Introduction

The Li/Mg ratio of CWCs provides a promising paleothermometer, as seen in chapter 6. But at times Li/Mg ratios in CWCs are particularly high resulting in physically unreasonable low reconstructed temperatures. The reason for these low temperatures are not yet understood. An altered Li concentration of the seawater might be one explanation. As the concentration of Li in seawater (∼180 ppb) is four orders of magnitude lower than the concentration of Mg (1.2 ‰). Thus, it is more likely to be altered through natural sources. As the primarily sources of lithium to the oceans highly differ in the δ^7Li signature, an additional input of lithium should also alter the isotopic composition of seawater and, thus, of carbonate skeletons precipitated from seawater.

Global changes in seawater lithium concentrations can be excluded, as extremely low temperatures are only found in particular locations like the Azores or the Gulf of Cadiz. Furthermore, Hall *et al.* (2005) and Cuny-Guirriec (2020) found constant δ^7Li values in foraminifera in the North Atlantic and CWCs in the Mediterranean Sea, respectively, arguing against a change in global Li concentrations on glacial/interglacial timescales. Increased local input of lithium into the ocean might, however, occur. As the continental weathering input through river and ground water discharge as well as hydrothermal vent fluids are by far the largest Li sources to the ocean, these have the highest potential to alter the local Li concentration and isotopic signature.

In the following chapters, this potential alteration in the Li isotopic signature will be investigated. Therefore, in a first step, the extraction of Li from the samples and the measurements of the Li isotopic signature on a MC-ICP-MS will be established (see chapter 8). Afterwards six samples from the Azores region will be analysed for their δ^7Li values and their specific Li isotope fractionation with respect to seawater. These samples were selected for their previously measured Li/Mg ratio and ϵ_{Nd} signature. No major river estuaries are present near the samples locations in the middle of the Atlantic. Instead, hydrothermal fluids are present near the mid-Atlantic ridge and can have a potential influence on the local Li concentration and δ^7Li signatures, thus, potentially influencing the Li/Mg thermometer in CWCs. This hypothesis will be tested in chapter 9.

8 Lithium isotopic analyses of cold-water corals

8.1 Introduction

In the following chapter the extraction of Li from carbonate and seawater samples and the subsequent measurement on an MC-ICP-MS will be described and discussed. Lithium isotope measurements using an ICP-MS are affected by the presence of matrix elements of the sample, i.e. Ca, Na and Sr. This results in changes of the ionization equilibrium in the ionising plasma, when matrix elements, i.e. non-analytes are ionised. Therefore, it is crucial to purify the samples solution before measurements. For marine samples it is especially important to separate Na and Ca from the samples to avoid matrix-induced effects (Misra and Froelich, 2009). Hereby, the separation of lithium from Na is rather difficult as both elements get extracted in close proximity during the purification process using an ion exchange column. Furthermore, rather strong fractionation occurs during the purification of lithium requiring a yield close to 100 %. Here, a single step separation of lithium from Na is tested following the protocol by Misra and Froelich (2009). In a second step, a measurement routine on the MC-ICP-MS is established and the reproducibility of sample measurements is tested.

8.2 Materials

Multiple different sample and standard solutions were used to establish a sample preparation and a mass spectrometric measurement routine for δ^7Li measurement in corals. The Li concentrations and isotopic composition are given in table 8.1.

Experiments to set up the chemical preparation and purification methods were mainly performed on the CWC specimen ICECTD PL501-6 C4 (HD Lab. No. 6118, 63.075 °N, 24.431 °W, 316 m). The same specimen is used as a reference coral for Li/Mg measurements (see chapter 4.3. Furthermore, Li extraction using ion exchange resins were obtained for seawater using seawater sample GeoB18154-1 (35.24975°N, 7.08380° ´W, 890 m water depth) from coastal waters off Morocco in the Atlantic Ocean

Table 8.1: Li concentration and isotopic signature of reference materials used to establish a δ^7Li preparation and measurement routine.

Material	Li conc.	δ^7Li
corals	1 ppm	17 -25 ‰ [1]
seawater	180 ppb	28.9 - 33.4 ‰ [2]
JCp-1	380 ppb [3]	18.8 ± 1.8 ‰ [4]
		20.2 ± 0.2 ‰ [5]
		20.3 ± 0.4 ‰ [6]
		17.0 ± 0.4 ‰ [7]
IRMM-016	18.8 % [8]	0.4018 ± 0.0016 ‰ [9]
Elemental solution	1000 ppm	

[1] Rollion-Bard *et al.* (2009)
[2] Carignan *et al.* (2004)
[3] Inoue *et al.* (2004)
[4] Bastian *et al.* (2018)
[5] Huang *et al.* (2010)
[6] Bohlin *et al.* (2017)
[7] Lin *et al.* (2019)
[8] Calculated from sample material being Li_2CO_3
[9] Calculated from the certified δ^6Li/δ^7Li ratios of the reference material IRMM-016 and LSVEC given in Qi *et al.* (1997).

(Hebbeln *et al.*, 2015).
Furthermore, tropical reference coral JCp-1 was analysed for interlaboratory comparison. JCp-1 is a coral of species *Porites* collected off the northeastwern coast of Japan. It is certified for major components like strontium, Na and magnesium. However, this reference material was previously also used for studies of its Li/Mg ratio and δ^7Li value by different authors (e.g. Montagna *et al.*, 2014; Bastian *et al.*, 2018; Bohlin *et al.*, 2017; Huang *et al.*, 2010).
For analytical tests multiple standard materials were used. The Lithium elemental standard from *Inorganic Ventures* was used as a available standard to test reproducibility. The isotopic lithium ratio of this standard is not certified, however, it is used for reproducibilty measurements. To get a larger range of δ^7Li in standards for analytical tests, the elemental standard was artificially modified in its isotopic ratio using the mass dependent isotope fractionation occurring during column chemistry.
As an isotope reference material IRMM-016 was used. This is a lithium carbonate certified to a Li isotopic ratio of $^6\text{Li}/^7\text{Li} = 0.082121 \pm 0.000087$ mol mol^{-1} and, thus, a δ^7Li value of 0.4018 ± 0.0016 ‰ (Qi *et al.*, 1997). The IRMM-016 is also used for mass bias and drift corrections when evaluating the analysis before normalizing the data to the LSVEC reference value when calculating the δ^7Li value.
Once the method was successfully established, first test measurements were performed on modern CWC and seawater samples from different locations in the Atlantic. Bottom water samples, collected using a ROV close to the sea floor were analysed from the Namibian margin (M122, GeoB20505-1, 20.733 °S, 12.817 °E, 232 m; Hebbeln *et al.*, 2017) and the Great Meteor Seamount (M151, GeoB23429-5, 30.086 °N, 28.727 °W, 895 m; -25-4, 29.565 °N, 28.339 °W, 948 m and -34-6, 29.656 °N, 29.013 °W, 757 m; Frank and the scientific crew of M151, 2018). Furthermore, seawater samples collected in the open ocean, i.e. far from the shelf, were also analysed to compare to the seawater δ^7Li values found in the literature. Two seawater samples from research cruise M151 at station GeoB23445-1 (30.904 °N, 23.960 °W) at 600 m and 1000 m water depth were selected for this purpose.
Modern CWC samples were analysed from three different locations. One live-collected *Lophelia pertusa* CWC was obtained from the Icelandic coast during N/O Thalassa research cruise ICE-CTD in 2012 (PL-497-2 A2, 63.874 °N, 13.998 °W, 259 m). One CWC from the Great Meteor seamount was collected during research cruise M151 (29.656 °N, 29.013 °W, 757 m) and the third modern CWC was sampled during research cruise M122 off the margin of Namibia (20.733 °S, 12.819 °E, 230 m).

8.3 Chemical extraction

8.3.1 Purification of Lithium

The chemical extraction and purification of Li from the sample material is necessary to eliminate matrix elemtents that would disturb the ionisation of Li in the plasma and, thus, change the ionisation equilibrium in the plasma (Misra and Froelich, 2009). To achieve the purification, column chromatography using an ion exchange resin, AG 50W-X8, was performed. Here, the single-step separation protocol by Misra and Froelich (2009) (updated in Misra and Froelich (2012)) was adopted. Misra and Froelich (2009) used 5 ml Teflon columns equipped with teflon frits having 2.0 ml resin volumn. The columns were than packed with BioRad AG 50W-X8 (100-200 mesh size) cation exchange resin. In a first step, the columns are pre-washed with 15 ml of 6 M HCl and afterwards back-washed and conditioned with 30 ml of 0.5 M HCl. Now the sample is loaded onto the column in 0.2 ml of 0.5 M HCl and eluted with 15 ml of 0.5 M HCl. The Li fraction is collected in acid cleaned Teflon beakers as the 6 ml to 11 ml eluate fraction.The pre-elution and post-elution fractions are collected for yield determination and to check for bleeding and tailing effects as a yield close to 1 is crucial due to strong isotope fracionation during chromatographic separation (see figure 8.3). The Li fracton is then evaporated to dryness at 80 °C and re-dissolved in 2 ml of 2 % HNO_3 for measurement.
This protocol was tested with different volumes of resin and two different mesh sizes of the BioRad AG 50W-X8 ion exchange resin to achieve the best possible separation of Li and Na, the latter being eluted directly after the Li fraction. In a first step about 400 mg of CWC sample 6118 was thoroughly mechanically cleaned and rinsed in MilliQ water. Then a disposable PP-Beaker was rinsed with 2 M HCl and MilliQ water before the CWC sample was covered in MilliQ water and dissolved in 7 M HNO_3 in the cleaned beaker. After dissolution the sample was evaporated to dryness over night. Lastly, the sample was re-dissolved in 5 ml of 0.5 M HCl. Using this sample solution, elution profiles were obtained to investigate the sorption behaviour at different resin volumns for the chosen column geometry. The Teflon columns used are characterised by a 20 cm long capillary tube with an internal diameter of 4 mm and a reservoir of 15 ml. They are equipped with 30 µm Teflon frits.
The experiments were conducted using two different mesh sizes of the same resin: AG 50W-X8 100-200 mesh and AG 50W-X8 200-400 mesh (see table 8.2). In preparation, the resin was transferred to a Teflon bottle and rinsed three times with MilliQ water until the disposed excess water was clear. Afterwards, the resin was stored in MilliQ water with a water head of about 1 cm above the resin.

Table 8.2: Different resin volumes used for elution profiles.

Sample Type	Resin	Amount
Coral	AG 50W-X8 100-200 mesh	1.5 ml
		2.0 ml
		3.0 ml
		3.5 ml
		4.5 ml
	AG 50W-X8 200-400 mesh	4.5 ml
Seawater	AG 50W-X8 100-200 mesh	3.5 ml
		4.5 ml
		5.5 ml
		6.0 ml

When preparing the columns, the capillary is filled with MilliQ water before adding the wet resin to the columns. This way, air bubbles in the resin column can be prevented. Afterwards, columns are prepared according to the method by Misra and Froelich (2009). In a first step, the resin was washed in 15 ml of 6 M HCl, before it was back-washed and conditioned using 2×15 ml of 0.5 M HCl. The sample containing about 30 ng of Li was loaded onto the column in 0.5 ml of 0.5 M HCl before eluting the Li fraction using 0.5 M HCl. For elution profiles, the eluent was applied in steps of 1 ml and beakers were exchanged after each step for individual analysis.
Afterwards, the eluate was evaporated to complete dryness and re-dissolved in 1 ml 0.5 M HNO_3 for concentration measurements using an ICP-Q-MS. The results of these extraction experiments can be found in figures 8.1 and 8.2.

In figure 8.1, the results can be found normalised to the total amount of Li and Na in the samples, respectively. It is apparent that, with larger amounts of resin, the elution profile becomes steadily broader and Li is extracted later from the resin. Furthermore, the extraction peaks of Li and Na are torn further apart with an increasing amount of resin. The resin volume of 2 ml does not separate the eluate peaks of Li and Na completely, hence a larger resin volume must be used. The maximum amount of resin that can be introduced into the capillary are about 4.5 ml of wet resin. In figure 8.1, a comparison between the same amounts of resin in different mesh sizes can be found. Here, the resin AG 50W-X8 100-200 mesh is compared to the finer resin of AG 50W-X8 200-400 mesh. With the same amount of resin, the elution peak of Li is much sharper for the finer resin. Furthermore, while for the resin AG 50W-X8 100-200 mesh, the peaks of Li and Na are still not fully separated at 4 ml, the separation of the extraction peaks of Li and Na is better for resin AG 50W-X8 200-400 mesh as the peaks are clearly separated here.

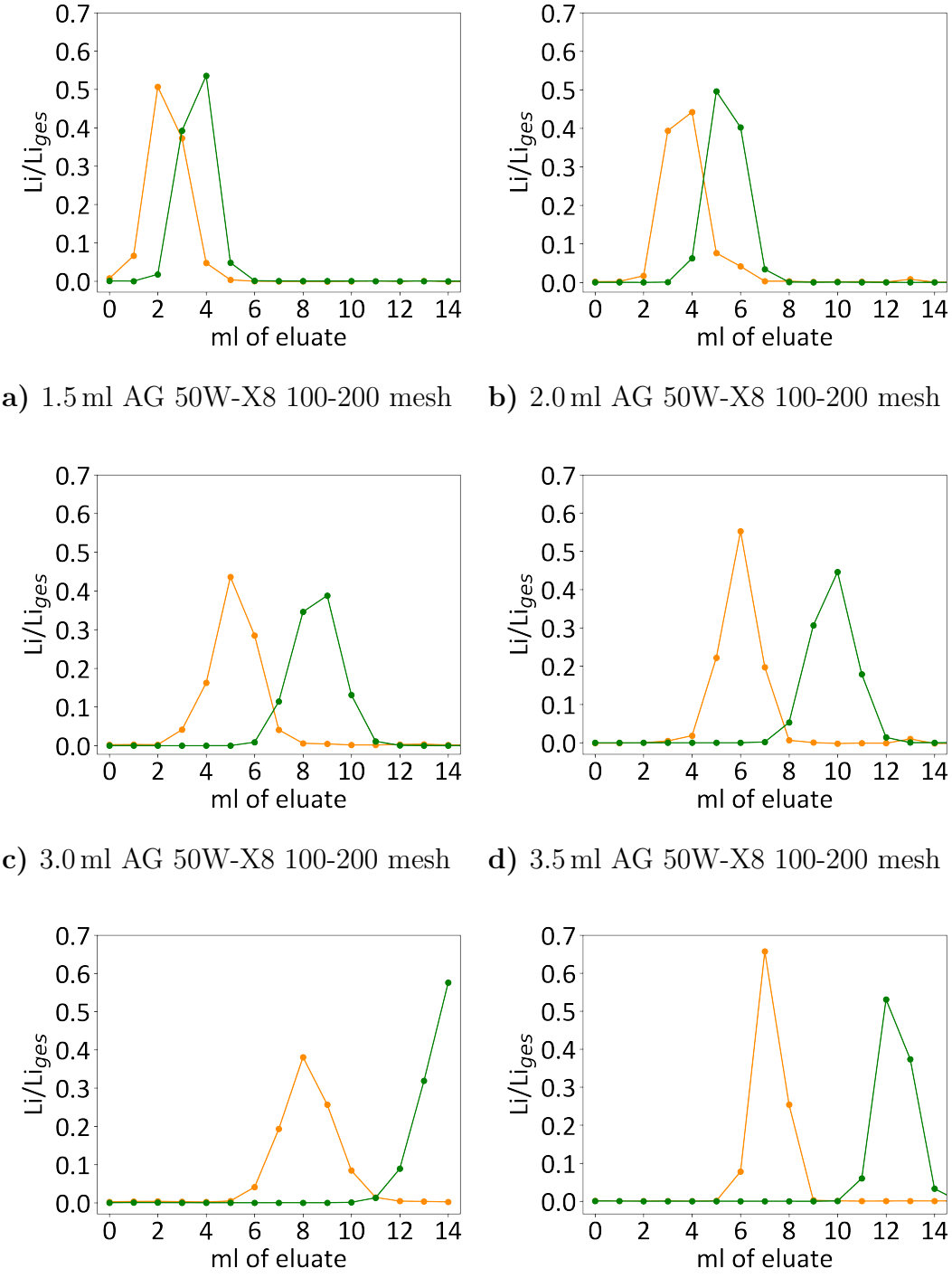

a) 1.5 ml AG 50W-X8 100-200 mesh **b)** 2.0 ml AG 50W-X8 100-200 mesh

c) 3.0 ml AG 50W-X8 100-200 mesh **d)** 3.5 ml AG 50W-X8 100-200 mesh

e) 4.5 ml AG 50W-X8 100-200 mesh **f)** 4.5 ml AG 50W-X8 200-400 mesh

Figure 8.1: Elution profiles of Li (orange) and Na (green) of CWC samples for different resin volumes. Best separation of Li from Na was obtained using 4.5 ml of AG 50W-X8 200-400 mesh resin (lower right graph).

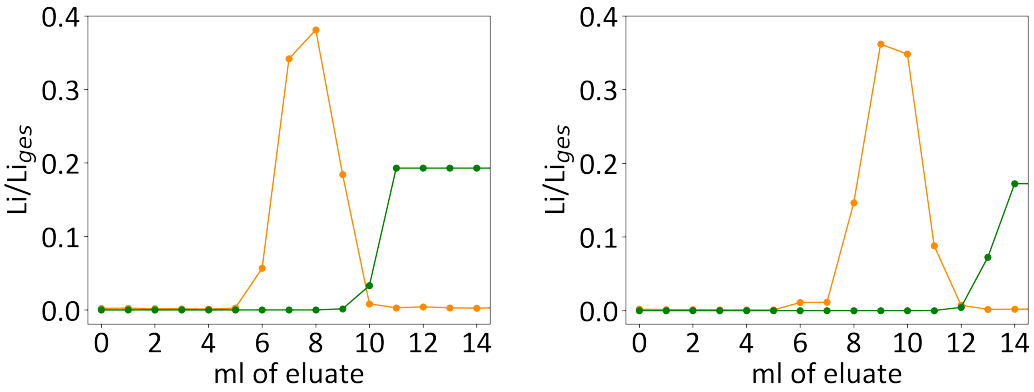

a) 3.5 ml AG 50W-X8 100-200 mesh

b) 4.5 ml AG 50W-X8 100-200 mesh

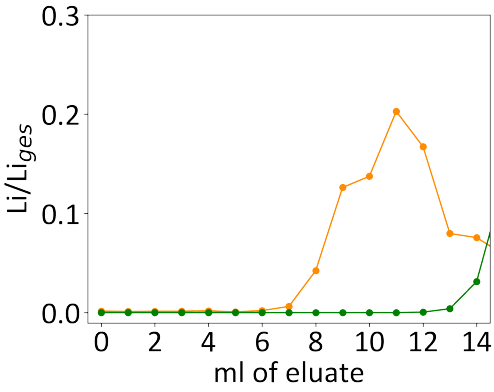

c) 5.5 ml AG 50W-X8 100-200 mesh

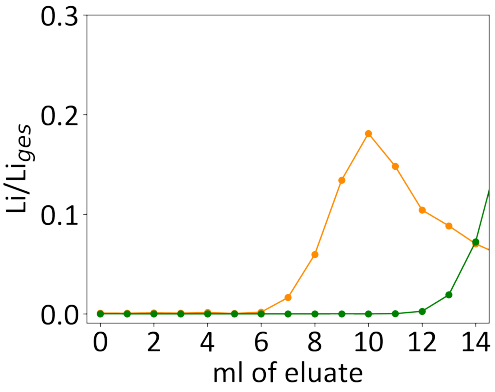

d) 6.0 ml AG 50W-X8 100-200 mesh

Figure 8.2: Elution profiles of Li (orange) and Na (green) of seawater samples for different resin volumes. For resin volumes > 4.5 ml tailing of the lithium elution peak is visible.

For seawater, based on the previously described results, a similar experiment was conducted (see figure 8.2). Four elution profiles with 3.5 ml to 6.0 ml of AG 50W-X8 100-200 mesh resin were produced. While elution profiles at 3.5 ml and 4.5 ml show the expected sharp peaks of Li, the respective profiles at 5.5 ml and 6.0 ml of resin do not show sharp elution profiles, but rather strong 'tailing' of Li towards the later elution steps inflicting with the elution of Na. As the maximum amount of wet resin that can be filled into the capillary of the columns is about 4.5 ml, for the elution profiles of 5.5 ml and 6.0 ml of resin, some of the resin was in the reservoir of the column rather than the capillary. Here, the extraction does not seem to be as effective as for the resin in the capillary, producing the tailing towards the end of the elution profile. Therefore, it is crucial for the resin to be within the capillary of the columns and to not spill into the reservoir.
For the elution profiles at a resin volume of 3.5 ml and 4.5 ml the results for seawater are similar to the coralline elution profiles. The Li fraction starts 6 ml of elution solution and ends at 13 ml, the elution profile of seawater at 3.5 ml of resin seems to be shifted by 2 ml compared to the coralline profile. The reason for this is unclear, as this shift cannot be found in the elution profile of 4.5 ml of resin.
All in all, best Li and Na separation can be achieved using 4.5 ml of AG 50W-X8 200-400 mesh. According to the elution profile in figure 8.1f) the Li fraction is eluted in between 7 ml to 10 ml of the elution solution of 0.5 M HCl. As Li is the first element to be eluted, but the elution of Na commences shortly after the Li peak, it is recommended to collect the fraction between the 5 and 11 ml. The elution fractions before and after the Li fraction need to be collected for yield measurements and quality control.

To calculate the fractionation occurring during the column chromatography, the measurement results of the elution profile using 4.5 ml of AG 50W-X8 100-200 mesh were used exemplarily. The concentrations of ^{7}Li and ^{6}Li were measured individually and used to calculate the fractionation between the isotopes via:

$$\text{Fractination} = \left(\frac{^{7}\text{Li}}{^{6}\text{Li}} - 1\right) * 1000 \ (‰) \tag{8.1}$$

The fractionation of the columns is shown in fig. 8.3. At the beginning ^{7}Li is enriched in the eluate by more than 50 ‰, while ^{6}Li mainly gets eluted towards the end of the Li fraction, resulting in a depletion of ^{7}Li by about 40 ‰. This immense fractionation during the column chromatography is also confirmed by e.g. Pistiner and Henderson (2003). This fractionation cannot be corrected for during the evaluation of measurements as there are no stable artifical Li isotopes that could be used for

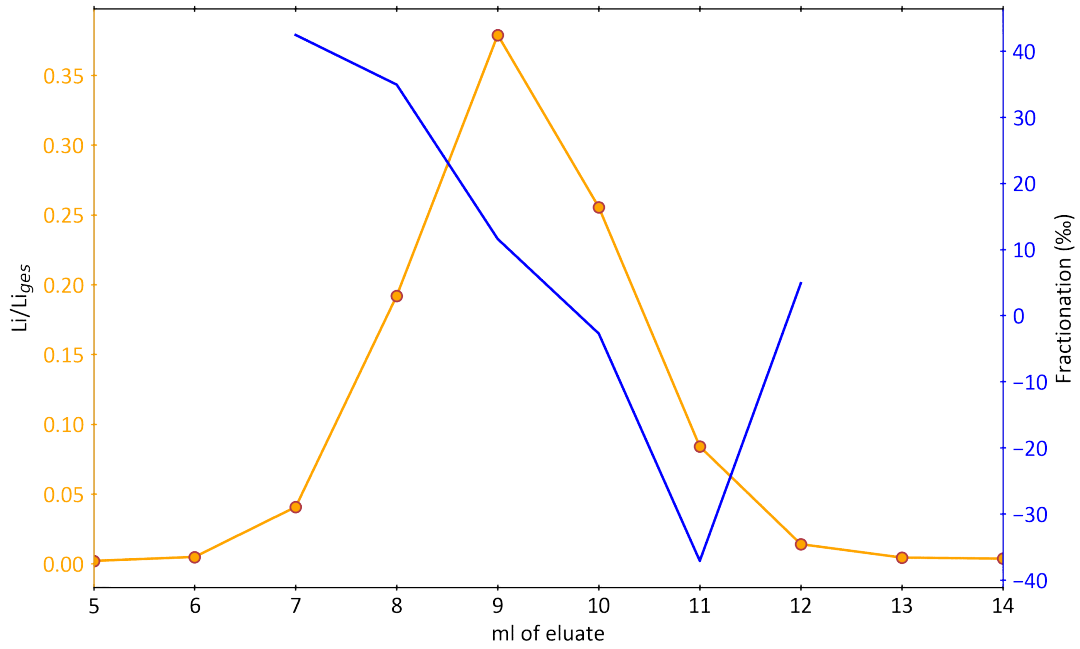

Figure 8.3: Exemplary fractionation of Li during column chromatography.

correction. Consequently, a yield of 100% during column chromatography is crucial for reliable Li isotopic measurements.

8.3.2 Yield

In the following, the yield was calculated from the elution profiles. The coral elution profiles were obtained using 40.6 mg of sample material. The mean Li/Ca ratio of the CWC with lab No. 6118 was measured to 2.05 ± 0.02 µg g^{-1} (n = 25). Using this information, the yield can be calculated as follows:
Calcium carbonate consists to 40.04 % of Ca. The amount of Ca per aliquot thus follows to 16.3 mg as each aliquot has a sample size of 40.6 mg. With the measured Li/Ca ratio of the sample, this yields 33.3 ng of Li in the sample. Li measured in the elution profile is normalized to this expected concentration to determine the achieved chemical extraction yield.

For the coralline elution profiles determined yields vary between 91 % and 125 % (see figure 8.4). Uncertainties of the yield are introduced during the dissolution and dilution of the samples, as these were not conducted gravimetrically but volumetrically. This uncertainty is estimated to about 6 %. For seawater elution profiles, 0.3 ml of the seawater samples were used. As the average seawater is about 180 ppb Li, the total

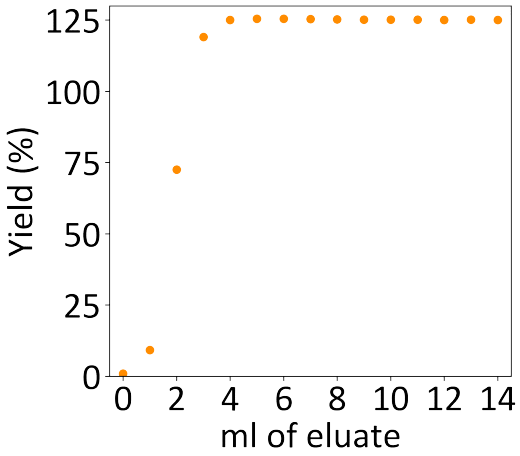

a) 1.5 ml AG 50W-X8 100-200 mesh

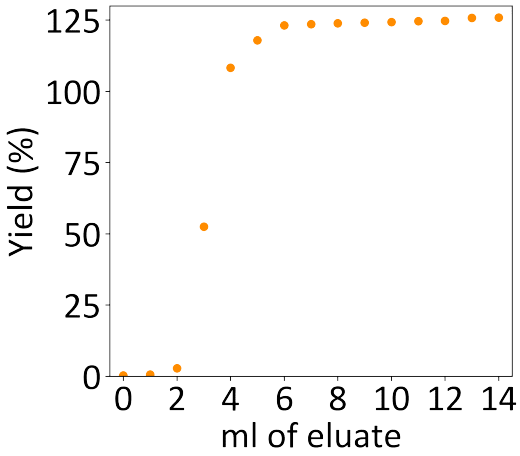

b) 2.0 ml AG 50W-X8 100-200 mesh

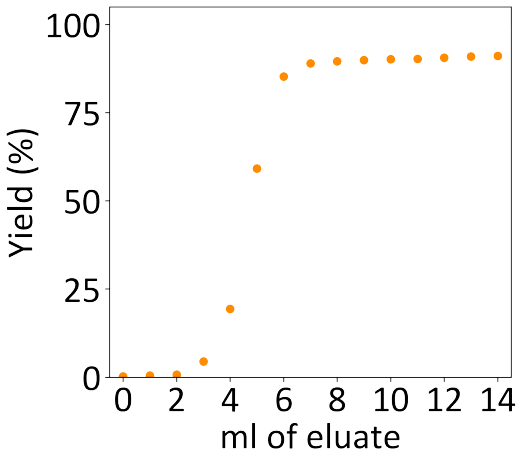

c) 3.0 ml AG 50W-X8 100-200 mesh

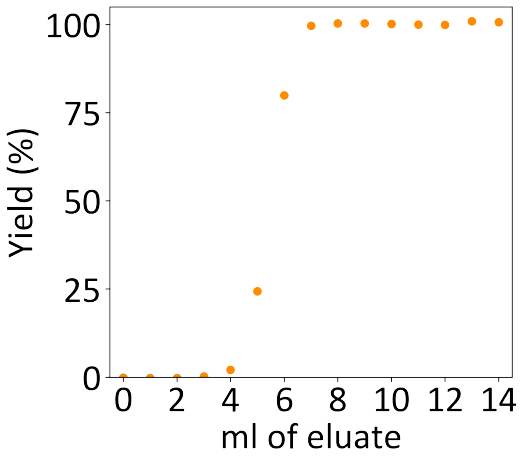

d) 3.5 ml AG 50W-X8 100-200 mesh

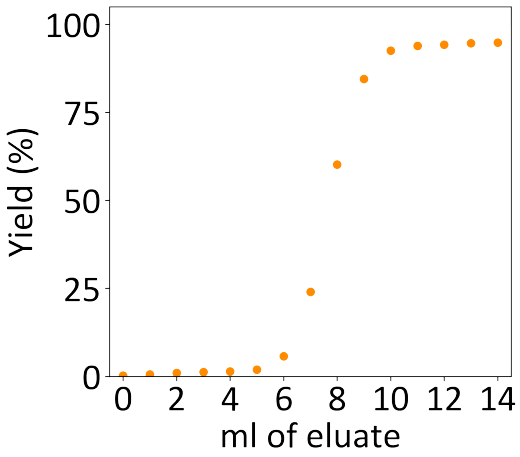

e) 4.5 ml AG 50W-X8 100-200 mesh

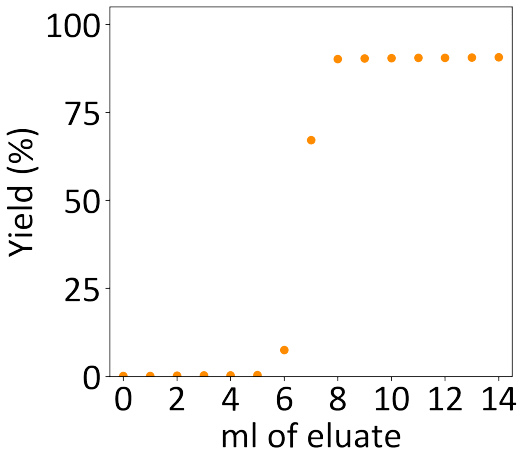

f) 4.5 ml AG 50W-X8 200-400 mesh

Figure 8.4: Accumulated yield of Li during extraction from CWC samples for different resin volumes.

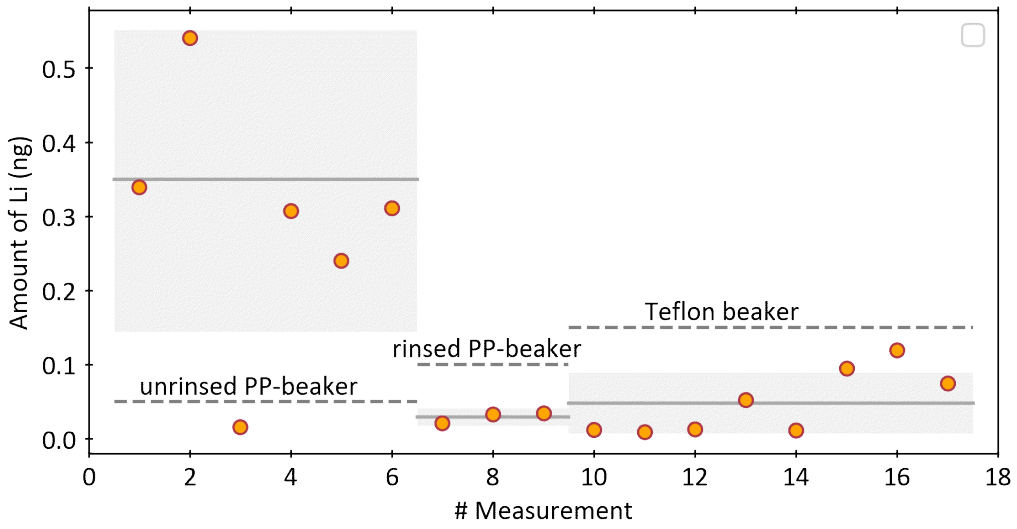

Figure 8.5: Procedual blanks for different beakers. The shaded areas denote the mean procedual blank and 2σ uncertainty.

amount of Li in the 0.3 ml of seawater can be estimated to 54 ng. For seawater elutions profiles a yield of 83 % to 96 % was determined. These are only rough estimates of the yield, as e.g. the Li concentration of the seawater was not precisely determined. Riley and Tongudai (1964) determined the average seawater concentration to 183 ± 3 ppb but found variation in the Li concentration between 140 ppb and 200 ppb. Pistiner and Henderson (2003) determined the Li concentration in seawater to 150 ± 15 ppb. When recalculating with this Li concentration yields of 95 % to 108 % are determined for seawater. Therefore, average column chromatographic yields of 89 ± 6 % to 102 ± 6 % are determined for seawater samples, indicating a successful extraction and purification of Li from marine samples.

8.3.3 Chemical Blank

Chemical blank experiments were conducted using different types of beakers: Teflon beakers and PP-beakers with and without acid precleaning. While PP-beakers are single-use beakers, Teflon beakers are multi-use beakers and need to be cleaned after every use in a time-consuming procedure. Column chemistry was performed as described in section 8.3 with 4.5 ml of wet AG 50W-X8 100-200 mesh resin without adding a Li-bearing sample. All test blanks were analysed for their Li concentration using an ICP-Q-MS and the results can be found in figure 8.5.

The chemical blank for unrinsed PP-beakers is highly variant and varies between

0.02 ng and 0.54 ng Li, in which five out of six samples contain between 0.24 ng to 0.54 ng of Li. Indicating a rather high Li blank for unrinsed PP-beakers. As Li is widely present today e.g in electronics and batteries, unrinsed PP-beakers are easily contaminated during the production process or transportation. Furthermore, since the caps are not screwed to the beakers when they arrive in the lab potentially contaminating particles are easily brought into the beakers. Therefore, rinsing the beakers is crucial before usage.
Li contents in blank samples were drastically improved when the PP-beakers are rinsed with 6 M HCl. Measured chemical blanks using these rinsed PP-beakers contain between 0.021 ng and 0.034 ng Li and are, therefore about a factor of 10 lower compared to the unrinsed PP-beaker.
The other option of beakers, Teflon beakers, do, in general, show a low chemical blank. These vary between 0.009 and 0.120 ng. A high variation in chemical blanks can be found here, as well. When comparing the mean chemical blank of the Teflon beakers to the mean chemical blank of the rinsed PP-beakers, both are similarly low at 0.048 ng for the Teflon beakers and 0.030 ng for the rinsed PP-beakers. As rinsing the PP-beakers is by far less time and acid consuming than cleaning Teflon beakers, while Teflon beakers seem to not offer an advantage, PP-beakers were chosen for the chemical preparation of samples for the Li isotopic measurements. All chemical blanks analysed during this study were smaller than 34 pg (n = 8). This corresponds to a blank contribution of about 1 ‰ to a typical sample and, hence, is negligible.

8.4 Mass spectrometric measurements

8.4.1 Mass spectrometer settings and measurement routine

Li isotopic measurements were conducted on an MC-ICP-MS (Neptune Plus, Thermo Fisher) allowing ^{6}Li and ^{7}Li to be measured simultaneously. The maximal adjustable positions between the outermost Faraday cups, H4 and L4, correspond to a relative mass deviation of 17 % (Millot *et al.*, 2004). As the isotopes ^{6}Li and ^{7}Li have a large relative mass difference of about 16.7 %, they were measured on these cups on the far end of the movable range. On the center cup, a 'dummy mass' of m/z = 6.475 was measured and all Faraday cups were equipped with $10^{11}\,\Omega$ resistors. The instrument settings, including gas flow rates, torch position and voltages to lenses and the electrostatic analyser were adjustes at the beginning of a measurement session to optimise the sample signal and sample/background ratio. A typical optimized instrumental setup can be found in table 8.3. The shape, alignment, and centering

of the beams were optimized at the beginning of each session and a peak center routine was performed regularly throughout the analysis session to confirm the alignment and centering of the beams.
The measured $^{7}Li/^{6}Li$ ratio of the IRMM-016 reference material typically ranged between 14.3 and 15.1. This corresponds to a mass bias of about 17.4 % to 24.0 % compared to a certified $^{7}Li/^{6}Li$ ratio of 12.18 (Qi *et al.*, 1997). To correct for this mass bias a standard bracketing measurement routine was applied:

Blk - IRMM-016 - Blk - Sample1 - Blk - Standard - Blk - IRMM-016 - ...

During evaluation, the measurements are blank, mass bias and drift corrected using the blank and IRMM-016 measurements and normalised to the LSVEC reference value (Qi *et al.*, 1997) according to equation 2.3.

Table 8.3: Typical mass spectrometer settings used during $\delta^{7}Li$ analyses.

Parameter	Value
Cup configuration	L4(^{6}Li), C(6.475), H4(^{7}Li)
Cones	Jet sampler cone + X skimmer cone
RF power	1200 W
Cool gas flow	16 l min^{-1}
Auxiliary gas flow	0.80 l min^{-1}
Sample gas flow	1.048 l min^{-1}
Torch z-position	0.780 mm
Extraction voltage	-1200 V
Zoom Optics	Focus Quad:
	Dispersion Quad:
Integration time	4.194 s
Cycles/blocks	30 cycles / 1 block

8.4.2 Choice of desolvating systems

For analyses on the MC-ICP-MS three different types of desolvating systems are available. The Scott is the standard form of a desolvating system provided with the Neptune Plus MC-ICP-MS. It is a glass dome consisting of two chambers. At the bottom, the sample solution enters as a spray through a nebulizer. Larger droplets are immediatly discarded through a tube at the bottom of the chamber connected to a peristaltic pump, while the fine drizzle is sucked into the upper glass chamber and into the mass spectrometer.

The second desolvating system available is the ESI Apex HF which aims to increase the sensitivity of the mass spectrometer by a factor of 3-5 through introducing a 'dry aerosol' into the ionization plasma. To achieve a 'dry aerosol', the sample solution is introducued into a heating chamber, heating the sample solution to about 140 °C before it is cooled again in a chamber of about 2 °C. Here, the water condensates and is pumped from the chamber while the now dry aerosol is introduced into the mass spectrometer.
The third desolvating system with the highest rate of sensitivity increase (up to 10 times) is the Cetac Aridus II system. This is a membrane desolvating system also providing a dry aerosol to the mass spectrometer.
To find out which desolvating system is best to use for Li isotope measurements a series of measurements of the reference material IRMM-016 were conducted using all three desolvating systems. All measurements were conducted on three consecutive days and the experiments ran for about 24 h each. Furthermore, for all measurements, the Li concentration of the sample solutions was adjusted to achieve a similar measurement signal for all experiments. The results of this measurement series can be found in figure 8.6.

The measurements using the Aridus desolvating system is highly variant and δ^7Li values vary between -3.27 ± 0.37 ‰ and 3.53 ± 0.22 ‰. The mean δ^7Li is at 0.5 ± 1.4 ‰ and agrees, due to a high uncertainty, well with the reference value of 0.4018 ± 0.0016 ‰. It is noticeable, that there seem to be 'dips' towards very low isotopic values of about -2.93 ± 0.20 ‰ on a regular basis.
The measurements using the Apex are less variant between -0.68 ± 0.93 ‰ and 2.57 ± 0.83 ‰, with a mean of 0.42 ± 0.54 ‰. This is also in good agreement with the reference value of 0.4018 ± 0.0016 ‰. Outliers are not as clearly distinguishable as for the Aridus measurements. Single measurement cycles are highly variable, however, which is indicated by high measurement uncertainites.
The Scott measurements do only vary little around the mean value of 0.39 ± 0.16 ‰, between -0.19 ± 0.21 ‰ and 0.68 ± 0.19 ‰.
In comparing all three measurement series, it is clearly visible that the Aridus measurements are the least stable, while Scott measurements are the most stable. One reason for the instabilities in the measurements using the Aridus disolvator might be the nitrogen gas flow added to the sample gas in the Aridus. As nitrogen has a atomic mass of 14, doubly ionised nitrogen atoms might influence the ^{7}Li measurements as isobaric interference. Due to high nitrogen supply through the added gas flow in the Aridus, this might also occur for very low doubly ionising rates as are expected for the ICP-MS (Becker, 2008). Slight instabilities in the gas flow or the plasma

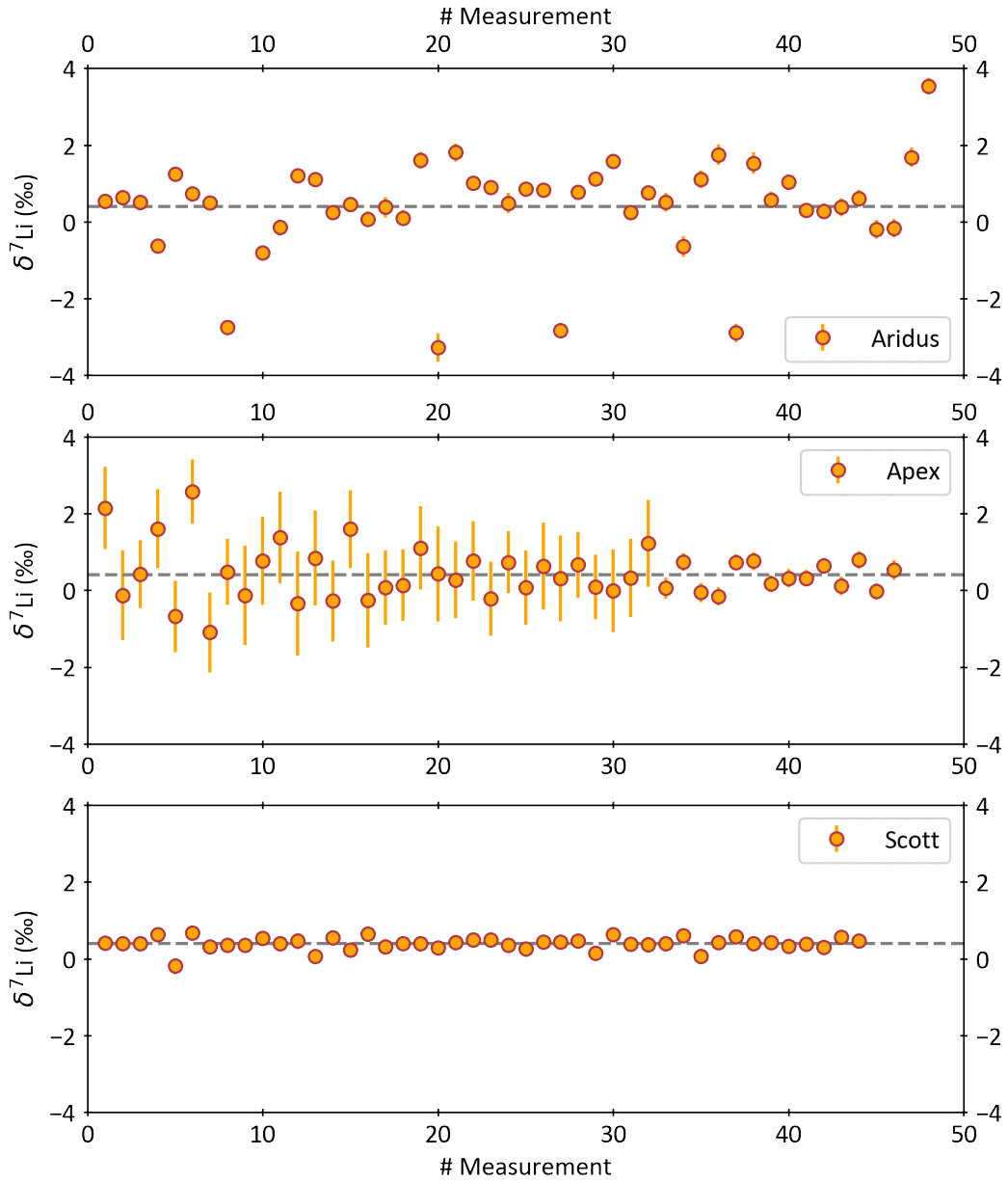

Figure 8.6: Measurement sequences for the three desolvating systems Aridus, Apex and Scott. The Scott desolvator provides best stability of all systems.

might, therefore, influence the stability of Li isotopic measurements. Another possible explanation for large deviations in the isotopic measurements that might also explain the discrete drops in Li isotopic values, is the Aridus itself and the usage of the Aridus at the Institute of Environmental Physics. The Aridus desolvating system is mainly used for U/Th measurements where the samples are dissolved in a mixture of HNO_3 and HF before measurement. HF and Li (hydroxide) can form Li fluoride (LiF), a hardly soluble crystal (Holleman and Wiberg, 2007). If remnants of the HF of U/Th measurements remain in the Aridus disolvator this might lead to the formation of LiF when Li samples are introduced into the Aridus. When these are dissolved later, they might influence the Li isotopic composition of single measurements and, therefore, increase the variance of the measurements using the Aridus dissolvator.
These explanations, however, cannot explain the variations in Apex measurements, as neither nitrogen gas is introduced here nor is the Apex used for U/Th measurements. Thus, the observed variability remains unexplaines at present. Since the measurements using the Scott injection system are by far the most stable, this desolvating system chamber is used for any further measurements.

8.4.3 Background

To process the raw measured Li signals the instrumental Li background has to be subtracted from the signal. This instrumental background results from Li traces that remain in the sample insertion and mass spectrometer system as well as from the 0.5 M HNO_3 the samples are dissolved in and which is, therefore, used as the blank solution. Prior to blank measurements, the internal passages are cleaned with 0.5 M HNO_3 for 5 minutes before the blank measurements were conducted. Blank measurements consisted of 30 cycles at 4.194 s integration time. In figure 8.7 an exemplary pattern of these wash and blank measurements can be found. Background signals are about two orders of magnitude smaller than the sample signal. At about 0.5 % and 1 % of the sample signal the background signal is sufficiently small for Li isotopic measurements.

A distinct pattern for the wash and the blank measurements can be seen here, as during the wash Li signals decrease fast before converging towards a low value. Once the solution is changed to the clean blank solution, the signal starts at a higher value, again, and decreases towards a stable value. These patterns are clearly visible for ^{7}Li measurements as blank levels are between 8 and 20 mV depending on the status of the instrument, the result of the daily tuning routine and the samples that were measured prior to the Li isotopic measurements. For ^{6}Li measurements the blanks are lower by a factor of about 10, as this is the lower abundant isotope. Therefore, the wash and

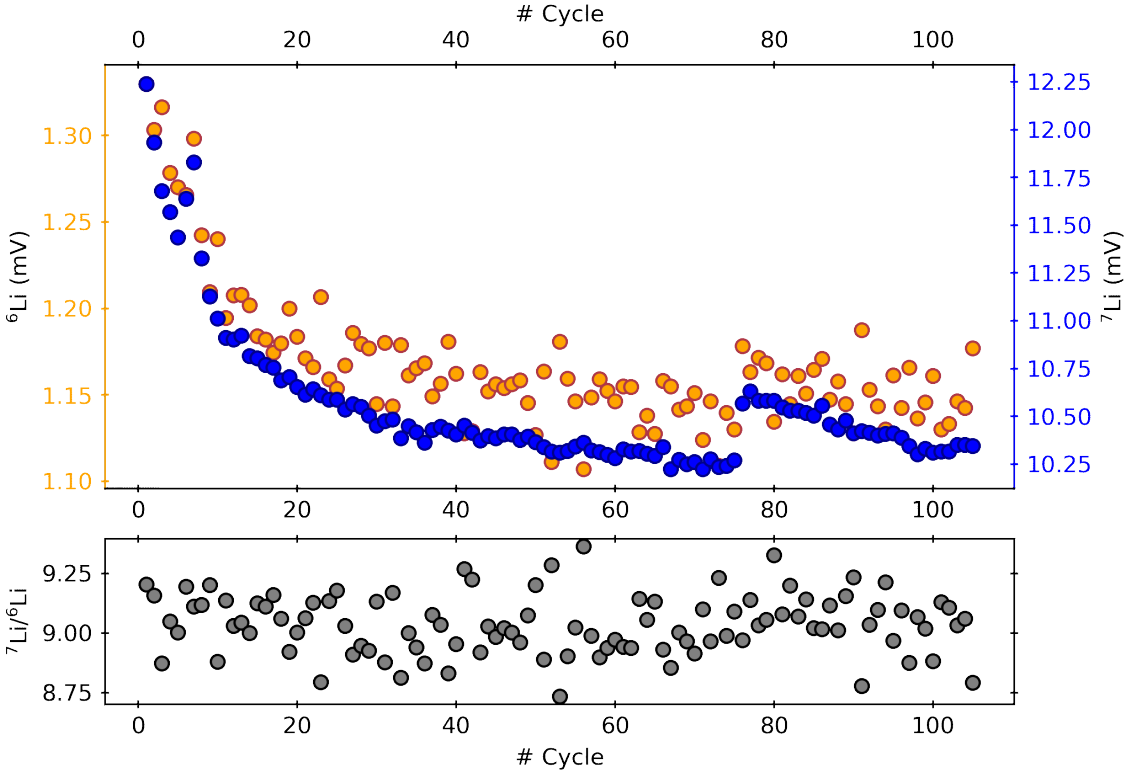

Figure 8.7: Exemplary wash and blank measurement. A clear jump in the signal is visible at the transition from wash to bank measurements.

blank signals are more scattered but show, in principle, the same pattern.
Even though blank signals are decreasing through all the blank measurement, this holds also true for the much longer wash signal. Therefore, it was decided on a routine of measuring 30 cycles for the blank correction, but only the mean of the last 5 cycles was actually used as the blank signal. At this point the majority of Li was washed out of the system and the signal reduction progresses much slower than at the beginning. However, it might be worth including the wash routine into the blank measurements to prevent the jump in the signal when changing from the wash to the blank solution. This would be possible as wash and blank solutions are the same and the solution uptake nozzle gets rinsed before changing from the sample to the wash solution to prevent contamination.

8.4.4 Influence of Na on the Li isotopic ratio

A strong influence of Na in Li isotopic measurements was reported (e.g. Jeffcoate *et al.*, 2004). The concentration of Na in CWC skeletons is with about 0.6 ‰ (e.g. Schleinkofer *et al.*, 2019) 500-times higher than the concentration of Li in CWCs at about 1 ppm (e.g. Montagna *et al.*, 2014, see chapter 6). As Na is eluted directly after the Li fraction, it has the highest risk of influencing the sample measurements. To test the influence of high Na contents in the samples on the Li isotopic MC-ICP-MS measurements, a measurement series adding various concentrations of a Na elemental standard to the reference standard IRMM-016 and the Li elemental standard was conducted. The results can be found in figure 8.8.
The measured δ^7Li values of the IRMM-016 reference material are between 0.21 ± 0.34 ‰ and 0.51 ± 0.31 ‰. All measurements are in good agreement with the reference value of 0.4018 ± 0.0016 ‰ within uncertainty. For the Li elemental standard, measured δ^7Li values are between 8.80 ± 0.33 ‰ and 9.24 ± 0.33 ‰, in agreement with the mean value of 9.18 ± 0.45 ‰ (n=65) measured for this standard.
Even 20-times more Na than Li soea not cause a measureable influence on the Li isotopic measurements of the standard material. This corresponds to about 4 % of the total Na content of CWCs. In contrast, previous studies found a large effect of Na on the Li isotopic ratio of the NIST LSVEC reference solution (Jeffcoate *et al.*, 2004). The authors measured a deviation of about -1.6 ‰ to the reference value at a Na/Li ratio of 10. This deviation could not be confirmed in this experiment.

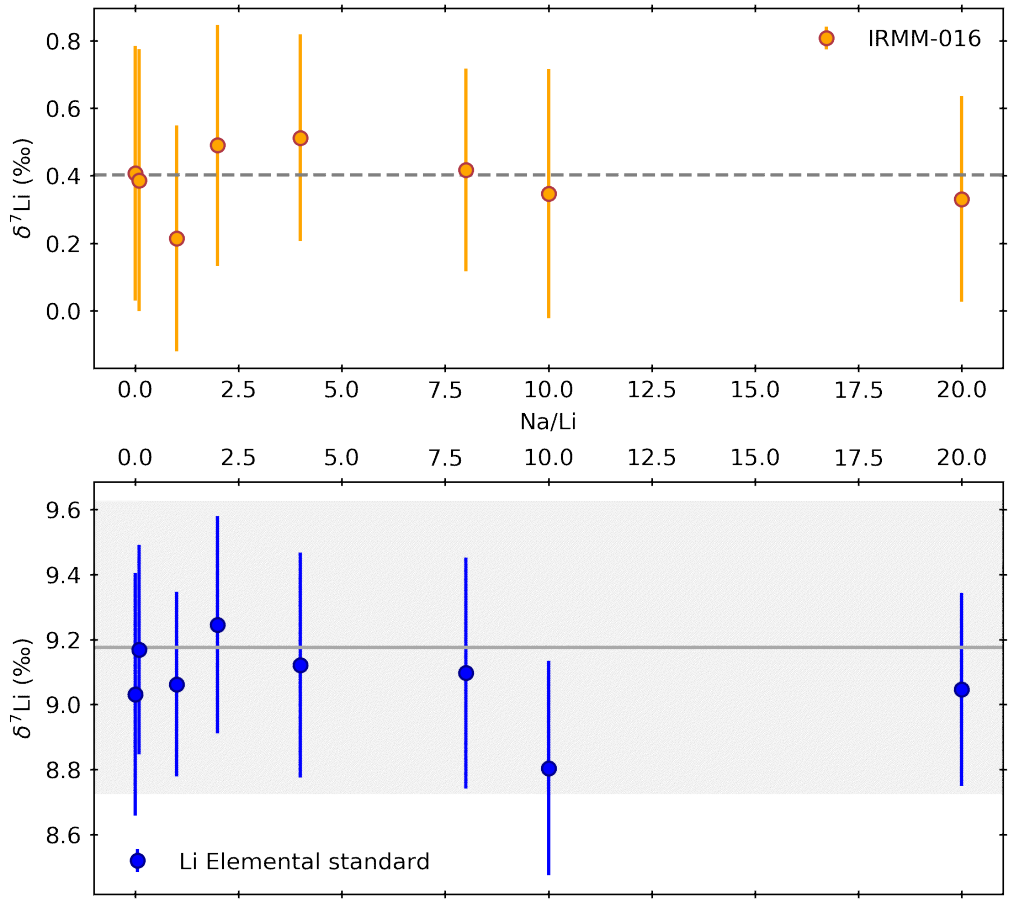

Figure 8.8: Test sequences to study the influence of Na on the Li isotopic measurements. Upper panel: The grey line marks the certified δ^7Li value of the IRMM-016 reference material. Lower panel: The grey line marks the average measured δ^7Li value for the Li elemental standard when measured without added Na. The grey shaded area shows the 2σ uncertainty of the average value.

8.5 Reproducibility

To determine the reproducibility of the Li isotopic measurements, three standard solutions were used. First of all, the reference standard IRMM-016 was used for standard bracketing but also frequently measured to be treated as a normal sample. Furthermore, two other reference solutions were used to broaden the range of isotopic values of the standards. Unlike the IRMM-016 reference material, the exact isotopic composition for these solutions was not known beforehand. Therefore, these are solely used to compare the internal reproducibility of the measurements over time.
The first one of these standards is a clean elemental Li standard from *Inorganic Ventures* that is normally used for concentration measurements. The other additional standard used in reproducibility measurements was a fractionated aliquot of the elemental Li standard. Here, the strong fractionation occurring during column chromatography was used. Only about 3/5 of the Li fraction was collected for the sample solution, fractionating the elemental standard to higher δ^7Li values.
The mean value and standard deviation of the reference material was determined to $\delta^7\text{Li} = 0.406 \pm 0.332\,‰$ ($n = 131$ over 10 months, $2\,\sigma$). This agrees well with the reference value of $0.4018 \pm 0.0016\,‰$. The elemental Li standard was measured to a mean value of $\delta^7\text{Li} = 9.18 \pm 0.45\,‰$ ($n = 65$ over 10 months, $2\,\sigma$). Lastly, the artificially fractionated elemental Li standard was determined to a mean value of $\delta^7\text{Li} = 39.66 \pm 0.96\,‰$ ($n = 23$ over 10 months, $2\,\sigma$). These measurement precisions and reproducibilities are in accordance with published data (e.g. Misra and Froelich, 2009; Vigier *et al.*, 2015).

8.5.1 Reference material

The reference material IRMM-016 was analysed after column chromatography, to compare to the untreated solution. The same solution was measured twice to $0.65 \pm 0.18\,‰$ and $0.75 \pm 0.25\,‰$ resulting in a mean δ^7Li value of $0.70 \pm 0.10\,‰$. This agrees within uncertainty with the measured mean value of the untreated solution of $\delta^7\text{Li} = 0.406 \pm 0.332\,‰$ and, hence, no fractionation occurs after successful column chromatography.
Furthermore, a coral reference material, the tropical coral JCp-1, was analysed for its Li isotopic composition to a value of $\delta^7\text{Li} = 18.2 \pm 0.8\,‰$. This is in good accordance to the value published by Bastian *et al.* (2018) of $18.8 \pm 1.8\,‰$. Previously published data Huang *et al.* (2010) and Bohlin *et al.* (2017) show slightly higher δ^7Li values of $20.2 \pm 0.2\,‰$ and $20.27 \pm 0.41\,‰$, respectively. However, Bastian *et al.* (2018) found strong isotope heterogeneity for small sample sizes of about 10 mg of powder, while Huang *et al.* (2010) and Bohlin *et al.* (2017) each used 100 mg of JCp-1 powder for

their analysis. For this study, 40 mg of sample material was used, matching the other coral samples. Therefore, some isotopic heterogeneity might influence the measured value.
The reference coral JCp-1 is a coral of the species *Porites*. Previously measured δ^7Li values for this species are 18.4 ‰ to 19.6 ‰ (Marriott *et al.*, 2004a) and 22.8 ± 0.8 ‰ for a specimen of P. lutea (Rollion-Bard *et al.*, 2009). This indicates a large range of variety of δ^7Li values for Porites corals and the value measured in this study agrees well within uncertainties with the range found before for this species.

8.5.2 Seawater and CWC samples

Furthermore, modern coral and bottom seawater samples collected at the sea floor using a ROV were analysed for their Li isotopic composition (see figure 8.9). Bottom water values were compared to open ocean seawater samples as well as the previously published value for the North Atlantic of 31.2 ± 0.4 ‰ (see e.g. Jeffcoate *et al.*, 2004; Millot *et al.*, 2004). The open ocean samples show an expected Li isotopic composition of 30.8 ± 0.3 ‰ at 1000 m water depth and 31.2 ± 0.8 ‰ at 600 m water depth and agree well within uncertainties with the previously measured seawater value of 31.2 ± 0.4 ‰. The same applies to the bottom water samples from the Great Meteor Seamount varying between 31.3 ± 0.1 ‰ and 32.2 ± 1.2 ‰ as well as for the Namibian margin where a bottom water δ^7Li value of 32.5 ± 0.9 ‰ was measured.
Modern CWCs were analysed from three different locations. One coral from the Great Meteor Seamount was analysed to a δ^7Li value of 18.3 ± 0.4 ‰. This coral is of species *Madrepora oculata*. No reference values are known for this species in particular, however, the δ^7Li value agrees well with the δ^7Li values published before for the CWC species *Lophelia pertusa* (19.0 ± 2.4 ‰) and *Desmophyllum cristagalli* (19.1 ± 1.4 ‰) (Rollion-Bard *et al.*, 2009). CWCs of species *Lophelia pertusa* were analysed from the Namibian and Icelandic margin. These revealed δ^7Li values of 19.2 ± 1.0 ‰ and 18.5 ± 0.8 ‰, respectively. This, again, perfectly agrees with the values published for this species of 19.0 ± 1.2 ‰ (Rollion-Bard *et al.*, 2009). No species specific difference in δ^7Li values were found for these three specimen of *Madrepora oculata* and *Lophelia pertusa*. This agrees well with the findings of Cuny-Guirriec (2020), who found a combined mean ratio of 18.3 ± 1.7 ‰ in the Mediterranean Sea over the last 55 ka for both species.
The fractionation between CWCs and seawater is about $\delta^7\text{Li}_{\text{mean,CWC}} - \delta^7\text{Li}_{\text{mean,sw}} = -12.6 \pm 1.5$ ‰. This is in excellent agreement with the fractionation previously meaasured for inorganic aragonite of -11.7 ± 0.8 ‰ (Marriott *et al.*, 2004b) and for CWCs of -12.8 ± 0.8 ‰ (Rollion-Bard *et al.*, 2009).

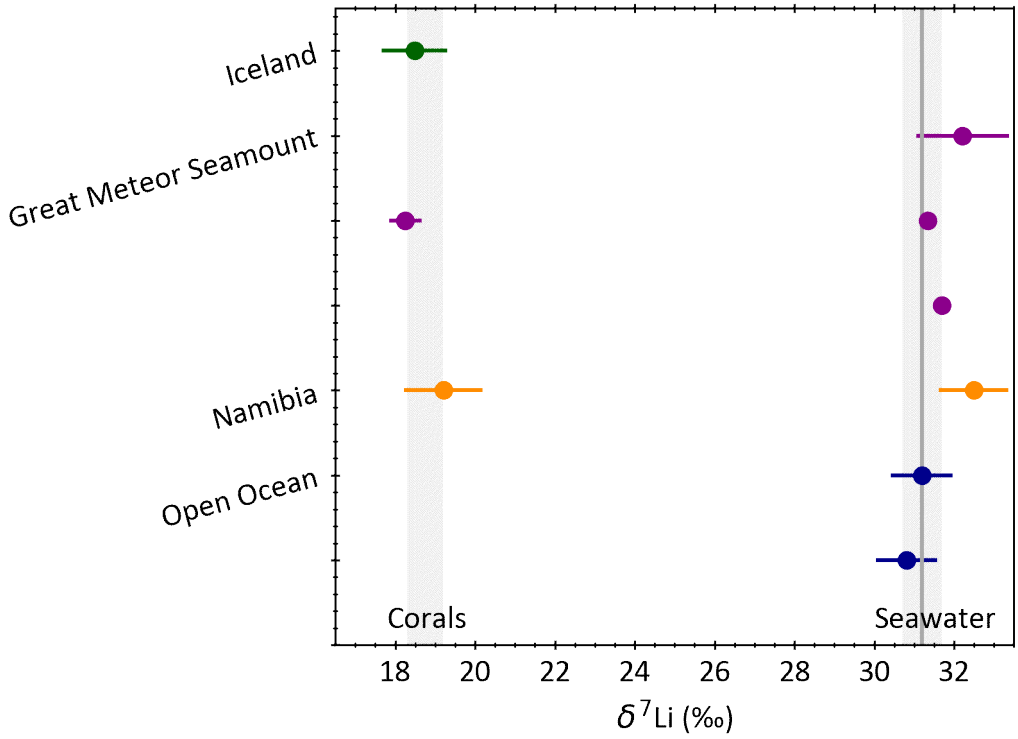

Figure 8.9: δ^7Li values of Holocene CWCs and seawater from different Atlantic locations. The grey shaded area on the left indicates the mean range found in previous publications. On the right, the average North Atlantic seawater value and 2σ uncertainty at 31.2 ± 0.4 ‰ are marked in grey.

8.6 Conclusions

Li isotopic analysis and measurements were established at the Institute of Environmental Physics at the Heidelberg University. It was shown, that Li can be extracted at high yields of $> 99\,\%$ from CWC and seawater samples. This is crucial due to a strong fractionation occurring during column chromatography.
Measurements using a MC-ICP-MS were successfully conducted at similar reproducibility levels as can be found in published studies. Furthermore, the typical values for seawater and CWC samples can be corroborated. The new results confirm the previously determined isotope fractionation between seawater and inorganic and biogenic aragonite precipitates, which is on average -12.4 $\pm$ 0.9 ‰. This demonstrates, that Li isotopic analyses can be successfully conducted, opening the pathway for further studies of the Li isotopic signals of CWCs.

9 Is the Li/Mg thermometer influenced by hydrothermal activity?

9.1 Introduction

During the last glacial, some CWCs show exceptionally high Li/Mg ratios resulting in physically unreasonable low reconstructed thermocline temperatures of as low as -5.0 ± 1.0 °C (see chapter 6). This leads to the hypothesis of increased seawater Li concentration resulting from local Li input.

At the Azores, some of these samples revealing unreasonable low temperatures were additionally analysed for their Nd isotopic signal which is used to track the provenance of water masses (e.g. Tachikawa *et al.*, 2017). Here, Nakajima (2016) found a correlation between ϵ_{Nd} values, hinting towards volcanic influence, and Li/Mg ratios. This lead to the hypothesis of an influence from hydrothermal fluids on the composition of the coralline skeletons as submarine volcanoes and fracture zones are widely present near the Azores archipelago possibly releasing hydrothemal fluids (Global Volcanism Program, 2013).

These physically unreasonable temperatures are primarily found near the Azores, i.e. in a region of hydrothermal activity, suggesting that hydrothermal fluids might be locally influencing the Li content of the seawater and therefore the Li content of CWCs and their Li/Mg ratios. As the Li isotopic signal of hydrothermal fluids is vastly different to the one of seawater, an additional hydrothermal Li source is thought to also change the isotopic composition of the CWCs. An increase in the flux of hydrothermal fluids of 20 % would lead to a significant change in the isotopic composition of the seawater. Assuming a conservative mixing behaviour between seawater (180 ppb Li, δ^7Li = 31.2 ± 0.4 ‰) and the hydrothermal fluids (3600 - 9000 ppb Li, δ^7Li = 3 - 11 ‰), such an increased flux would result in a mixed δ^7Li_m of 25.4 - 27 ‰. Hence, a drop in δ^7Li of about 4.2 - 5.8 ‰. To test this hypothesis of local influences on Li, in this study six corals from the Azores were analysed for their Li isotopic signal.

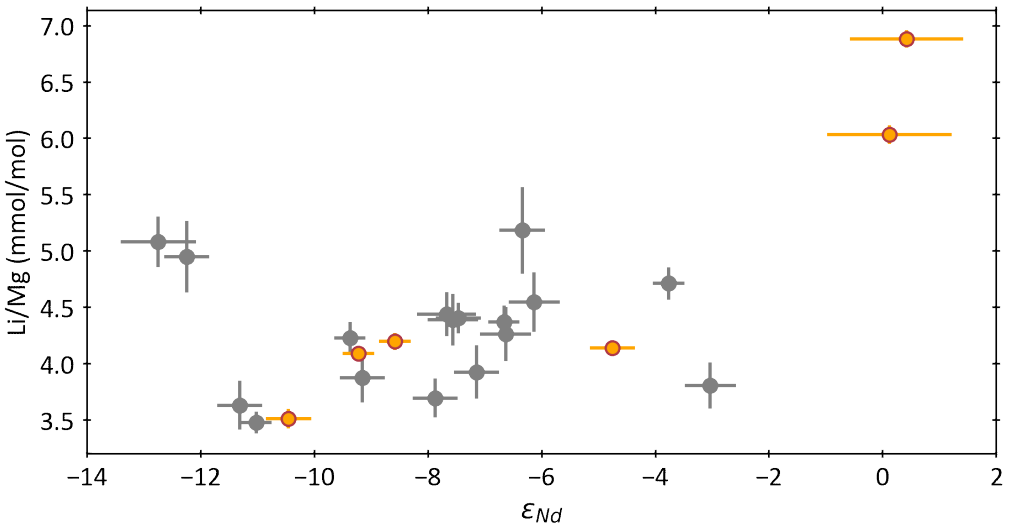

Figure 9.1: ϵ_{Nd} and Li/Mg ratio of the CWCs in the Azores region. Selected CWCs are shown in orange, further avaialble data is shown in grey dots.

9.2 Materials and Methods

To test the hypothesis of an additional Li source influencing the Li/Mg thermometer and the Li isotopic composition of the corals, six different corals from the Azores region were analysed. The precise locations of all studied corals used is given in table C.4 and shown in figure 9.2. All of these corals were U/Th dated before and were selected for their Li/Mg ratio and ϵ_{Nd} signal (see table C.4). Three aliquots of all six samples were prepared and analysed twice for their Li isotopic composition.

These samples were prepared for measurements on the MC-ICP-MS according to the results in chapter 8.3 using about 40 mg of sample material per aliquot. In the end, all samples were evaporated to dryness before being redissolved in 0.5 M HNO_3 and transfered to measurement tubes. The control samples that were extracted before and after the Li fraction were analysed on a ICP-Q-MS (Thermo Fisher ICap Q) for their Li concentration while the Li fraction was analysed for its Li isotopic composition on a MC-ICP-MS (Thermo Fisher Neptune Plus).

9.3 Results

Three aliquots of six individual samples were analysed twice for their Li isotopic ratio. The results of all single measurements are ahown in figure 9.3. The δ^7Li values of all single measurements are in the same range varying between 14.6 ± 0.7 ‰ and 20.7 ± 0.8 ‰, with 89 % of all values between 17.1 ± 1.4 ‰ and 19.7 ± 0.6 ‰. The mean

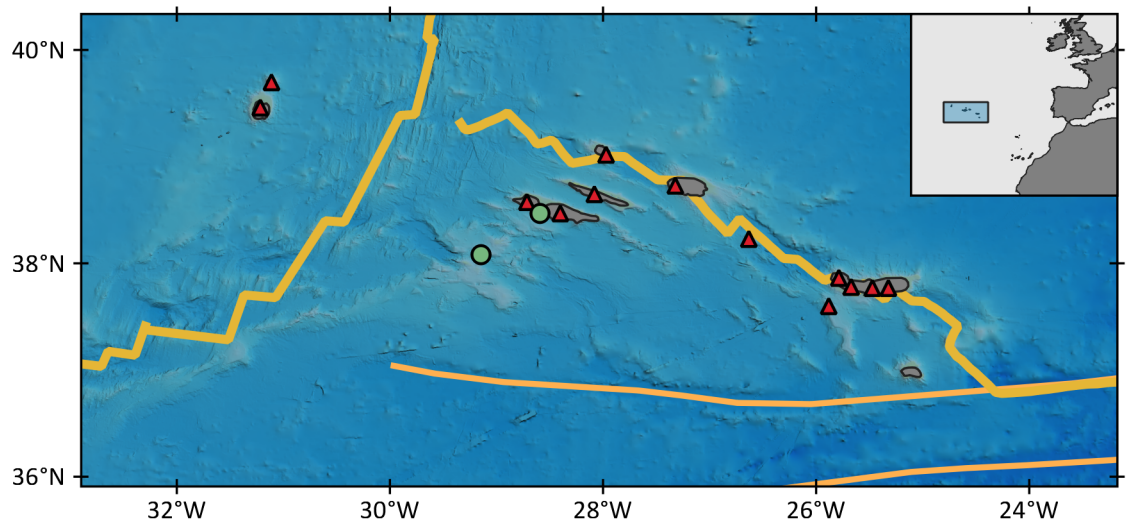

Figure 9.2: Map of the Azores region. Samples locations are shown as green dots. The mid-Atlantic ridge as well as fracture zones are marked as orange lines, volcanoes active during the late Pleistocene or Holocene are shown as red triangles.

δ^7Li values vary between 17.3 ± 3.0 ‰ and 18.6 ± 1.6 ‰.

9.4 Discussion

9.4.1 Quality control

As described before, the yield of the column chromatography is crucial for Li isotopic measurements. Therefore, the Li concentration was measured in the 4 ml before and after the Li fraction. From this, the yield was calculated as the ratio between the Li content in these solutions to the mean total Li content in the samples. All samples with a yield < 99 % were discarded from the discussion, as these samples probably do not reflect the Li isotopic composition of the CWC samples. Therefore, six out of 18 samples were discarded. Three of these discarded samples still had a high yield of 97.5 % to 99 %, whereas the lowest yield achieved was only 78.4 %.

In figure 9.4 the course of the ^{7}Li/^{6}Li ratio of the used reference standard IRMM-016, is shown for the measurement campaign. At the beginning, a measurement sequence consisting of the IRMM-016 standard, the Li elemental solution and the fractionated Li elemental solution is shown ('standardmeasurement'). Here, the ^{7}Li/^{6}Li ratios of the IRMM-016 standard reveal a small increase, but are fairly constant throughout the measurement. Once the samples are measured, the ^{7}Li/^{6}Li ratio of the IRMM-016

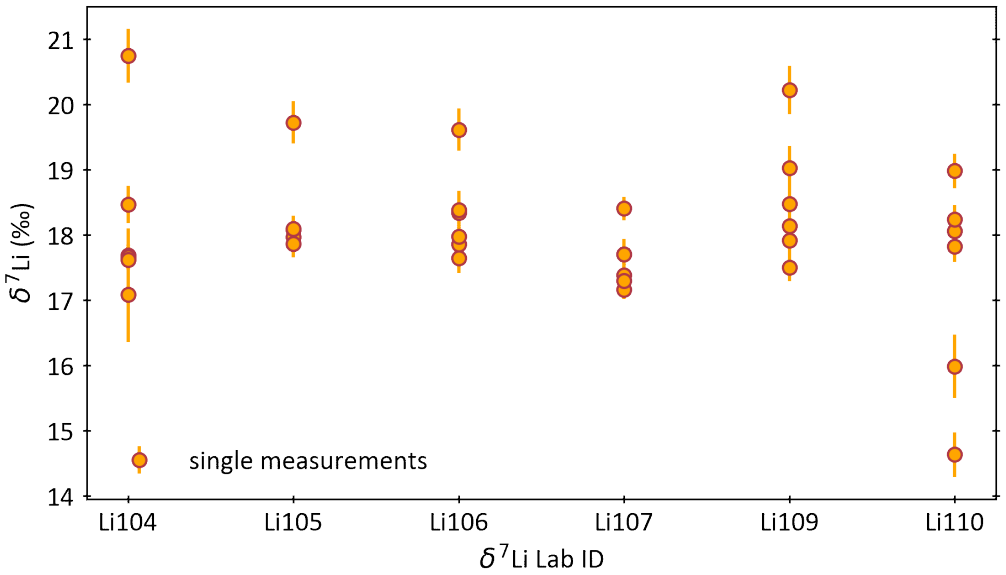

Figure 9.3: All δ^7Li results of the measurements of CWCs from the Azores.

standard gets highly variable throughout the measurement ('sample sequence 1'). The exact reason for this development is not known, yet. A possible explanation might be that the inlet system is not rinsed well enough in between samples and that remains of the sample solution build up in dissolvator and mass spectrometer system, despite a return to low blank intensities. As the CWC samples have a much higher ^{7}Li/^{6}Li ratio than the standard, this would possibly lead to an increase in the measured ^{7}Li/^{6}Li ratio of the standard. Therefore, the decrease in ^{7}Li/^{6}Li ratios in the second half of the measurement sequence cannot be explained by a build up of samples solution in the system. Furthermore, a build up of sample solution would particularly influence the instrumental blank measurements, as these are easily altered with low amounts of additional Li. However, in figure 9.5 is shown, that the intensity of the blank signal increases in parts of the sequence, but decreases with time for the overall sequence. Furthermore, the ^{7}Li/^{6}Li ratio of the blank signal would be expected to increase if sample solution remains in the system as blank signals are srongly depleted in ^{7}Li. However, the blank ^{7}Li/^{6}Li ratio as well does not increase. Therefore, a build up of sample solution influencing the standard measurements cannot explain the variation in standard ^{7}Li/^{6}Li ratios.

Another explanation might be, that the separation of Li from the the matrix elements of the CWC samples was not sufficient, leading to an influence of the matrix elements on the ionization of Li. To have an influence on the standard measurements, this, however, would again need to lead to a build up of sample solution in the system.

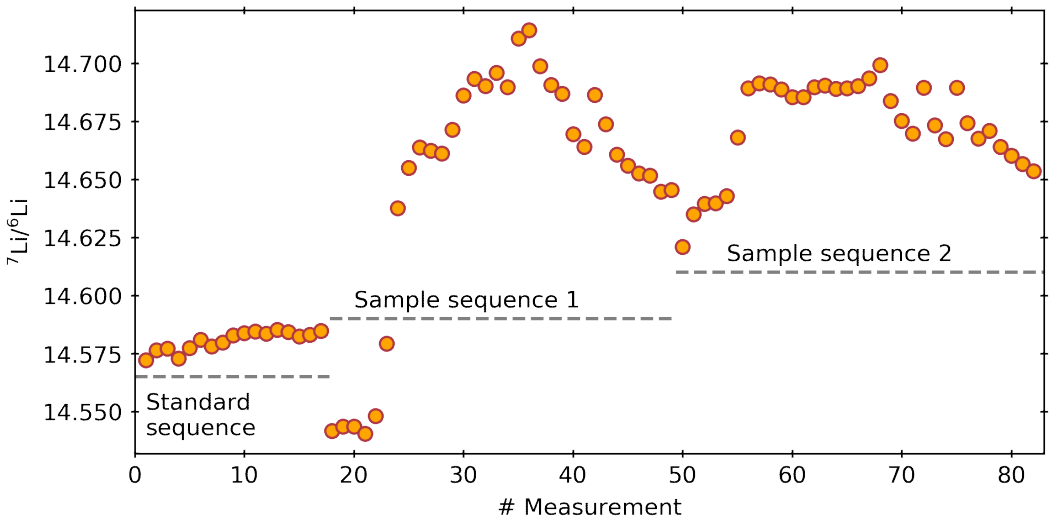

Figure 9.4: ^{7}Li/^{6}Li ratio of the IRMM-016 reference standard during the measurement sequences. This standard is used for corrections of the measurements in the standard bracketing method.

This is unlikely due to the previously explained reasons. However, matrix elements cannot only build up in the inlet system, but also on the cones leading the ion beam from the plasma chamber into the high-vacuum domain of the mass spectrometer. If matrix elements like Na form deposits on these cones, the change in cone geometry might influence the measurement of ^{7}Li and ^{6}Li and, therefore, the measured ^{7}Li/^{6}Li ratio. Furthermore, this would influence the measurement of the standard as well as the measurements of the sample. This can be accounted for using the standard bracketing technique. The δ^7Li values of the Azores samples after the quality control are shown in figure 9.6.

9.4.2 Does hydrothermal activity influence the Li/Mg thermometer near the Azores?

The remaining measurements are not equally distributed throughout the samples. While for sample Li110 all three aliquots were purified with the required yield, only one aliquot of coral Li104 can be used for further discussions. This also reflects in the standard deviation of the mean of each sample. While the two measurements of the same aliquot of sample Li104 are identical within uncertainties, for sample Li110 a large deviation of the single measurements is found. Measurements for this coral are between 14.6 ± 0.3 ‰ and 20.5 ± 0.4 ‰. While higher δ^7Li values might be influenced by a low yield, this is unlikely to be the case for low δ^7Li values, as heavy isotopes are

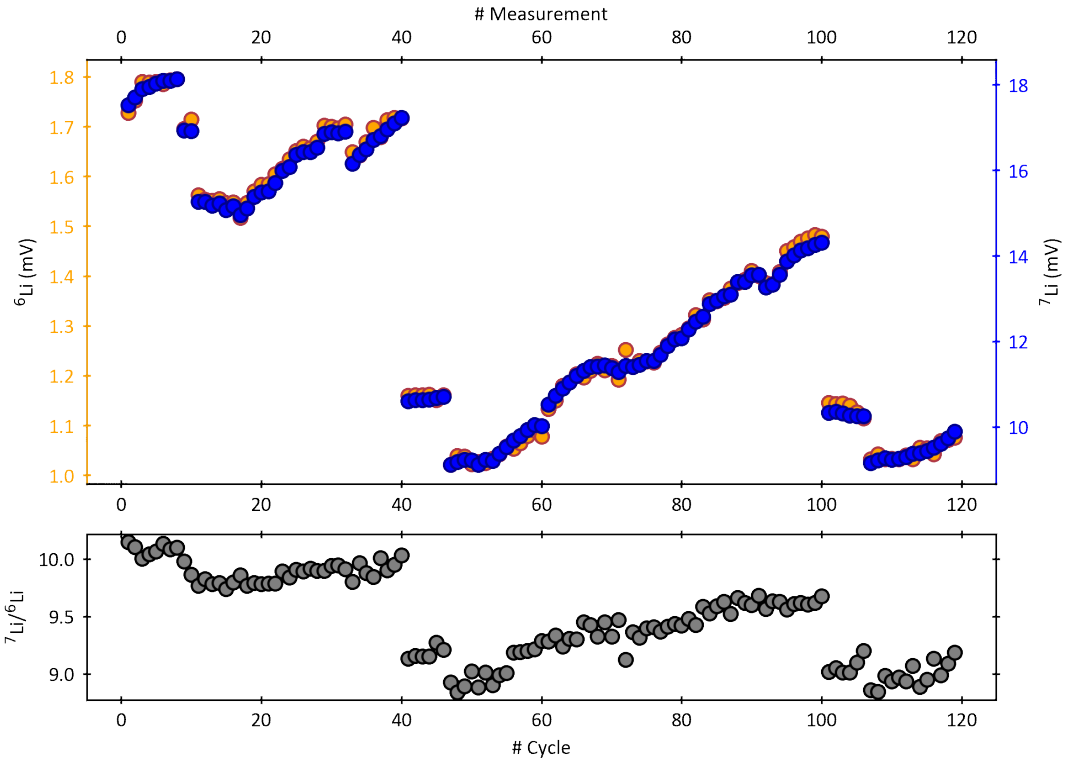

Figure 9.5: Blank sequence during measurement of CWCs from the Azores. Upper panel: Signal intensity of ^{6}Li (orange) and ^{7}Li (blue) blank measurements. Blank measurements decrease during the overall sequence but are increasing in periods inbetween. Lower panel: ^{7}Li/^{6}Li ratios of blank measurements.

eluted first. Sharp rises or decreases in the Li isotopic ratio of the standard solution as seen during the measurements (see figure 9.4) might lead to a slight overcorrection or undercorrection of Li isotopic ratios of the coral samples during evaluation. The same applies to the short peaks in the standards ratio seen towards the end of the second sample sequence.

Apart from potentially influenced measurements, all corals show similar δ^7Li values between 17.3 ± 3.0 ‰ and 18.5 ± 2.0 ‰. These values compare very well to the ones found in other locations far away from hydrothermal influences as seen in chapter 8.5.2. Additionally, the δ^7Li values of the CWCs analysed here are slightly lower than the average δ^7Li values of 19.0 ± 2.4 ‰ for L. pertusa and 19.1 ± 1.4 ‰ for D. cristagalli reported by Rollion-Bard *et al.* (2009), but agree within uncertainty. Furthermore, the mean value of 17.9 ± 1.0 ‰ for all six analysed CWCs agrees with the mean δ^7Li of 18.3 ± 1.7 ‰ observed by Cuny-Guirriec (2020) in the Mediterranean basin for the last 55 ka.

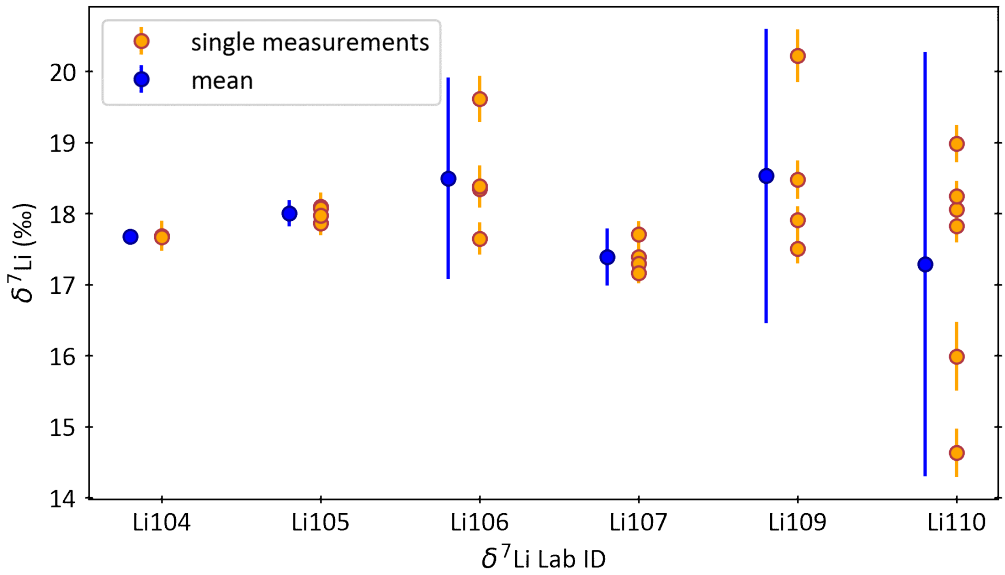

Figure 9.6: Results of δ^7Li values after quality control. Orange dots show single measurements of the CWC aliquots. Blue dots show respective means.

When comparing the δ^7Li values of the CWCs analysed here to their respective Li/Mg ratios, no correlation between these two proxies was found (see figure 9.7) contrasting to the correlation of ϵ_{Nd} and Li/Mg as described above. This was expected from the constant δ^7Li values and argues against a local volcanic influence on the Li composition of the coralline skeletons.

Therefore, at the current precision of Li isotopic measurements an influence of hydrothermal activity on the Li/Mg ratio in the seawater and, thus, in the coralline skeletons cannot be confirmed and cannot explain the unreasonable low reconstructed temperatures.

9.5 Conclusions

Here, first measurements of δ^7Li of fossil CWCs from the Azores region were presented to study a possible influence of hydrothermal fluids on Li incorporation into the coralline skeleton. Six corals were selected due to previous anexpected Li/Mg and ϵ_{Nd} measurements. An average δ^7Li value of 17.9 ± 1.0 ‰ was found for all six corals. The δ^7Li values are independent of the Li concentration in the corals and do not correlate with the Li/Mg ratios. Therefore, no influence of hydrothermal fluids on the Li isotopic composition of the CWCs was found. This also excludes an influence of

hydrothermal fluids on the Li/Mg ratio of the CWCs and leaves the observation of physically unreasonable low reconstructed temperatures unexplained.

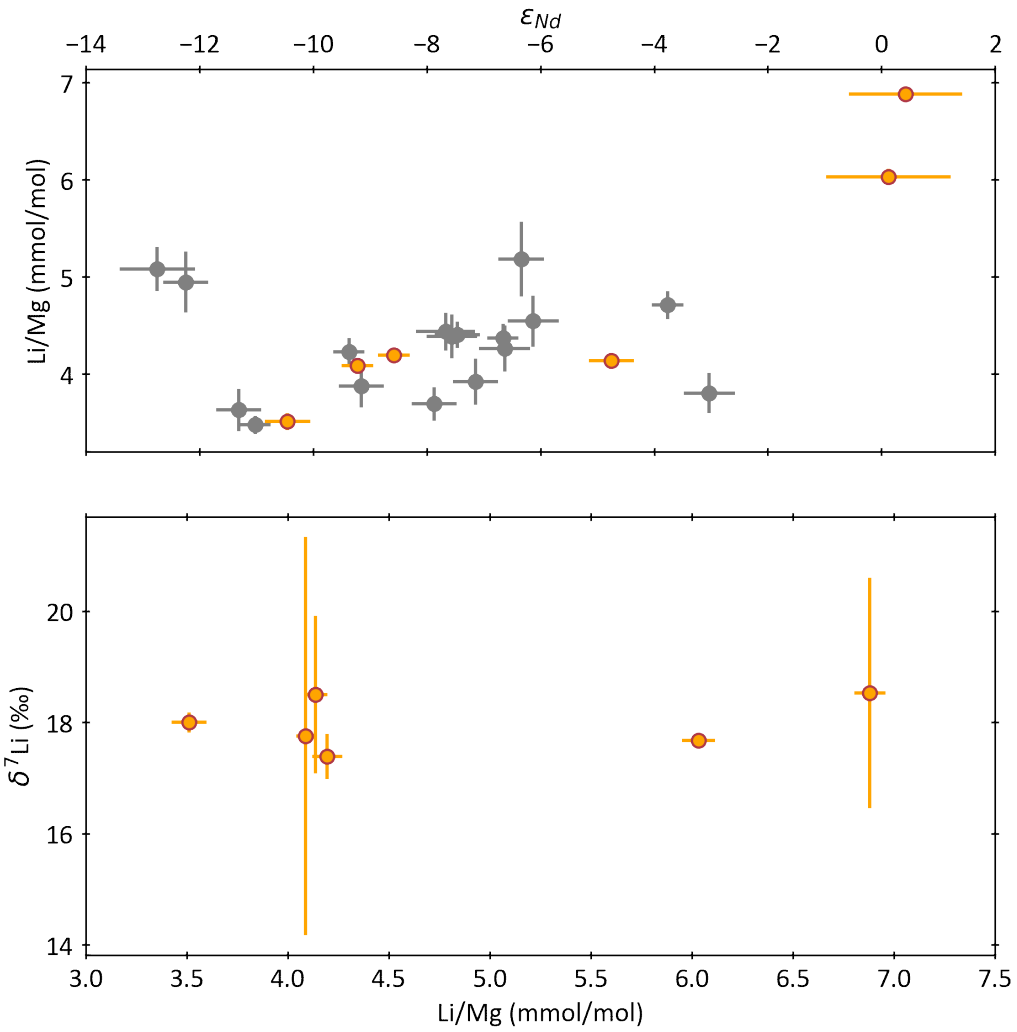

Figure 9.7: δ^7Li values do not show a correlation with Li/Mg ratios as is seen between Li/Mg ratios and ϵ_{Nd} values. Upper panel: ϵ_{Nd} and Li/Mg ratio of the CWCs in the Azores region. Selected CWCs are shown in orange, further avaialble data is shown in grey dots. Lower panel: δ^7Li values and Li/Mg ratios of the same corals.

10 Conclusions and Outlook

In this thesis, CWCs were used as an environmental archive for temperature reconstructions and changes in water pathways. Li/Mg ratios were measured as a temperature proxy, using the calibration curve of Montagna *et al.* (2014). More recent calibration curves are published by Cuny-Guirriec *et al.* (2019) and Stewart *et al.* (2020), however, they all agree within uncertainty. For the analysis of changes in water pathways, a compilation of published radiocarbon measurements was used. Some CWCs revealed extremely high Li/Mg ratios translating into physically unreasonable low temperatures. To possibly find an explanation for high Li/Mg contents in the CWCs, in a second part, the samples were analysed for their lithium isotopic composition. The aim was to study if hydrothermal fluids might locally influence the Li composition of the ocean and, thus, the Li/Mg ratio measured in CWCs.

Reconstruction of past ocean properties using CWCs in the Atlantic

In a first study, the thermal and ventilation patterns for the upper thermocline eastern South Atlantic over the past 34 ka were reconstructed. CWCs from three coral bearing gravity cores, complemented with surface samples were analysed. U/Th dating revealed nearly continous coral growth for the last 34 ka with three major hiatuses from 31 ka to 25 ka, from 23 ka to 19 ka and from about 17 ka to 14 ka. Therefore, the coral site off the Angolan margin are one of the few locations worldwide, where CWCs can be studied during interglacial as well as during glacial times.

The CWCs were also analysed for their radiocarbon age and Li/Mg ratio to obtain changes in glacial thermocline water properties near todays ABF. While temperatures are at a constant low value during the glacial, ventilation ages increase towards the LGM coiciding with the aging of thermocline equatorial North Atlantic and Antarctic circumpolar current waters (Chen *et al.*, 2015).

Strong glacial thermocline cooling indicates a shoaling of the thermocline during the last glacial. At the start of H1, Li/Mg temperatures begin to rise in a sharp and intense

increase. Modern-day temperatures are observed for the last 14 ka. Surface water temperatures increase more gradually and reach their modern day values not before later in the holocene. This hints towards a deepening of the thermocline occuring simultaneously to the sea level rise.
An enhanced Hadley circulation and, thus, an enhanced, cold BeC are a likely candidate for the observed water mass properties. As the BeC lacks the influx of warm water from the Indian ocean via the Angulhas leakage, cut off by a thermal barrier at the tip of Africa during the glacial periods, it transports cold waters towards the north. Alternatively an enhanced coastal upwelling could lead to the observed cooling and aging of thermocline waters. However, changes in upwelling intensity occur in sharp events (Little *et al.*, 1997a), this cannot explain the gradually aging of thermocline waters. Nevertheless, increased upwelling cannot be completely ruled out.
Both hypotheses imply an enhanced northward wind most likely caused by an intensification of the Hadley circulation. If the hypothesis of an advection of cold and aged polar water masses is valid, a major temperature drop during the glacial throughout the entire thermocline Atlantic would be expected. A shoaling of the thermocline would, furthermore, reduce vertical mixing near the surface in the mid-depth Atlantic ocean. This hypothesis was tested in the following chaper 6. Li/Mg ratios of CWCs from six locations throughout the Atlantic were analysed revealing similar and synchronous temporal patterns coinciding with atmospheric ice core data. Two published Atlantic data sets from the Gulf of Cadiz and the Rockall Bank agree well with the presented data. These temporal temperature patterns are clearly systematic and cannot be explained by vital effects, diagenesis, incorporated organic matter or changes in seawater Li/Mg ratios as these would produce more randomly distributed data. Therefore, the presented CWC temperature data is assumed to reflect changes in thermocline water temperatures (ThWT). During the LGM all ThWTs are at similar low values of about 2 ± 1 °C in the North and South Atlantic. However, some locations show physically unreasonable low temperatures of down to -5 °C. The reason for such low reconstructed temperatures resulting from extremely high Li/Mg ratios is not understood yet. The hypothesis of local Li input at these locations was tested in chapter 9.
While temperatures in the South Atlantic start to rise at the beginning of H1, coinciding with the Vostok ice core, CWCs in the North Atlantic disappear at that time before reappearing at modern-day temperatures just before the Bølling-Allerød stadial at about 15 ka. Near the Azores Front, CWC data shows a different pattern as temperatures stay relatively low and are highly variant during the Termination 1 until modern day temperatures are observed just after the Younger Dryas at about 11.5 ka. A reasonable explanation for the glacial cooling, again, is the equatorward advection

of polar waters.
To obtain further information on the origin of the water masses and their pathways, reservoir ages were obtained through coralline radiocarbon ages. These seem to confirm the hypothesis of polar water advection. Water masses in the South Atlantic become poorer ventilated during the LGM, while coralline radiocarbon data near the Azores Front and the North Atlantic reveal better ventilated water masses. Furthermore ventilation ages during the glacial and the deglacation are highly variable, while Holocene ventilation ages are more stable. A comparison between coralline paleo- and modern seawater $\Delta^{14}C_{sw}$ data further hints towards a strong influence of the Azores Front on the Atlantic thermocline water pathways.

Do hydrothermal fluids influence the Li/Mg thermometer near the Azores?

In the second part of this thesis, the hypothesis of hydrothermal fluids influencing the seawater Li concentration and, thus, the Li/Mg ratio in CWCs was tested. In a first step, Li isotopic analysis and measurements were established. It was shown, that lithium can be extracted at high yields of $> 99\,\%$ from CWC and seawater samples. This is crucial due to a strong fractionation occuring during column chromatography. Furthermore, suitable low procedual blanks are achieved.
Measurements using a MC-ICP-MS were successfully conducted at similar reproducibility levels as can be found in published studies. The common values for seawater and CWC samples can be corroborated. This demonstrates, that lithium isotopic analyses can be successfully conducted, opening the pathway for further studies of the lithium isotopic signals of CWCs.
In a second step, a study using six fossil CWCs from the Azores region was conducted. First measurements of δ^7Li of fossil CWCs were produced to study a possible influence of hydrothermal fluids on Li incorporation into the coralline skeleton. The six corals were selected due to previous unexpected Li/Mg and ϵ_{Nd} measurements (Lausecker, 2015; Nakajima, 2016). An average δ^7Li value of $17.9 \pm 1.0\,‰$ was found for all six corals. This value agrees with the formerly published CWC data (Vigier *et al.*, 2015; Rollion-Bard *et al.*, 2009; Cuny-Guirriec, 2020). The δ^7Li values are independent of the Li/Mg ratio and do not correlate with the ϵ_{Nd} measurements of the CWCs. Therefore, no influence of hydrothermal fluids on the Li isotopic composition of the CWCs was found. This also excludes an influence of hydrothermal fluids on the Li/Mg ratio of

the corals and, thus, cannot explain the unreasonable low reconstructed temperatures.

Outlook

As presented for the Angolan margin, locations where CWC growth is found during glacial and interglacial periods, are a unique opportunity for the reconstruction of thermocline waters. Therefore, it would be helpful to find and study more of such locations. The Azores archipelago might be a candidate for continuous CWC growth during glacial and interglacial periods as CWC are found at various times during the last 50 ka. As there are no CWC mounds in this region, no continuous record of CWC growth from coral-bearing sediment cores can be obtained. Therefore, it is, yet, unclear, if periods of missing CWC samples are due to a sampling bias of the surface samples or if no CWC growth occurred during these times. This can only be solved by analysing more samples from this region. One candidate worthwhile to study in more detail is the a small mount near the Azores which was discovered during RV Meteor research cruise M151 and named 'Little brother'. During sampling, the associated fauna that was collected together with the CWCs hinted towards a living or at least 'recently died' CWC reef. The few CWC samples which are analysed yet, however, all revealed a U/Th age of about 45 ka to 50 ka. Therefore, further studies require more analyses in this region.

Furthermore, more analyses on the western site of the Atlantic are necessary to obtain a full picture of the glacial thermocline waters. Most CWCs analysed here originate from the eastern basin boundary of the Atlantic with the exception of the Brazilian data set. To gain further insights into the glacial water pathways and to prove the hypothesis of Arctic waters propagating along the western basin boundary leading to the extremely high reservoir ages found at the Brazilian margin, more data along the way is needed. Candidates for suitable CWC locations might be the New England Seamounts or the canyons along the Georges Bank off the coast of the USA and the region around the Lesser Antilles in the south, where the Arctic water masses would need to pass on their way to the south.

Another proxy to trace the water mass provenance is the Nd isotopic composition of the CWC samples. As was observed e.g. near the Azores, this proxy is not suitable for every location. For the Brazilian margin, however, this might by a another helpful tool to be able to make a statement about the origin of the extremely poor ventilated water masses.

The findings of the North Atlantic are mainly based on the Galicia Bank and the Gulf

of Cadiz. It would be neccessary to confirm these finding at further locations, like the Rockall Bank and Porcupine Seabight or the Reykjanes Ridge off Iceland. For most of the known North Atlantic locations, however, little to know coral growth is observed during the LGM. Therefore, a multi-archive analysis using the findings of this CWC study combined with data from e.g. mid-depth sediment cores might be useful to obtain further clarity on the water pathways and provenance during the glacial.

The mechanism influencing the Li/Mg thermometer to extremely high Li/Mg ratios in some regions remains still unknown. To better understand the Li/Mg thermometer it is crucial to find the influences causing these high Li/Mg ratios. Another hypothesis might be a stress induced change the Li incorporation during the calcification process of the CWCs at very low temperatures. As the CWCs revealing extremely high Li/Mg ratios probably did not live at favourable conditions, i.e. at low seawater temperatures, this might induce stress on the organisms. However, this hypothesis is not investigated as easily, as such an experiment most likely must be conducted using cultured CWCs which grew in controlled environments.

Furthermore, a possible variation of the Li isotopic composition of the CWCs might be smaller than the currently achieved precision of δ^7Li measurements. Therefore, to further study a possible influence of hydrothermal fluids it might be helpful to analyse modern samples known to have grown in direct neighbourhood to hydrothermal sources, where hydrothermal influences would be largest. Such a location would be e.g. the Menez Gwen hydrothermal vent field near the Azores. Further analyses of the seawater and hydrothermal fluids at the CWC location can provide further insights into the possible disturbances of the Li isotopic composition through hydrothermal fluids.

Nevertheless, δ^7Li measurements are a common tool for weathering analyses. Therefore, changes in freshwater discharge and river run-off might be studied through δ^7Li measurements. A potential effect would be best observed using e.g. tropical corals near a large freshwater source like the Amazon river.

Appendix

A Coral locations

Table A.1: Compiled sample locations. Gear abbreviations are: Grab sampler (GS), Box Corer (BC), Giant Box Corer (GBC), Gravity Core (GC), Piston Core (PC), TV-Grab (TVG), Remotely operated vehicle (ROV).

	Station ID/Core ID	Gear	Location	Latitude N	Longitude E	water depth m
Galicia Bank	DR17	Dredge	Galicia Bank	42° 40.866'	-11° 36.642'	813
	DR19	Dredge	Galicia Bank	42° 43.632'	-11° 50.232'	796
	DR20	Dredge	Galicia Bank	42° 34.536'	-11° 44.262'	806
	DR22	Dredge	Galicia Bank	42° 39.780'	-11° 56.964'	919
	DR23	Dredge	Galicia Bank	42° 48.618'	-11° 43.350'	861.5
	DR24	Dredge	Galicia Bank	42° 48.618'	-12° 5.148'	1241.5
Azores	GeoB23106-1	GS	José Gaspar seamount	37° 40.522´	-25° 42.996´	314
	GeoB23109-1	GS	Mar da Prata NW	37° 40.112'	-25° 55.562'	834
	GeoB23113-1	GS	Mar da Prata NW	37° 39.914'	-25° 57.755'	944
	GeoB23120-1	GS	Mar da Prata NW	37° 39.922'	-25° 57.876'	949
	GeoB23121-1	GS	Mar da Prata NW	37° 39.930'	-25° 57.968'	961
	GeoB23125-1	GS	Albatroz seamount	38° 06.932'	-27° 10.893'	770
	GeoB23147-1	GS	Acor Bank South	38° 01.872'	-29° 25.558'	830
	GeoB23153-1	GS	Acor Bank South	38° 01.875'	-29° 25.565'	832
	GeoB23161-1	BC	José Gaspar seamount	37° 40.526'	-25° 42.995'	311
	GeoB23182-1	ROV	Jose Gaspar seamount	37° 40.509'	-25° 43.048'	293
	Faial Pico Channel 400m	Dredge	Faial Pico Channel	38° 28.122'	-28° 35.415'	400
	M128-755-ROV	ROV	Pico Ridge	38° 23.253'	-27° 55.615'	504
	M128-827-TVG	TVG	rift zone N of Capelinhos	38° 40.692'	-28° 47.509'	647
	M128-811-TVG	TVG	cone SW Capelinos	38° 11.779'	-29° 33.673'	720
	MG	Dredge	Menez Gwen hydrothermal vent field	37° 51.710'	-31° 31.162'	850
	Acor	Dredge	Acor Seamount	38° 04.916'	-29° 08.649'	893

Continued on next page

Table A.1 – *Continued from previous page*

	Station ID/Core ID	Gear	Location	Latitude N	Longitude E	water depth m
Great Meteor Seamount	GeoB23415-1 Rov1	ROV	Great Meteor Seamount North	30° 14.743'	-28° 26.289'	985
	GeoB23415-1 Rov3	ROV	Great Meteor Seamount North	30° 14.681'	-28° 26.312'	971
	GeoB23415-1 Rov4	ROV	Great Meteor Seamount North	30° 14.460'	-28° 26.353'	894
	GeoB23415-1 Rov5	ROV	Great Meteor Seamount North	30° 14.353'	-28° 26.352'	822
	GeoB23415-1 Rov7	ROV	Great Meteor Seamount North	30° 14.206'	-28° 26.442'	751
	GeoB23425-1 Rov1	ROV	Great Meteor Seamount South	29° 33.893'	-28° 20.334'	946
	GeoB23425-1 Rov6	ROV	Great Meteor Seamount South	29° 33.923'	-28° 20.352'	943
	GeoB23425-1 Rov8	ROV	Great Meteor Seamount South	29° 33.999'	-28° 20.384'	902
	GeoB23425-1 Rov9	ROV	Great Meteor Seamount South	29° 34.070'	-28° 20.408'	883
	GeoB23429-1 Rov5	ROV	Great Meteor Seamount NW	30° 46.617'	-28° 43.617'	895
	GeoB23429-1 Rov8	ROV	Great Meteor Seamount NW	30° 05.173'	-28° 43.552'	906
	GeoB23434-1 Rov2	ROV	Little Meteor Bank North	29° 39.206'	-29° 00.924'	893
	GeoB23436-1	GS	Little Meteor Bank North	29° 39.235'	-29° 00.881'	852
	GeoB23437-1	GS	Little Meteor Bank North	29° 39.262'	-29° 00.827'	811
Mauritania	GeoB 14884-1	GC	Timiris deep coral mound chain	18° 57.803'	-16° 52.123'	492
	GeoB 14905-2	GC	Banda slide	17° 32.456'	-16° 39.999'	493
	GeoB14890-2	GC	Canyon S of Timiris mound chain	18° 38.792'	-16° 43.698'	580
	GeoB14899-1	GC	Banda mounds	17° 40.191'	-16° 40.329'	485
Angola	GeoB20907-1	GS	Valentine Mound	-9° 44.092'	12° 42.410'	517
	GeoB20908-2	GC	Valentine Mound	-9° 43.605'	12° 42.893	439
	GeoB20909-1	GS	Valentine Mound	-9° 42.871'	12° 42.997'	396
	GeoB20910-1	GS	Twin Mounds	-9° 43.573'	12° 44.664'	334
	GeoB20913-1	GS	Anna Ridge	-9° 47.296'	12° 46.401'	307
	GeoB20917-1 #6	ROV	Valentine Mound	-9° 43.626'	12° 42.898'	446

Continued on next page

Table A.1 – *Continued from previous page*

	Station ID/Core ID	Gear	Location	Latitude N	Longitude E	water depth m
	GeoB20927-1 #9	ROV	Buffalo Mounds	-9° 41.998'	12° 43.883'	356
	GeoB20928-1	GC	Valentine Mound	-9° 43.388'	12° 42.899'	457
	GeoB20930-4 #3	ROV	Scary Mound	-9° 49.372'	12° 46.436'	374
	GeoB20930-6 #5	ROV	Scary Mound	-9° 49.354'	12° 46.540'	361
	GeoB20933-1	GC	Scary Mound	-9° 49.331'	12° 46.565'	338
	GeoB20934-2	GS	Scary Mound	-9° 49.362'	12° 46.543'	382
	GeoB20935-1	GS	Scary Mound	-9° 49.384'	12° 46.514'	412
	GeoB20951-1	ROV	Buffalo Mounds	-9° 42.096'	12° 43.746'	357
	GeoB20953-2	GBC	Snake Mound	-9° 43.022'	12° 45.996'	259
	GeoB20955-1	GS	Anna Ridge	-9° 44.680'	12° 46.896'	299
	GeoB20958-1	GS	Castle Mound	-9° 39.898'	12° 42.937'	453
Brazil	MXL-030	PC	Santos Basin	-24° 37.567'	-44° 01.150'	808
	C1	PC	Campos Basin	-22° 24.767'	-40° 08.683'	621
	C2	PC	Santos Basin	-24° 15.400'	-43° 12.100'	781
	K-GLC-PPT-06	PC	Campos Basin	-23° 29.450'	-41° 06.667'	626
	M125-4-2	GC	Off Paraiba do Sul	-21° 56.957'	-39° 53.117'	866

B Li/Mg data

Table B.1: Li/Mg data of CWCs from the Galicia Bank.

Lab.No.	Sample ID	Dredge ID	Age ka	2σ	Li/Ca µg/g	σ	Mg/Ca mg/g	σ	Li/Mg mg/g	σ	Li/Mg* mmo/mol	σ	Temperature	2σ
8889[1]	DR17 Vario 1/1 17.23	DR17	0.73	0.03	1.03	0.03	1.29	0.02	0.80	0.02	3.42	0.08	9.4	1.2
8638[1]	BT1 DR17 17.1	DR17	11.69	0.04	2.14	0.03	2.10	0.02	1.02	0.02	3.76	0.03	7.4	1.0
8637[1]	BT1 DR17 17.4	DR17	11.74	0.04	1.72	0.03	2.09	0.03	0.82	0.02	3.03	0.02	11.8	1.0
8643[1]	BT1 DR17 17.9	DR17	12.15	0.06	2.15	0.06	2.11	0.04	1.02	0.03	3.74	0.07	7.5	1.0
8642[1]	BT1 DR17 17.8	DR17	12.42	0.05	2.45	0.05	2.56	0.04	0.96	0.02	3.52	0.05	8.8	1.0
8886[1]	DR17 Vario 1/1 17.20	DR17	14.82	0.09	1.31	0.03	1.69	0.01	0.78	0.02	3.31	0.07	10.0	1.2
8892[1]	DR19 3/3 19.1	DR19	14.01	0.03	2.48	0.05	3.10	0.01	0.80	0.02	3.01	0.06	12.0	1.3
8680[1]	M.O.DR 20 20.14	DR20	0.07	0.00	1.84	0.03	2.05	0.02	0.89	0.01	3.29	0.04	10.1	1.0
8676[1]	M.O.DR 20 20.2	DR20	0.09	0.00	1.70	0.03	1.92	0.02	0.89	0.01	3.27	0.04	10.3	1.0
8675[1]	M.O.DR 20 20.1	DR20	0.13	0.00	1.94	0.03	2.21	0.02	0.88	0.01	3.22	0.02	10.6	1.0
8639[1]	M.o. DR20 1/1 20.9	DR20	0.18	0.01	1.81	0.03	2.07	0.03	0.88	0.02	3.23	0.03	10.5	1.0
8679[1]	M.O.DR 20 20.12	DR20	0.19	0.00	1.70	0.03	1.89	0.03	0.90	0.01	3.31	0.04	10.1	1.0
8678[1]	M.O.DR 20 20.11	DR20	0.20	0.02	1.77	0.02	1.95	0.02	0.91	0.01	3.35	0.03	9.8	1.0
8640	M.o. DR20 1/1 20.16	DR20	0.23	0.02	1.84	0.03	2.02	0.04	0.91	0.02	3.34	0.02	9.8	1.0
8677[1]	M.O.DR 20 20.8	DR20	0.24	0.01	1.43	0.03	1.63	0.02	0.88	0.01	3.22	0.04	10.6	1.0
8686[1]	Fl.DR 20 20.25	DR20	0.71	0.02	1.10	0.03	1.04	0.01	1.06	0.02	4.50	0.10	3.7	1.0
8685[1]	Fl.DR 20 20.24	DR20	1.01	0.04							2.74	0.04	13.9	1.3
8924*	DR22 2/2 b 22.1	DR22	14.67	0.04									11.2	1.2
8924a[1]		DR22			1.72	0.04	2.43	0.04	0.71	0.01	3.03	0.05	11.8	1.2
8924b		DR22			2.90	0.05	3.39	0.02	0.86	0.02	3.22	0.06	10.6	1.2
6686	0710Dr.22 2/2a	DR22	15.26	0.57	2.42	0.07	2.93	0.02	0.82	0.02	3.05	0.09	11.7	1.5
8923[1]	DR22 2/2 b 22.1	DR22	21.53	0.06	3.01	0.09	2.77	0.07	1.09	0.02	4.63	0.08	3.2	1.0

Continued on next page.

Table B.1 – *Continued from previous page*

Lab.No.	Sample ID	Dredge ID	Age ka	2σ	Li/Ca µg/g	σ	Mg/Ca mg/g	σ	Li/Mg mg/g	σ	Li/Mg* mmo/mol	σ	Temperature	2σ
8682[1]	M.O.DR 23 23.12	DR23	0.09	0.00	1.99	0.04	2.38	0.02	0.84	0.01	3.07	0.05	11.5	1.1
8683[1]	M.O.DR 23 23.14	DR23	0.10	0.01	2.08	0.02	2.45	0.02	0.85	0.01	3.12	0.03	11.2	1.0
8645[1]	M.o. DR23 23.3	DR23	0.11	0.02	1.87	0.03	2.14	0.02	0.88	0.01	3.23	0.03	10.5	1.0
8681[1]	M.O.DR 23 23.11	DR23	0.12	0.01	1.78	0.02	2.07	0.02	0.86	0.01	3.17	0.04	10.9	1.0
8684[1]	M.O.DR 23 23.15	DR23	0.14	0.01	1.92	0.03	2.31	0.02	0.83	0.01	3.07	0.04	11.5	1.1
8646[1]	M.o. DR23 23.7	DR23	0.20	0.01	2.00	0.03	2.25	0.02	0.89	0.01	3.27	0.03	10.3	1.0
8644[1]	M.o. DR23 23.2	DR23	0.21	0.00	2.08	0.03	2.28	0.03	0.91	0.02	3.36	0.02	9.8	1.0
8673[1]	M.o. DR24 24.9	DR24	0.08	0.00	1.78	0.02	1.91	0.01	0.94	0.01	3.45	0.04	9.2	1.0
8672[1]	M.o. DR24 24.8	DR24	0.17	0.01	2.11	0.02	2.14	0.02	0.98	0.01	3.62	0.04	8.2	1.0
8674[1]	M.O.DR 24 24.13	DR24	0.18	0.01	2.11	0.02	2.15	0.02	0.98	0.01	3.61	0.03	8.2	1.0
8647[1]	M.o. DR24 24.1	DR24	0.19	0.02	1.80	0.03	1.77	0.02	1.01	0.01	3.73	0.04	7.6	1.0
8671[1]	M.o. DR24 24.7	DR24	0.19	0.01	2.21	0.04	2.17	0.02	1.02	0.02	3.75	0.06	7.5	1.0
8670[1]	M.o. DR24 24.3	DR24	0.21	0.03	1.82	0.03	2.01	0.02	0.91	0.01	3.34	0.04	9.8	1.0
8648[1]	M.o. DR24 24.4	DR24	0.35	0.02	1.85	0.02	2.06	0.02	0.90	0.01	3.31	0.02	10.1	1.0

* Mean of multiple measurements of the same CWC. Single measurements are marked as a,b.

[1] from Glasder (2018).

Table B.2: Li/Mg data of CWCs from the Azores.

Lab.No.	Sample ID	Age ka	2σ	Li/Ca µg/g	σ	Mg/Ca mg/g	σ	Li/Mg mg/g	σ	Li/Mg* mmo/mol	σ	Temperature	2σ
6623[1]	Acor14	2.06	0.19	2.22	0.03	2.11	0.02	1.05	0.01	3.48	0.05	9.0	1.0
5993[1]	Acor 15	11.22	0.24	2.09	0.05	1.97	0.02	1.06	0.03	3.52	0.09	8.8	1.2
7721[2]	Acor 08/2010 (5C)	11.54	0.11	1.74	0.05	1.75	0.02	1.00	0.03	3.88	0.11	6.8	1.3
6014[1]	Acor 10	11.94	0.30	2.10	0.04	1.88	0.02	1.12	0.02	3.70	0.09	7.8	1.2
7717[2]	Acor 08/2010 (5A)	12.18	0.09	1.92	0.07	1.69	0.06	1.13	0.02	4.40	0.07	4.2	1.0
6300[1]	Acor7	12.78	0.28	2.58	0.04	1.95	0.01	1.32	0.02	4.37	0.07	4.4	1.0
7718[2]	Acor 08/2010 (2B)	13.04	0.15	2.29	0.08	1.71	0.05	1.34	0.03	5.16	0.14	1.0	1.1
6041[1]	Acor 1	13.07	0.27	2.28	0.03	1.82	0.01	1.25	0.02	4.14	0.06	5.4	1.0
6299[1]	Acor2	13.10	0.30	2.82	0.04	2.09	0.02	1.35	0.02	4.46	0.06	3.9	1.0
6012[1]	Acor 8	13.12	0.27	2.60	0.04	2.05	0.01	1.27	0.02	4.20	0.07	5.2	1.0
7720[2]	Acor 08/2010 (5B)	13.27	0.09	1.88	0.06	1.72	0.02	1.09	0.03	4.26	0.12	4.9	1.2
6013[1]	Acor 9	13.57	0.21	2.97	0.04	2.08	0.01	1.43	0.02	4.71	0.07	2.8	1.0
7716[2]	Acor 08/2010 (6A)	14.02	0.21	1.87	0.10	1.60	0.08	1.17	0.03	4.55	0.13	3.5	1.2
5995[1]	Acor 17	14.04	0.23	2.24	0.04	1.76	0.01	1.28	0.02	4.23	0.07	5.0	1.0
6015[1]	Acor 11	14.20	0.33	2.36	0.03	2.09	0.01	1.13	0.01	3.72	0.06	7.6	1.0
5994[1]	Acor 16	14.66	0.41	2.28	0.02	1.84	0.02	1.24	0.02	4.09	0.05	5.7	1.0
6010[1]	Acor 6	16.97	0.51	2.38	0.04	1.89	0.00	1.26	0.02	4.16	0.07	5.3	1.0
7683[2]	Acor 08/2010 (2A)	37.58	0.32	1.83	0.06	1.61	0.04	1.14	0.03	4.44	0.10	4.0	1.0
7722*	Faial Pico Channel 400m (4B)	0.04	0.03									4.8	1.1
7722a				1.33	0.08	1.23	0.07	1.08	0.09	4.16	0.04	5.4	1.0
7722b[2]										4.39	0.11	4.3	1.1
7715*	Faial Pico Channel 400m (4E)	0.10	0.01									6.2	1.0
7715a[2]				1.38	0.04	1.35	0.01	1.02	0.03	3.92	0.12	6.6	1.4
7715b				1.29	0.08	1.21	0.07	1.06	0.09	4.07	0.08	5.8	1.0

Continued on next page.

Table B.2 – *Continued from previous page*

Lab.No.	Sample ID	Age ka	2σ	Li/Ca µg/g	σ	Mg/Ca mg/g	σ	Li/Mg mg/g	σ	Li/Mg* mmo/mol	σ	Temperature	2σ
7684[2]	Faial Pico Channel 400m (4A)	0.14	0.01	1.34	0.05	1.43	0.03	0.93	0.03	3.63	0.11	8.1	1.4
7723[2]	Faial Pico Channel 400m (4C)	0.17	0.06							3.80	0.10	7.2	1.3
7681[2,5]	Menez Gwen (Azores) (3A)	12.59	0.09	1.90	0.08	1.50	0.05	1.27	0.04	4.95	0.16	1.8	1.3
8845*	M128-755-ROV5-3	0.24	0.09									5.7	4.4
8845a[3]										3.67	0.07	7.9	1.0
8845b				1.34	0.07	1.13	0.03	1.18	0.07	4.54	0.20	3.6	1.8
8837[3]	M128-811-TVG-4	0.74	0.02	2.37	0.03	2.40	0.00	0.99	0.01	3.57	0.04	8.5	1.0
8765[3]	M128-811-TVG-3	0.90	0.02	2.01	0.03	2.03	0.03	0.99	0.01	3.67	0.03	7.9	1.0
8862[3]	M128-811-TVG-6	0.92	0.01	1.87	0.04	1.83	0.01	1.02	0.02	3.69	0.08	7.8	1.1
8757[3]	M128-755-ROV5-2	0.92	0.05	1.78	0.03	2.09	0.03	0.85	0.01	3.14	0.04	11.1	1.0
8764[3]	M128-811-TVG-1	1.12	0.07	2.18	0.03	2.11	0.02	1.03	0.01	3.81	0.04	7.1	1.0
8844[3]	M128-827-TVG-5	39.93	0.11	2.60	0.03	1.67	0.01	1.56	0.02	5.62	0.07	-0.8	1.0
10794[4]	GeoB23161 - 1	0.00	0	1.51	0.11	2.03	0.15	0.74	0.08	2.81	0.03	13.4	1.2
10136[4]	GeoB23182-4	0.05	0.02	1.58	0.09	2.25	0.12	0.70	0.06	2.69	0.05	14.3	1.4
10848[4]	GeoB23106-1-3	0.07	0.02	1.41	0.12	1.51	0.12	0.93	0.11	3.55	0.06	8.6	1.0
10085[4]	GeoB23125-1 GS F	0.15	0.03	1.80	0.12	1.78	0.12	1.01	0.10	3.87	0.06	6.8	1.0
10079[4]	GeoB23121-1 GS S.v.II	0.36	0.16	1.64	0.09	1.41	0.08	1.16	0.09	4.44	0.04	4.1	1.0
10515	GeoB23109-1 M.o.	10.99	0.08	1.90	0.13	1.99	0.13	0.96	0.09	3.65	0.07	8.0	1.0
10087[4]	GeoB23147-1 GS M.b.	12.26	0.06	1.86	0.15	2.18	0.18	0.85	0.10	3.24	0.05	10.5	1.0
10086[4]	GeoB23147-1 GS L.p.	12.27	0.07	1.72	0.10	1.58	0.09	1.09	0.09	4.12	0.06	5.5	1.0
10088	GeoB23153-1 GS M.o.	12.42	0.06	1.87	0.15	1.75	0.14	1.07	0.12	4.03	0.07	6.0	1.0
10089	GeoB23153-1 GS L.p.	13.12	0.07	2.17	0.17	1.83	0.15	1.19	0.14	4.49	0.12	3.8	1.2
10460*[5]	GeoB23109-1 GS L.p.	17.33	0.07									-2.7	1.1
10460a				3.00	0.08	2.00	0.05	1.50	0.01	6.03	0.06	-2.2	1.0

Continued on next page.

Table B.2 – *Continued from previous page*

Lab.No.	Sample ID	Age ka	2σ	Li/Ca µg/g	σ	Mg/Ca mg/g	σ	Li/Mg mg/g	σ	Li/Mg* mmo/mol	σ	Temperature	2σ
10460b[4]				2.65	0.19	1.58	0.11	1.67	0.01	6.35	0.07	-3.3	1.0
10080*	GeoB23121-1 GS S.v.III	18.41	0.11									-0.6	2.1
10080a[4]				2.64	0.19	1.89	0.13	1.39	0.14	5.30	0.11	0.4	1.0
10080b										5.88	0.15	-1.7	1.1
10386*[5]	GeoB23120-1 S.v.?	18.94	0.12									-5.0	1.0
10386a				3.08	0.08	1.80	0.04	1.71	0.02	6.88	0.08	-4.9	1.0
10386b[4]				2.33	0.15	1.33	0.08	1.75	0.15	6.95	0.16	-5.1	1.0
10385[4,5]	GeoB23120-1 D.dianthus top	19.71	0.09	2.85	0.20	1.56	0.10	1.83	0.18	6.74	0.19	-4.5	1.2
10408[4,5]	GeoB23120-1 D.dianthus bottom	19.79	0.09	2.65	0.19	1.58	0.11	1.67	0.17	6.65	0.08	-4.2	1.0
10384[4,5]	GeoB23113-1 M.o.?	19.94	0.07	2.06	0.15	1.16	0.08	1.78	0.17	6.48	0.08	-3.7	1.0
10078[4,5]	GeoB23121-1 GS S.v.I	22.17	0.09	2.46	0.14	1.43	0.08	1.72	0.14	6.50	0.07	-3.8	1.0
10383[4,5]	GeoB23113-1 S.v.?	22.39	0.07	2.49	0.16	1.45	0.09	1.72	0.16	6.81	0.12	-4.7	1.0

* Mean of multiple measurements of the same CWC. Single measurements are marked as a,b.

[1] from Lausecker (2015).

[2] from Nakajima (2016).

[3] from Rosenthal (2018).

[4] from Rampmeier (2021).

[5] Excluded after quality control.

Table B.3: Li/Mg data of CWCs from the Great Meteor Seamount.

Lab.No.	Sample ID GeoB234	Age ka	2σ	Li/Ca µg/g	σ	Mg/Ca mg/g	σ	Li/Mg mg/g	σ	Li/Mg* mmo/mol	σ	Temperature	2σ
9819[1]	34-1 (jung)	0.083	0.011	1.489	0.036	1.623	0.034	0.917	0.012	3.21	0.04	10.6	1.0
10128[2]	34-1 Rov2	0.094	0.003	1.362	0.073	1.281	0.070	1.063	0.081	3.93	0.07	6.5	1.0
9823*	15-1 Rov4	0.097	0.003									7.9	1.5
9823a[1]				1.599	0.037	1.583	0.030	1.010	0.014	3.54	0.05	8.7	1.0
9823b[2]				1.507	0.089	1.466	0.083	1.028	0.084	3.79	0.08	7.2	1.0
9825[1]	15-1 Rov5A(2)	0.098	0.003	1.564	0.044	1.533	0.033	1.020	0.019	3.57	0.07	8.5	1.0
10034*	25-1 Rov1(2)	0.113	0.003	2.366	0.082	1.836	0.043	1.289	0.034			6.9	1.6
10034a[1]				1.586	0.039	1.498	0.030	1.059	0.014	3.71	0.05	7.7	1.0
10034b[2]				1.520	0.084	1.398	0.075	1.088	0.084	4.01	0.06	6.1	1.0
10035*	25-1 Rov1(3)	0.121	0.004									6.5	1.0
10035a[2]										3.90	0.08	6.7	1.0
10035b[1]				1.692	0.045	1.490	0.035	1.136	0.015	3.98	0.05	6.3	1.0
9960[1]	15-1 bulk(2)	0.132	0.005	1.564	0.047	1.552	0.036	1.008	0.020	3.53	0.07	8.7	1.1
9861[1]	15-1 Rov7(2)	0.157	0.004	1.509	0.036	1.523	0.030	0.991	0.013	3.47	0.05	9.1	1.0
9822[1]	15-1 Rov3	0.166	0.005	1.554	0.044	1.498	0.036	1.038	0.016	3.63	0.06	8.1	1.0
9860[1]	15-1 Rov7(1)	0.180	0.004	1.469	0.038	1.530	0.032	0.960	0.015	3.36	0.05	9.7	1.0
10032[1]	25-1 Rov1(1)	0.199	0.006	1.610	0.039	1.483	0.033	1.085	0.010	3.80	0.04	7.2	1.0
9824[1]	15-1 Rov5A(1)	0.223	0.003	1.427	0.033	1.408	0.028	1.014	0.013	3.55	0.05	8.6	1.0
9827[1]	15-1 Rov5A(4)	0.233	0.010	1.623	0.038	1.635	0.037	0.993	0.007	3.48	0.03	9.0	1.0
9821[1]	15-1 Rov1	0.257	0.009	1.610	0.044	1.490	0.035	1.080	0.015	3.78	0.05	7.3	1.0
9820[1]	34-1 (alt)	0.352	0.015	1.594	0.037	1.815	0.032	0.878	0.013	3.08	0.05	11.5	1.1
10074[1]	29-1 Rov5(3)	0.459	0.007	2.543	0.060	1.758	0.037	1.447	0.016	3.56	0.05	8.5	1.0
9961[1]	29-1 Rov5(1)	0.547	0.021	1.536	0.050	1.466	0.042	1.048	0.017	3.70	0.07	7.8	1.0
10075[1]	29-1 Rov5(4)	0.554	0.009	2.035	0.058	1.735	0.044	1.173	0.016	3.65	0.10	8.1	1.3

Continued on next page.

Table B.3 – *Continued from previous page*

Lab.No.	Sample ID GeoB234	Age ka	2σ	Li/Ca µg/g	σ	Mg/Ca mg/g	σ	Li/Mg mg/g	σ	Li/Mg* mmo/mol	σ	Temperature	2σ
9962[1]	29-1 Rov5(2)	0.561	0.013	2.028	0.053	2.016	0.047	1.006	0.014	3.53	0.05	8.7	1.0
10037[1]	25-1 Rov6(2)	0.663	0.074	1.851	0.048	1.655	0.036	1.118	0.016	3.92	0.06	6.6	1.0
10038[1]	25-1 Rov6(3)	1.614	0.015	1.691	0.040	1.515	0.033	1.116	0.012	3.91	0.04	6.6	1.0
10077*	29-1 Rov8(2)	10.411	0.066									6.8	1.0
10077a[1]				1.468	0.036	1.343	0.029	1.093	0.015	3.86	0.05	6.9	1.0
10077b[2]				1.454	0.081	1.366	0.074	1.064	0.082	3.91	0.06	6.6	1.0
10076*	29-1 Rov8(1)	10.980	0.038									5.2	1.0
10076a[1]				1.510	0.037	1.283	0.030	1.177	0.011	4.15	0.04	5.4	1.0
10076b[2]				1.380	0.077	1.196	0.064	1.154	0.089	4.23	0.09	5.0	1.0
10040[1]	25-1 Rov8(2)	11.209	0.059	2.055	0.041	2.650	0.044	0.775	0.009	3.69	0.09	7.8	1.2
10043*	25-1 Rov9(3)	12.295	0.033									6.8	1.2
10043a[1]				1.565	0.040	1.464	0.036	1.069	0.008	3.77	0.04	7.4	1.0
10043b[2]				1.508	0.085	1.385	0.075	1.089	0.085	4.00	0.06	6.2	1.0
10041[1]	25-1 Rov9(1)	12.648	0.512	1.657	0.058	1.571	0.037	1.055	0.027	5.08	0.06	1.3	1.0
10042*	25-1 Rov9(2)	13.455	0.132									6.5	1.0
10042a[1]				1.905	0.045	1.674	0.032	1.138	0.015	4.00	0.06	6.2	1.0
10042b[2]				1.814	0.097	1.721	0.085	1.054	0.077	3.87	0.09	6.8	1.1
10459[2]	37-1 solitär	14.161	0.063	1.784	0.100	1.459	0.079	1.223	0.095	4.50	0.08	3.8	1.0
10140*	36-1 GS M.o. "alt"	16.227	0.048									0.7	1.0
10140a[2]				2.030	0.097	1.458	0.070	1.392	0.095	5.12	0.12	1.1	1.0
10140b										5.32	0.04	0.3	1.0
10511*	37-1 M.o.?	18.399	0.051									-1.1	1.0
10511a[2]				2.055	0.042	1.347	0.018	1.525	0.038	5.62	0.14	-0.8	1.0
10511b				2.393	0.064	1.669	0.040	1.434	0.017	5.77	0.07	-1.3	1.0

Continued on next page.

Table B.3 – *Continued from previous page*

Lab.No.	Sample ID GeoB234	Age ka	2σ	Li/Ca µg/g	σ	Mg/Ca mg/g	σ	Li/Mg mg/g	σ	Li/Mg* mmo/mol	σ	Temperature	2σ
10143[2]	36-1 GS Lip.	21.221	0.042	2.345	0.130	1.463	0.081	1.603	0.126	5.91	0.16	-1.8	1.1

* Mean of multiple measurements of the same CWC. Single measurements are marked as a,b.

[1] from Dardoufas (2019).

[2] from Rampmeier (2021).

Table B.4: Li/Mg data of CWCs from off the coast of Mauritania. All data from Schneider (2018)

Lab.No.	Core ID GeoB14	Core-depth cm	Age ka	2σ	Li/Ca µg/g	σ	Mg/Ca mg/g	σ	Li/Mg mg/g	σ	Li/Mg* mmo/mol	σ	Temperature	2σ
8052	884-1	19	19.80	0.07	2.64	0.07	1.92	0.03	1.37	0.03	4.82	0.11	2.4	1.0
8799	884-1	145.5	36.56	0.09	2.01	0.03	2.43	0.03	0.83	0.01	4.15	0.05	5.4	1.0
8054	884-1	119	36.57	0.11	2.49	0.08	2.04	0.03	1.22	0.03	4.28	0.12	4.8	1.2
8053	884-1	99	36.71	0.10	2.10	0.05	1.89	0.03	1.11	0.02	3.91	0.08	6.6	1.0
8801	884-1	228	37.46	0.10	2.26	0.04	2.00	0.03	1.13	0.01	4.16	0.05	5.4	1.0
8230	905-2	1	13.13	0.06	1.87	0.03	2.21	0.03	0.84	0.01	3.49	0.03	9.0	1.0
8231	905-2	199	13.67	0.07	2.17	0.02	2.07	0.01	1.05	0.01	4.35	0.03	4.4	1.0
8232	905-2	281	14.18	0.09	1.84	0.02	2.19	0.01	0.84	0.01	3.44	0.04	9.2	1.0
8233	905-2	429	14.31	0.06	1.78	0.02	2.11	0.02	0.85	0.01	3.47	0.02	9.1	1.0
8813	905-2	491.5	14.32	0.05	2.17	0.04	2.23	0.01	0.97	0.01	3.51	0.05	8.8	1.0
8814	905-2	557.5	19.97	0.03	2.97	0.03	2.22	0.00	1.34	0.02	4.82	0.06	2.3	1.0
8235	905-2	590.5	20.88	0.11	1.93	0.03	2.09	0.03	0.92	0.01	4.95	0.05	1.8	1.0
8815	905-2	667	34.13	0.09	2.72	0.03	2.20	0.01	1.24	0.01	4.46	0.05	3.9	1.0
8816	905-2	837.5	34.53	0.16	2.37	0.05	2.04	0.01	1.16	0.02	4.19	0.08	5.2	1.0
8236	905-2	741	34.78	0.25	2.59	0.05	2.18	0.04	1.19	0.01	4.59	0.03	3.3	1.0
8237	905-2	953	36.88	0.14	2.51	0.04	2.27	0.03	1.11	0.01	3.42	0.03	9.4	1.0
9154	890-2	20.5	10.18	0.04	1.96	0.07	1.99	0.07	0.99	0.02	3.66	0.06	8.0	1.0
9155	890-2	53	12.59	0.04	1.77	0.03	1.89	0.03	0.94	0.01	3.48	0.03	9.0	1.0
9156	890-2	109	13.60	0.04	2.35	0.05	2.06	0.03	1.14	0.02	4.23	0.07	5.0	1.0
9158[1]	890-2	228	25.56	0.07	3.20	0.12	1.99	0.07	1.61	0.03	5.99	0.11	-2.1	1.0
9160	890-2	350	34.42	0.09	2.84	0.03	2.01	0.01	1.41	0.02	5.26	0.06	0.6	1.0
9157	890-2	203	34.60	0.12	2.52	0.02	1.88	0.01	1.34	0.01	4.99	0.04	1.6	1.0
9159	890-2	309	34.91	0.08	2.49	0.05	2.17	0.02	1.15	0.02	4.27	0.07	4.8	1.0

Continued on next page.

Table B.4 – *Continued from previous page*

Lab.No.	Core ID GeoB14	Core-depth cm	Age ka	2σ	Li/Ca µg/g	σ	Mg/Ca mg/g	σ	Li/Mg mg/g	σ	Li/Mg* mmo/mol	σ	Temperature	2σ
8930	899-1	15	34.07	0.11	2.57	0.09	2.15	0.07	1.20	0.01	4.45	0.05	4.0	1.0
8929	899-1	10.5	35.65	0.08	2.31	0.08	2.05	0.06	1.13	0.02	4.19	0.06	5.2	1.0
8931	899-1	25	36.56	0.14	2.24	0.05	1.88	0.04	1.19	0.01	4.43	0.04	4.1	1.0
8936	899-1	225	36.98	0.21	2.24	0.03	1.89	0.02	1.19	0.02	4.42	0.08	4.1	1.0
8935	899-1	160.5	37.08	0.09	2.40	0.07	2.26	0.06	1.07	0.01	3.96	0.05	6.4	1.0
8933	899-1	110	37.37	0.19	2.30	0.06	2.30	0.05	1.00	0.01	3.72	0.05	7.7	1.0
8940	899-1	335.5	38.12	0.19	3.02	0.13	2.18	0.09	1.39	0.02	5.15	0.08	1.0	1.0
8941	899-1	398.75	38.85	0.12	2.78	0.03	1.96	0.02	1.42	0.01	5.27	0.05	0.5	1.0

[1] Excluded after quality control.

Table B.5: Li/Mg data of CWCs from off the coast of Angola

Lab.No.	Core GeoB209	Core-depth cm	Age ka	2σ	Li/Ca µg/g	σ	Mg/Ca mg/g	σ	Li/Mg mg/g	σ	Li/Mg* mmo/mol	σ	Temperature	2σ
10530	28-0	242	11.576	0.029	2.341	0.071	2.504	0.007	0.935	0.029	3.518	0.108	8.78	1.44
10663	28-0	277.5	11.706	0.027	2.574	0.040	2.772	0.008	0.929	0.015	3.494	0.056	8.9	1.00
10664	28-0	335.5	13.254	0.030	2.608	0.048	2.565	0.002	1.017	0.019	3.826	0.071	7.07	1.00
10666	28-0	373	13.232	0.034	2.675	0.053	2.551	0.005	1.048	0.021	3.945	0.079	6.45	1.00
10531	28-1	382.5	13.560	0.033	1.837	0.048	1.798	0.038	1.021	0.034	3.845	0.063	6.97	1.00
10534	28-1	613.5	24.335	0.062	2.426	0.086	1.939	0.049	1.251	0.055	4.710	0.129	2.83	1.14
10547	28-1	687.5	25.054	0.091	2.740	0.070	2.082	0.052	1.316	0.047	4.956	0.071	1.79	1.00
10605	28-1	447.5	16.839	0.050	2.098	0.069	2.142	0.047	0.980	0.039	3.689	0.094	7.82	1.22
10607	28-1	475	17.067	0.043	2.397	0.052	2.007	0.040	1.194	0.035	4.497	0.041	3.77	1.00
10609	28-1	525.5	17.646	0.040	2.365	0.062	1.917	0.041	1.233	0.041	4.644	0.070	3.12	1.00
10613	28-1	465	16.834	0.059	2.014	0.054	1.868	0.041	1.079	0.037	4.061	0.066	5.85	1.00
10614	28-1	485.5	17.075	0.054	2.695	0.064	2.096	0.040	1.286	0.039	4.841	0.073	2.27	1.00
10617	28-1	567	23.918	0.074	2.661	0.078	2.117	0.043	1.257	0.045	4.733	0.103	2.73	1.00
10619	28-1	598.5	24.156	0.071	2.400	0.050	1.890	0.036	1.270	0.036	4.781	0.038	2.52	1.00
10620	28-1	515	17.423	0.044	2.538	0.068	1.962	0.041	1.294	0.044	4.872	0.081	2.14	1.00
10667	28-1	414	13.588	0.074	1.763	0.055	1.783	0.044	0.989	0.039	3.722	0.075	7.63	1.04
10532*	28-1	430	16.685	0.035									6.0	1.0
10532a					1.965	0.057	1.938	0.050	1.014	0.013	4.081	0.053	5.75	1.00
10532b					2.041	0.069	1.935	0.045	1.055	0.043	3.972	0.099	6.30	1.14
10533*	28-1	547.5	17.665	0.045									9.6	1.1
10533a					2.596	0.080	2.109	0.056	1.231	0.020	4.954	0.079	1.80	1.00
10533b					2.477	0.076	1.989	0.047	1.245	0.048	4.689	0.098	2.92	1.00
7917[1]	33-1	0.5	0.465	0.029	1.907	0.023	1.908	0.022	0.999	0.010	3.370	0.032	9.66	1.00
7918[1]	33-1	8.5	1.861	0.007	1.714	0.021	1.702	0.019	1.007	0.014	3.396	0.046	9.51	1.00

Continued on next page.

Table B.5 – *Continued from previous page*

Lab.No.	Core GeoB209	Core-depth cm	Age ka	2σ	Li/Ca µg/g	σ	Mg/Ca mg/g	σ	Li/Mg mg/g	σ	Li/Mg* mmo/mol	σ	Temperature	2σ
7919[1]	33-1	34	3.013	0.012	1.859	0.030	1.889	0.030	0.984	0.011	3.320	0.039	9.96	1.00
7920[1]	33-1	79.5	3.668	0.015	1.964	0.021	1.817	0.018	1.081	0.012	3.645	0.040	8.06	1.00
7921[1]	33-1	114.5	6.305	0.032	2.067	0.023	2.036	0.020	1.015	0.011	3.424	0.037	9.33	1.00
7923[1]	33-1	179.5	7.423	0.047	2.213	0.023	2.176	0.020	1.017	0.010	3.430	0.035	9.30	1.00
7924[1]	33-1	204.5	9.344	0.026	2.047	0.017	1.872	0.020	1.093	0.008	3.687	0.025	7.83	1.00
7925[1]	33-1	208.5	9.396	0.048	2.069	0.028	1.898	0.015	1.090	0.014	3.676	0.049	7.88	1.00
7927[1]	33-1	273	10.617	0.033	1.748	0.019	1.754	0.013	0.996	0.011	3.361	0.036	9.72	1.00
7928[1]	33-1	301.5	10.663	0.038	1.815	0.022	1.805	0.015	1.005	0.011	3.391	0.038	9.53	1.00
7929[1]	33-1	329.5	10.903	0.039	1.639	0.023	1.674	0.020	0.979	0.009	3.301	0.031	10.08	1.00
7930[1]	33-1	384	11.483	0.032	1.837	0.025	1.827	0.017	1.005	0.010	3.391	0.034	9.53	1.00
7931[1]	33-1	412.5	11.463	0.036	1.785	0.020	1.848	0.023	0.966	0.007	3.258	0.023	10.35	1.00
7932[1]	33-1	428	13.258	0.037	1.822	0.023	1.801	0.024	1.012	0.009	3.413	0.031	9.40	1.00
7933[1]	33-1	486	13.484	0.045	1.896	0.035	1.851	0.021	1.025	0.017	3.455	0.056	9.15	1.00
7934[1]	33-1	522.5	13.592	0.045	1.984	0.030	1.897	0.025	1.046	0.011	3.528	0.035	8.73	1.00
7935[1]	33-1	560	13.895	0.040	1.913	0.021	1.871	0.021	1.023	0.008	3.449	0.027	9.19	1.00
7936[1]	33-1	579.5	19.312	0.043	2.423	0.036	1.717	0.025	1.411	0.016	4.760	0.053	2.61	1.00
7937[1]	33-1	630	23.184	0.099	2.507	0.034	1.919	0.039	1.307	0.027	4.482	0.092	3.84	1.00
7938[1]	33-1	662.5	23.070	0.077	2.402	0.030	1.858	0.044	1.293	0.030	4.433	0.103	4.06	1.01
7939[1]	33-1	684.5	25.108	0.081	2.307	0.033	1.678	0.044	1.375	0.037	4.714	0.127	2.81	1.13
7940[1]	33-1	708	26.786	0.101	2.522	0.034	1.903	0.038	1.326	0.021	4.546	0.071	3.55	1.00
7941[1]	33-1	730	26.825	0.062	2.509	0.032	1.801	0.041	1.393	0.030	4.777	0.102	2.54	1.00
7942[1]	33-1	761	31.406	0.096	2.016	0.057	1.511	0.039	1.334	0.049	4.575	0.169	3.42	1.54
7943[1]	33-1	788.5	31.737	0.142	2.560	0.040	1.780	0.035	1.438	0.029	4.931	0.098	1.89	1.00
7944[1]	33-1	815	31.688	0.134	2.287	0.030	1.698	0.039	1.347	0.028	4.618	0.094	3.23	1.00
7945[1]	33-1	834.5	31.919	0.089	2.300	0.025	1.751	0.039	1.313	0.026	4.504	0.090	3.74	1.00

Continued on next page.

Table B.5 – *Continued from previous page*

Lab.No.	Core GeoB209	Core-depth cm	Age ka	2σ	Li/Ca µg/g	σ	Mg/Ca mg/g	σ	Li/Mg mg/g	σ	Li/Mg* mmo/mol	σ	Temperature	2σ
7946[1]	33-1	868	32.162	0.139	2.151	0.043	1.619	0.039	1.329	0.040	4.556	0.138	3.50	1.27
7947[1]	33-1	889.5	32.490	0.074	2.238	0.022	1.658	0.033	1.350	0.027	4.630	0.093	3.18	1.00
7948[1]	33-1	916	32.722	0.149	2.212	0.023	1.802	0.033	1.227	0.023	4.209	0.079	5.12	1.00
7949[1]	33-1	937	33.547	0.087	2.147	0.025	1.703	0.034	1.261	0.026	4.324	0.088	4.57	1.00
7950[1]	33-1	960	33.580	0.082	2.268	0.020	1.827	0.034	1.241	0.023	4.256	0.079	4.89	1.00
8186[1]	33-1	562	13.761	0.057	1.725	0.029	1.652	0.037	1.044	0.028	3.581	0.095	8.42	1.29
8187[1]	33-1	564.5	13.810	0.054	1.946	0.026	1.894	0.033	1.027	0.020	3.523	0.070	8.75	1.08
8188[1]	33-1	567	13.876	0.074	1.865	0.022	1.807	0.045	1.032	0.025	3.539	0.087	8.66	1.23
8189[1]	33-1	568.5	19.114	0.224	2.514	0.023	1.802	0.034	1.395	0.024	4.784	0.084	2.51	1.00
8190[1]	33-1	571.5	19.123	0.081	2.392	0.025	1.760	0.038	1.359	0.029	4.661	0.101	3.04	1.00
8191[1]	33-1	573.5	19.251	0.075	2.443	0.046	1.732	0.024	1.410	0.019	4.756	0.063	2.63	1.00
8192[1]	33-1	574.5	19.284	0.089	2.564	0.031	1.775	0.021	1.445	0.018	4.873	0.062	2.13	1.00
8193[1]	33-1	575.5	19.045	0.103	2.426	0.031	1.666	0.017	1.456	0.013	4.911	0.043	1.98	1.00
8194[1]	33-1	603.5	22.683	0.271	2.169	0.023	1.577	0.018	1.376	0.012	4.639	0.040	3.14	1.00
8195[1]	33-1	616	23.114	0.103	2.292	0.032	1.637	0.021	1.400	0.011	4.721	0.036	2.78	1.00
8196[1]	33-1	739.5	31.189	0.212	2.557	0.034	1.777	0.021	1.439	0.019	4.852	0.066	2.22	1.00
8197[1]	33-1	746	30.984	0.165	2.679	0.038	1.866	0.035	1.436	0.020	4.842	0.067	2.27	1.00
8198[1]	33-1	752	31.400	0.149	2.472	0.038	1.718	0.031	1.439	0.020	4.855	0.068	2.21	1.00
8199[1]	33-1	756	31.264	0.163	2.351	0.028	1.628	0.018	1.444	0.015	4.871	0.051	2.14	1.00
8200[1]	33-1	758	31.268	0.120	2.188	0.025	1.582	0.016	1.383	0.013	4.665	0.043	3.02	1.00
10402	35-1	0	12.528	0.055	2.565	0.039	2.871	0.003	0.894	0.014	3.362	0.051	9.71	1.00
10403	53-2	0	18.036	0.058	2.676	0.085	2.028	0.051	1.319	0.027	5.311	0.108	0.38	1.00
7676	53-2 17-20 A	18.5	18.618	0.062	2.275	0.056	2.062	0.040	1.103	0.017	4.442	0.069	4.02	1.00
10406	58-1	0	21.899	0.078	3.434	0.038	2.670	0.011	1.286	0.015	4.838	0.057	2.28	1.00

Continued on next page.

Table B.5 – *Continued from previous page*

Lab.No.	Core GeoB209	Core-depth cm	Age ka	2σ	Li/Ca µg/g	σ	Mg/Ca mg/g	σ	Li/Mg mg/g	σ	Li/Mg* mmo/mol	σ	Temperature	2σ

* Mean of multiple measurements of the same CWC. Single measurements are marked as a,b.

[1] from Roesch (2017).

Table B.6: Li/Mg data of CWCs from off the coast of Brazil

Lab.No.	Sample ID	Core depth cm	Age ka	2σ	Li/Ca µg/g	σ	Mg/Ca mg/g	σ	Li/Mg mg/g	σ	Li/Mg* mmo/mol	σ	Temperature	2σ
5251*	MXL-030	51	12.16	0.10									11.1	1.0
5251a[1]											3.13	0.05[3]	11.2	1.0
5251b[1]											3.17	0.05[3]	10.9	1.0
5464*	MXL-030	86	15.51	0.22									8.9	1.0
5464a[1]											3.49	0.05[3]	9.0	1.0
5464b[1]											3.50	0.05[3]	8.9	1.0
5293[1]	MXL-030	154	34.34	0.31							4.85	0.05[3]	2.2	1.0
4674*	C1	113	14.44	0.30									9.2	1.5
4674a[1]											3.33	0.05[3]	9.9	1.0
4674b[1]											3.58	0.05[3]	8.4	1.0
4673*	C1	295	18.87	0.21									3.5	1.0
4673a[1]											4.55	0.05[3]	3.5	1.0
4673b[1]											4.56	0.05[3]	3.5	1.0
4679[1]	C2	36	5.69	0.07							3.17	0.05[3]	10.9	1.0
4502[1,2]	C2		16.33	0.07							5.99	0.05[3]	-2.1	1.0
5183*	C2	94	37.06	0.45									4.5	1.0
5183a[1]											4.22	0.05[3]	5.1	1.0
5183b[1]											4.30	0.05[3]	4.7	1.0
5183c[1]											4.36	0.05[3]	4.4	1.0
5183d[1]											4.38	0.05[3]	4.3	1.0
5183e[1]											4.41	0.05[3]	4.2	1.0
5288*	K-GLC-PPT-06	124	19.57	0.11									1.8	1.0
5288a[1]											4.95	0.05[3]	1.8	1.0

Continued on next page.

Table B.6 – *Continued from previous page*

Lab.No.	Sample ID	Core depth cm	Age ka	2σ	Li/Ca µg/g	σ	Mg/Ca mg/g	σ	Li/Mg mg/g	σ	Li/Mg* mmo/mol	σ	Temperature	2σ
5288b[1]											4.95	0.05[3]	1.8	1.0
5470[1]	K-GLC-PPT-06	146	20.32	0.23							4.81	0.05[3]	2.4	1.0
5249*	K-GLC-PPT-06	394	27.08	0.21									2.5	1.0
5249a[1]											4.70	0.05[3]	2.9	1.0
5249b[1]											4.89	0.05[3]	2.1	1.0
8650	M125-34-2	6	13.65	0.06	1.69	0.08	1.49	0.04	1.14	0.06	4.61	0.14	3.2	1.2
8651	M125-34-2	13	14.34	0.11	1.92	0.07	1.67	0.04	1.15	0.05	4.68	0.15	3.0	1.3
8735	M125-34-2	91	16.44	0.07	2.13	0.10	1.93	0.04	1.10	0.06	4.87	0.09	2.2	1.0
8734	M125-34-2	89	16.48	0.07	2.11	0.10	1.92	0.05	1.10	0.06	4.47	0.08	3.9	1.0
8733	M125-34-2	80	16.54	0.07	2.34	0.20	1.91	0.05	1.22	0.11	4.87	0.14	2.1	1.2
8652	M125-34-2	91	16.67	0.16	2.34	0.07	2.18	0.06	1.07	0.04	4.26	0.06	4.9	1.0
9765	M125-34-2	102	16.90	0.07	2.50	0.07	1.84	0.04	1.36	0.05	5.49	0.18	-0.3	1.3
9766	M125-34-2	105	16.99	0.08	2.60	0.10	1.83	0.04	1.42	0.06	5.65	0.16	-0.9	1.1
9768	M125-34-2	106	17.00	0.12	2.61	0.11	1.83	0.04	1.42	0.05	5.59	0.12	-0.7	1.0
9767	M125-34-2	105	17.01	0.10	2.51	0.11	1.83	0.04	1.37	0.06	5.50	0.10	-0.3	1.0

* Mean of multiple measurements of the same CWC. Single measurements are marked as a,b.

[1] Measured at the LSCE in Gif-sur-Yvette, France.

[2] Excluded after quality control.

[3] Mean external uncertainty.

C δ^7Li data

Table C.1: Yield achieved for the different resin volumes.

Sample type	Resin	Resin volume ml	Yield %
Coral	AG 50W-X8 100-200 mesh	1.5	125 ± 6
		2	126 ± 6
		3	91 ± 6
		3.5	100 ± 6
		4.5	95 ± 6
	AG 50W-X8 200-400 mesh	4.5	91 ± 6
Seawater	AG 50W-X8 100-200 mesh	3.5	89 ± 6
		4.5	102 ± 6
		5.5	92 ± 6
		6	92 ± 6

Table C.2: Results of procedual blank experiment using different beakers.

Beaker	Amount of Li ng	Mean ng
unrinsed PP	0.34	
	0.54	
	0.02	
	0.31	
	0.24	
	0.31	$\mathbf{0.29 \pm 0.31}$
rinsed PP	0.021	
	0.033	
	0.034	$\mathbf{0.029 \pm 0.012}$
Teflon	0.012	
	0.009	
	0.012	
	0.052	
	0.011	
	0.095	
	0.120	
	0.074	$\mathbf{0.048 \pm 0.041}$

Table C.3: δ^7Li values of modern coral and seawater samples as well as the reference material JCp-1.

	δ^7Li Lab ID	Sample ID	Location	Longitude N	Latitude E	water depth m	Age ka	2σ ka	δ^7Li ‰	2σ ‰
Seawater	Li056*	GeoB23425-2 948m	GMS	29° 33.893'	-28° 20.334'	948			**31.34**	**0.08**
	Li056a								31.38	0.15
	Li056b								31.30	0.17
	Li057*	GeoB23434-6 757m	GMS	29° 39.289'	-29° 00.774'	757			**31.69**	**0.01**
	Li057a								31.69	0.21
	Li057b								31.70	0.23
	Li065	GeoB23429-1	GMS	30° 05.191'	-28° 43.617'	895			**32.21**	**1.16**
	Li067	GeoB20504-1	Namibia	-20° 44.067'	12° 49.330	220			**32.49**	**0.87**
	Li068	GeoB23445-1 600m	Open Ocean	30° 54.260'	-23° 57.605'	600			**31.19**	**0.78**
	Li070*	GeoB23445-1 1000m	Open Ocean	30° 54.260'	-23° 57.605'	1000			**30.81**	**0.77**
	Li070a								30.68	0.23
	Li070b								31.33	0.23
	Li070c								30.41	0.78
Coral	Li063*	GeoB23434-1 ROV6	GMS	29° 39.289'	-29° 00.774'	757	0.083	0.011	**18.25**	**0.41**
	Li063a								18.34	0.21
	Li063b								18.45	0.27
	Li063c								17.98	1.59
	Li071*	GeoB20510-1	Namibia	-20° 43.962'	12° 49.119'	230	5.031	0.272	**19.21**	**0.99**
	Li071a								19.09	0.27
	Li071b								18.67	0.29
	Li071c								19.87	1.84
	Li072*	PL-497-2 A2	Iceland	63° 52.320'	-14° 00.78'	330	live		**18.48**	**0.83**
	Li072a								18.09	0.21
	Li072b								18.31	0.24

Continued on next page.

Table C.3 – *Continued from previous page*

	δ^7Li Lab ID	Sample ID	Location	Longitude N	Latitude E	water depth m	Age ka	2σ ka	δ^7Li ‰	2σ ‰
	Li072c								19.05	1.13
Reference material	Li069*	JCp-1							**18.22**	**0.77**
	Li069a								18.74	0.39
	Li069b								17.82	0.33
	Li069c								18.09	2.16

* Mean of multiple measurements of the same aliquot. Single measurements are marked as a-c.

Table C.4: Li/Mg ratios and ϵ_{Nd} values of the CWCs selected for δ^7Li analysis.

δ^7Li Lab ID	U/Th Lab ID	Sample ID	Age ka	2σ ka	Li/Mg mmol/mol	σ mmol/mol	T °C	2σ °C	ϵ_{Nd}	2σ	δ^7Li ‰	2σ ‰
Li104	7680	Faial Pico Channel 900m (1B)	17.411	0.112	6.03	0.08	-2.2	1.0	0.12	1.10	17.67	0.02
Li105	5993	Acor 15	11.126	0.235	3.51	0.09	8.8	1.2	-10.45	0.40	18.00	0.18
Li106	6041	Acor1	13.070	0.280	4.14	0.06	5.5	1.00	-4.75	0.40	18.49	1.42
Li107	6012	Acor 8	12.425	0.153	4.20	0.07	5.2	1.0	-8.58	0.28	17.39	0.40
Li109	7679	Faial Pico Channel 900m (1A)	17.589	0.124	6.88	0.08	-4.9	1.0	0.42	1.00	18.53	2.07
Li110	5994	Acor 16	14.658	0.410	4.09	0.05	5.7	1.0	-9.22	0.28	17.75	3.58

Table C.5: δ^7Li results of CWCs from the Azores region.

δ^7Li Sample ID		Longitude N	Latitude E	water depth m	δ^7Li ‰	2σ ‰	mean ‰	2σ ‰
Li104.1a	Faial Pico Channel 900m (1B)	38° 28.122'	-28° 35.415'	400	17.69	0.21	17.67	0.02
Li104.1b					17.66	0.19		
Li104.2a$^+$					17.09	0.73		
Li104.2b$^+$					17.62	0.48		
Li104.3a$^+$					18.47	0.29		
Li104.3b$^+$					20.74	0.41		
Li105.1a	Acor 15	38° 04.916'	-29° 08.649'	893	17.86	0.17	18.00	0.18
Li105.1b					18.07	0.22		
Li105.2a					17.97	0.17		
Li105.2b					18.09	0.17		
Li105.3a$^+$					17.87	0.22		
Li105.3b$^+$					19.72	0.33		
Li106.1a$^+$	Acor1	38° 04.916'	-29° 08.649'	893	17.86	0.22	18.5	1.4
Li106.1b$^+$					17.97	0.23		
Li106.2a					18.34	0.26		
Li106.2b					17.65	0.23		
Li106.3a					18.38	0.30		
Li106.3b					19.61	0.33		
Li107.1a	Acor 8	38° 04.916'	-29° 08.649'	893	17.39	0.20	17.39	0.40
Li107.1b					17.71	0.19		
Li107.2a$^+$					18.40	0.19		
Li107.2b$^+$					17.70	0.24		
Li107.3a					17.16	0.14		

Continued on next page.

Table C.5 – *Continued from previous page*

δ^7Li Sample ID		Longitude N	Latitude E	water depth m	δ^7Li ‰	2σ ‰	mean ‰	2σ ‰
Li107.3a					17.30	0.14		
Li109.1a	Faial Pico Channel 900m (1A)	38° 28.122'	-28° 35.415'	400	17.50	0.21	18.5	2.1
Li109.1b					17.91	0.19		
Li109.2a					18.47	0.27		
Li109.2b					20.22	0.37		
Li109.3a$^+$					19.03	0.34		
Li109.3b$^+$					18.13	0.24		
Li110.1a	Acor 16	38° 04.916'	-29° 08.649'	893	17.82	0.23	17.3	3.0
Li110.1b					18.98	0.27		
Li110.2a					18.06	0.25		
Li110.2b					18.24	0.22		
Li110.3a					15.99	0.49		
Li110.3b					14.63	0.34		

$^+$ Samples are rejected after quality control due to low yield of lithium extraction.

List of Figures

List of Tables

Bibliography

Addamo, A.M., Vertino, A., Stolarski, J., García-Jiménez, R., Taviani, M., Machordom, A. (2016): Merging scleractinian genera: the overwhelming genetic similarity between solitary Desmophyllum and colonial Lophelia. *BMC Evolutionary Biology* **16**.

Adkins, J.F. (1998): *Deep-Sea Corals: A New Oceanic Archive*. Ph.D. thesis, Massachusetts Institute of Technology.

Adkins, J.F. (2013): The role of deep ocean circulation in setting glacial climates. *Paleoceanography* **28**, 539–561.

Adkins, J.F., Boyle, E.A. (1997): Changing atmospheric Δ^{14}C and the record of deep water paleoventilation ages. *Paleoceanographic Currents* **12**, 337–344.

Adkins, J.F., Cheng, H., Boyle, E.A., Druffel, E.R.M., Edwards, R.L. (1998): Deep-Sea Coral Evidence for Rapid Change in Ventilation of the Deep North Atlantic 15,400 Years Ago. *Science* **280**, 725–728.

Adkins, J.F., McIntyre, K., Schrag, D.P. (2002): The Salinity, Temperature, and δ^{18}O of the Glacial Deep Ocean. *Science* **298**, 1769–1773.

Adkins, J.F., Boyle, E.A., Curry, W.B., Lutringer, A. (2003): Stable isotopes in deep-sea corals and a new mechanism for "vital effects". *Geochimica et Cosmochimica Acta* **67**, 1129–1143.

Adkins, J.F., Henderson, G.M., Wang, S.L., O'Shea, S., Mokadem, F. (2004): Growth rates of the deep-sea scleractinia Desmophyllum cristagalli and Enallopsammia rostrata. *Earth and Planetary Science Letters* **227**, 481–490.

Allemand, D., Tambutté, É., Zoccola, D., Tambutté, S. (2010): Coral Calcification, Cells to Reefs. In: *Coral Reefs: An Ecosystem in Transition*, 119–150, Springer Netherlands.

Allison, N., Finch, A.A., Sutton, S.R., Newville, M. (2001): Strontium heterogeneity and speciation in coral aragonite: implications for the strontium paleothermometer. *Geochimica et Cosmochimica Acta* **65**, 2669–2676.

Allison, N., Finch, A.A., Webster, J.M., Clague, D.A. (2007): Palaeoenvironmental records from fossil corals: The effects of submarine diagenesis on temperature and climate estimates. *Geochimica et Cosmochimica Acta* **71**, 4693–4703.

Anand, P., Elderfield, H., Conte, M.H. (2003): Calibration of Mg/Ca thermometry in planktonic foraminifera from a sediment trap time series. *Paleoceanography* **18**.

Andersen, M.B., Stirling, C.H., Zimmermann, B., Halliday, A.N. (2010): Precise determination of the open ocean $^{234}U/^{238}U$ composition. *Geochemistry, Geophysics, Geosystems* **11**.

Annan, J.D., Hargreaves, J.C. (2013): A new global reconstruction of temperature changes at the Last Glacial Maximum. *Climate of the Past* **9**, 367–376.

Annan, J.D., Hargreaves, J.C. (2015): A perspective on model-data surface temperature comparison at the Last Glacial Maximum. *Quaternary Science Reviews* **107**, 1–10.

Arps, J. (2017): *Towards ϵ-Precisionof U-series Age Determinations of Secondary Carbonates*. Ph.D. thesis, Institute of Environmental Physics, Department of Physics and Astronomy, Heidelberg University.

Auffret, G.A., Richter, T., Reyss, J.L., Organo, C., Deloule, E., Gaillard, J.F., Dennielou, B., Mueller, C., Thomas, B., Watremez, P., Grousset, F., Boelaert, A., Cambon, P., Etoubleau, J. (1996): Record of hydrothermal activity in sediments from the Mid-Atlantic Ridge south of the Azores. *Comptes Rendus de l'Academie des Sciences, Serie IIa: Sciences de la Terre et des Planetes* **323**, 583–590.

Bashmachnikov, I., Neves, F., Calheiros, T., Carton, X. (2015): Properties and pathways of Mediterranean water eddies in the Atlantic. *Progress in Oceanography* **137**, 149–172.

Bastian, L., Vigier, N., Reynaud, S., Kerros, M.E., Revel, M., Bayon, G. (2018): Lithium Isotope Composition of Marine Biogenic Carbonates and Related Reference Materials. *Geostandards and Geoanalytical Research* **42**, 403–415.

Batchelor, C.L., Margold, M., Krapp, M., Murton, D.K., Dalton, A.S., Gibbard, P.L., Stokes, C.R., Murton, J.B., Manica, A. (2019): The configuration of Northern Hemisphere ice sheets through the Quaternary. *Nature Communications* **10**.

Bazin, L., Landais, A., Lemieux-Dudon, B., Toyé Mahamadou Kele, H., Veres, D., Parrenin, F., Martinerie, P., Ritz, C., Capron, E., Lipenkov, V.Y., Loutre, M.F., Raynaud, D., Vinther, B.M., Svensson, A.M., Rasmussen, S.O., Severi, M., Blunier, T., Leuenberger, M.C., Fischer, H., Masson-Delmotte, V., Chappellaz, J.A., Wolff, E.W. (2013a): delta 18O measured on ice core NGRIP on AICC2012 chronology.

Bazin, L., Landais, A., Lemieux-Dudon, B., Toyé Mahamadou Kele, H., Veres, D., Parrenin, F., Martinerie, P., Ritz, C., Capron, E., Lipenkov, V.Y., Loutre, M.F., Raynaud, D., Vinther, B.M., Svensson, A.M., Rasmussen, S.O., Severi, M., Blunier, T., Leuenberger, M.C., Fischer, H., Masson-Delmotte, V., Chappellaz, J.A., Wolff, E.W. (2013b): delta Deuterium measured on ice core Vostok on AICC2012 chronology. dataset.

Beck, J.W., Edwards, R.L., Ito, E., Taylor, F.W., Recy, J., Rougerie, F., Joannot, P., Henin, C. (1992): Sea-Surface Temperature from Coral Skeletal Strontium/Calcium Ratios. *Science* **257**, 644–647.

Becker, S. (2008): *Inorganic Mass Spectrometry: Principles and Applications*. WILEY.

Beisel, E. (2021): *Interhemisphärische Gradienten von Radiokohlenstoff im Zwischenwasser des Atlantiks seit der letzten Eiszeit*. Master's thesis, Institute of Environmental Physics, Department of Physics and Astronomy, Heidelberg University.

Bell, N., Smith, J. (1999): Coral growing on North Sea oil rigs. *Nature* **402**, 601.

Bereiter, B., Shackleton, S., Baggenstos, D., Kawamura, K., Severinghaus, J. (2018): Mean global ocean temperatures during the last glacial transition. *Nature* **553**, 39–44.

Berner, E.K., Berner, R.A. (2012): *Global Environment: Water, Air, and Geochemical Cycles*. Princeton University press, 2 edition.

Böhm, E., Lippold, J., Gutjahr, M., Frank, M., Blaser, P., Antz, B., Fohlmeister, J., Frank, N., Andersen, M.B., Deininger, M. (2015): Strong and deep Atlantic meridional overturning circulation during the last glacial cycle. *Nature* **517**, 73–76.

Biastoch, A., Böning, C.W., Lutjeharms, J.R.E. (2008): Agulhas leakage dynamics affects decadal variability in Atlantic overturning circulation. *Nature* **456**, 489–492.

Biastoch, A., Durgadoo, J.V., Morrison, A.K., van Sebille, E., Weijer, W., Griffies, S.M. (2015): Atlantic multi-decadal oscillation covaries with Agulhas leakage. *Nature Communications* **6**.

Bohlin, M.S., Misra, S., Lloyd, N., Elderfield, H., Bickle, M.J. (2017): High-precision determination of lithium and magnesium isotopes utilising single column separation and multi-collector inductively coupled plasma mass spectrometry. *Rapid Communications in Mass Spectrometry* **32**, 93–104.

Bond, G.C., Lotti, R. (1995): Iceberg Discharges into the North Atlantic on Millennial Time Scales During the Last Glaciation. *Science* **267**, 1005–1010.

Bondevik, S. (2006): Changes in North Atlantic Radiocarbon Reservoir Ages During the Allerod and Younger Dryas. *Science* **312**, 1514–1517.

Bonneau, L., Colin, C., Pons-Branchu, E., Mienis, F., Tisnérat-Laborde, N., Blamart, D., Elliot, M., Collart, T., Frank, N., Foliot, L., Douville, E. (2018): Imprint of Holocene Climate Variability on Cold-Water Coral Reef Growth at the SW Rockall Trough Margin, NE Atlantic. *Geochemistry, Geophysics, Geosystems* **19**, 2437–2452.

Border, E.C. (2020): *Variability of $\delta^{234}U$ in the Mediterranean Sea, Amazon Estuary, and Atlantic Ocean*. Ph.D. thesis, Institute of Environmental Physics, Department of Physics and Astronomy, Heidelberg University.

Boyer, D.C., Hampton, I. (2001): An overview of the living marine resources of Namibia. *South African Journal of Marine Science* **23**, 5–35.

Brambilla, E., Talley, L.D. (2008): Subpolar Mode Water in the northeastern Atlantic: 1. Averaged properties and mean circulation. *Journal of Geophysical Research* **113**.

Broecker, W.S., Andree, M., Wolfli, W., Oeschger, H., Bonani, G., Kennett, J., Peteet, D. (1988): The chronology of the last Deglaciation: Implications to the cause of the Younger Dryas Event. *Paleoceanography* **3**, 1–19.

Bryan, S.P., Marchitto, T.M. (2008): Mg/Ca-temperature proxy in benthic foraminifera: New calibrations from the Florida Straits and a hypothesis regarding Mg/Li. *Paleoceanography* **23**.

Burke, A., Robinson, L.F. (2012): The Southern Ocean's Role in Carbon Exchange During the Last Deglaciation. *Science* **335**, 557–561.

Burles, S., Nollett, K.M., Turner, M.S. (2001): Big Bang Nucleosynthesis Predictions for Precision Cosmology. *The Astrophysical Journal* **552**, L1–L5.

Burton, K.W., Vigier, N. (2011): Lithium Isotopes as Tracers in Marine and Terrestrial Environments. In: *Advances in Isotope Geochemistry*, 41–59, Springer Berlin Heidelberg.

Butzin, M., Prange, M., Lohmann, G. (2005): Radiocarbon simulations for the glacial ocean: The effects of wind stress, Southern Ocean sea ice and Heinrich events. *Earth and Planetary Science Letters* **235**, 45–61.

Cairns, S.D. (1982): Antarctic and Subantarctic Scleractinia. *Antarctic Research Series* **34**, 1–74.

Cairns, S.D. (1984): New Records of Ahermatypic Corals (Scleractinia) from the Hawaiian Line Islands. *Bishop Museum Occasional Papers* **25**.

Cairns, S.D. (2007): Deep-water corals: An overview with special reference to diversity and distribution of deep-water scleractinian corals. *Bulletin of Marine Science* **81**, 311–322.

Candela, J. (2001): Chapter 5.7 Mediterranean water and global circulation. In: *International Geophysics*, 419–XLVIII, Elsevier.

Cao, L., Fairbanks, R., Mortlock, R., Risk, M. (2007): Radiocarbon reservoir age of high latitude North Atlantic surface water during the last deglacial. *Quaternary Science Reviews* **26**, 732–742.

Carignan, J., Cardinal, D., Eisenhauer, A., Galy, A., Rehkamper, M., Wombacher, F., Vigier, N. (2004): A Reflection on Mg, Cd, Ca, Li and Si Isotopic Measurements and Related Reference Materials. *Geostandards and Geoanalytical Research* **28**, 139–148.

Case, D.H., Robinson, L.F., Auro, M.E., Gagnon, A.C. (2010): Environmental and biological controls on Mg and Li in deep-sea scleractinian corals. *Earth and Planetary Science Letters* **300**, 215–225.

Chan, L.H., Edmond, J., Thompson, G., Gillis, K. (1992): Lithium isotopic composition of submarine basalts: implications for the lithium cycle in the oceans. *Earth and Planetary Science Letters* **108**, 151–160.

Chan, L.H., Edmond, J.M., Thompson, G. (1993): A lithium isotope study of hot springs and metabasalts from Mid-Ocean Ridge Hydrothermal Systems. *Journal of Geophysical Research* **98**, 9653–9659.

Chan, L.H., Gieskes, J.M., Chen-Feng, Y., Edmond, J.M. (1994): Lithium isotope geochemistry of sediments and hydrothermal fluids of the Guaymas Basin, Gulf of California. *Geochimica et Cosmochimica Acta* **58**, 4443–4454.

Chan, L.H., Alt, J.C., Teagle, D.A. (2002): Lithium and lithium isotope profiles through the upper oceanic crust: a study of seawater–basalt exchange at ODP Sites 504B and 896A. *Earth and Planetary Science Letters* **201**, 187–201.

Chan, L.H., Leeman, W.P., Plank, T. (2006): Lithium isotopic composition of marine sediments. *Geochemistry, Geophysics, Geosystems* **7**.

Chen, T., Robinson, L.F., Burke, A., Southon, J., Spooner, P., Morris, P.J., Ng, H.C. (2015): Synchronous centennial abrupt events in the ocean and atmosphere during the last deglaciation. *Science* **349**, 1537–1541.

Chen, T., Robinson, L.F., Beasley, M.P., Claxton, L.M., Andersen, M.B., Gregoire, L.J., Wadham, J., Fornari, D.J., Harpp, K.S. (2016): Ocean mixing and ice-sheet control of seawater $^{234}U/^{238}U$ during the last deglaciation. *Science* **354**, 626–629.

Cheng, H., Adkins, J., Edwards, R.L., Boyle, E.A. (2000a): U-Th dating of deep-sea corals. *Geochimica et Cosmochimica Acta* **64**, 2401–2416.

Cheng, H., Edwards, R.L., Hoff, J., Gallup, C.D., Richards, D.A., Asmerom, Y. (2000b): The half-lives of uranium-234 and thorium-230. *Chemical Geology* **169**, 17–33.

Clark, P.U., Pisias, N.G., Stocker, T.F., Weaver, A.J. (2002): The role of the thermohaline circulation in abrupt climate change. *Nature* **415**, 863–869.

Clark, P.U., Dyke, A.S., Shakun, J.D., Carlson, A.E., Clark, J., Wohlfarth, B., Mitrovica, J.X., Hostetler, S.W., McCabe, A.M. (2009): The Last Glacial Maximum. *Science* **325**, 710–714.

Clement, A.C., Peterson, L.C. (2008): Mechanisms of abrupt climate change of the last glacial period. *Reviews of Geophysics* **46**.

Cohen, A.L., Owens, K.E., Layne, G.D., Shimizu, N. (2002): The Effect of Algal Symbionts on the Accuracy of Sr/Ca Paleotemperatures from Coral. *Science* **296**, 331–333.

Cohen, A.L., Gaetani, G.A., Lundälv, T., Corliss, B.H., George, R.Y. (2006): Compositional variability in a cold-water scleractinian, *Lophelia pertusa*: New insights into "vital effects". *Geochemistry, Geophysics, Geosystems* **7**.

Colin, C., Frank, N., Copard, K., Douville, E. (2010): Neodymium isotopic composition of deep-sea corals from the NE Atlantic: implications for past hydrological changes during the Holocene. *Quaternary Science Reviews* **29**, 2509–2517.

Cuny-Guirriec, K. (2020): *Le rapport élémentaire Li/Mg dans les coraux scléractiniaires : un nouveau et puissant traceur des paléo-températures de l'océan?* Ph.d. thesis, Université Paris-Saclay.

Cuny-Guirriec, K., Douville, E., Reynaud, S., Allemand, D., Bordier, L., Canesi, M., Mazzoli, C., Taviani, M., Canese, S., McCulloch, M., Trotter, J., Rico-Esenaro, S.D., Sanchez-Cabeza, J.A., Ruiz-Fernández, A.C., Carricart-Ganivet, J.P., Scott, P.M., Sadekov, A., Montagna, P. (2019): Coral Li/Mg thermometry: Caveats and constraints. *Chemical Geology* **523**, 162–178.

Currie, L. (2004): The remarkable metrological history of radiocarbon dating [II]. *Journal of Research of the National Institute of Standards and Technology* **109**, 185.

Dansgaard, W., Johnsen, S.J., Clausen, H.B., Dahl-Jensen, D., Gundestrup, N.S., Hammer, C.U., Hvidberg, C.S., Steffensen, J.P., Sveinbjörnsdottir, A.E., Jouzel, J., Bond, G. (1993): Evidence for general instability of past climate from a 250-kyr ice-core record. *Nature* **364**, 218–220.

Dardoufas, T. (2019): *Age determination and temperature reconstructionusing cold water corals*. Bachelor's thesis, Institute of Environmental Physics, Department of Physics and Astronomy, Heidelberg University.

Davies, A.J., Guinotte, J.M. (2011): Global Habitat Suitability for Framework-Forming Cold-Water Corals. *PLoS ONE* **6**, e18483.

Davies, A.J., Wisshak, M., Orr, J.C., Roberts, J.M. (2008): Predicting suitable habitat for the cold-water coral Lophelia pertusa (Scleractinia). *Deep Sea Research Part I: Oceanographic Research Papers* **55**, 1048–1062.

Davies, A.J., Duineveld, G.C.A., Lavaleye, M.S.S., Bergman, M.J.N., van Haren, H., Roberts, J.M. (2009): Downwelling and deep-water bottom currents as food supply mechanisms to the cold-water coral Lophelia pertusa (Scleractinia) at the Mingulay Reef Complex. *Limnology and Oceanography* **54**, 620–629.

de Villiers, S., Nelson, B.K., Chivas, A.R. (1995): Biological Controls on Coral Sr/Ca and δ^{18}O Reconstructions of Sea Surface Temperatures. *Science* **269**, 1247–1249.

Dellinger, M., West, A.J., Paris, G., Adkins, J.F., von Strandmann, P.A.P., Ullmann, C.V., Eagle, R.A., Freitas, P., Bagard, M.L., Ries, J.B., Corsetti, F.A., Perez-Huerta, A., Kampf, A.R. (2018): The Li isotope composition of marine biogenic carbonates: Patterns and mechanisms. *Geochimica et Cosmochimica Acta* **236**, 315–335.

Dorschel, B., Hebbeln, D., Rüggeberg, A., Dullo, W.C., Freiwald, A. (2005): Growth and erosion of a cold-water coral covered carbonate mound in the Northeast Atlantic during the Late Pleistocene and Holocene. *Earth and Planetary Science Letters* **233**, 33–44.

Douarin, M., Elliot, M., Noble, S.R., Moreton, S.G., Long, D., Sinclair, D., Henry, L.A., Roberts, J.M. (2016): North Atlantic ecosystem sensitivity to Holocene shifts in Meridional Overturning Circulation. *Geophysical Research Letters* **43**, 291–298.

Dubois-Dauphin, Q., Bonneau, L., Colin, C., Montero-Serrano, J.C., Montagna, P., Blamart, D., Hebbeln, D., Rooij, D.V., Pons-Branchu, E., Hemsing, F., Wefing, A.M., Frank, N. (2016): South Atlantic intermediate water advances into the Northeast Atlantic with reduced Atlantic meridional overturning circulation during the last glacial period. *Geochemistry, Geophysics, Geosystems* **17**, 2336–2353.

Edwards, R.L., Gallup, C.D., Cheng, H. (2003): Uranium-series Dating of Marine and Lacustrine Carbonates. *Reviews in Mineralogy and Geochemistry* **52**, 363–405.

Eisele, M., Frank, N., Wienberg, C., Hebbeln, D., López Correa, M., Douville, E., Freiwald, A. (2011): Productivity controlled cold-water coral growth periods during the last glacial off Mauritania. *Marine Geology* **280**, 143–149.

Elmore, A.C., McClymont, E.L., Elderfield, H., Kender, S., Cook, M.R., Leng, M.J., Greaves, M., Misra, S. (2015): Antarctic Intermediate Water properties since 400 ka recorded in infaunal (Uvigerina peregrina) and epifaunal (Planulina wuellerstorfi) benthic foraminifera. *Earth and Planetary Science Letters* **428**, 193–203.

Emiliani, C., Hudson, J.H., Shinin, E.A., George, R.Y. (1978): Oxygen and Carbon Isotopic Growth Record in a Reef Coral from the Florida Keys and a Deep-Sea Coral from Blake Plateau. *Science* **202**, 627–629.

Eynaud, F., de Abreu, L., Voelker, A., Schönfeld, J., Salgueiro, E., Turon, J.L., Penaud, A., Toucanne, S., Naughton, Filipa andSánchez Goñi, M.F., Malaizé, B., Cacho, I. (2009): Position of the Polar Front along the western Iberian margin during key cold episodes of the last 45 ka. *Geochemistry, Geophysics, Geosystems* **10**.

Falkner, K.K., Church, M., Measures, C.I., Lebaron, G., Thouron, D., Jeandel, C., Stordal, M.C., Gill, G.A., Mortlock, R., Froelich, P., Chan, L.H. (1997): Minor and trace element chemistry of Lake Baikal, its tributaries, and surrounding hot springs. *Limnology and Oceanography* **42**, 329–345.

Flatau, M.K., Talley, L., Niiler, P.P. (2003): The North Atlantic Oscillation, Surface Current Velocities, and SST Changes in the Subpolar North Atlantic. *Journal of Climate* **16**, 2355–2369.

Flesch, G., Anderson, A., Svec, H. (1973): A secondary isotopic standard for $^{6}Li/^{7}Li$ determinations. *International Journal of Mass Spectrometry and Ion Physics* **12**, 265–272.

Flögel, S., Dullo, W.C., Pfannkuche, O., Kiriakoulakis, K., Rüggeberg, A. (2014): Geochemical and physical constraints for the occurrence of living cold-water corals. *Deep Sea Research Part II: Topical Studies in Oceanography* **99**, 19–26.

Fosså, J.H., Mortensen, P. B., F.D.M. (2000): Lophelia-Korallrev langs Norskekysten forekomst og tilstand. *Fisken og Havet* 4–94.

Foustoukos, D.I., James, R.H., Berndt, M.E., Seyfried, W.E. (2004): Lithium isotopic systematics of hydrothermal vent fluids at the Main Endeavour Field, Northern Juan de Fuca Ridge. *Chemical Geology* **212**, 17–26.

Frank, M. (2002): Radiogenic isotopes: Tracers of past ocean circulation and erosional input. *Reviews of Geophysics* **40**.

Frank, M., Eckhardt, J.D., Eisenhauer, A., Kubik, P.W., Dittrich-Hannen, B., Segl, M., Mangini, A. (1994): Beryllium 10, thorium 230, and protactinium 231 in Galapagos microplate sediments: Implications of hydrothermal activity and paleoproductivity changes during the last 100,000 years. *Paleoceanography* **9**, 559–578.

Frank, N., Hemsing, F. (2020): Dating of Corals and Other Geological Samples via the Radioactive Disequilibrium of Uranium and Thorium Isotopes. In: *Frontiers in Earth Sciences*, 89–100, Springer International Publishing.

Frank, N., the scientific crew of M151 (2018): Short Cruise Report - M151 - Atlantic Thermocline Ocean and Ecosystems Dynamic during Natural Climate Change. Research report.

Frank, N., Paterne, M., Ayliffe, L., van Weering, T., Henriet, J.P., Blamart, D. (2004): Eastern North Atlantic deep-sea corals: tracing upper intermediate water $\Delta^{14}C$ during the Holocene. *Earth and Planetary Science Letters* **219**, 297–309.

Frank, N., Freiwald, A., López Correa, M., Wienberg, C., Eisele, M., Hebbeln, D., van Rooij, D., Henriet, J.P., Colin, C., van Weering, T., de Haas, H., Buhl-Mortensen, P., Roberts, J.M., de Mol, B., Douville, E., Blamart, D., Hatte, C. (2011): Northeastern Atlantic cold-water coral reefs and climate. *Geology* **39**, 743–746.

Fratantoni, D.M. (2001): North Atlantic surface circulation during the 1990's observed with satellite-tracked drifters. *Journal of Geophysical Research: Oceans* **106**, 22067–22093.

Freeman, E., Skinner, L.C., Tisserand, A., Dokken, T., Timmermann, A., Menviel, L., Friedrich, T. (2015): An Atlantic–Pacific ventilation seesaw across the last deglaciation. *Earth and Planetary Science Letters* **424**, 237–244.

Freiwald, A. (2002): Reef-Forming Cold-Water Corals. In: *Ocean Margin Systems*, 365–385, Springer Berlin Heidelberg.

Freiwald, A., Roberts, J.M. (eds.) (2005): *Cold-Water Corals and Ecosystems*. Springer.

Freiwald, A., Fosså, J.H., Grehan, A., Koslow, T., Roberts, J.M. (2004): *Cold-water Coral Reefs: Out of sight - no longer out of mind*. Biodiversity Series 22, UNEP-WCMC, Biodiversity Series 22, Cambridge, UK.

Freiwald, A., Rogers, A., Hall-Spencer, J., Guinotte, J.M., Davies, A.J., Yesson, C., Martin, C.S., Weatherdon, L.V. (2017): Global distribution of cold-water corals (version 5.0). Fifth update to the dataset in Freiwald et al. (2004) by UNEP-WCMC, in collaboration with Andre Freiwald and John Guinotte. Cambridge (UK): UN Environment World Conservation Monitoring Centre. .

Friedman, I., O'Neil, J., Cebula, G. (1982): Two New Carbonate Stable-Isotope Standards. *Geostandards and Geoanalytical Research* **6**, 11–12.

Förstel, J. (2014): *Messung von Lithium-Magnesium-Verhältnissen an einem iCAP Q™ Quadrupol-Massenspektrometer mit induktiv gekoppelter Plasmaionenquelle*. Bachelor's thesis, Institute of Environmental Physics, Department of Physics and Astronomy, Heidelberg University.

Gagnon, A.C., Adkins, J.F., Fernandez, D.P., Robinson, L.F. (2007): Sr/Ca and Mg/Ca vital effects correlated with skeletal architecture in a scleractinian deep-sea coral and the role of Rayleigh fractionation. *Earth and Planetary Science Letters* **261**, 280–295.

Garzoli, S.L., Gordon, A.L., Kamenkovich, V., Pillsbury, D., Duncombe-Rae, C. (1996): Variability and sources of the southeastern Atlantic circulation. *Journal of Marine Research* **54**, 1039–1071.

Ghosh, P., Adkins, J., Affek, H., Balta, B., Guo, W., Schauble, E.A., Schrag, D., Eiler, J.M. (2006): 13C–18O bonds in carbonate minerals: A new kind of paleothermometer. *Geochimica et Cosmochimica Acta* **70**, 1439–1456.

Gladfeiter, E.H. (1982): Skeletal development in Acropora cervicornis: I. Patterns of calcium carbonate accretion in the axial corallite. *Coral Reefs* **1**, 45–51.

Glasder, A. (2018): *Rekonstruktion der Nordwärtsbewegungvon Mittelmeerwasser-anhand von Tiefseekorallen*. Master's thesis, Institute of Environmental Physics, Department of Physics and Astronomy, Heidelberg University.

Global Volcanism Program (2013): Volcanoes of the World, v. 4.10.1. (29 Jun 2021). Data, Smithsonian Institution.

Glogowski, S., Dullo, W.C., Feldens, P., Liebetrau, V., von Reumont, J., Hühnerbach, V., Krastel, S., Wynn, R.B., Flögel, S. (2015): The Eugen Seibold coral mounds offshore western Morocco: oceanographic and bathymetric boundary conditions of a newly discovered cold-water coral province. *Geo-Marine Letters* **35**, 257–269.

Godwin, H. (1962): Half-life of Radiocarbon. *Nature* **195**, 984–984.

Gordon, A.L., Lutjeharms, J.R.E., Gründlingh, M.L. (1987): Stratification and circulation at the Agulhas Retroflection. *Deep Sea Research Part A. Oceanographic Research Papers* **34**, 565–599.

Gowan, E.J., Zhang, X., Khosravi, S., Rovere, A., Stocchi, P., Hughes, A.L.C., Gyllencreutz, R., Mangerud, J., Svendsen, J.I., Lohmann, G. (2021): A new global ice sheet reconstruction for the past 80 000 years. *Nature Communications* **12**.

Guilderson, T.P., Fairbanks, R.G., Rubenstone, J.L. (1994): Tropical Temperature Variations Since 20,000 Years Ago: Modulating Interhemispheric Climate Change. *Science* **263**, 663–665.

Guo, L., Santschi, P.H., Baskaran, M., Zindler, A. (1995): Distribution of dissolved and particulate230Th and232Th in seawater from the Gulf of Mexico and off Cape Hatteras as measured by SIMS. *Earth and Planetary Science Letters* **133**, 117–128.

Hain, M.P., Sigman, D.M., Haug, G.H. (2011): Shortcomings of the isolated abyssal reservoir model for deglacial radiocarbon changes in the mid-depth Indo-Pacific Ocean. *Geophysical Research Letters* **38**, n/a–n/a.

Hall, J.M., Chan, L.H., McDonough, W.F., Turekian, K.K. (2005): Determination of the lithium isotopic composition of planktic foraminifera and its application as a paleo-seawater proxy. *Marine Geology* **217**, 255–265.

Hathorne, E.C., James, R. (2006): Temporal record of lithium in seawater: A tracer for silicate weathering? *Earth and Planetary Science Letters* **246**, 393–406.

Hathorne, E.C., Felis, T., Suzuki, A., Kawahata, H., Cabioch, G. (2013): Lithium in the aragonite skeletons of massive Porites corals: A new tool to reconstruct tropical sea surface temperatures. *Paleoceanography* **28**, 143–152.

Hebbeln, D., Wienberg, C., Bartels, M., Bergenthal, M., Frank, N., Gaide, S., Henriet, J.P., Kaszemeik, K., Klar, S., Klein, T., Krengel, T., Kuhnert, M., Meyer-Schack, B., Noorlander, C., Reuter, M., Rosiak, U., Schmidt, W., Seeba, H., Seiter, C., Stange, N., Terhzaz, L., Van Rooij, D. (2015): MoccoMeBo Climate-driven development of Moroccan cold-water coral mounds revealed by MeBo-drilling: Atlantic vs. Mediterranean settings - Cruise MSM36 - February 18 - March 17, 2014 - Malaga (Spain) - Las Palmas (Spain). Technical report.

Hebbeln, D., Wienberg, C., Bender, M., Bergmann, F., Dehning, K., Dullo, W.C., Eichstädter, R., Flöter, S., Freiwald, A., Gori, A., Haberkern, J., Hoffmann, L., João, F., Lavaleye, M., Leymann, T., Matsuyama, K., Meyer-Schack, B., Mienis, F., Moçambique, I., Nowald, N., Orejas, C., Ramos Cordova, C., Saturov, D., Seiter, C., Titschack, J., Vittori, V., Wefing, A.M., Wilsenack, M., Wintersteller, P. (2017): ANNA Cold-Water Coral Ecosystems off Angola and Namibia - Cruise No. M122 - December 30, 2015 - January 31, 2016 - Walvis Bay (Namibia) - Walvis Bay (Namibia). Technical report.

Hebbeln, D., Wienberg, C., Dullo, W.C., Freiwald, A., Mienis, F., Orejas, C., Titschack, J. (2020): Cold-water coral reefs thriving under hypoxia. *Coral Reefs* **39**, 853–859.

Heinrich, H. (1988): Origin and Consequences of Cyclic Ice Rafting in the Northeast Atlantic Ocean During the Past 130,000 Years. *Quaternary Research* **29**, 142–152.

Hemming, S.R. (2004): Heinrich events: Massive late Pleistocene detritus layers of the North Atlantic and their global climate imprint. *Reviews of Geophysics* **42**.

Hemsing, F. (2017): *Cold-Water Corals as Archives for Ocean Dynamics, Environmental Conditions and Glacial Reef Accumulation*. Ph.D. thesis, Institute of Environmental Physics, Department of Physics and Astronomy, Heidelberg University.

Hennige, S.J., Morrison, C.L., Form, A.U., Büscher, J., Kamenos, N.A., Roberts, J.M. (2014): Self-recognition in corals facilitates deep-sea habitat engineering. *Scientific Reports* **4**.

Henry, L.A., Frank, N., Hebbeln, D., Wienberg, C., Robinson, L., van de Flierdt, T., Dahl, M., Douarin, M., Morrison, C.L., Correa, M.L., Rogers, A.D., Ruckelshausen, M., Roberts, J.M. (2014): Global ocean conveyor lowers extinction risk in the deep sea. *Deep Sea Research Part I: Oceanographic Research Papers* **88**, 8–16.

Hensen, C., Nuzzo, M., Hornibrook, E., Pinheiro, L.M., Bock, B., Magalhães, V.H., Brückmann, W. (2007): Sources of mud volcano fluids in the Gulf of Cadiz—indications for hydrothermal imprint. *Geochimica et Cosmochimica Acta* **71**, 1232–1248.

Hoefs, J., Sywall, M. (1997): Lithium isotope composition of quaternary and tertiary biogene carbonates and a global lithium isotope balance. *Geochimica et Cosmochimica Acta* **61**, 2679–2690.

Hogg, A.G., Heaton, T.J., Hua, Q., Palmer, J.G., Turney, C.S.M., Southon, J., Bayliss, A., Blackwell, P.G., Boswijk, G., Bronk Ramsey, C., Pearson, C., Petchey, F., Reimer, P., Reimer, R., Wacker, L. (2020): SHCal20 Southern Hemisphere Calibration, 0–55,000 Years cal BP. *Radiocarbon* **62**, 759–778.

Holleman, A.F., Wiberg, E. (2007): *Lehrbuch der anorganischen Chemie*. de Gruyter, Berlin.

Huang, K.F., You, C.F., Liu, Y.H., Wang, R.M., Lin, P.Y., Chung, C.H. (2010): Low-memory, small sample size, accurate and high-precision determinations of lithium isotopic ratios in natural materials by MC-ICP-MS. *Journal of Analytical Atomic Spectrometry* **25**, 1019–1024.

Hughen, K.A., Schrag, D.P., Jacobsen, S.B., Hantoro, W. (1999): El Niño during the Last Interglacial Period recorded by a fossil coral from Indonesia. *Geophysical Research Letters* **26**, 3129–3132.

Huh, Y., Chan, L.H., Zhang, L., Edmond, J.M. (1998): Lithium and its isotopes in major world rivers: implications for weathering and the oceanic budget. *Geochimica et Cosmochimica Acta* **62**, 2039–2051.

Imbrie, J., Hays, J.D., Martinson, D.G., McIntyre, A., Mix, A.C., Morley, J.J., Pisias, N.G., Prell, W.L., Shackleton, N.J. (1984): The orbital theory of Pleistocene climate:

support from a revised chronology of the marine δ^{18}O record. In: *Milankovich and Climate Part 1*, edited by A. Berger, J. Imbrie, J. Hays, G. Kukla, B. Saltzman, D. Reidel Publishing Company.

Inoue, M., Nohara, M., Okai, T., Suzuki, A., Kawahata, H. (2004): Concentrations of Trace Elements in Carbonate Reference Materials Coral JCp-1 and Giant Clam JCt-1 by Inductively Coupled Plasma-Mass Spectrometry. *Geostandards and Geoanalytical Research* **28**, 411–416.

Ivanovich, M., Harmon, R.S. (eds.) (1982): *Uranium Series Disequilibrium : Applications to Environmental Problems*. Clarendon Press, Oxford.

Jansen, J.H.F., Ufkes, E., Schneider, R.R. (1996): Late Quaternary Movements of the Angola-Benguela Front, SE Atlantic, and Implications for Advection in the Equatorial Ocean. In: *The South Atlantic*, 553–575, Springer Berlin Heidelberg.

Jeffcoate, A., Elliott, T., Kasemann, S., Ionov, D., Cooper, K., Brooker, R. (2007): Li isotope fractionation in peridotites and mafic melts. *Geochimica et Cosmochimica Acta* **71**, 202–218.

Jeffcoate, A.B., Elliott, T., Thomas, A., Bouman, C. (2004): Precise/ Small Sample Size Determinations of Lithium Isotopic Compositions of Geological Reference Materials and Modern Seawater by MC-ICP-MS. *Geostandards and Geoanalytical Research* **28**, 161–172.

Johnsen, S.J., Clausen, H.B., Dansgaard, W., Fuhrer, K., Gundestrup, N., Hammer, C.U., Iversen, P., Jouzel, J., Stauffer, B., steffensen, J.P. (1992): Irregular glacial interstadials recorded in a new Greenland ice core. *Nature* **359**, 311–313.

Kano, A., Ferdelman, T.G., Williams, T., Henriet, J.P., Ishikawa, T., Kawagoe, N., Takashima, C., Kakizaki, Y., Abe, K., Sakai, S., Browning, E.L., and, X.L. (2007): Age constraints on the origin and growth history of a deep-water coral mound in the northeast Atlantic drilled during Integrated Ocean Drilling Program Expedition 307. *Geology* **35**, 1051.

Keffer, T., Martinson, D.G., Corliss, B.H. (1988): The Position of the Gulf Stream During Quaternary Glaciations. *Science* **241**, 440–442.

Keigwin, L.D., Boyle, E.A. (1989): Late quaternary paleochemistry of high-latitude surface waters. *Palaeogeography, Palaeoclimatology, Palaeoecology* **73**, 85–106.

Keigwin, L.D., Jones, G.A., Lehman, S.J., Boyle, E.A. (1991): Deglacial meltwater discharge, North Atlantic Deep Circulation, and abrupt climate change. *Journal of Geophysical Research* **96**, 16811–16826.

Knutti, R., Flückiger, J., Stocker, T.F., Timmermann, A. (2004): Strong hemispheric coupling of glacial climate through freshwater discharge and ocean circulation. *Nature* **430**, 851–856.

Korn, A.J., Grundahl, F., Richard, O., Barklem, P.S., Mashonkina, L., Collet, R., Piskunov, N., Gustafsson, B. (2006): A probable stellar solution to the cosmological lithium discrepancy. *Nature* **442**, 657–659.

Krengel, T. (2016): *Temporal and spatial cold-water coral occurrence in the Alboran Sea and the Gulf of Cádiz during previous glacial-interglacial cycles*. Master's thesis, Institute of Earth Science, Heidelberg University.

Krengel, T. (2020): *550,000 years of marine climate variability in the western Mediterranean Sea revealed by cold-water corals*. Ph.d. thesis, Institute of Earth Science, Heidelberg University.

Kromer, B., Lindauer, S., Synal, H.A., Wacker, L. (2013): MAMS – A new AMS facility at the Curt-Engelhorn-Centre for Achaeometry, Mannheim, Germany. *Nuclear Instruments and Methods in Physics Research Section B: Beam Interactions with Materials and Atoms* **294**, 11–13.

Lambeck, K., Rouby, H., Purcell, A., Sun, Y., Sambridge, M. (2014): Sea level and global ice volumes from the Last Glacial Maximum to the Holocene. *Proceedings of the National Academy of Sciences* **111**, 15296–15303.

Lausecker, M. (2015): *Das Lithium - Magnesium - Verhaltnis alsTemperaturproxy in Tiefseekorallen: Temperaturkalibration und Temperaturrekonstruktion*. Bachelor's thesis, Institute of Environmental Physics, Department of Physics and Astronomy, Heidelberg University.

Libby, W.F. (1946): Atmospheric Helium Three and Radiocarbon from Cosmic Radiation. *Physical Review* **69**, 671–672.

Lin, J., Liu, Y., Hu, Z., Chen, W., Zhang, L., Chen, H. (2019): Accurate Measurement of Lithium Isotopes in Eleven Carbonate Reference Materials by MC-ICP-MS with Soft Extraction Mode and 10^12 Ω Resistor High-Gain Faraday Amplifiers. *Geostandards and Geoanalytical Research* **43**, 277–289.

Lippold, J., Pöppelmeier, F., Süfke, F., Gutjahr, M., Goepfert, T.J., Blaser, P., Friedrich, O., Link, J.M., Wacker, L., Rheinberger, S., Jaccard, S.L. (2019): Constraining the Variability of the Atlantic Meridional Overturning Circulation During the Holocene. *Geophysical Research Letters* **46**, 11338–11346.

Little, M.G., Schneider, R.R., Kroon, D., Price, B., Bickert, T., Wefer, G. (1997a): Rapid palaeoceanographic changes in the Benguela Upwelling System for the last 160,000 years as indicated by abundances of planktonic foraminifera. *Palaeogeography, Palaeoclimatology, Palaeoecology* **130**, 135–161.

Little, M.G., Schneider, R.R., Kroon, D., Price, B., Summerhayes, C.P., Segl, M. (1997b): Trade wind forcing of upwelling, seasonality, and Heinrich events as a response to sub-Milankovitch climate variability. *Paleoceanography* **12**, 568–576.

López Correa, M., Montagna, P., Joseph, N., Rüggeberg, A., Fietzke, J., Flögel, S., Dorschel, B., Goldstein, S.L., Wheeler, A., Freiwald, A. (2012): Preboreal onset of cold-water coral growth beyond the Arctic Circle revealed by coupled radiocarbon and U-series dating and neodymium isotopes. *Quaternary Science Reviews* **34**, 24–43.

Lozier, M.S. (1999): The impact of mid-depth recirculations on the distribution of tracers in the North Atlantic. *Geophysical Research Letters* **26**, 219–222.

Lütkes, L. (2021): *East Atlantic Thermocline Circulation During the Last 58 ka - Viewed Through Neodymium Isotopes in Cold-Water Corals*. Master's thesis, Institute of Environmental Physics, Department of Physics and Astronomy, Heidelberg University.

Lu, J., Vecchi, G.A., Reichler, T. (2007): Expansion of the Hadley cell under global warming. *Geophysical Research Letters* **34**.

Lund, D.C., Asimow, P.D., Farley, K.A., Rooney, T.O., Seeley, E., Jackson, E.W., Durham, Z.M. (2016): Enhanced East Pacific Rise hydrothermal activity during the last two glacial terminations. *Science* **351**, 478–482.

Lynch-Stieglitz, J., Ito, T., Michel, E. (2016): Antarctic density stratification and the strength of the circumpolar current during the Last Glacial Maximum. *Paleoceanography* **31**, 539–552.

Mangini, A., Lomitschka, M., Eichstädter, R., Frank, N., Vogler, S., Bonani, G., Hajdas, I., Patzold, J. (1998): Coral provides way to age deep water. *Nature* **392**, 347–348.

Mangini, A., Godoy, J.M., Godoy, M.L., Kowsmann, R., Santos, G.M., Ruckelshausen, M., Schroeder-Ritzrau, A., Wacker, L. (2010): Deep sea corals off Brazil verify a poorly ventilated Southern Pacific Ocean during H2, H1 and the Younger Dryas. *Earth and Planetary Science Letters* **293**, 269–276.

MARGO Project Members (2009): Constraints on the magnitude and patterns of ocean cooling at the Last Glacial Maximum. *Nature Geoscience* **2**, 127–132.

Marriott, C.S., Henderson, G.M., Belshaw, N.S., Tudhope, A.W. (2004a): Temperature dependence of δ^7Li, δ^{44}Ca and Li/Ca during growth of calcium carbonate. *Earth and Planetary Science Letters* **222**, 615–624.

Marriott, C.S., Henderson, G.M., Crompton, R., Staubwasser, M., Shaw, S. (2004b): Effect of mineralogy, salinity, and temperature on Li/Ca and Li isotope composition of calcium carbonate. *Chemical Geology* **212**, 5–15.

McConnaughey, T. (1989): ^{13}C and ^{18}O isotopic disequilibrium in biological carbonates: II. *In vitro* simulation of kinetic isotope effects. *Geochimica et Cosmochimica Acta* **53**, 163–171.

McManus, J.F., Francois, R., Gherardi, J.M., Keigwin, L.D., Brown-Leger, S. (2004): Collapse and rapid resumption of Atlantic meridional circulation linked to deglacial climate changes. *Nature* **428**, 834–837.

Meeuwis, J.M., Lutjeharms, J.R.E. (1990): Surface thermal characteristics of the Angola-Benguela front. *South African Journal of Marine Science* **9**, 261–279.

Meibom, A., Cuif, J.P., Houlbreque, F., Mostefaoui, S., Dauphin, Y., Meibom, K.L., Dunbar, R. (2008): Compositional variations at ultra-structure length scales in coral skeleton. *Geochimica et Cosmochimica Acta* **72**, 1555–1569.

Messing, C.G., Neumann, A.C., Lang, J.C. (1990): Biozonation of Deep-Water Lithoherms and Associated Hardgrounds in the Northeastern Straits of Florida. *Palaios* **5**, 15–33.

Middleton, J.L., Langmuir, C.H., Mukhopadhyay, S., McManus, J.F., Mitrovica, J.X. (2016): Hydrothermal iron flux variability following rapid sea level changes. *Geophysical Research Letters* **43**, 3848–3856.

Mienis, F., van der Land, C., de Stigter, H.C., van de Vorstenbosch, M., de Haas, H., Richter, T., van Weering, T.C.E. (2009): Sediment accumulation on a cold-water carbonate mound at the Southwest Rockall Trough margin. *Marine Geology* **265**, 40–50.

Mienis, F., de Stigter, H.C., de Haas, H., van der Land, C., van Weering, T.C.E. (2012): Hydrodynamic conditions in a cold-water coral mound area on the Renard Ridge, southern Gulf of Cadiz. *Journal of Marine Systems* **96-97**, 61–71.

Milliman, J.D. (1993): Production and accumulation of calcium carbonate in the ocean: Budget of a nonsteady state. *Global Biogeochemical Cycles* **7**, 927–957.

Millot, R., Guerrot, C., Vigier, N. (2004): Accurate and High-Precision Measurement of Lithium Isotopes in Two Reference Materials by MC-ICP-MS. *Geostandards and Geoanalytical Research* **28**, 153–159.

Millot, R., Petelet-Giraud, E., Guerrot, C., Négrel, P. (2010): Multi-isotopic composition (δ7Li–δ11B–δD–δ18O) of rainwaters in France: Origin and spatio-temporal characterization. *Applied Geochemistry* **25**, 1510–1524.

Miltner, M. (2020): *Radiocarbon in the Northeast Atlantic*. Master's thesis, Institute of Environmental Physics, Department of Physics and Astronomy, Heidelberg University.

Misra, S., Froelich, P.N. (2009): Measurement of lithium isotope ratios by quadrupole-ICP-MS: application to seawater and natural carbonates. *Journal of Analytical Atomic Spectrometry* **24**, 1524–1533.

Misra, S., Froelich, P.N. (2012): Lithium Isotope History of Cenozoic Seawater: Changes in Silicate Weathering and Reverse Weathering. *Science* **335**, 818–823.

Mitsuguchi, T., Matsumoto, E., Abe, O., Uchida, T., Isdale, P.J. (1996): Mg/Ca Thermometry in Coral Skeletons. *Science* **274**, 961–963.

Mitsuguchi, T., Dang, P.X., Kitagawa, H., Uchida, T., Shibata, Y. (2008): Coral Sr/Ca and Mg/Ca records in Con Dao Island off the Mekong Delta: Assessment of their potential for monitoring ENSO and East Asian monsoon. *Global and Planetary Change* **63**, 341–352.

Mollenhauer, G., Schneider, R.R., Müller, P.J., Spieß, V., Wefer, G. (2002): Glacial/interglacial variablity in the Benguela upwelling system: Spatial distribution and budgets of organic carbon accumulation. *Global Biogeochemical Cycles* **16**.

Montagna, P., McCulloch, M., Douville, E., López Correa, M., Trotter, J., Rodolfo-Metalpa, R., Dissard, D., Ferrier-Pagès, C., Frank, N., Freiwald, A., Goldstein, S., Mazzoli, C., Reynaud, S., Rüggeberg, A., Russo, S., Taviani, M. (2014): Li/Mg systematics in scleractinian corals: Calibration of the thermometer. *Geochimica et Cosmochimica Acta* **132**, 288–310.

Montero-Serrano, J.C., Frank, N., Colin, C., Wienberg, C., Eisele, M. (2011): The climate influence on the mid-depth Northeast Atlantic gyres viewed by cold-water corals. *Geophysical Research Letters* **38**, n/a–n/a.

Mortensen, P.B., Hovland, T., Fosså, J.H., Furevik, D.M. (2001): Distribution, abundance and size of Lophelia pertusa coral reefs in mid-Norway in relation to seabed characteristics. *Journal of the Marine Biological Association of the United Kingdom* **81**, 581–597.

Murakami, S., Ohgaito, R., Abe-Ouchi, A., Crucifix, M., Otto-Bliesner, B.L. (2008): Global-Scale Energy and Freshwater Balance in Glacial Climate: A Comparison of Three PMIP2 LGM Simulations. *Journal of Climate* **21**, 5008–5033.

Nakajima, K. (2016): *Local overprinting of ϵNd and Li/Mg in deep-sea corals of the Azores*. Bachelor's thesis, Institute of Environmental Physics, Department of Physics and Astronomy, Heidelberg University.

New, A.L., Jia, Y., Coulibaly, M., Dengg, J. (2001): On the role of the Azores Current in the ventilation of the North Atlantic Ocean. *Progress in Oceanography* **48**, 163–194.

Olsen, A., Lange, N., Key, R.M., Tanhua, T., Álvarez, M., Becker, S., Bittig, H.C., Carter, B.R., da Cunha, L.C., Feely, R.A., van Heuven, S., Hoppema, M., Ishii, M., Jeansson, E., Jones, S.D., Jutterström, S., Karlsen, M.K., Kozyr, A., Lauvset, S.K., Monaco, C.L., Murata, A., Pérez, F.F., Pfeil, B., Schirnick, C., Steinfeldt, R., Suzuki, T., Telszewski, M., Tilbrook, B., Velo, A., Wanninkhof, R. (2019): GLODAPv2.2019 – an update of GLODAPv2. *Earth System Science Data* **11**, 1437–1461.

Pahnke, K., Goldstein, S.L., Hemming, S.R. (2008): Abrupt changes in Antarctic Intermediate Water circulation over the past 25,000 years. *Nature Geoscience* **1**, 870–874.

Pedro, J.B., Jochum, M., Buizert, C., He, F., Barker, S., Rasmussen, S.O. (2018): Beyond the bipolar seesaw: Toward a process understanding of interhemispheric coupling. *Quaternary Science Reviews* **192**, 27–46.

Penaud, A., Eynaud, F., Turon, J.L., Blamart, D., Rossignol, L., Marret, F., Lopez-Martinez, C., Grimalt, J.O., Malaizé, B., Charlier, K. (2010): Contrasting paleoceanographic conditions off Morocco during Heinrich events (1 and 2) and the Last Glacial Maximum. *Quaternary Science Reviews* **29**, 1923–1939.

Penaud, A., Eynaud, F., Voelker, A., Kageyama, M., Marret, F., Turon, J.L., Blamart, D., Mulder, T., Rossignol, L. (2011): Assessment of sea surface temperature changes in the Gulf of Cadiz during the last 30 ka: implications for glacial changes in the regional hydrography. *Biogeosciences* **8**, 2295–2316.

Pistiner, J.S., Henderson, G.M. (2003): Lithium-isotope fractionation during continental weathering processes. *Earth and Planetary Science Letters* **214**, 327–339.

Pons-Branchu, E., Hillaire-Marcel, C., Deschamps, P., Ghaleb, B., Sinclair, D.J. (2005): Early diagenesis impact on precise U-series dating of deep-sea corals: Example of a 100–200-year old Lophelia pertusa sample from the northeast Atlantic. *Geochimica et Cosmochimica Acta* **69**, 4865–4879.

Qi, H., Taylor, P., Berglund, M., Bièvre, P.D. (1997): Calibrated measurements of the isotopic composition and atomic weight of the natural Li isotopic reference material IRMM-016. *International Journal of Mass Spectrometry and Ion Processes* **171**, 263–268.

Raddatz, J., Rüggeberg, A. (2019): Constraining past environmental changes of cold-water coral mounds with geochemical proxies in corals and foraminifera. *The Depositional Record* .

Raddatz, J., Liebetrau, V., Rüggeberg, A., Hathorne, E., Krabbenhöft, A., Eisenhauer, A., Böhm, F., Vollstaedt, H., Fietzke, J., López Correa, M., Freiwald, A., Dullo, W.C. (2013): Stable Sr-isotope, Sr/Ca, Mg/Ca, Li/Ca and Mg/Li ratios in the scleractinian cold-water coral Lophelia pertusa. *Chemical Geology* **352**, 143–152.

Raddatz, J., Rüggeberg, A., Flögel, S., Hathorne, E.C., Liebetrau, V., Eisenhauer, A., Dullo, W.C. (2014): The influence of seawater pH on U/Ca ratios in the scleractinian cold-water coral *Lophelia pertusa*. *Biogeosciences* **11**, 1863–1871.

Rahmstorf, S. (2002): Ocean circulation and climate during the past 120,000 years. *Nature* **419**, 207–214.

Rahmstorf, S. (2003): Timing of abrupt climate change: A precise clock. *Geophysical Research Letters* **30**, n/a–n/a.

Ramos, A., Sanz, J.L., Ramil, F., Agudo, L.M., Presas-Navarro, C. (2017): The Giant Cold-Water Coral Mounds Barrier Off Mauritania. In: *Deep-Sea Ecosystems Off Mauritania*, 481–525, Springer Netherlands.

Rampmeier, J.L. (2021): *Glaziale Zwischenwassertemperaturen nahe der Azorenfront: Li/Mg-Verhältnis in Kaltwasserkorallen unter dem Einfluss hydrothermaler Aktivität*. Bachelor's thesis, Institute of Environmental Physics, Department of Physics and Astronomy, Heidelberg University.

Rasmussen, S.O., Andersen, K.K., Svensson, A.M., Steffensen, J.P., Vinther, B.M., Clausen, H.B., Siggaard-Andersen, M.L., Johnsen, S.J., Larsen, L.B., Dahl-Jensen, D., Bigler, M., Röthlisberger, R., Fischer, H., Goto-Azuma, K., Hansson, M.E., Ruth, U. (2006): A new Greenland ice core chronology for the last glacial termination. *Journal of Geophysical Research* **111**.

Reimer, P.J., Austin, W.E.N., Bard, E., Bayliss, A., Blackwell, P.G., Ramsey, C.B., Butzin, M., Cheng, H., Edwards, R.L., Friedrich, M., Grootes, P.M., Guilderson, T.P., Hajdas, I., Heaton, T.J., Hogg, A.G., Hughen, K.A., Kromer, B., Manning, S.W., Muscheler, R., Palmer, J.G., Pearson, C., van der Plicht, J., Reimer, R.W., Richards, D.A., Scott, E.M., Southon, J.R., Turney, C.S.M., Wacker, L., Adolphi, F., Büntgen, U., Capano, M., Fahrni, S.M., Fogtmann-Schulz, A., Friedrich, R., Köhler, P., Kudsk, S., Miyake, F., Olsen, J., Reinig, F., Sakamoto, M., Sookdeo, A., Talamo, S. (2020): The IntCal20 Northern Hemisphere Radiocarbon Age Calibration Curve (0–55 cal kBP). *Radiocarbon* **62**, 725–757.

Reynaud, S., Ferrier-Pagès, C., Meibom, A., Mostefaoui, S., Mortlock, R., Fairbanks, R., Allemand, D. (2007): Light and temperature effects on Sr/Ca and Mg/Ca ratios in the scleractinian coral Acropora sp. *Geochimica et Cosmochimica Acta* **71**, 354–362.

Rühlemann, C., Mulitza, S., Lohmann, G., Paul, A., Prange, M., Wefer, G. (2004): Intermediate depth warming in the tropical Atlantic related to weakened thermohaline circulation: Combining paleoclimate data and modeling results for the last deglaciation. *Paleoceanography* **19**.

Richardson, P.L., Bower, A.S., Zenk, W. (2000): A census of Meddies tracked by floats. *Progress in Oceanography* **45**, 209–250.

Riley, J.P., Tongudai, M. (1964): The lithium content of sea water. *Deep Sea Research and Oceanographic Abstracts* **11**, 563–568.

Roberts, J.M., Long, D., Wilson, J.B., Mortensen, P.B., Gage, J.D. (2003): The cold-water coral Lophelia pertusa (Scleractinia) and enigmatic seabed mounds along the north-east Atlantic margin: are they related? *Marine Pollution Bulletin* **46**, 7–20.

Roberts, J.M., Wheeler, A.J., Freiwald, A., Cairns, S.D. (2009): *Cold-water corals : the biology and geology of deep-sea coral habitats*. Cambridge University Press, Cambridge, UK New York.

Robinson, L.F. (2004): Climatic Control of Riverine and Seawater Uranium-Isotope Ratios. *Science* **305**, 851–854.

Robinson, L.F., van de Flierdt, T. (2009): Southern Ocean evidence for reduced export of North Atlantic Deep Water during Heinrich event 1. *Geology* **37**, 195–198.

Robinson, L.F., Adkins, J.F., Frank, N., Gagnon, A.C., Prouty, N.G., Roark, E.B., van de Flierdt, T. (2014): The geochemistry of deep-sea coral skeletons: A review of vital effects and applications for palaeoceanography. *Deep Sea Research Part II: Topical Studies in Oceanography* **99**, 184–198.

Roesch, C. (2017): *Tiefseekorallen vor Angola: Archive der tropischen Zwischenwasserdynamik seit der letzten Eiszeit*. Bachelor's thesis, Institute of Environmental Physics, Department of Physics and Astronomy, Heidelberg University.

Rogerson, M., Rohling, E.J., Weaver, P.P.E., Murray, J.W. (2004): The Azores Front since the Last Glacial Maximum. *Earth and Planetary Science Letters* **222**, 779–789.

Rollion-Bard, C., Chaussidon, M., France-Lanord, C. (2003): pH control on oxygen isotopic composition of symbiotic corals. *Earth and Planetary Science Letters* **215**, 275–288.

Rollion-Bard, C., Vigier, N., Meibom, A., Blamart, D., Reynaud, S., Rodolfo-Metalpa, R., Martin, S., Gattuso, J.P. (2009): Effect of environmental conditions and skeletal ultrastructure on the Li isotopic composition of scleractinian corals. *Earth and Planetary Science Letters* **286**, 63–70.

Rollion-Bard, C., Blamart, D., Cuif, J.P., Dauphin, Y. (2010): In situ measurements of oxygen isotopic composition in deep-sea coral, Lophelia pertusa: Re-examination of the current geochemical models of biomineralization. *Geochimica et Cosmochimica Acta* **74**, 1338–1349.

Romero, O., Mollenhauer, G., Schneider, R.R., Wefer, G. (2003): Oscillations of the siliceous imprint in the central Benguela Upwelling System from MIS 3 through to the early Holocene: the influence of the Southern Ocean. *Journal of Quaternary Science* **18**, 733–743.

Rosenthal, H.S. (2018): *Tiefseekorallen als Archiv eiszeitlicherTemperaturentwicklung der Thermokline nahe der Azorenfront*. Bachelor's thesis, Institute of Environmental Physics, Department of Physics and Astronomy, Heidelberg University.

Roy-Barman, M., Chen, J., Wasserburg, G. (1996): 230Th232Th systematics in the central Pacific Ocean: The sources and the fates of thorium. *Earth and Planetary Science Letters* **139**, 351–363.

Rozanski, K., Stichler, W., Gonfiantini, R., Scott, E.M., Beukens, R.P., Kromer, B., Plicht, J.V.D. (1992): The IAEA 14C Intercomparison Exercise 1990. *Radiocarbon* **34**, 506–519.

Ruckelshausen, M. (2013): *Cold-water corals: A paleoceanographic archive; Tracing past ocean circulation changes in the mid-depth subtropical western South Atlantic off Brazil for the last 40 ka BP*. Ph.d. thesis, Institute of Environmental Physics, Department of Physics and Astronomy, Heidelberg University.

Rutberg, R.L., Goldstein, S.L., Hemming, S.R., Anderson, R.F. (2005): Sr isotope evidence for sources of terrigenous sediment in the southeast Atlantic Ocean: Is there increased available Fe for enhanced glacial productivity? *Paleoceanography* **20**.

Sachs, J.P., Anderson, R.F., Lehman, S.J. (2001): Glacial Surface Temperatures of the Southeast Atlantic Ocean. *Science* **293**, 2077–2079.

Schiebel, R., Schmuker, B., Alves, M., Hemleben, C. (2002): Tracking the Recent and late Pleistocene Azores front by the distribution of planktic foraminifers. *Journal of Marine Systems* **37**, 213–227.

Schiller, A., Mikolajewicz, U., Voss, R. (1997): The stability of the North Atlantic thermohaline circulation in a coupled ocean-atmosphere general circulation model. *Climate Dynamics* **13**, 325–347.

Schleinkofer, N., Raddatz, J., Freiwald, A., Evans, D., Beuck, L., Rüggeberg, A., Liebetrau, V. (2019): Environmental and biological controls on Na/Ca ratios in scleractinian cold-water corals. *Biogeosciences* **16**, 3565–3582.

Schlitzer, R. (2020): Ocean Data View. https://odv.awi.de.

Schneider, H.S. (2018): *Cold-water corals: Reconstruction of paleoenvironmental history off Mauritania*. Master's thesis, Institute of Earth Science, Heidelberg University.

Schneider, R.R., Müller, P.J., Ruhland, G., Meinecke, G., Schmidt, H., Wefer, G. (1996): Late Quaternary Surface Temperatures and Productivity in the East-Equatorial South Atlantic: Response to Changes in Trade/Monsoon Wind Forcing and Surface Water Advection. In: *The South Atlantic*, 527–551, Springer Berlin Heidelberg.

Schröder-Ritzrau, A., Mangini, A., Lomitschka, M. (2003): Deep-sea corals evidence periodic reduced ventilation in the North Atlantic during the LGM/Holocene transition. *Earth and Planetary Science Letters* **216**, 399–410.

Schwab, C., Kinkel, H., Weinelt, M., Repschläger, J. (2012): Coccolithophore paleoproductivity and ecology response to deglacial and Holocene changes in the Azores Current System. *Paleoceanography* **27**.

Shen, G.T., Dunbar, R.B. (1995): Environmental controls on uranium in reef corals. *Geochimica et Cosmochimica Acta* **59**, 2009–2024.

Sherwood, O.A., Risk, M.J. (2007): Chapter Twelve Deep-Sea Corals: New Insights to Paleoceanography. In: *Developments in Marine Geology*, 491–522, Elsevier.

Shirai, K., Kusakabe, M., Nakai, S., Ishii, T., Watanabe, T., Hiyagon, H., Sano, Y. (2005): Deep-sea coral geochemistry: Implication for the vital effect. *Chemical Geology* **224**, 212–222.

Sinclair, D.J., Williams, B., Risk, M. (2006): A biological origin for climate signals in corals—Trace element "vital effects" are ubiquitous in Scleractinian coral skeletons. *Geophysical Research Letters* **33**.

Skinner, L.C., Fallon, S., Waelbroeck, C., Michel, E., Barker, S. (2010): Ventilation of the Deep Southern Ocean and Deglacial CO2 Rise. *Science* **328**, 1147–1151.

Skinner, L.C., Primeau, F., Freeman, E., de la Fuente, M., Goodwin, P.A., Gottschalk, J., Huang, E., McCave, I.N., Noble, T.L., Scrivner, A.E. (2017): Radiocarbon constraints on the glacial ocean circulation and its impact on atmospheric CO2. *Nature Communications* **8**.

Smith, J.E., Schwarcz, H.P., Risk, M.J. (2002): Patterns of isotopic disequilibria in azooxanthellate coral skeletons. *Hydrobiologia* **471**, 111–115.

Spiro, B., Roberts, M., Gage, J., Chenery, S. (2000): $^{18}O/^{16}O$ and $^{13}C/^{12}C$ in an ahermatypic deep-water coral Lophelia pertusa from the North Atlantic: a case of disequilibrium isotope fractionation. *Rapid Communications in Mass Spectrometry* **14**, 1332–1336.

Spite, M., Spite, F. (1982): Lithium abundance at the formation of the Galaxy. *Nature* **297**, 483–485.

Spooner, P.T., Guo, W., Robinson, L.F., Thiagarajan, N., Hendry, K.R., Rosenheim, B.E., Leng, M.J. (2016): Clumped isotope composition of cold-water corals: A role for vital effects? *Geochimica et Cosmochimica Acta* **179**, 123–141.

Stewart, J.A., Robinson, L.F., Day, R.D., Strawson, I., Burke, A., Rae, J.W.B., Spooner, P.T., Samperiz, A., Etnoyer, P.J., Williams, B., Paytan, A., Leng, M.J., Häussermann, V., Wickes, L.N., Bratt, R., Pryer, H. (2020): Refining trace metal temperature proxies in cold-water scleractinian and stylasterid corals. *Earth and Planetary Science Letters* **545**, 116412.

Stocker, T.F., Johnsen, S.J. (2003): A minimum thermodynamic model for the bipolar seesaw. *Paleoceanography* **18**.

Stocker, T.F., Mysak, L.A., Wright, D.G. (1992): A Zonally Averaged, Coupled Ocean-Atmosphere Model for Paleoclimate Studies. *Journal of Climate* **5**, 773–797.

Stoffynegli, P., Mackenzie, F.T. (1984): Mass balance of dissolved lithium in the oceans. *Geochimica et Cosmochimica Acta* **48**, 859–872.

Stolarski, J. (2003): Three- dimensional micro- and nanostructural characteristics of the scleractinian coral skeleton: A biocalcification proxy. *Acta palaeontologica Polonica* **48**, 497–530.

Stoll, H.M., Schrag, D.P., Clemens, S.C. (1999): Are seawater Sr/Ca variations preserved in quaternary foraminifera? *Geochimica et Cosmochimica Acta* **63**, 3535–3547.

Stramma, L. (2001): Current Systems In The Atlantic Ocean. In: *Encyclopedia of Ocean Sciences*, 589–598, Elsevier.

Stramma, L., Peterson, R.G. (1989): Geostrophic Transport in the Benguela Current Region. *Journal of Physical Oceanography* **19**, 1440–1448.

Stuiver, M., Polach, H.A. (1977): Discussion Reporting of ^{14}C Data. *Radiocarbon* **19**, 355–363.

Stuiver, M., Suess, H.E. (1966): On the Relationship Between Radiocarbon Dates and True Sample Ages. *Radiocarbon* **8**, 534–540.

Tachikawa, K., Arsouze, T., Bayon, G., Bory, A., Colin, C., Dutay, J.C., Frank, N., Giraud, X., Gourlan, A.T., Jeandel, C., Lacan, F., Meynadier, L., Montagna, P., Piotrowski, A.M., Plancherel, Y., Pucéat, E., Roy-Barman, M., Waelbroeck, C. (2017): The large-scale evolution of neodymium isotopic composition in the global modern and Holocene ocean revealed from seawater and archive data. *Chemical Geology* **457**, 131–148.

Talley, L.D. (1996): Antarctic Intermediate Water in the South Atlantic. In: *The South Atlantic*, 219–238, Springer Berlin Heidelberg.

Talley, L.D. (2008): Freshwater transport estimates and the global overturning circulation: Shallow, deep and throughflow components. *Progress in Oceanography* **78**, 257–303.

Talley, L.D., Pickard, G.L., Emery, W.J., Swift, J.H. (2011): *Descriptive physical oceanography : an introduction*. Academic Press, Boston.

Taylor, T.I., Urey, H.C. (1938): Fractionation of the Lithium and Potassium Isotopes by Chemical Exchange with Zeolites. *The Journal of Chemical Physics* **6**, 429–438.

Teng, F.Z., McDonough, W., Rudnick, R., Dalpé, C., Tomascak, P., Chappell, B., Gao, S. (2004): Lithium isotopic composition and concentration of the upper continental crust. *Geochimica et Cosmochimica Acta* **68**, 4167–4178.

Therre, S., Proß, L., Friedrich, R., Trüssel, M., Frank, N. (2021): Heidelberg Radiocarbon Lab - Establishing a new carbon dioxide extraction line for carbonate samples. *Radiocarbon* **63**, 915–924.

Thiagarajan, N., Adkins, J., Eiler, J. (2011): Carbonate clumped isotope thermometry of deep-sea corals and implications for vital effects. *Geochimica et Cosmochimica Acta* **75**, 4416–4425.

Thiagarajan, N., Subhas, A.V., Southon, J.R., Eiler, J.M., Adkins, J.F. (2014): Abrupt pre-Bølling–Allerød warming and circulation changes in the deep ocean. *Nature* **511**, 75–78.

Thornalley, D.J.R., Bauch, H.A., Gebbie, G., Guo, W., Ziegler, M., Bernasconi, S.M., Barker, S., Skinner, L.C., Yu, J. (2015): A warm and poorly ventilated deep Arctic Mediterranean during the last glacial period. *Science* **349**, 706–710.

Tomascak, P.B., Langmuir, C.H., le Roux, P.J., Shirey, S.B. (2008): Lithium isotopes in global mid-ocean ridge basalts. *Geochimica et Cosmochimica Acta* **72**, 1626–1637.

Tomascak, P.B., Magna, T., Dohmen, R. (2016): *Advances in Lithium Isotope Geochemistry*. Springer International Publishing.

Tsuchiya, M. (1989): Circulation of the Antarctic Intermediate Water in the North Atlantic Ocean. *Journal of Marine Research* **47**, 747–755.

Vaughan, T.W. (1940): Ecology of modern marine organisms with reference to paleogeography. *Geological Society of America Bulletin* **51**, 433–468.

Veitch, J., Penven, P., Shillington, F. (2010): Modeling Equilibrium Dynamics of the Benguela Current System. *Journal of Physical Oceanography* **40**, 1942–1964.

Veitch, J.A., Penven, P. (2017): The role of the Agulhas in the Benguela Current system: A numerical modeling approach. *Journal of Geophysical Research: Oceans* **122**, 3375–3393.

Vigier, N., Rollion-Bard, C., Spezzaferri, S., Brunet, F. (2007): In situ measurements of Li isotopes in foraminifera. *Geochemistry, Geophysics, Geosystems* **8**.

Vigier, N., Rollion-Bard, C., Levenson, Y., Erez, J. (2015): Lithium isotopes in foraminifera shells as a novel proxy for the ocean dissolved inorganic carbon (DIC). *Comptes Rendus Geoscience* **347**, 43–51.

Vogler, S., Scholten, J., van der Loeff, M.R., Mangini, A. (1998): ^{230}Th in the eastern North Atlantic: the importance of water mass ventilation in the balance of ^{230}Th. *Earth and Planetary Science Letters* **156**, 61–74.

Wacongne, S., Piton, B. (1992): The near-surface circulation in the northeastern corner of the South Atlantic ocean. *Deep Sea Research Part A. Oceanographic Research Papers* **39**, 1273–1298.

Waelbroeck, C., Duplessy, J.C., Michel, E., Labeyrie, L., Paillard, D., Duprat, J. (2001): The timing of the last deglaciation in North Atlantic climate records. *Nature* **412**, 724–727.

Weaver, A.J. (2003): Meltwater Pulse 1A from Antarctica as a Trigger of the Bolling-Allerod Warm Interval. *Science* **299**, 1709–1713.

Weber, J.N. (1973): Deep-sea ahermatypic scleractinian corals: isotopic composition of the skeleton. *Deep Sea Research and Oceanographic Abstracts* **20**, 901–909.

Weber, J.N., Woodhead, P.M.J. (1970): Carbon and oxygen isotope fractionation in the skeletal carbonate of reef-building corals. *Chemical Geology* **6**, 93–117.

Wefing, A.M., Arps, J., Blaser, P., Wienberg, C., Hebbeln, D., Frank, N. (2017): High precision U-series dating of scleractinian cold-water corals using an automated chromatographic U and Th extraction. *Chemical Geology* **475**, 140–148.

Weijer, W., van Sebille, E. (2014): Impact of Agulhas Leakage on the Atlantic Overturning Circulation in the CCSM4. *Journal of Climate* **27**, 101–110.

Wheat, C.G., Mottl, M.J. (2000): Composition of pore and spring waters from Baby Bare: global implications of geochemical fluxes from a ridge flank hydrothermal system. *Geochimica et Cosmochimica Acta* **64**, 629–642.

White, M. (2006): Benthic dynamics at the carbonate mound regions of the Porcupine Sea Bight continental margin. *International Journal of Earth Sciences* **96**, 1–9.

Wienberg, C., Titschack, J. (2017): Framework-Forming Scleractinian Cold-Water Corals Through Space and Time: A Late Quaternary North Atlantic Perspective. In: *Marine Animal Forests*, 1–34, Springer International Publishing.

Wienberg, C., Frank, N., Mertens, K.N., Stuut, J.B., Marchant, M., Fietzke, J., Mienis, F., Hebbeln, D. (2010): Glacial cold-water coral growth in the Gulf of Cádiz: Implications of increased palaeo-productivity. *Earth and Planetary Science Letters* **298**, 405–416.

Wienberg, C., Titschack, J., Freiwald, A., Frank, N., Lundälv, T., Taviani, M., Beuck, L., Schröder-Ritzrau, A., Krengel, T., Hebbeln, D. (2018): The giant Mauritanian cold-water coral mound province: Oxygen control on coral mound formation. *Quaternary Science Reviews* **185**, 135–152.

Wilson, J.B. (1979): 'Patch' development of the deep-water coral Lophelia Pertusa (L.) on Rockall Bank. *Journal of the Marine Biological Association of the United Kingdom* **59**, 165–177.

You, C.F., Chan, L.H. (1996): Precise determination of lithium isotopic composition in low concentration natural samples. *Geochimica et Cosmochimica Acta* **60**, 909–915.

Zhang, X., Lohmann, G., Knorr, G., Purcell, C. (2014): Abrupt glacial climate shifts controlled by ice sheet changes. *Nature* **512**, 290–294.

Danksagung

"Niemand hätte jemals den Ozean überquert, wenn er die Möglichkeit gehabt hätte, bei Sturm das Schiff zu verlassen."
Charles Kettering

An dieser Stelle gebührt Dank all denjenigen, die in den letzten Jahren dieses Schiff getragen haben:

Zuallererst möchte ich Norbert Frank für die Betreuung meiner Dokotrarbeit danken. Ich hatte immer die Möglichkeit Neues auszuprobieren und habe dabei sehr viele Freiheiten erfahren, auch wenn nicht immer alles auf Anhieb funktioniert hat. Seine Begeisterung für Korallen war immer motivierend, ansteckend und überhaupt der Grund, warum ich in der Paläoozeanograpphie gelandet bin. Danke auch für das mir entgegengebrachte Vertrauen, ich hoffe, ich hab es nicht enttäuscht.
Prof. Werner Aeschbach möchte ich dafür danken, dass er sich bereit erklärt hat, Zweitgutachter meiner Dissertation zu sein. Danke auch an apl. Prof. Monica Dunford und und Jun.-Prof. Susanne Westhoff, die sich bereit erklärt haben, Teil meines Prüfungskomitees zu sein.
Ein wichtiger Baustein in den letzten Jahren waren natürlich die PUAs, mit allen aktuellen Mitgliedern und all jenen, die das IUP in den letzten Jahren schon vor mir verlassen haben. Danke für die schöne Arbeitsatmosphäre und dafür, dass jederzeit eure Türen offen stehen. Egal ob es um eine 'kurze' Teepause geht oder ein Problem gelöst werden muss. Egal ob in 'echt' oder virtuell während der letzten Monate, ich konnte immer sicher sein, dass jemand da ist. Danke vor allem Jasmin, Thomas, Steffen, Evan und Julius, dafür, dass ihr immer ein offenes Ohr hattet, für die aufbauenden Gespräche und viele schöne Mittagspausen.
Diese Arbeit wäre ohne die Hilfe von vielen Menschen nicht möglch gewesen. Da wäre zum einen Andrea Schröder-Ritzrau, die immer die passenden Proben parat hatte, mich schon während meiner Bachelorarbeit immer unterstützt hat und sich immer Zeit für Fragen genommen hat (und mögen sie noch so offensichtlich gewesen sein). Danke auch an René Eichstädter, für die Einführung an der Neptune und dafür, dass er immer

mit Rat und Tat zur Seite stand, wenn die Massenspektrometer mal wieder nicht das gemacht haben was ich wollte. An dieser Stelle sei auch Julius Förstel, Patrick Blaser und Benny Antz gedankt, die mir das Messen an der ICap begebracht haben. Charlotte König danke dafür, dass sie mich zu Beginn der Promotion bei den Elementmessungen unterstützt hat und mir damit vor allem auch die 'nebenbei' Messungen abgenommen hat. Natürlich auch ein großes Danke an all jene, deren Daten ich in dieser Arbeit nutze, in die so viele Bachelor- und Masterarbeiten eingeflossen sind: Elvira Beisel, Tamara Dardoufas, Amrei Glasder, Thomas Krengel, Markus Miltner, Kai Nakajima, Johanna Rampmeier, Carla Roesch, Hanna Rosenthal und Hannah Schneider.
Thomas, Steffen, Andrea, Elvira und Jasmin danke ich für eure Korrekturen und Kommentare zu dieser Arbeit. Danke, dass ihr euch dafür Zeit genommen habt.
Ich durfte in den letzten Jahren einige Erlebnisse machen, die ich so schnell nicht vergessen werde. Da wären zum einen die beiden Schifffahrten auf der RV Meteor mit einem neu entdeckten Lophelia Riff. Ich bin sicher, das waren meine ersten aber nicht meine letzten Schifffahrten. Danke Norbert, dass ich dabei sein und Neues lernen durfte. Einen besseren Start in meine Promotionszeit hätte ich mir nicht vorstellen können. Nur ein Hurrican muss beim nächsten Mal nicht wieder in der Nähe sein...
Außerdem gab es einige unvergessliche Reisen auf Konferenzen nach Paris, mit fast der ganzen Gruppen, nach Trondheim und nach Sydney. Danke an dieser Stelle auch der HGSFP, die mir die Konferenz in Sydney finanziert und damit überhaupt ermöglicht hat.

Aber auch außerhalb der Arbeitsgruppe und des Instituts gibts es viele Menschen, die mich immer unterstützt und damit das hier möglich gemacht haben.
Das sind zum einen Laura, Lena, Gesa und Martin, ohne die ich wahrscheinlich nicht bis hier hin durchgehalten hätte. Ihr seid großartig! Ich freue mich auf die nächsten Jahre, wir haben noch viel vor.
Meiner Familie bin ich dankbar für die Unterstützung, die ich erfahren durfte und die mir überhaupt ermöglicht hat diesen Weg einzuschlagen. Danke für euren Rückhalt in jeder Situation, ich weiß, dass ich immer auf euch zählen kann!
Und zu guter Letzt ein großes Danke! an Thomas, der mich auch in den letzten, anstrengenden Wochen immer unterstützt hat. Der mich immer wieder aufgebaut hat und zeitweise mehr an meine Fähigkeiten geglaubt hat als ich selber. Ich bin dir unendlich dankbar, dass du mich und meine Launen in den letzten Wochen ausgehalten und freue mich auf alles, was noch vor uns liegt.